University of Bremen

Stability, Bifurcations and Explicit Solutions in Geophysical Fluid Models with Simplified Backscatter

by

Artur Prugger

A dissertation for the attainment of the degree
— *Dr. rer. nat.* —

Submitted to

Department of Mathematics
University of Bremen

October 2022

Supervisor: Prof. Dr. Jens Rademacher (Universität Bremen)
Second Reviewer: Prof. Dr. Christian Kühn (Technische Universität München)

Date of the defense: December 19, 2022

Acknowledgements

First of all, I would like to express my deep sense of gratitude to Jens Rademacher for the opportunity to work under his supervision and being part of the "Applied Analysis" working group. This thesis and my development as researcher would not have been possible without his support, knowledge, time and valuable advices. I am also very thankful to him for providing some numerical implementations used in this thesis.

I would also like to thank Christian Kühn for taking the time and immediately agreeing to be part of the examination board as well as to review this thesis.

I am thankful for having Jichen as my office mate and I am enormously grateful to him for the fruitful, inspiring and instructive cooperation, which was the key for writing this thesis, as well as for creating and providing some figures used in this thesis.

I thank the former working group "Applied Analysis": Jens Rademacher, Ivan, Lars, Hendrik, Jichen, Miriam, Dennis, Antoine, Rüdiger, Paul and Luby. It was a great time with valuable support and interesting meetings, projects and discussions. Also many thanks to Katie for her great help with bureaucratic issues.

A lot of thanks to Marcel Oliver and Stephan Juricke for their help and input regarding the backscatter topic, as well as the TRR for the support and great community.

I am also thankful to my brother Andrej, and in particular I am deeply grateful to my mother for her huge support in everything, which was always providing me the opportunity to freely choose and go my way, even resulting in writing this thesis.

I am very grateful to my best friend Pascal for having so many things in common, talking about everything, his honest and reflected opinions, understanding me so well and making the time always funny and relaxed.

Also thanks a lot to the rest of the "Knorzergruppe" and my precious friends Miriam, Alex and Kos for their support, the great time and various activities together.

I highly appreciate the precious time together with Cilia, which was important for me to get through all of this. I also thank her dog Campi for providing the required amount of cuteness.

Thanks to MARUM and GLOMAR for the interesting research topics and courses they offer. Thanks to Gualtiero Badin for being part of my thesis committee, together with Jens Rademacher and Marcel Oliver, and the fruitful discussions about my work.

This work is funded by the Deutsche Forschungsgemeinschaft (DFG, German Research Foundation) in the framework of the project M2 (Systematic multi-scale modelling and analysis for geophysical flow) of the Collaborative Research Centre TRR 181 "Energy Transfers in Atmosphere and Ocean" with project number 274762653.

Abstract

For the numerical simulations of geophysical flows it is necessary to model the effects of unresolved small scales on the resolved large scales, in order to ensure energy consistency and provide more realistic results. Such modeling is called subgrid parameterization and one method that comes to frequent use is the kinetic energy backscatter scheme. We investigate this numerical scheme analytically and point out some possible issues, that might occur in the numerical computations.

In the first part we present certain functions in plane wave or traveling wave form, that generate a vanishing or gradient nonlinear advection term in fluid equations. This allows us to reduce nonlinear fluid equations to linear problems. We show that certain superposition among such functions retains the targeted form of the advection term. This in particular means, that solutions of the presented form solve the linear and nonlinear equations at the same time and possess a certain linear behavior. Using these functions and their properties, we study the occurrence of linear spaces of explicit solutions to incompressible Euler and Navier–Stokes equations in $\mathbb{R}^n$ with arbitrary $n \geq 2$, as well as the rotating Boussinesq equations in $\mathbb{R}^3$. In the latter we discover explicit solutions that we characterize with known classes of flows, namely the parallel flows, Kolmogorov flows and monochromatic inertia gravity waves. Afterwards, we show that forcing terms of corresponding plane wave type in more general fluid equations yield explicit solutions by linear variation of constants. In the end of this part the new contributions of our presented solutions are pointed out and a comparison of them with already known ones is provided. Our approach offers another view on known explicit solutions of different fluid models from a plane wave perspective and provides transparent nonlinear interactions between different flow components.

In the second part we investigate the rotating shallow water and Boussinesq equations with horizontal simplified kinetic energy backscatter and hyperviscosity. With the help of the functions presented in the first part, we study the impact of this energy input and find that backscatter generates numerous solutions that grow exponentially and unboundedly in time. This indicates the possibility of undesired energy concentration into specific modes due to the backscatter. We also analyze the stability of trivial and nontrivial steady solutions in the same plane wave or traveling wave form, where some of these can be characterized as classes of flows mentioned in the first part. Possible superposition with unboundedly growing solutions provides a sufficient condition for instability. For certain steady barotropic flows we provide numerical evidence of eigenmodes whose growth rates are proportional to the free amplitude factor of the flow. For all other arising steady solutions we prove that this is not possible.

In the third part we extend the rotating shallow water equations with backscatter and hyperdiffusion by additional linear and non-smooth quadratic bottom drag terms, which represent energy loss through simple bottom topography. Our results show that the interplay between the backscatter, hyperdiffusion and bottom drag terms cause amplification and selection effects, which are undesired for the targeted realistic energy distribution. By decreasing the linear bottom drag we find that the trivial flow becomes unstable after a certain threshold, which generates nonlinear flows. For isotropic backscatter and hyperdiffusion we determine the simultaneous supercritical bifurcation of (steady) Rossby waves and (temporally oscillating) inertia-gravity waves, while in the anisotropic case only Rossby waves primarily bifurcate. For the bifurcation analysis we use Lyapunov–Schmidt reduction, where care has to be taken due to the missing smoothness and since the hyperdiffusion terms prevent a spectral gap at large wave numbers. We illustrate the bifurcation results by numerical computations and extend branches in parameter space beyond our analytical investigations. Furthermore, we find that purely smooth bottom drag cannot completely suppress the occurrence of explicit solutions as presented in the second part for the shallow water equations, so that steady and unboundedly growing explicit flows can exist in this case as well.

Zusammenfassung

Für numerische Simulationen von geophysikalischen Strömungen ist es notwendig, die Einflüsse von nicht berechneten kleinskaligen Bewegungen auf berechnete großskalige Flüsse zu modellieren, um Energiekonsistenz und realistischere Ergebnisse zu gewährleisten. Solch eine Modellierung wird "subgrid parameterization" genannt und ein Verfahren, das häufig eingesetzt wird, ist das sogenannte "kinetic energy backscatter" Modell. Wir untersuchen dieses numerische Modell mit analytischen Methoden und weisen auf mögliche Probleme hin, die in numerischen Berechnungen auftreten könnten.

Im ersten Abschnitt stellen wir gewisse Funktionen in Form von ebenen Wellen oder Wanderwellen vor, die die Advektionsterme in Fluidgleichungen verschwinden lassen oder in eine Gradientenform überführen. Damit sind wir in der Lage nichtlineare Fluidgleichungen auf lineare Probleme zu reduzieren. Wir zeigen, dass bestimmte Superpositionen dieser Funktionen die gewünschte Form des Advektionsterms erhält. Insbesondere bedeutet das, dass die Lösungen in der vorgestellten Form die linearen und nichtlinearen Gleichungen gleichzeitig lösen, weswegen sie ein bestimmtes lineares Verhalten aufweisen. Auf Grundlage dieser Funktionen und ihrer Eigenschaften untersuchen wir das Vorkommen linearer Räume aus expliziten Lösungen, sowohl von inkompressiblen Euler und Navier–Stokes Gleichungen in $\mathbb{R}^n$ für beliebiges $n \geq 2$, als auch von rotierenden Boussinesq Gleichungen in $\mathbb{R}^3$. In Letzteren finden wir explizite Lösungen, die sich durch bekannte Klassen von Strömungen charakterisieren lassen, und zwar den sogenannten "parallel flows", "Kolmogorov flows" und "monochromatic inertia gravity waves". Danach zeigen wir, dass antreibende Terme in Form von bestimmten ebenen Wellen in allgemeineren Fluidgleichungen zu expliziten Lösungen führen, die man durch lineare Variation der Konstanten erhalten kann. Am Ende dieses Abschnittes heben wir hervor, was an den vorgestellten Lösungen neu ist und vergleichen sie mit bereits bekannten Lösungen. Unser Ansatz zeigt einen anderen Blickwinkel auf bekannte Lösungen von verschiedenen Fluidgleichungen und bietet eine transparente Sicht auf nichtlineare Wechselwirkungen zwischen einzelnen Bestandteilen bestimmter Strömungen.

Im zweiten Abschnitt analysieren wir sowohl die rotierenden Flachwassergleichungen, als auch die rotierenden Boussinesq Gleichungen, beide erweitert durch horizontalen, vereinfachten "kinetic energy backscatter" und horizontale Hyperviskosität. Mithilfe der im ersten Abschnitt vorgestellten Funktionen untersuchen wir den Einfluss der zusätzlichen Energiezufuhr und stellen fest, dass die "backscatter" Terme eine Vielzahl expliziter Lösungen generieren, die zeitlich unbeschränkt und exponentiell wachsen. Dies deutet auf die Möglichkeit hin, dass sich Energie durch den "backscatter" unerwünscht in bestimmte Moden konzentriert. Wir analysieren zudem die Stabilität von trivialen und

nichttrivialen stationären Lösungen, die dieselbe Form von ebenen Wellen oder Wanderwellen besitzen, wobei einige wie im ersten Abschnitt durch bekannte Klassen von Flüssen charakterisiert werden können. Eine hinreichende Bedingung für Instabilität ist gegeben durch mögliche Superposition mit unbeschränkt und exponentiell wachsenden Lösungen. Für bestimmte barotrope Flüsse geben wir numerische Hinweise für Eigenmoden, dessen Wachstumsraten proportional sind zu den frei wählbaren Amplituden der Flüsse. Für alle anderen stationären Flüsse zeigen wir, dass das nicht der Fall ist.

Im dritten Abschnitt erweitern wir dann die rotierenden Flachwassergleichungen mit "backscatter" und Hyperviskosität durch sowohl lineare als auch nicht glatte und quadratische Bodenreibungsterme, die den Energieverlust durch einfache Topographie des Grundes darstellen. Unsere Ergebnisse zeigen ein gewisses Zusammenspiel von "backscatter", Hyperviskosität und Bodenreibung, die eine Verstärkung und Selektierung verursachen, die für realistische Energieverteilungen unerwünscht sind. Es stellt sich heraus, dass durch Abschwächung der Bodenreibung die triviale Lösung ab einem bestimmten Schwellenwert instabil wird, was zusätzliche nichtlineare Lösungen erzeugt. Wir ermitteln für isotropen "backscatter" und Hyperviskosität eine gleichzeitige superkritische Verzweigung von (stationären) Rossby-Wellen und (zeitlich oszillierenden) "inertia-gravity waves", während im anisotropen Fall nur Rossby-Wellen zuerst verzweigen. Für die Verzweigungsanalyse verwenden wir die Lyapunov–Schmidt Reduktion. Dabei ist insbesondere die fehlende Glattheit des Problems als auch die durch die Hyperviskosität induzierte, fehlende spektrale Lücke für große Wellenzahlen zu berücksichtigen. Wir veranschaulichen die Verzweigungsergebnisse mit numerischen Berechnungen und erweitern die Zweige im Parameterraum über unsere analytischen Untersuchungen hinaus. Zudem stellen wir fest, dass eine rein glatte Bodenreibung das Vorkommen von expliziten Lösungen, ähnlich wie im zweiten Abschnitt für die Flachwassergleichungen, nicht komplett verhindern kann. Damit können auch in diesem Fall explizite stationäre und unbeschränkt wachsende Lösungen existieren.

Contents

List of Figures

List of Symbols and Notations

$\mathbb{N}$	Set of natural numbers $\{0, 1, 2, \dots\}$
$\mathbb{Z}$	Set of integers $\{\dots, -2, -1, 0, 1, 2, \dots\}$
$\mathbb{R}$	Set of real numbers
$\mathbb{R}_{\geq 0}$	Set of non-negative real numbers
$\mathbb{R}^n$	n-dimensional real Euclidean space for $n \geq 2$
$\mathbb{C}$	Set of complex numbers
$\mathbb{C}^n$	n-dimensional complex space for $n \geq 2$
$\boldsymbol{v}$	Vector $\boldsymbol{v} := (v_1, \dots, v_n)^\intercal \in \mathbb{C}^n$ for $n \geq 2$
Re	Real part of a complex number
Im	Imaginary part of a complex number
$\bar{z}$, $\bar{\boldsymbol{v}}$	Complex conjugate of complex number z or each component of complex vector $\boldsymbol{v}$
$X \times Y$	Cartesian product of two sets X and Y
$\operatorname{span} S$, $\operatorname{span}(S)$	Linear span of vector set S
Id	Identity matrix or operator
$\operatorname{sgn}(\cdot)$	Sign function
$\lfloor \cdot \rfloor$	Rounding down of a real number
$\boldsymbol{v}^\intercal$, $A^\intercal$	Transpose of vector $\boldsymbol{v}$ or matrix A
$\lvert \cdot \rvert$	Absolute value in $\mathbb{C}$, norm $\lvert\boldsymbol{v}\rvert := \sqrt{\boldsymbol{v}^\intercal \cdot \bar{\boldsymbol{v}}}$ in $\mathbb{C}^n$ for $n \geq 2$
$\det(A)$	Determinant of matrix A
$\ker(L)$	Kernel of linear operator L
$\operatorname{range}(L)$	Range of linear operator L
$\sphericalangle(\boldsymbol{v}_1, \boldsymbol{v}_2)$	Interior angle between vectors $\boldsymbol{v}_1$ and $\boldsymbol{v}_2$
$\boldsymbol{v}_1 \cdot \boldsymbol{v}_2$	Scalar product of vectors $\boldsymbol{v}_1$ and $\boldsymbol{v}_2$
$\boldsymbol{v}_1 \perp \boldsymbol{v}_2$, $S_1 \perp S_2$	Orthogonality of vectors $\boldsymbol{v}_1$ and $\boldsymbol{v}_2$ or vector spaces S_1 and S_2
$\boldsymbol{v}_1 \times \boldsymbol{v}_2$	Cross product of vectors $\boldsymbol{v}_1$ and $\boldsymbol{v}_2$ for $n = 3$

$\frac{\partial}{\partial x}$, ∂_x	Partial derivative in x
div	Divergence operator
∇	Gradient operator
$(\boldsymbol{v} \cdot \nabla)\boldsymbol{\zeta}$	Advection operator of quantity $\boldsymbol{\zeta}$ with background flow $\boldsymbol{v}$
$\frac{\mathrm{D}}{\mathrm{D}t}$	Material derivative
Δ	Laplace operator
Δ^2	Bi-Laplace operator
curl$(\cdot)$	Curl operator $\mathrm{curl}(\boldsymbol{F}) = \nabla \times \boldsymbol{F}$ for functions $\boldsymbol{F} : \mathbb{R}^3 \to \mathbb{R}^3$
$\mathcal{L}$	Linear differential operator
$\widehat{\mathcal{L}}$	Fourier transform of linear differential operator $\mathcal{L}$
$\mathcal{L}^*$	Adjoint of linear differential operator $\mathcal{L}$
I	Interval in $\mathbb{R}$
Ω	Domain in $\mathbb{R}^n$ for $n \geq 2$
$C(X, Y)$	Space of continuous functions mapping from X to Y
$C^k(X, Y)$	Space of k-times continuously differentiable functions mapping from X to Y for $k \geq 1$, space $C(X, Y)$ for $k = 0$
$C^{k,\alpha}(X, Y)$	Space of functions from $C^k(X, Y)$ with Hölder continuous k-th derivatives for $k \in \mathbb{N}$ and $0 < \alpha \leq 1$
$\|\cdot\|_{C^{k,\alpha}}$	Norm in $C^{k,\alpha}(X, Y)$ for $k \in \mathbb{N}$ and $0 < \alpha \leq 1$, norm in $C^k(X, Y)$ for $\alpha = 0$
L^p, $L^p(\Omega)$	Lebesgue space from domain Ω to $\mathbb{R}$ or $\mathbb{C}$ for $1 \leq p \leq \infty$
$\|\cdot\|_p$	Norm in Lebesgue space L^p for $1 \leq p \leq \infty$
$\langle\cdot,\cdot\rangle_{L^2}$	Inner product in Lebesgue space L^2
H^k, $H^k(\Omega)$	Sobolev space $H^k = W^{k,2}$ from domain Ω to $\mathbb{R}$ or $\mathbb{C}$ for $1 \leq k < \infty$
H^k_{per}, $H^k_{\mathrm{per}}(\Omega)$	Sobolev space H^k with periodic boundary condition on bounded domain Ω for $1 \leq k < \infty$
$\|\cdot\|_{H^k}$	Norm in Sobolev space H^k for $1 \leq k < \infty$
$\langle\cdot,\cdot\rangle_{H^2}$	Inner product in Sobolev space H^2
$\mathcal{O}(\varepsilon)$	Asymptotic O-notation $\limsup_{\varepsilon\to 0}\lvert\mathcal{O}(\varepsilon)/\varepsilon\rvert = C < \infty$
$o(\varepsilon)$	Asymptotic o-notation $\lim_{\varepsilon\to 0}\lvert o(\varepsilon)/\varepsilon\rvert = 0$

Declaration of changes

This version of the PhD thesis (February 6, 2023) contains only minor edits compared with the examined version (October 28, 2022), that do not change the meanings or results. The date of the defense was added and typing as well as linguistic mistakes corrected. In a few places more detailed comments are provided, Remark 3.1.2 added and the software used for this work are mentioned. A few more references are included and the information about Prugger et al. (2022a) updated.

1. Introduction

1.1. Geophysical flows and subgrid-scale parameterization

The understanding of large scale geophysical flows is of great interest. The focus lies not only on large scale atmospheric flows for the prediction of weather and climate, but also on large scale oceanic currents, which are the main transporting systems of various quantities in the oceans, as e.g. temperature, and they are even coupled with the climate systems as well. This interest and importance increased in the last years due to the global warming and climate change.

The analytical investigations of the corresponding geophysical fluid models experienced a great progress, which have a high impact on the understanding of large scale processes. One is e.g. able to show and characterize analytically some types of flows, which are also observed in atmosphere and oceans, as e.g. the stationary *Rossby waves* or the propagating *inertia-gravity waves*. For this topic we recommend the books Pedlosky (1987); Vallis (2017). Such realistic and complex problems are not solvable with only analytical research, e.g. due to complicated topographical circumstances. Therefore, numerical computations are indispensable for the investigations, simulations and predictions of large scale flow phenomena.

Even though the numerical simulations are very accurate nowadays and provide possibilities to determine, analyze and predict geophysical flows, which would not be possible with pure analytical methods, there are still some challenging issues in numerical modeling. The major issue is that flows in atmosphere and oceans consist of a large variety of motions in different scales, which are all connected and influence each other, from the small and short-living turbulence to the large planetary currents existing for weeks. Even though one is essentially interested in large scale phenomena when investigating geophysical flows, one cannot neglect the impact of small scale motions on the large scale. Energy is not just dissipating from large to small scales, there is a more complex interplay between the different scales, where even energy can be reinjected from small to large scales, see e.g. Jansen and Held (2014); Rubio et al. (2014).

The issue lies not only in the complex interplay between the different scales, but also in the computations of the small scale motions. Due to the lack of computational power and the limited memory, as well as the observational possibilities to provide data, the resolutions of the spatial grids for the numerical models is limited, in particular when e.g. simulating and investigating geophysical flows throughout the whole ocean. The result is, that there are scales of flows which are too small to be computed explicitly, since their structures lie between the grids. Such small scales are therefore also called *subgrid scales*. As already pointed out, even though one is in particular interested in

the large scale flows, one cannot just neglect the subgrid scale flows due to the connection with and the importance for the resolved larger scales. In order to overcome this problem, one uses so-called *subgrid parameterizations*, where the influence of the subgrid scale on the larger scales is modeled and simulated depending on the data from the resolved large scale flows. Furthermore, such models of subgrid effects should also ensure stable numerical simulations, as well as energy consistency for the computed results. The use of subgrid parameterizations improves the numerical simulations of geophysical flows clearly, verified by comparisons with observational data and higher resolution simulations, see e.g. Jansen and Held (2014); Juricke et al. (2020).

There are different subgrid models satisfying the required properties, as e.g. stochastic parameterizations (Porta Mana and Zanna, 2014; Zanna et al., 2017), but here we focus on certain deterministic models, the so-called *kinetic energy backscatter schemes*, which have come to frequent use. They are in a way build up by negative horizontal viscosity together with hyperviscosity, see e.g. Jansen and Held (2014); Zurita-Gotor et al. (2015); Jansen et al. (2019); Juricke et al. (2020); Perezhogin (2020), and for a detailed discussion and relations to other approaches Danilov et al. (2019). Numerical simulations with backscatter schemes have been found to provide energy "at the right places" and the results are matching more closely to observational data and comparisons with high resolution simulations.

We pick up the characteristics of the backscatter parameterization and study different geophysical fluid models adjusted by simplified versions of such schemes analytically. To the best of our knowledge, an analytic investigation of such backscatter modifications on geophysical fluid models has not been done in the continuum setting. Even though the ideas for backscatter are derived and used for improving numerical computations of geophysical flows, i.e. for discrete settings, the investigations of such models in the continuum setting is eminent for the understanding and improving the corresponding numerical models.

We focus here on two geophysical fluid models. First, we consider the rotating shallow water equations, which is a simpler model describing the horizontal motions in a thin fluid layer with constant density, where the depth of the fluid layer is much smaller than the horizontal scales. Second, we study the rotating Boussinesq equations, in which vertical motions are also determined and the density, described by the buoyancy, is not constant. We realize the backscatter in these models by destabilizing negative horizontal viscosity and the dissipation by stabilizing horizontal hyperviscosity with constant parameters. By comparison, the backscatter terms in the numerical schemes have non-constant coefficients, which are coupled with energy equations in order to regulate energy flux and provide energy consistency during the runtime. With our simplified consideration on the continuum level we are able to analytically investigate properties, dynamics and energy distributions, so that our results point out potential issues in the discrete setting and can provide hints for improvements and further studies of backscatter schemes.

In Prugger (2017) similar linear damping and forcing terms are investigated for the rotating shallow water equations. The dissipation is realized there by usual viscosity, while the linear forcing by the flow itself. For this model it turns out that the trivial steady flow can become unstable due to perturbations of waves with finite wavelength, when certain parameters are varied, which also causes the emergence of nontrivial flows. These results give hints for similar dynamics in models with backscatter and hyperviscosity due to similar roles of the terms, which motivated us to consider and analyze such backscatter models.

In some simulations with data-driven subgrid scale models, build up by other realizations of backscatter, one has observed numerical blow-up and physically unrealistic flows, see Guan et al. (2022) and the references therein. Indeed, we find similar phenomenon in our analytical investigations with the presented simplified backscatter. We not only prove the instability of the trivial flow in these settings, but in certain cases also the existence of explicit solutions, that grow exponentially and unboundedly in time. In fact, they do not blow up in finite time, as mentioned in Guan et al. (2022), but still have similar unbounded temporal behavior. Furthermore, we investigate the shallow water equations with backscatter and bottom drag, which has an additional stabilizing effect. Nevertheless, the bottom drag is not able to prevent backscatter-induced instabilities completely. As a result, we prove in this setting the emergence of nontrivial flows, when the trivial flow becomes unstable. These nontrivial flows could also be physically unrealistic flows, as indicated in Guan et al. (2022), since they only arise due to backsatter from numerical subgrid parameterization. Such solutions, that only arise from numerical subgrid models, should be avoided in simulations of realistic flows.

The relevance of our analytical approach comes from the fact, that numerical solutions on the discrete space approximate analytical solutions on the continuous space. Thus, solutions on the discrete space with backscatter approximate those on the continuous space with similar backscatter. The finer the resolution, the better usually the approximations.

For infinite resolution of the numerical models, the backscatter terms in the numerical schemes would vanish, which one can for instance see from the description of backscatter in Perezhogin (2020). Even though the investigations on the continuum level correspond to such infinite resolution, where backscatter terms vanish, we still keep them in a simplified way. Moreover, the analytical results that we show in this thesis are also provided by arbitrarily small backscatter terms. In particular we will see, that the range of wavelength for unstable perturbations depends on the ratio between the backscatter and the hyperviscosity parameter, but not their magnitudes. Thus, the numerical models with constant backscatter parameter and arbitrarily high resolutions can also possess the phenomena we identify here analytically. This underlines our conjecture, that the behavior and properties of our analytical solutions with simplified backscatter can provide hints for the behavior and properties of discrete solutions with similar non-constant backscatter realizations in the numerical simulations.

We note that other subgrid parameterizations may perform better regarding possible issues found here analytically. However, analytical investigations of other subgrid models and comparisons with them is not subject of this work and beyond the scope here.

1.2. Mathematical analyses

In this thesis we pick up the aforementioned idea of backscatter parameterization and study it from the analytical perspective. Such analytical investigations of the problem are not only valuable for improving the mathematical understanding in the field of (geophysical) fluid models, but can be also very crucial for the development of the corresponding numerical schemes. For instance, the analytical results might be important for testing the numerics, which should correspondingly behave as predicted analytically. Furthermore, certain analytical aspects of the problem might also indicate possible problems in the numerical computations or give hints for developing and improving them. Summing up the message with the words by Schneider and Uecker (2017): *"A numerical simulation of a PDE requires an analytical understanding of the PDE".*

Partial differential equations (PDEs) are mathematical models describing physical problems and laws, but also in other natural sciences, which can be investigated analytically and numerically. PDEs consist of differential operators and the solutions of such equations are functions $\boldsymbol{u} = \boldsymbol{u}(t, \boldsymbol{x})$ from a suitable function space. Here we analyze PDEs of the form

$$\frac{\partial \boldsymbol{u}}{\partial t} = G(\boldsymbol{u}) = \mathcal{L}_G \boldsymbol{u} + N_G(\boldsymbol{u}) \,, \tag{1.1}$$

with linear differential operator $\mathcal{L}_G$ in $\boldsymbol{u}$, meaning that $\mathcal{L}_G$ contains constant terms and spatial derivatives $\partial_{x_j}^k$ in its coefficients for $\boldsymbol{k} \geq 1$, as well as the nonlinear differential operator N_G. This form of PDE can be even more general, when e.g. prescribing space and time dependent operators $\mathcal{L}_G = \mathcal{L}_G(t, \boldsymbol{x})$ and $N_G = N_G(t, \boldsymbol{x}, \boldsymbol{u})$, or taking higher order time-derivatives ∂_t^k with $k \geq 2$, but we will not consider such problems here.

1.2.1. Dynamical systems

Finding solutions to nonlinear PDEs is pretty challenging, since well-studied general methods are not available as for linear problems. Each nonlinear problem has different properties and behaviors, so that individual methods and approaches are usually required. It is therefore not surprising, that determining explicit solutions, which can be explicitly described by analytical expressions, is not only difficult, but sometimes even not possible. However, there are methods and tools in order to prove existence of solutions, as well as to approximate them and to determine their properties and (temporal) behaviors. The research field of *dynamical systems* investigates the temporal behavior and evolution of a system, i.e. of the solutions it contains.

In the first place we are interested in *steady solutions*, since they are starting points for finding and analyzing other solutions. Steady solutions $\boldsymbol{u}_s$, which are also called *steady states* or *fixed points*, are solutions of (1.1) satisfying $G(\boldsymbol{u}_s) = 0$. One can easily see in the PDE (1.1), that in this case there is no temporal change for $\boldsymbol{u}$, so it remains steady. An important characteristic of steady solutions for the analysis of the dynamics is its stability. If we choose an initial value $\boldsymbol{u}_0$ close to the steady state $\boldsymbol{u}_s$, then $\boldsymbol{u}_s$ is called *stable*, if for any $\varepsilon > 0$ there is a $\delta > 0$, so that for $\|\boldsymbol{u}_0 - \boldsymbol{u}_s\| < \delta$ it follows $\|\boldsymbol{u}(t, \boldsymbol{u}_0) - \boldsymbol{u}_s\| < \varepsilon$ for all $t \geq 0$, where $\|\cdot\|$ is a suitable norm of the considered function space. It means, small perturbations of $\boldsymbol{u}_s$ remain small for all $t \geq 0$. The steady solution $\boldsymbol{u}_s$ is called *asymptotically stable*, if in addition $\|\boldsymbol{u}(t, \boldsymbol{u}_0) - \boldsymbol{u}_s\| \to 0$ for $t \to \infty$ and $\|\boldsymbol{u}_0 - \boldsymbol{u}_s\| < \delta$, so small deviations from $\boldsymbol{u}_s$ converge to $\boldsymbol{u}_s$. In such a case $\boldsymbol{u}_s$ is also called *attractor*. If $\boldsymbol{u}_s$ does not satisfy the condition for a stable steady solutions, then it is called *unstable*.

In order to determine the stability of a steady solution $\boldsymbol{u}_s$, one often approximates the problem by linearizing it in $\boldsymbol{u}_s$, so that one studies the behavior of the steady state locally with respect to G. It is reasonable to do this for the analysis of the stability, since it is a local characteristic of a steady state $\boldsymbol{u}_s$ as well. Having a steady solution $\boldsymbol{u}_s$, we then investigate small deviations $\boldsymbol{u} = \boldsymbol{u}_s + \boldsymbol{v}$ from it, with perturbation $\boldsymbol{v}$. If G is smooth enough, we can approximate and simplify the problem by using Taylor expansion of G in $\boldsymbol{u}_s$ and obtain for (1.1)

$$\frac{\partial \boldsymbol{v}}{\partial t} = \frac{\partial \boldsymbol{u}}{\partial t} = G(\boldsymbol{u}) = G(\boldsymbol{u}_s + \boldsymbol{v}) = \mathrm{D}_{\boldsymbol{u}} G|_{\boldsymbol{u}_s} \boldsymbol{v} + \mathcal{O}(\|\boldsymbol{v}\|^2)\,.$$

So the temporal behavior of small perturbations $\boldsymbol{v}$ is approximated by a remaining linear problem, the Fréchet derivative of G in the steady solution $\boldsymbol{u}_s$, when disregarding the higher order terms $\mathcal{O}(\|\boldsymbol{v}\|^2)$.

Linear problems are well-studied and the most important here are the eigenvalues λ, which are defined by $\mathcal{L}\boldsymbol{e} = \lambda \boldsymbol{e}$ for a linear operator $\mathcal{L}$ and a corresponding eigenmode $\boldsymbol{e}$. Thus, on the linear level, this provides perturbations satisfying $\partial_t \boldsymbol{v} = \mathrm{D}_{\boldsymbol{u}} G|_{\boldsymbol{u}_s} \boldsymbol{v} = \lambda \boldsymbol{v}$, so $\boldsymbol{v}$ consists of a factor $\mathrm{e}^{\lambda t}$ and a time-independent profile or spacial shape. The real part $\mathrm{Re}(\lambda)$ of the eigenvalue describes the temporal behavior on the linear level: $\boldsymbol{v}$ is exponentially decaying for $\mathrm{Re}(\lambda) < 0$ and growing for $\mathrm{Re}(\lambda) > 0$. This determines the instability of the steady state $\boldsymbol{u}_s$. If $\mathrm{D}_{\boldsymbol{u}} G|_{\boldsymbol{u}_s}$ has an eigenvalue λ with $\mathrm{Re}(\lambda) > 0$, then $\boldsymbol{u}_s$ is unstable due to the perturbation and eigenmode $\boldsymbol{v}$ of λ, which is growing in time.

Even though the eigenmode is growing exponentially and unboundedly in time, the perturbation $\boldsymbol{v}$ usually does not do the same in the full nonlinear setting. The reason is, that for larger perturbations the nonlinear terms, which we neglected by the rest term $\mathcal{O}(\|\boldsymbol{v}\|^2)$, have more and decisive influence on them, forcing them to another behavior. For a linear problem $N_G \equiv 0$ such perturbations grow unboundedly. Nevertheless, in this thesis we will see, that even in presence of nonlinear terms there might be perturbations, that grow exponentially and unboundedly in the full nonlinear setting. We call steady solutions, which have such growing perturbations, *unboundedly unstable* here.

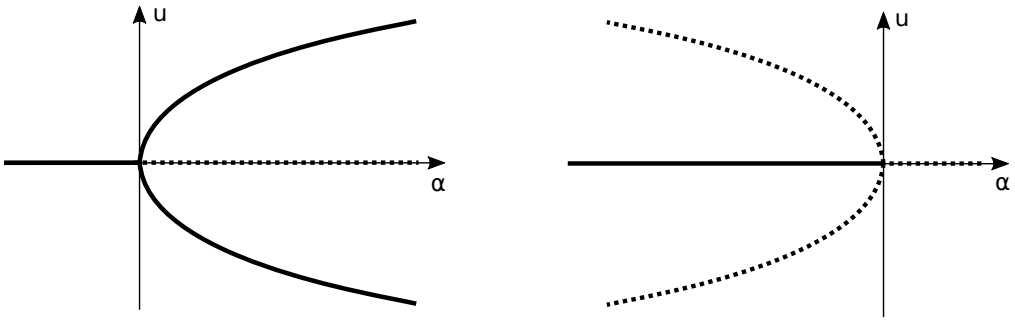

(a) Supercritical (b) Subcritical

Figure 1.1.: Illustration of both types of pitchfork bifurcations. Bold branches represent stable solutions and dotted branches unstable solutions.

The stability property of a steady solution $\boldsymbol{u}_s$ of (1.1) directly depends on G and is not necessarily the same for all parameter choices. If for instance $\boldsymbol{u}_s$ is stable for certain parameters of G, then it might become unstable when varying a parameter beyond a certain threshold. such a change of stability changes the dynamics near $\boldsymbol{u}_s$ and other solutions bifurcate. We illustrate this phenomenon with a simple example of an ordinary differential equation (ODE), where solutions depend on time t only. This example shows one of the fundamental types of bifurcations, which we will also find later in the thesis.

We consider the one-dimensional ODE

$$\frac{\mathrm{d}u}{\mathrm{d}t} = G(u, \alpha) = u(\alpha - u^2)\,, \tag{1.2}$$

with parameter $\alpha \in \mathbb{R}$ and $u(t) \in \mathbb{R}$. One immediately sees the trivial solution $u_1 = 0$, which exists for all parameter values $\alpha \in \mathbb{R}$. The linearization of $G(\cdot, \alpha)$ in u_1 is just α, which directly gives the eigenvalues in the one-dimensional problem. Thus, u_1 is stable for $\alpha < 0$ and unstable for $\alpha > 0$, which means a stability change occurs at the threshold $\alpha = 0$. Furthermore, two other steady solutions bifurcate at $\alpha = 0$ from u_1, namely $u_2 = \sqrt{\alpha}$ and $u_3 = -\sqrt{\alpha}$, which exist for $\alpha \geq 0$. Linearizing $G(\cdot, \alpha)$ in u_2 or u_3 both give -2α, which is also the eigenvalue and implying that $u_{2,3}$ are stable. Summarized, for $\alpha < 0$ we only have one stable steady solution u_1. For $\alpha > 0$ we have one unstable steady solution u_1 and two stable ones $u_{2,3}$, which bifurcate from u_1 at $\alpha = 0$. This form of bifurcation is called *pitchfork bifurcation*, and since the trivial steady solution u_1 is unstable, while at the same time the bifurcating ones are stable, it is called *supercritical pitchfork bifurcation*, c.f. Figure 1.1(a).

If we change the sign of the cubic term in (1.2), so $G(u, \alpha) = u(\alpha + u^2)$, then the dynamics are exactly the other way round: The stability of the trivial steady solution u_1 remains unchanged, but the bifurcating solutions $u_2 = \sqrt{-\alpha}$ and $u_3 = -\sqrt{-\alpha}$ only exist for $\alpha < 0$ and are unstable. This dynamical situation is then called *subcritical pitchfork bifurcation*, c.f. Figure 1.1(b).

There are also other types of bifurcations, e.g. the *transcritical bifurcation* or the *saddle-node bifurcation*. It is also possible, that not steady solutions are bifurcating from the trivial one, as shown here, but solutions that oscillate in time. This occurs, when not a real eigenvalue is critical, i.e. has zero real part, but purely imaginary ones. Such a bifurcation is called *Andronov-Hopf bifurcation* and will also occur later in this thesis. We will not show these types of bifurcations here, but instead we recommend the book of Schneider and Uecker (2017) for more details about the presented methods and phenomena, as well as for more aspects of dynamical systems and nonlinear PDEs.

1.2.2. Nonlinear fluid equations and explicit solutions

The nonlinear PDEs, which we investigate in this thesis, are certain selected incompressible (geophysical) fluid equations. Such equations describe the motions in a fluid, represented by the velocity $\boldsymbol{v}$, and other quantities transported in the fluid, as e.g. temperature, salinity or density. There are two viewpoints for the description of temporal and spatial behaviors of motions and other quantities in the fluid:

In the *Lagrangian point of view* one considers a fluid parcel (or several parcels for the whole setting) and describes the evolution of its position and other quantities in time. This representation is convenient for derivations of physical models, since one can investigate how such a parcel behaves in response to forces and other influences from outside. However, such a representation is too complex for mathematical studies and often too expensive for numerical computations as well.

For mathematical purposes it is better to fix the coordinates and describe the quantities for fixed positions $\boldsymbol{x}$ at time t. This representation is called *Eulerian point of view* and this means, that one determines for a fixed position $\boldsymbol{x}$ (or all positions for the whole setting) the quantities of the fluid parcel, that is at this position at time t.

Now, in order to use the knowledge about the physical properties of fluid parcels from the Lagrangian point of view in mathematical investigations, one needs to transform the corresponding mathematical models into the Eulerian point of view. Let us consider a fluid element at the point $\boldsymbol{x}_0$ for initial time $t = 0$, where a fluid element is an infinitesimally small fluid parcel. Furthermore, we denote the position of that fluid element at time $t \geq 0$ by $\tilde{\boldsymbol{x}}(\boldsymbol{x}_0, t)$, with $\tilde{\boldsymbol{x}}(\boldsymbol{x}_0, 0) = \boldsymbol{x}_0$. The derivative $\partial_t \tilde{\boldsymbol{x}}(\boldsymbol{x}_0, t)$ at time t is then the velocity of the fluid element $\boldsymbol{x}_0$ at time t, which is at the position $\tilde{\boldsymbol{x}}(\boldsymbol{x}_0, t)$. Considering now the setting from the Eulerian point of view, then we denote $\boldsymbol{v}(\boldsymbol{x}, t)$ as the velocity at the position $\boldsymbol{x}$ at time t. This in particular also means from the explanation above

$$\frac{\partial}{\partial t} \tilde{\boldsymbol{x}}(\boldsymbol{x}_0, t) = \boldsymbol{v}(\tilde{\boldsymbol{x}}(\boldsymbol{x}_0, t), t) \,.$$

For any fluid quantity $\boldsymbol{\zeta}(\boldsymbol{x}, t)$ in the Eulerian point of view we can represent this quantity for the fluid element at time t by $\boldsymbol{\zeta}(\tilde{\boldsymbol{x}}(\boldsymbol{x}_0, t), t)$. Now for the investigation of the temporal evolution of fluid quantities we always have the time derivative $\partial_t \boldsymbol{\zeta}$ in the equations. For the time derivative of the quantity of the fluid element $\boldsymbol{x}_0$ we in particular obtain by

chain rule

$$\frac{\mathrm{d}}{\mathrm{d}t}\boldsymbol{\zeta}(\tilde{\boldsymbol{x}}(\boldsymbol{x}_0,t),t) = \frac{\partial}{\partial t}\boldsymbol{\zeta} + \frac{\partial}{\partial t}\tilde{\boldsymbol{x}}(\boldsymbol{x}_0,t)\cdot\nabla\boldsymbol{\zeta} = \frac{\partial}{\partial t}\boldsymbol{\zeta} + \boldsymbol{v}\cdot\nabla\boldsymbol{\zeta} = \frac{\mathrm{D}}{\mathrm{D}t}\boldsymbol{\zeta}(\tilde{\boldsymbol{x}}(\boldsymbol{x}_0,t),t)\,. \tag{1.3}$$

This means, it does not matter for the time derivative of any quantity $\boldsymbol{\zeta}$ at $\tilde{\boldsymbol{x}}$, to which fluid element this quantity belongs or where it comes from, since we can use the so-called *material derivative* $\frac{\mathrm{D}}{\mathrm{D}t}$ from (1.3) with background flow $\boldsymbol{v}$, which does not depend on the fluid element for fixed position $\tilde{\boldsymbol{x}}$. Thus, we can represent the time derivative in the Lagrangian point of view completely in terms of the coordinates in the Eulerian point of view. For more details about the material derivative and the derivation of fluid equations we recommend the book of Vallis (2017).

The message here is, that all Eulerian fluid equations contain the nonlinear advection term $\boldsymbol{v}\cdot\nabla$ from the material derivative. Hence, we always consider nonlinear PDEs, where the nonlinearity comes at least from the advection term. This makes the analysis of fluid models more complicated, analytically as well as numerically. However, there are analytical tools for finding and analyzing solutions, even explicit solutions. Much has been done for instance in the direction of existence, uniqueness or regularity of solutions for the Navier–Stokes equations (e.g. Foias and Temam (1989); Doering and Gibbon (1995); Temam (1995, 2001)) as well as exact solutions (e.g. Majda and Bertozzi (2001); Schneider and Uecker (2017)). For the Euler equations there is for instance the non-uniqueness of weak solutions, which can be shown by the reduction to Burgers' equation (e.g. Schneider and Uecker (2017)), and even the existence of infinitely many global weak solutions for any space dimension and divergence-free initial condition (Wiedemann, 2011). The book by Majda and Bertozzi (2001) for instance provides a comprehensive collection of results about Euler and Navier–Stokes equations. As an example for geophysical fluid models, see e.g. Petcu et al. (2009) for results regarding existence, uniqueness and regularity of solutions for the primitive equations.

Even though it is not that usual to find nontrivial explicit solutions in complicated nonlinear PDEs, and solutions can be analyzed with analytical tools and determined numerically, one is still highly interested in them and they are of great importance. Explicit solutions form a cornerstone in analytical and numerical studies of nonlinear models in fluids and other contexts (as e.g. Weinbaum and O'Brien (1967); Majda (2003); Achatz (2006); Drazin and Riley (2006); Majda and Wang (2006); van der Toorn (2019); Chai et al. (2020); Dyck and Straatman (2020)) and also for investigations of turbulence (as e.g. Lelong and Dunkerton (1998); Ghaemsaidi and Mathur (2019); Onuki et al. (2021)). With such solutions one has a better understanding of the structures and properties of nonlinear mathematical models. The knowledge about these explicit analytical solutions are valuable for testing the corresponding numerical schemes, which highlights possible issues in such numerical models and helps to improve them. Explicit solutions also build starting points for further relevant analyses of dynamics, similar as shown above. One studies for instance their vicinity by perturbation methods, which are often build from wave-like structures. These can reveal the stability of such explicit solutions and the

existence of solutions, which cannot be expressed explicitly.

Since explicit solutions in nonlinear PDEs are rather rare, it is surprising that nonlinear fluid equations possess large sets and subspaces of explicit solutions. In this thesis we also investigate the occurrence and properties of explicit solutions in different fluid models, which are of certain traveling or plane wave form in the whole space $\mathbb{R}^n$. For the studies of geophysical flows in observations and simulations it is customary to consider linear wave modes, see e.g. Pedlosky (1987); Olbers et al. (2012); Vallis (2017), which also classify certain large scale wave phenomena. Thus, the consideration of traveling or plane wave explicit solutions is also useful in the applications.

The explicit flows that we study are chosen in such a way, that they solve the full nonlinear and the linear equations at the same time, by dropping the nonlinear advection terms. Due to this, these explicit solutions span certain linear subspaces, since they have a free amplitude scaling and restricted superposition among them is possible. These almost linear behaviors of such explicit solutions are very useful for the investigations of the full nonlinear fluid models. They allow to find steady, exponentially decaying or unboundedly growing solutions, which point out potential issues in the models. For the backscatter models this can mean, that energy is accumulating in certain scales, in contrast to the pursued energy distribution and consistency. Furthermore, it is also possible to study nonlinear interactions with the explicit flows, which is an important question for instance for the investigations of energy transfers between different scales.

Explicit solutions with such linear behavior are unusual in generic nonlinear evolution equations, but it is well known that these can occur in fluid models with nonlinear advection terms. Simple monochromatic explicit wave solutions of this kind, i.e. consisting of a single Fourier mode, are for instance presented in Meshalkin and Sinai (1961); Mied (1976); Drazin (1977). Various solutions of Eulerian fluid equations in space dimensions $n = 2$ or $n = 3$ can be classified in terms of different types of so-called *Beltrami flows*. Solutions of fluid equations are called Beltrami flows, if they satisfy

$$\boldsymbol{v} \times \operatorname{curl}(\boldsymbol{v}) = 0\,,$$

where $\boldsymbol{v}$ is the velocity of the solution, $\times$ the cross product of vectors and $\operatorname{curl}(\cdot)$ the curl operator defined by $\operatorname{curl}(\boldsymbol{v}) = \nabla \times \boldsymbol{v}$ for gradient operator ∇. They are for instance discussed in Wang (1989); Majda and Bertozzi (2001); Drazin and Riley (2006). If the solutions satisfy

$$\operatorname{curl}\big(\boldsymbol{v} \times \operatorname{curl}(\boldsymbol{v})\big) = 0\,,$$

then they are called *generalized Beltrami flows*, which are for instance studied in Wang (1989, 1990); Drazin and Riley (2006). There is also the class of *extended Beltrami flows*, which is presented in Dyck and Straatman (2020). The solutions we consider here belong to the class of generalized Beltrami flows, but not to the other two.

As already mentioned, the coefficients of the additional backscatter and hyperdiffusion terms can be arbitrarily small and we still obtain the same phenomena, as for instance the existence of explicit solutions. A small choice of these parameters suggests to consider the backscatter models as a regularization of the (rotating) Euler equations, i.e. a perturbation of these equations with higher derivative terms. The explicit solutions presented here might be important to understand the dynamics of this regularization, which then provide a better understanding of the solutions and dynamics of the (rotating) Euler equations as well, when the hyperdiffusion and backscatter parameter tend to zero. For this purpose, one additionally has to study the well-posedness of the backscatter models, which is not done in this work here.

The idea and procedure of using a regularization in order to have a clearer understanding of the dynamics of the underlying model is the analogous to the Burgers' equation (Bateman, 1915; Burgers, 1948). The inviscid Burgers' equation has a discontinuous shock as weak traveling wave solution, which is not unique for given initial condition. In contrast, viscous Burgers' equation has certain unique traveling wave solutions approximating the shock solution in the inviscid case, when the viscosity parameter tends to zero. For more details see e.g. Schneider and Uecker (2017).

1.3. Outline

This thesis has the following structure.

In Chapter 2, we present how certain functions can explicitly solve nonlinear fluid equations, in which the nonlinearity stems from the material derivative only. We first characterize flows that generate a vanishing or gradient nonlinear advection operator. This allows us to simplify and reduce nonlinear fluid models to linear equations. Due to that, the corresponding explicit solutions of the full nonlinear problem inherit certain linear behavior. We analyze the influence of such functions on the nonlinear advection operator and further properties in detail, in particular possible superposition.

Afterwards, we use these flows in non-rotating Euler and Navier–Stokes equations with arbitrary dimensions $n \geq 2$, and then in the Boussinesq equations as a geophysical rotating fluid model as well, in order to analyze the occurrence and sets of such explicit solutions, as well as possible superposition. In the latter model we also characterize the determined explicit solutions as some known classes of flows. Then we show how the presented functions can be applied to a more general fluid model with adapted forcing. In the end, we compare the discovered explicit solutions with already known solutions and classify them.

The contents of this chapter, except for the detailed proofs and stating the results in theorems, as well as further explanations, some differing notations, minor corrections, the overall structure itself and the corresponding Appendix A, have been published in Prugger and Rademacher (2021).

In Chapter 3, we investigate two different geophysical fluid models with horizontal simplified backscatter and hyperdiffusion. The first part is about the rotating shallow

water equations, while in the second part the rotating Boussinesq equations are studied. We primarily study the occurrence and behavior of explicit solutions in those models and characterize them. In particular, we investigate in which cases steady and unboundedly growing explicit flows exist. Furthermore, we determine the stability of steady solutions, which also includes the unbounded growth of perturbations, which is caused by possible superposition with unboundedly growing explicit solutions. Since the steady solutions have a free amplitude scaling from their certain linear behavior, we also study their stability in the limit of small and large amplitude. In the Boussinesq equations with backscatter similar classes of flows occur as in the usual viscous models, but with different properties and conditions for the existence, which we also analyze in detail.

The contents of this chapter, except for some differing notations and minor changes, have been published in Prugger et al. (2022a).

In Chapter 4, we again consider the rotating shallow water equations with horizontal backscatter and hyperdiffusion, but augmented with additional bottom drag terms. Such friction terms have a stabilizing effect on solutions and varying the parameters can change the stability of the trivial steady flow, so that nontrivial solutions bifurcate. After clarifying the setting in the beginning of this chapter, we continue with spectrum and stability analysis of the trivial flow. We in particular determine the critical value of the bottom drag parameter, when the trivial flow changes stability, as well as the spectral picture and the critical eigenvalues.

It turns out, that in the anisotropic case the critical eigenvalues are real, while in the isotropic case they are real and purely imaginary at the same time, indicating the simultaneous bifurcation of steady and temporal oscillating flows. Based on the results of the linear analysis, we then investigate the bifurcations of nontrivial solutions, that can be classified as so-called *Rossby waves* and *inertia-gravity waves*, which are well-known phenomena in the research of geophysical flows. We study the bifurcation of both wave types separately by the Lyapunov–Schmidt reduction (Stakgold, 1971; Schneider and Uecker, 2017).

Afterwards, the occurrence and behavior of explicit solutions in such a model are examined, in particular steady and unboundedly growing solutions, and we relate them with the bifurcation results before. The existence of particularly unboundedly growing explicit flows in this model means, that stabilizing bottom drag cannot prevent such undesired solutions completely. In the end of this chapter we present some numerical results of the bifurcations in this model.

The contents of this chapter and of the corresponding Appendix B, C, D, except for minor changes and the consideration of the parameter A_0 together with in this regard additional investigations, have been submitted for publication (Prugger et al., 2022b).

In Chapter 5, we give an outlook about further ideas for research topics, which are connected with the investigations and results presented in this thesis.

In Appendices we move some technical proofs in order to improve the readability in Chapter 2 and Chapter 4.

For the numerical computations and plots we have used MATLAB. The computations for the bifurcating branches in Chapter 4 were done with the MATLAB package *pde2path* (Uecker et al., 2014; Uecker, 2022). Some results in Chapter 2 have been checked with Wolfram Alpha. The sketches in Chapter 1 and Chapter 5 have been made with Inkscape.

The author of this thesis, Artur Prugger, contributed to the here presented analyses under the supervision of Jens D. M. Rademacher, except for the numerical computations for some spectra and the bifurcations, which are contributed by Jens D. M. Rademacher, as well as some figures in Chapter 4, which are contributed by Jichen Yang.

2. Explicit Solutions in Fluid Models

Finding analytical solutions to nonlinear problems is particularly challenging, since general methods are missing and for each problem one has to find a different way to solve it. Eulerian fluid models possess a nonlinear operator, which has different names, e.g. material derivative, advective derivative, convective derivative or hydrodynamic derivative. It stems from the transformation of the problem from the Lagrangian to the Eulerian point of view, as shown in Section 1.2.2. The material derivative consists of a nonlinear term (advection term) created by the scalar product of the flow and the gradient of the considered fluid quantity, see (1.3). With functions in certain plane wave forms we can use this special nonlinear structure in order to create gradient or vanishing nonlinear advection terms. In this way we are able to reduce a system of nonlinear equations to a linear problem, which we can solve and analyze. Additionally, the fact that solutions of the remaining linear equations also solve the full nonlinear equations, leads to certain superposition and a certain linear subspace of explicit solutions. This is in general unusual for nonlinear equations, but also known in fluid models. Such linear behaviors and properties of explicit solutions are very useful for further analysis.

In Section 2.1 we present such functions, their influence on the nonlinear advection term and further properties. Afterwards, we show in Section 2.2 how one can use these functions in order to explicitly solve different nonlinear fluid problems, here the Euler and Navier–Stokes equations with arbitrary dimensions $n \geq 2$. In Section 2.3 we extend the investigation to a geophysical fluid model, namely the rotating Boussinesq equations. In both sections we compare and analyze the explicit solutions, especially possible superposition of such explicit flows. As a preparation for the following chapters about fluid models with backscatter, which act as forcing terms in the corresponding equations, we shortly show in Section 2.4 how a more general adapted forcing can be treated with the functions studied in this chapter. In the end of this chapter, in Section 2.5, we discuss the presented explicit solutions and classify them among already known solutions used in different works.[1]

2.1. Advection operator and certain plane wave flows

We consider a velocity field $\boldsymbol{v} = \boldsymbol{v}(t, \boldsymbol{x}) \in \mathbb{R}^n$ of the fluid on the space $\boldsymbol{x} \in \mathbb{R}^n$ with $n \geq 2$ and at time $t \geq 0$. Usually, the flows are represented in a two- or three-dimensional space, but in this section we keep it more general and provide solutions and results in higher space dimensions as well. For any quantity $\boldsymbol{\zeta} = \boldsymbol{\zeta}(t, \boldsymbol{x}) \in \mathbb{R}^m$ transported by the fluid

[1] The main results presented in this chapter have been published in Prugger and Rademacher (2021).

(as e.g. the density, temperature, salinity or the velocity field $\boldsymbol{v}$ itself) with $m \geq 1$, the material derivative of $\boldsymbol{\zeta}$ is defined by

$$\frac{\mathrm{D}\boldsymbol{\zeta}}{\mathrm{D}t} := \frac{\partial \boldsymbol{\zeta}}{\partial t} + (\boldsymbol{v} \cdot \nabla)\boldsymbol{\zeta}\,.$$

The advection operator $(\boldsymbol{v} \cdot \nabla)$ is meant to act on each component of $\boldsymbol{\zeta}$. This means, the values of the nonlinear advection term from the material derivative are also m-dimensional and each of its component $1 \leq j \leq m$ is defined by $\big((\boldsymbol{v} \cdot \nabla)\boldsymbol{\zeta}\big)_j := \boldsymbol{v} \cdot \nabla \zeta_j$.

For our purpose of finding explicit solutions in this chapter we are in particular interested in functions, for which the nonlinear term of the material derivative vanishes. This has the advantage of reducing a system of nonlinear equations to a system of linear equations, which are simpler to handle. In order to create a vanishing nonlinear advection term, a simple general idea is to make the gradient of each component of $\boldsymbol{\zeta}$ orthogonal to the velocity $\boldsymbol{v}$. This means for all $\boldsymbol{x} \in \mathbb{R}^n$, $t \geq 0$ and $1 \leq j \leq m$

$$\boldsymbol{v}(t, \boldsymbol{x}) \cdot \nabla \zeta_j(t, \boldsymbol{x}) = 0\,.$$

It is well known, that this is satisfied for certain pure plane waves or traveling waves. In the following lemma we classify such wave-like functions, which are fundamental for a large part of this work.

Lemma 2.1. *Let $\boldsymbol{\zeta} : \mathbb{R}_{\geq 0} \times \mathbb{R}^n \to \mathbb{R}^m$ be of the traveling wave form*

$$\boldsymbol{\zeta}(t, \boldsymbol{x}) = \boldsymbol{\phi}(t, \boldsymbol{k} \cdot \boldsymbol{x} + \omega t)\,, \tag{2.1}$$

for any $m \geq 1$, $n \geq 2$, wave shape $\boldsymbol{\phi} \in C^1(\mathbb{R}_{\geq 0} \times \mathbb{R}, \mathbb{R}^m)$, wave vector $\boldsymbol{k} \in \mathbb{R}^n$ and temporal frequency $\omega \in \mathbb{R}$, and the velocity field $\boldsymbol{v} : \mathbb{R}_{\geq 0} \times \mathbb{R}^n \to \mathbb{R}^n$ of the form

$$\boldsymbol{v}(t, \boldsymbol{x}) = \psi(t, \boldsymbol{x})\boldsymbol{a} + \boldsymbol{c}\,, \tag{2.2}$$

for any flow shape $\psi \in C(\mathbb{R}_{\geq 0} \times \mathbb{R}^n, \mathbb{R})$, constant flow direction $\boldsymbol{a} \in \mathbb{R}^n$ and constant drift $\boldsymbol{c} \in \mathbb{R}^n$. If wave vector $\boldsymbol{k}$ and flow direction $\boldsymbol{a}$ satisfy the orthogonality condition $\boldsymbol{a} \cdot \boldsymbol{k} = 0$, then the nonlinear advection operator becomes

$$(\boldsymbol{v} \cdot \nabla)\boldsymbol{\zeta} = (\boldsymbol{c} \cdot \boldsymbol{k})\frac{\partial \boldsymbol{\phi}}{\partial \xi}\,, \tag{2.3}$$

where ξ denotes the second variable of $\boldsymbol{\phi}$.

Proof. The advection operator $(\boldsymbol{v} \cdot \nabla)\boldsymbol{\zeta}$ maps to an m-dimensional vector field. We consider its j-th component, with arbitrary $1 \leq j \leq m$. Using the definition of the advection operator, as well as (2.1) and (2.2), it follows

$$\big((\boldsymbol{v}\cdot\nabla)\boldsymbol{\zeta}\big)_j = \boldsymbol{v}\cdot(\nabla\zeta_j) = (\psi\boldsymbol{a}+\boldsymbol{c})\cdot\frac{\partial\phi_j}{\partial\xi}\boldsymbol{k} = (\boldsymbol{a}\cdot\boldsymbol{k})\psi\frac{\partial\phi_j}{\partial\xi} + (\boldsymbol{c}\cdot\boldsymbol{k})\frac{\partial\phi_j}{\partial\xi}\,.$$

Due to the orthogonality $\boldsymbol{a}\cdot\boldsymbol{k}=0$, the first term on the right-hand side vanishes and the remaining term is precisely the j-th component of (2.3). Since j was arbitrary, it holds for all $1\leq j\leq m$, which proves the full statement (2.3). □

The statement in Lemma 2.1 can be generalized by replacing the linear time-dependent phase shift ωt in (2.1) with a more general and nonlinear form $\omega(t)$. Since we will (and can) use only the linear form ωt in the following sections, we formulate the statements with this phase shift.

Furthermore, in this work we will mostly consider a velocity field without a constant drift $\boldsymbol{c}$. Some fluid equations do not allow velocity fields with such a constant drift, in particular those with a Coriolis term, and some fluid equations have a so-called Galileian invariance, which allows us to restrict to $\boldsymbol{c}=0$. Additionally, we are in particular interested in functions, which cause a vanishing nonlinear advection term $(\boldsymbol{v}\cdot\nabla)\boldsymbol{\zeta}\equiv 0$, since they allow us to find certain linear sets of explicit solutions of various fluid equations.

Usually, in presence of nonlinear terms in the equations, superposition of functions are coupled nonlinearly due to these terms. A very important property of the functions in Lemma 2.1 is the possibility of certain superpositions, which still keeps the nonlinear advection term in the form (2.3). This provides the possibility to decouple such superposed functions in fluid equations, even in presence of the nonlinear advection operator. This means, we obtain a linear behavior of such superposed functions in nonlinear equations, so that each function in the superposition has to solve the remaining linear equations on its own. With this we are able to form certain linear spaces of explicit solutions of the full nonlinear equations. We formulate such a superposition and the corresponding nonlinear advection term in the following theorem.

Theorem 2.2. *Let $\boldsymbol{\zeta}:\mathbb{R}_{\geq 0}\times\mathbb{R}^n\to\mathbb{R}^m$ be of the superposed traveling wave form*

$$\boldsymbol{\zeta}(t,\boldsymbol{x}) = \sum_{j=1}^{M}\boldsymbol{\phi}_j(t,\boldsymbol{k}_j\cdot\boldsymbol{x}+\omega_j t)\,, \tag{2.4}$$

with $m,M\geq 1$, $n\geq 2$, wave shapes $\boldsymbol{\phi}_j\in C^1(\mathbb{R}_{\geq 0}\times\mathbb{R},\mathbb{R}^m)$, wave vectors $\boldsymbol{k}_j\in\mathbb{R}^n$ and temporal frequencies $\omega_j\in\mathbb{R}$ for any $1\leq j\leq M$. Furthermore, let the velocity field $\boldsymbol{v}:\mathbb{R}_{\geq 0}\times\mathbb{R}^n\to\mathbb{R}^n$ be of the superposed form

$$\boldsymbol{v}(t,\boldsymbol{x}) = \sum_{j=1}^{N}\psi_j(t,\boldsymbol{x})\boldsymbol{a}_j+\boldsymbol{c}\,, \tag{2.5}$$

with $1\leq N<n$, constant drift $\boldsymbol{c}\in\mathbb{R}^n$, flow shapes $\psi_j\in C(\mathbb{R}_{\geq 0}\times\mathbb{R}^n,\mathbb{R})$ and constant, as well as linearly independent flow directions $\boldsymbol{a}_j\in\mathbb{R}^n$ for any $1\leq j\leq N$. If each flow

direction $\boldsymbol{a}_j$ *is orthogonal to every wave vector* $\boldsymbol{k}_\ell$*, i.e.* $\boldsymbol{a}_j \cdot \boldsymbol{k}_\ell = 0$ *for all* $1 \leq j \leq N$ *and* $1 \leq \ell \leq M$*, then the nonlinear advection operator becomes*

$$(\boldsymbol{v} \cdot \nabla)\boldsymbol{\zeta} = \sum_{\ell=1}^{M} (\boldsymbol{c} \cdot \boldsymbol{k}_\ell) \frac{\partial \boldsymbol{\phi}_\ell}{\partial \xi}\,, \tag{2.6}$$

where ξ *refers to the phase variables of each* $\boldsymbol{\phi}_\ell$*, respectively.*

Proof. We use the linearity of the gradient operator and the bilinearity of the scalar product, as well as the forms (2.4) and (2.5), in order to rewrite the advection operator

$$\begin{aligned}(\boldsymbol{v} \cdot \nabla)\boldsymbol{\zeta} &= (\boldsymbol{v} \cdot \nabla)\left(\sum_{\ell=1}^{M} \boldsymbol{\phi}_\ell\right) = \sum_{\ell=1}^{M} (\boldsymbol{v} \cdot \nabla)\boldsymbol{\phi}_\ell = \sum_{\ell=1}^{M} \left(\left(\sum_{j=1}^{N} \psi_j \boldsymbol{a}_j + \boldsymbol{c}\right) \cdot \nabla\right) \boldsymbol{\phi}_\ell \\ &= \sum_{\ell=1}^{M} \left(\sum_{j=1}^{N} (\psi_j \boldsymbol{a}_j \cdot \nabla)\boldsymbol{\phi}_\ell + (\boldsymbol{c} \cdot \nabla)\boldsymbol{\phi}_\ell\right)\,.\end{aligned}$$

Since any $\psi_j \boldsymbol{a}_j$ is of the form (2.2) and any $\boldsymbol{\phi}_\ell$ of the form (2.1), with each flow direction $\boldsymbol{a}_j$ being orthogonal to every wave vector $\boldsymbol{k}_\ell$, we can use Lemma 2.1 for every $1 \leq j \leq N$ and $1 \leq \ell \leq M$ and obtain

$$(\boldsymbol{v} \cdot \nabla)\boldsymbol{\zeta} = \sum_{\ell=1}^{M} \left(\sum_{j=1}^{N} (\psi_j \boldsymbol{a}_j \cdot \nabla)\boldsymbol{\phi}_\ell + (\boldsymbol{c} \cdot \nabla)\boldsymbol{\phi}_\ell\right) = \sum_{\ell=1}^{M} (\boldsymbol{c} \cdot \boldsymbol{k}_\ell) \frac{\partial \boldsymbol{\phi}_\ell}{\partial \xi}\,.$$

□

The most important quantity that we use for $\boldsymbol{\zeta}$ is the velocity $\boldsymbol{v}$ itself, since it appears in the momentum equations of every fluid model that we consider in this work. So in order to get $(\boldsymbol{v} \cdot \nabla)\boldsymbol{v} \equiv 0$ the velocity $\boldsymbol{v}$ must not only have the form (2.2), but also the form (2.1). This in particular means, that the velocity is also of a traveling wave form with a wave vector orthogonal to its own flow direction. Due to its importance here, we formulate the following theorem for such flows together with the possible superpositions.

Theorem 2.3. *Let the velocity field* $\boldsymbol{v} : \mathbb{R}_{\geq 0} \times \mathbb{R}^n \to \mathbb{R}^n$ *be of the superposed traveling wave form*

$$\boldsymbol{v}(t, \boldsymbol{x}) = \sum_{j=1}^{N} \left(\sum_{\ell=1}^{M_j} \psi_{j,\ell}(t, \boldsymbol{k}_{j,\ell} \cdot \boldsymbol{x} + \omega_{j,\ell} t)\right) \boldsymbol{a}_j + \boldsymbol{c}\,, \tag{2.7}$$

with $n \geq 2$*,* $1 \leq N < n$*, constant drift* $\boldsymbol{c} \in \mathbb{R}^n$ *and* $M_j \geq 1$*, constant and linearly independent flow directions* $\boldsymbol{a}_j \in \mathbb{R}^n$*, wave shapes* $\psi_{j,\ell} \in C^1(\mathbb{R}_{\geq 0} \times \mathbb{R}, \mathbb{R})$*, wave vectors* $\boldsymbol{k}_{j,\ell} \in \mathbb{R}^n$*, temporal frequencies* $\omega_{j,\ell} \in \mathbb{R}$ *for all* $1 \leq \ell \leq M_j$ *and* $1 \leq j \leq N$*. If the wave*

vectors and flow directions satisfy the orthogonality condition

$$\boldsymbol{a}_j \cdot \boldsymbol{k}_{\ell,m} = 0 \qquad \text{for all} \quad 1 \le m \le M_\ell \quad \text{and} \quad 1 \le j,\, \ell \le N\,, \tag{2.8}$$

then the nonlinear advection operator becomes

$$(\boldsymbol{v}\cdot\nabla)\boldsymbol{v} = \sum_{j=1}^{N}\sum_{\ell=1}^{M_j}(\boldsymbol{c}\cdot\boldsymbol{k}_{j,\ell})\frac{\partial\psi_{j,\ell}}{\partial\xi}\boldsymbol{a}_j\,, \tag{2.9}$$

where ξ denotes the second variable of each of $\psi_{j,\ell}$, respectively.

Proof. The velocity field (2.7) has the form (2.5) and that of $\boldsymbol{\zeta}$ in (2.4), with $\boldsymbol{\phi}_{j,\ell} = \psi_{j,\ell}\boldsymbol{a}_j$ for all $1 \le \ell \le M_j$ and $1 \le j \le N$ and an additional $\boldsymbol{\phi}_0 \equiv \boldsymbol{c}$. Since the conditions in Theorem 2.2 are satisfied as well, in particular the orthogonality condition, it follows from Theorem 2.2

$$(\boldsymbol{v}\cdot\nabla)\boldsymbol{v} = \sum_{j=1}^{N}\sum_{\ell=1}^{M_j}(\boldsymbol{c}\cdot\boldsymbol{k}_{j,\ell})\frac{\partial\boldsymbol{\phi}_{j,\ell}}{\partial\xi} = \sum_{j=1}^{N}\sum_{\ell=1}^{M_j}(\boldsymbol{c}\cdot\boldsymbol{k}_{j,\ell})\frac{\partial\psi_{j,\ell}}{\partial\xi}\boldsymbol{a}_j\,.$$

□

A very important property of such flows is the incompressibility, which is an frequently posed condition in fluid models, also in this work. This additionally underlines the suitability of the consideration of such flows. We show the incompressibility for the single wave velocity first and afterwards formulate it for the velocity field from Theorem 2.3.

Lemma 2.4. *Let the velocity field $\boldsymbol{v} : \mathbb{R}_{\ge 0} \times \mathbb{R}^n \to \mathbb{R}^n$ be of the traveling wave form*

$$\boldsymbol{v}(t,\boldsymbol{x}) = \psi(t, \boldsymbol{k}\cdot\boldsymbol{x} + \omega t)\boldsymbol{a}\,, \tag{2.10}$$

with $n \ge 2$, arbitrary wave shape $\psi \in C^1(\mathbb{R}_{\ge 0}\times\mathbb{R},\mathbb{R})$, wave vector $\boldsymbol{k} \in \mathbb{R}^n$, constant flow direction $\boldsymbol{a} \in \mathbb{R}^n$ and temporal frequency $\omega \in \mathbb{R}$. If wave vector $\boldsymbol{k}$ and flow direction $\boldsymbol{a}$ are orthogonal, then $\boldsymbol{v}$ is divergence-free:

$$\operatorname{div}\boldsymbol{v} := \nabla\cdot\boldsymbol{v} = \sum_{j=1}^{n}\frac{\partial v_j}{\partial x_j} \equiv 0\,. \tag{2.11}$$

Proof. By inserting the definition of $\boldsymbol{v}$ it follows directly

$$\operatorname{div}\boldsymbol{v} = \sum_{j=1}^{n}\frac{\partial v_j}{\partial x_j} = \sum_{j=1}^{n}\frac{\partial\psi}{\partial x_j}a_j = \sum_{j=1}^{n}k_j a_j\frac{\partial\psi}{\partial\xi} = (\boldsymbol{k}\cdot\boldsymbol{a})\frac{\partial\psi}{\partial\xi} \equiv 0\,,$$

since $\boldsymbol{k}\cdot\boldsymbol{a} = 0$, where ξ denotes the second variable of ψ. □

Theorem 2.5. *The flow (2.7) defined in Theorem 2.3 is divergence-free.*

Proof. It follows directly from the linearity of the divergence operator $\operatorname{div} \boldsymbol{v}$ in $\boldsymbol{v}$ and Lemma 2.4. □

For the material derivative of the velocity field $\boldsymbol{v}$ there is also another way to remove the corresponding nonlinear term and reduce the problem to a system of linear equations. Such material derivatives of $\boldsymbol{v}$ always appear in the momentum equations, which often contain the pressure gradient as well. The idea is to define the velocity $\boldsymbol{v}$ in such a way, that the resulting nonlinear advection term is a gradient and can be fully compensated by the pressure gradient, since the pressure is often not specified elsewhere. We start with a more intuitive flow for this purpose in the following theorem.

Theorem 2.6. *Let the velocity field $\boldsymbol{v} : \mathbb{R}_{\geq 0} \times \mathbb{R}^n \to \mathbb{R}^n$ be of the traveling wave form*

$$\boldsymbol{v}(t, \boldsymbol{x}) = \sum_{j=1}^{N} \psi_j(t, \boldsymbol{k}_j \cdot \boldsymbol{x} + \omega_j t)\boldsymbol{k}_j + \boldsymbol{c}\,, \tag{2.12}$$

with $n \geq 2$, $N \geq 1$ and arbitrary wave shapes $\psi_j \in C^1(\mathbb{R}_{\geq 0} \times \mathbb{R}, \mathbb{R})$, wave vectors and constant flow directions $\boldsymbol{k}_j$, $\boldsymbol{c} \in \mathbb{R}^n$ and temporal frequencies $\omega_j \in \mathbb{R}$ for any $1 \leq j \leq N$. The nonlinear advection term from the material derivative of $\boldsymbol{v}$ then becomes

$$(\boldsymbol{v} \cdot \nabla)\boldsymbol{v} = \sum_{j=1}^{N} (\boldsymbol{c} \cdot \boldsymbol{k}_j) \frac{\partial \psi_j}{\partial \xi} \boldsymbol{k}_j + \nabla h\,, \tag{2.13}$$

where ξ denotes the second variable of each function ψ_j, respectively, and the function $h \in C^1(\mathbb{R}_{\geq 0} \times \mathbb{R}^n, \mathbb{R})$ is defined by

$$h(t, \boldsymbol{x}) = \frac{1}{2} \sum_{j=1}^{N} \sum_{\ell=1}^{N} (\boldsymbol{k}_j \cdot \boldsymbol{k}_\ell) \psi_j(t, \boldsymbol{k}_j \cdot \boldsymbol{x} + \omega_j t) \psi_\ell(t, \boldsymbol{k}_\ell \cdot \boldsymbol{x} + \omega_\ell t)\,. \tag{2.14}$$

Proof. If we insert $\boldsymbol{v}$ of the form (2.12) into $(\boldsymbol{v} \cdot \nabla)\boldsymbol{v}$ we get

$$\begin{aligned}
(\boldsymbol{v} \cdot \nabla)\boldsymbol{v} &= \left(\left(\sum_{j=1}^{N} \psi_j \boldsymbol{k}_j + \boldsymbol{c} \right) \cdot \nabla \right) \left(\sum_{\ell=1}^{N} \psi_\ell \boldsymbol{k}_\ell + \boldsymbol{c} \right) \\
&= (\boldsymbol{c} \cdot \nabla) \left(\sum_{\ell=1}^{N} \psi_\ell \boldsymbol{k}_\ell + \boldsymbol{c} \right) + \sum_{j=1}^{N} (\psi_j \boldsymbol{k}_j \cdot \nabla) \left(\sum_{\ell=1}^{N} \psi_\ell \boldsymbol{k}_\ell + \boldsymbol{c} \right) \\
&= \sum_{\ell=1}^{N} (\boldsymbol{c} \cdot \nabla) \psi_\ell \boldsymbol{k}_\ell + \sum_{j=1}^{N} \sum_{\ell=1}^{N} (\psi_j \boldsymbol{k}_j \cdot \nabla) \psi_\ell \boldsymbol{k}_\ell
\end{aligned}$$

$$= \sum_{\ell=1}^{N} (\boldsymbol{c} \cdot \boldsymbol{k}_\ell) \frac{\partial \psi_\ell}{\partial \xi} \boldsymbol{k}_\ell + \sum_{j=1}^{N} \sum_{\ell=1}^{N} (\psi_j \boldsymbol{k}_j \cdot \boldsymbol{k}_\ell) \frac{\partial \psi_\ell}{\partial \xi} \boldsymbol{k}_\ell$$

$$= \sum_{\ell=1}^{N} (\boldsymbol{c} \cdot \boldsymbol{k}_\ell) \frac{\partial \psi_\ell}{\partial \xi} \boldsymbol{k}_\ell + \sum_{j=1}^{N} \sum_{\ell=1}^{N} (\boldsymbol{k}_j \cdot \boldsymbol{k}_\ell) \psi_j \frac{\partial \psi_\ell}{\partial \xi} \boldsymbol{k}_\ell \,.$$

The first sum on the right-hand side is the same as the first sum in (2.13), but with index variable ℓ instead of j. The double sum on the right-hand side is exactly ∇h with h as in (2.14), since

$$\nabla h = \nabla \left(\frac{1}{2} \sum_{j=1}^{N} \sum_{\ell=1}^{N} (\boldsymbol{k}_j \cdot \boldsymbol{k}_\ell) \psi_j \psi_\ell \right) = \frac{1}{2} \sum_{j=1}^{N} \sum_{\ell=1}^{N} (\boldsymbol{k}_j \cdot \boldsymbol{k}_\ell) \nabla (\psi_j \psi_\ell)$$

$$= \frac{1}{2} \sum_{j=1}^{N} \sum_{\ell=1}^{N} (\boldsymbol{k}_j \cdot \boldsymbol{k}_\ell) (\psi_\ell \nabla \psi_j + \psi_j \nabla \psi_\ell)$$

$$= \frac{1}{2} \sum_{j=1}^{N} \sum_{\ell=1}^{N} (\boldsymbol{k}_j \cdot \boldsymbol{k}_\ell) \left(\psi_\ell \frac{\partial \psi_j}{\partial \xi} \boldsymbol{k}_j + \psi_j \frac{\partial \psi_\ell}{\partial \xi} \boldsymbol{k}_\ell \right)$$

$$= \frac{1}{2} \sum_{j=1}^{N} \sum_{\ell=1}^{N} (\boldsymbol{k}_j \cdot \boldsymbol{k}_\ell) \psi_\ell \frac{\partial \psi_j}{\partial \xi} \boldsymbol{k}_j + \frac{1}{2} \sum_{j=1}^{N} \sum_{\ell=1}^{N} (\boldsymbol{k}_j \cdot \boldsymbol{k}_\ell) \psi_j \frac{\partial \psi_\ell}{\partial \xi} \boldsymbol{k}_\ell$$

$$= \frac{1}{2} \sum_{j=1}^{N} \sum_{\ell=1}^{N} (\boldsymbol{k}_j \cdot \boldsymbol{k}_\ell) \psi_j \frac{\partial \psi_\ell}{\partial \xi} \boldsymbol{k}_\ell + \frac{1}{2} \sum_{j=1}^{N} \sum_{\ell=1}^{N} (\boldsymbol{k}_j \cdot \boldsymbol{k}_\ell) \psi_j \frac{\partial \psi_\ell}{\partial \xi} \boldsymbol{k}_\ell$$

$$= \sum_{j=1}^{N} \sum_{\ell=1}^{N} (\boldsymbol{k}_j \cdot \boldsymbol{k}_\ell) \psi_j \frac{\partial \psi_\ell}{\partial \xi} \boldsymbol{k}_\ell \,.$$

Thus, we get (2.13) with (2.14). □

Unlike the flow in Theorem 2.3, where the wave vector of each wave is orthogonal to its own and others flow directions, the waves of the flow in Theorem 2.6 have wave vectors, which are the same as their own flow directions. Due to this missing orthogonality, the waves are interacting with each other by the advection term $(\boldsymbol{v} \cdot \nabla)\boldsymbol{v}$ and due to their traveling wave structure they create a gradient nonlinear term ∇h of the form (2.14). The momentum equations can be reduced to systems of linear equations with such flows, since the pressure gradient can compensate the remaining nonlinear and gradient term ∇h. However, the problem of this kind of flows is, that they are not incompressible.

Since we focus on incompressible fluid models, we cannot consider these flows, but they may be of interest for other fluid models, like those for compressible flow. Nevertheless, there is another type of such superposed flows, which uses a similar idea of producing gradient nonlinear terms and is incompressible at the same time. In order to simplify the proofs for the upcoming results regarding these kind of flows, we first show in the

following lemma the behavior of the material derivative when splitting the velocity field in different orthogonal linear subspaces.

Lemma 2.7. *Let the space $\mathbb{R}^n$ with dimension $n \geq 2$ be split into the Cartesian product $\mathbb{R}^n = S_1 \times \ldots \times S_N$, with $N \leq n$ and linear subspaces $S_j \subseteq \mathbb{R}^n$ for all $1 \leq j \leq N$, which are mutually orthogonal, i.e. $S_j \perp S_\ell$ for all $1 \leq j, \ell \leq N$, $j \neq \ell$. Furthermore, let the velocity $\boldsymbol{v}$ be divided into $\boldsymbol{v} = \sum_{j=1}^{N} \boldsymbol{v}_j$, with $\boldsymbol{v}_j(\boldsymbol{x}) \in S_j$ and $\boldsymbol{v}_j(\boldsymbol{x}) = \boldsymbol{v}_j(\boldsymbol{x}_j)$ for all $\boldsymbol{x} \in \mathbb{R}^n$ and any $1 \leq j \leq N$, where $\boldsymbol{x}_j \in S_j$ is the projection of $\boldsymbol{x}$ onto S_j. Then the material derivative of the velocity $\boldsymbol{v}$ can be split into*

$$(\boldsymbol{v} \cdot \nabla)\boldsymbol{v} = \sum_{j=1}^{N} (\boldsymbol{v}_j \cdot \nabla)\boldsymbol{v}_j \,. \tag{2.15}$$

Proof. Since for any $1 \leq j \leq N$ the velocity term $\boldsymbol{v}_j$ depends only on the direction $\boldsymbol{x}_j \in S_j$, it follows $\nabla(\boldsymbol{v}_j)_m \in S_j$ for each component $1 \leq m \leq n$. Due to $\boldsymbol{v}_\ell(\boldsymbol{x}) \in S_\ell$ for all $\boldsymbol{x} \in \mathbb{R}^n$ and the orthogonality $S_\ell \perp S_j$ for any $1 \leq j, \ell \leq N$ and $j \neq \ell$ we then obtain

$$(\boldsymbol{v} \cdot \nabla)\boldsymbol{v} = \sum_{\ell=1}^{N} (\boldsymbol{v}_\ell \cdot \nabla)\boldsymbol{v} = \sum_{j=1}^{N} \sum_{\ell=1}^{N} (\boldsymbol{v}_\ell \cdot \nabla)\boldsymbol{v}_j = \sum_{j=1}^{N} (\boldsymbol{v}_j \cdot \nabla)\boldsymbol{v}_j \,.$$

□

This lemma shows, that if we split the velocity field $\boldsymbol{v}$ into parts, which lie in different orthogonal linear subspaces, then the material derivative of $\boldsymbol{v}$ can be split into a sum of material derivatives of each velocity part. This gives us the opportunity to split the considered fluid equations into these linear subspaces, which do not affect each other, if there are no further terms coupling the different linear subspaces.

In general, the flows in Theorem 2.3 do not belong to those of Lemma 2.7, since all waves with different flow directions $\boldsymbol{a}_j$ can have wave vectors that are linearly dependent. Thus, the linear subspaces which are build from the wave vectors and flow directions of the waves are in general not orthogonal to each other.

However, the flows we present now do belong to such splitting as in Lemma 2.7 and we will see, that they are different from those in Theorem 2.3. In order to simplify the derivation of these flows, we first show a simple version of them as a superposition of two waves in the following lemma and generalize them for arbitrary number of superpositions afterwards.

Lemma 2.8. *For $n \geq 2$, let the velocity field $\boldsymbol{v} : \mathbb{R}_{\geq 0} \times \mathbb{R}^n \to \mathbb{R}^n$ be of the traveling wave form*

$$\boldsymbol{v}(t, \boldsymbol{x}) = A_1(t) \sin(\boldsymbol{k}_1 \cdot \boldsymbol{x} + \omega_1 t)\boldsymbol{a}_1 + A_2(t) \sin(\boldsymbol{k}_2 \cdot \boldsymbol{x} + \omega_2 t)\boldsymbol{a}_2 + \boldsymbol{c} \,, \tag{2.16}$$

with time-dependent amplitude factors $A_1, A_2 \in C^1(\mathbb{R}_{\geq 0}, \mathbb{R})$*, linearly independent wave vectors* $\boldsymbol{k}_1, \boldsymbol{k}_2 \in \mathbb{R}^n$*, temporal frequencies* $\omega_1, \omega_2 \in \mathbb{R}$ *and constant flow directions* $\boldsymbol{a}_1, \boldsymbol{a}_2 \in \operatorname{span}\{\boldsymbol{k}_1, \boldsymbol{k}_2\} \subseteq \mathbb{R}^n$ *as well as* $\boldsymbol{c} \in \mathbb{R}^n$*. Furthermore, we presume that the wave vectors have the same length* $|\boldsymbol{k}_1| = |\boldsymbol{k}_2| = \mu > 0$ *and the flow directions are unit vectors and orthogonal to the wave vector of their own wave, i.e.* $|\boldsymbol{a}_1| = |\boldsymbol{a}_2| = 1$ *as well as* $\boldsymbol{a}_1 \cdot \boldsymbol{k}_1 = 0$ *and* $\boldsymbol{a}_2 \cdot \boldsymbol{k}_2 = 0$*. Under these conditions, the nonlinear advection term becomes*

$$(\boldsymbol{v} \cdot \nabla)\boldsymbol{v} = (\boldsymbol{c} \cdot \nabla)\boldsymbol{v} + \nabla h\,, \tag{2.17}$$

where $h \in C^1(\mathbb{R}_{\geq 0} \times \mathbb{R}^n, \mathbb{R})$ *is defined by*

$$h(t, \boldsymbol{x}) := \delta_{1,2} A_1(t) A_2(t) \left(\cos(\xi_1)\cos(\xi_2) + \frac{\boldsymbol{k}_1 \cdot \boldsymbol{k}_2}{\mu^2} \sin(\xi_1)\sin(\xi_2) \right), \tag{2.18}$$

with phase variables $\xi_1 := \boldsymbol{k}_1 \cdot \boldsymbol{x} + \omega_1 t$*,* $\xi_2 := \boldsymbol{k}_2 \cdot \boldsymbol{x} + \omega_2 t$ *and the additional factor* $\delta_{1,2} := -\operatorname{sgn}(\boldsymbol{a}_1 \cdot \boldsymbol{k}_2)\operatorname{sgn}(\boldsymbol{a}_2 \cdot \boldsymbol{k}_1)$*.*

Proof. Inserting $\boldsymbol{v}$ of the form (2.16) into $(\boldsymbol{v} \cdot \nabla)\boldsymbol{v}$ yields

$$\begin{aligned}
(\boldsymbol{v} \cdot \nabla)\boldsymbol{v} &= (\boldsymbol{c} \cdot \nabla)\boldsymbol{v} + (A_1 \sin(\xi_1)\boldsymbol{a}_1 \cdot \nabla)\boldsymbol{v} + (A_2 \sin(\xi_2)\boldsymbol{a}_2 \cdot \nabla)\boldsymbol{v} \\
&= (\boldsymbol{c} \cdot \nabla)\boldsymbol{v} + A_1^2 \sin(\xi_1)\cos(\xi_1) \underbrace{(\boldsymbol{a}_1 \cdot \boldsymbol{k}_1)}_{=0} \boldsymbol{a}_1 + A_1 A_2 \sin(\xi_1)\cos(\xi_2)(\boldsymbol{a}_1 \cdot \boldsymbol{k}_2)\boldsymbol{a}_2 \\
&\quad + A_1 A_2 \sin(\xi_2)\cos(\xi_1)(\boldsymbol{a}_2 \cdot \boldsymbol{k}_1)\boldsymbol{a}_1 + A_2^2 \sin(\xi_2)\cos(\xi_2) \underbrace{(\boldsymbol{a}_2 \cdot \boldsymbol{k}_2)}_{=0} \boldsymbol{a}_2 \\
&= (\boldsymbol{c} \cdot \nabla)\boldsymbol{v} + A_1 A_2 \Big(\sin(\xi_1)\cos(\xi_2)(\boldsymbol{a}_1 \cdot \boldsymbol{k}_2)\boldsymbol{a}_2 + \cos(\xi_1)\sin(\xi_2)(\boldsymbol{a}_2 \cdot \boldsymbol{k}_1)\boldsymbol{a}_1 \Big)\,.
\end{aligned}$$

The first term on the right-hand side is the same as the first term on the right-hand side of (2.17). It remains to show, that the remaining terms on the right-hand side are the same as ∇h:

$$\nabla h = A_1 A_2 \Big(\sin(\xi_1)\cos(\xi_2)(\boldsymbol{a}_1 \cdot \boldsymbol{k}_2)\boldsymbol{a}_2 + \cos(\xi_1)\sin(\xi_2)(\boldsymbol{a}_2 \cdot \boldsymbol{k}_1)\boldsymbol{a}_1 \Big)\,. \tag{2.19}$$

In order to prove (2.19), we first need two results regarding the vectors $\boldsymbol{a}_1$, $\boldsymbol{a}_2$, $\boldsymbol{k}_1$ and $\boldsymbol{k}_2$ with the given conditions as a preparation. Since all these four vectors are in the two-dimensional linear subspace $\operatorname{span}\{\boldsymbol{k}_1, \boldsymbol{k}_2\}$, and due to the orthogonalities $\boldsymbol{a}_1 \cdot \boldsymbol{k}_1 = 0$ and $\boldsymbol{a}_2 \cdot \boldsymbol{k}_2 = 0$, the pairs of vectors $\frac{1}{|\boldsymbol{k}_1|}\boldsymbol{k}_1$ and $\boldsymbol{a}_1$, as well as $\frac{1}{|\boldsymbol{k}_2|}\boldsymbol{k}_2$ and $\boldsymbol{a}_2$, form orthonormal basis of $\operatorname{span}\{\boldsymbol{k}_1, \boldsymbol{k}_2\}$. Thus, we can represent the vectors

$$\boldsymbol{k}_1 = \frac{\boldsymbol{k}_1 \cdot \boldsymbol{k}_2}{|\boldsymbol{k}_2|^2}\boldsymbol{k}_2 + (\boldsymbol{k}_1 \cdot \boldsymbol{a}_2)\boldsymbol{a}_2 \qquad \text{and} \qquad \boldsymbol{a}_1 = \frac{\boldsymbol{a}_1 \cdot \boldsymbol{k}_2}{|\boldsymbol{k}_2|^2}\boldsymbol{k}_2 + (\boldsymbol{a}_1 \cdot \boldsymbol{a}_2)\boldsymbol{a}_2\,, \tag{2.20a}$$

$$\boldsymbol{k}_2 = \frac{\boldsymbol{k}_2 \cdot \boldsymbol{k}_1}{|\boldsymbol{k}_1|^2}\boldsymbol{k}_1 + (\boldsymbol{k}_2 \cdot \boldsymbol{a}_1)\boldsymbol{a}_1 \qquad \text{and} \qquad \boldsymbol{a}_2 = \frac{\boldsymbol{a}_2 \cdot \boldsymbol{k}_1}{|\boldsymbol{k}_1|^2}\boldsymbol{k}_1 + (\boldsymbol{a}_2 \cdot \boldsymbol{a}_1)\boldsymbol{a}_1\,. \tag{2.20b}$$

This is the first result of the preparation we need. For the second one we use another description of the scalar product, namely $\boldsymbol{k}_1 \cdot \boldsymbol{k}_2 = |\boldsymbol{k}_1||\boldsymbol{k}_2| \cos(\sphericalangle(\boldsymbol{k}_1, \boldsymbol{k}_2))$, where $\sphericalangle(\boldsymbol{k}_1, \boldsymbol{k}_2)$ denotes the interior angle between the vectors $\boldsymbol{k}_1$ and $\boldsymbol{k}_2$. Since $\boldsymbol{a}_1$, $\boldsymbol{a}_2$, $\boldsymbol{k}_1$ and $\boldsymbol{k}_2$ are in the same two-dimensional linear subspace and due to the orthogonalities $\boldsymbol{a}_1 \perp \boldsymbol{k}_1$ and $\boldsymbol{a}_2 \perp \boldsymbol{k}_2$, it follows

$$\sphericalangle(\boldsymbol{a}_1, \boldsymbol{a}_2) = \sphericalangle(\boldsymbol{k}_1, \boldsymbol{k}_2) + \theta \,,$$

with $\theta \in \{-\pi, 0\}$. To be accurate, in case $\theta = -\pi$ the interior angle between $\boldsymbol{a}_1$ and $\boldsymbol{a}_2$ is positive by $\pi - \sphericalangle(\boldsymbol{k}_1, \boldsymbol{k}_2)$, but for simplicity we also use negative values of the angles, since both signs mean exactly the same for our purpose. With this, we obtain

$$\begin{aligned} \boldsymbol{a}_1 \cdot \boldsymbol{a}_2 = \cos(\sphericalangle(\boldsymbol{a}_1, \boldsymbol{a}_2)) &= \frac{|\boldsymbol{k}_1||\boldsymbol{k}_2| \cos(\sphericalangle(\boldsymbol{a}_1, \boldsymbol{a}_2))}{|\boldsymbol{k}_1||\boldsymbol{k}_2|} \\ &= \pm \frac{|\boldsymbol{k}_1||\boldsymbol{k}_2| \cos(\sphericalangle(\boldsymbol{k}_1, \boldsymbol{k}_2))}{|\boldsymbol{k}_1||\boldsymbol{k}_2|} = \pm \frac{\boldsymbol{k}_1 \cdot \boldsymbol{k}_2}{|\boldsymbol{k}_1||\boldsymbol{k}_2|} \,, \end{aligned}$$

where the upper case with "+" corresponds to $\theta = 0$ and the lower case with "−" to $\theta = -\pi$. Now we can use this, the orthogonality $\boldsymbol{a}_1 \perp \boldsymbol{k}_1$ as well as (2.20a) and obtain

$$\begin{aligned} 0 = \boldsymbol{k}_1 \cdot \boldsymbol{a}_1 &= \boldsymbol{k}_1 \cdot \left(\frac{\boldsymbol{a}_1 \cdot \boldsymbol{k}_2}{|\boldsymbol{k}_2|^2} \boldsymbol{k}_2 + (\boldsymbol{a}_1 \cdot \boldsymbol{a}_2) \boldsymbol{a}_2 \right) \\ &= \boldsymbol{a}_1 \cdot \boldsymbol{k}_2 \frac{\boldsymbol{k}_1 \cdot \boldsymbol{k}_2}{|\boldsymbol{k}_2|^2} + (\boldsymbol{k}_1 \cdot \boldsymbol{a}_2)(\boldsymbol{a}_1 \cdot \boldsymbol{a}_2) \\ &= \boldsymbol{a}_1 \cdot \boldsymbol{k}_2 \frac{\boldsymbol{k}_1 \cdot \boldsymbol{k}_2}{|\boldsymbol{k}_2|^2} \pm \boldsymbol{k}_1 \cdot \boldsymbol{a}_2 \frac{\boldsymbol{k}_1 \cdot \boldsymbol{k}_2}{|\boldsymbol{k}_1||\boldsymbol{k}_2|} \\ &= (\boldsymbol{a}_1 \cdot \boldsymbol{k}_2 \pm \boldsymbol{k}_1 \cdot \boldsymbol{a}_2) \frac{\boldsymbol{k}_1 \cdot \boldsymbol{k}_2}{\mu^2} \,, \end{aligned}$$

where the last equation follows from the condition $|\boldsymbol{k}_1| = |\boldsymbol{k}_2| = \mu$. Thus, for the case $\boldsymbol{k}_1 \cdot \boldsymbol{k}_2 \neq 0$, we obtain

$$\boldsymbol{a}_1 \cdot \boldsymbol{k}_2 = \mp \boldsymbol{a}_2 \cdot \boldsymbol{k}_1 \,. \tag{2.21}$$

For the case $\boldsymbol{k}_1 \cdot \boldsymbol{k}_2 = 0$ it follows from (2.20) that $\boldsymbol{k}_1 = \pm|\boldsymbol{k}_1|\boldsymbol{a}_2$ and $\boldsymbol{k}_2 = \pm|\boldsymbol{k}_2|\boldsymbol{a}_1$, since $\boldsymbol{a}_1$ and $\boldsymbol{a}_2$ are unit vectors. The signs of their factors are not in conjunction with θ here, but they always correspond to one of the two cases (2.21), since

$$|\boldsymbol{a}_1 \cdot \boldsymbol{k}_2| = |\pm|\boldsymbol{k}_2|\boldsymbol{a}_1 \cdot \boldsymbol{a}_1| = |\boldsymbol{k}_2| = \mu = |\boldsymbol{k}_1| = |\pm|\boldsymbol{k}_1|\boldsymbol{a}_2 \cdot \boldsymbol{a}_2| = |\boldsymbol{a}_2 \cdot \boldsymbol{k}_1| \,.$$

Thus, for both cases $\boldsymbol{k}_1 \cdot \boldsymbol{k}_2 \neq 0$ and $\boldsymbol{k}_1 \cdot \boldsymbol{k}_2 = 0$ we have always one of the two cases in (2.21).
Now, with (2.20) and (2.21), we have everything to prove (2.19). We just use the

conditions from the lemma as well as (2.20) and (2.21) and obtain

$$\begin{aligned}
\nabla h &\overset{(2.18)}{=} \delta_{1,2}A_1A_2\left(\nabla(\cos(\xi_1)\cos(\xi_2)) + \frac{\boldsymbol{k}_1\cdot\boldsymbol{k}_2}{\mu^2}\nabla(\sin(\xi_1)\sin(\xi_2))\right)\\
&= \delta_{1,2}A_1A_2\Big(-\sin(\xi_1)\cos(\xi_2)\boldsymbol{k}_1 - \cos(\xi_1)\sin(\xi_2)\boldsymbol{k}_2\\
&\qquad + \frac{\boldsymbol{k}_1\cdot\boldsymbol{k}_2}{\mu^2}(\cos(\xi_1)\sin(\xi_2)\boldsymbol{k}_1 + \sin(\xi_1)\cos(\xi_2)\boldsymbol{k}_2)\Big)\\
&\overset{(2.20)}{=} \delta_{1,2}A_1A_2\Big(-\sin(\xi_1)\cos(\xi_2)\frac{\boldsymbol{k}_1\cdot\boldsymbol{k}_2}{|\boldsymbol{k}_2|^2}\boldsymbol{k}_2 - \sin(\xi_1)\cos(\xi_2)(\boldsymbol{k}_1\cdot\boldsymbol{a}_2)\boldsymbol{a}_2\\
&\qquad - \cos(\xi_1)\sin(\xi_2)\frac{\boldsymbol{k}_2\cdot\boldsymbol{k}_1}{|\boldsymbol{k}_1|^2}\boldsymbol{k}_1 - \cos(\xi_1)\sin(\xi_2)(\boldsymbol{k}_2\cdot\boldsymbol{a}_1)\boldsymbol{a}_1\\
&\qquad + \frac{\boldsymbol{k}_1\cdot\boldsymbol{k}_2}{\mu^2}(\cos(\xi_1)\sin(\xi_2)\boldsymbol{k}_1 + \sin(\xi_1)\cos(\xi_2)\boldsymbol{k}_2)\Big)\\
&\overset{|\boldsymbol{k}_1|=|\boldsymbol{k}_2|=\mu}{=} -\delta_{1,2}A_1A_2\Big(\sin(\xi_1)\cos(\xi_2)(\boldsymbol{k}_1\cdot\boldsymbol{a}_2)\boldsymbol{a}_2 + \cos(\xi_1)\sin(\xi_2)(\boldsymbol{k}_2\cdot\boldsymbol{a}_1)\boldsymbol{a}_1\Big)\\
&\overset{(2.21)}{=} \pm\,\delta_{1,2}A_1A_2\Big(\sin(\xi_1)\cos(\xi_2)(\boldsymbol{a}_1\cdot\boldsymbol{k}_2)\boldsymbol{a}_2 + \cos(\xi_1)\sin(\xi_2)(\boldsymbol{a}_2\cdot\boldsymbol{k}_1)\boldsymbol{a}_1\Big)\,.
\end{aligned}$$

On the right-hand side of the last equation, the upper case with "+" corresponds to the case of $\boldsymbol{a}_1\cdot\boldsymbol{k}_2$ and $\boldsymbol{a}_2\cdot\boldsymbol{k}_1$ having different signs, while the lower case with "-" when they have the same sign. Due to the presumed linear independence of $\boldsymbol{k}_1$ and $\boldsymbol{k}_2$ in the statement of the lemma, we have $\boldsymbol{a}_1\cdot\boldsymbol{k}_2 \neq 0$ and $\boldsymbol{a}_2\cdot\boldsymbol{k}_1 \neq 0$, otherwise one would get $\boldsymbol{k}_2 = \pm\boldsymbol{k}_1$ by the orthogonalities with $\boldsymbol{a}_1$ and $\boldsymbol{a}_2$, which is a contradiction (one can also see it in (2.20)). This means we have for the upper case $+\delta_{1,2} = -\mathrm{sgn}(\boldsymbol{a}_1\cdot\boldsymbol{k}_2)\mathrm{sgn}(\boldsymbol{a}_2\cdot\boldsymbol{k}_1) = 1$ and the lower case $-\delta_{1,2} = \mathrm{sgn}(\boldsymbol{a}_1\cdot\boldsymbol{k}_2)\mathrm{sgn}(\boldsymbol{a}_2\cdot\boldsymbol{k}_1) = 1$. Thus, we get for both cases

$$\nabla h = A_1A_2\Big(\sin(\xi_1)\cos(\xi_2)(\boldsymbol{a}_1\cdot\boldsymbol{k}_2)\boldsymbol{a}_2 + \cos(\xi_1)\sin(\xi_2)(\boldsymbol{a}_2\cdot\boldsymbol{k}_1)\boldsymbol{a}_1\Big)\,,$$

which is exactly (2.19). □

In contrast to the flow in Theorem 2.3, the flow directions $\boldsymbol{a}_1, \boldsymbol{a}_2$ of the velocity (2.16) in Lemma 2.8 must be orthogonal to the wave vector of the corresponding plane wave only, and not to the wave vectors of the other waves. This results in nonlinear interactions between these waves by the advection operator, which can be described by the gradient term ∇h. However, compared with Theorem 2.3, the wave shapes of the velocity in Lemma 2.8 are not arbitrary but in sinusoidal form. Furthermore, the flow directions $\boldsymbol{a}_1, \boldsymbol{a}_2$ are restricted to the two-dimensional linear subspace of $\mathbb{R}^n$ spanned by the wave vectors $\boldsymbol{k}_1$ and $\boldsymbol{k}_2$.

Remark 2.8.1. One needs two different wave vectors $\boldsymbol{k}_1$ and $\boldsymbol{k}_2$ in Lemma 2.8 in order to span a two-dimensional linear subspace, where the flow directions $\boldsymbol{a}_1, \boldsymbol{a}_2$ also lie in. If we instead choose the wave vectors to be linearly dependent, so $\boldsymbol{k}_2 = s\boldsymbol{k}_1$ for any

$s \in \mathbb{R}$, with arbitrary but still orthogonal flow directions, then we technically get the same result as in Theorem 2.3 with vanishing nonlinear terms. The function h as in (2.18) is indeed zero in this case as well, since $\delta_{1,2} = 0$.

Remark 2.8.2. In Lemma 2.8 we restrict the wave vectors and flow directions to be in the same two-dimensional linear subspace of $\mathbb{R}^n$. The problem in considering the vectors in a three-dimensional (or higher) linear subspace lies in the issue of clear interplay between vectors in more than two dimensions, as described in (2.20) and (2.21), which are necessary for the proof of the lemma. It might be possible to prove Lemma 2.8 with a three- or higher-dimensional linear subspace in a similar or another way, but we omit such an analysis here.

Theorem 2.9. *For $n \geq 2$ and $1 \leq N \leq n/2$ let $S_j \subseteq \mathbb{R}^n$ be two-dimensional linear subspaces with $S_j \perp S_\ell$ for all $1 \leq j, \ell \leq N$, $j \neq \ell$. Consider the velocity field $\boldsymbol{v} : \mathbb{R}_{\geq 0} \times \mathbb{R}^n \to \mathbb{R}^n$ of the traveling wave form*

$$\boldsymbol{v}(t, \boldsymbol{x}) = \sum_{j=1}^{N} \sum_{\ell=1}^{M_j} A_{j,\ell}(t) \sin(\boldsymbol{k}_{j,\ell} \cdot \boldsymbol{x} + \omega_{j,\ell} t) \boldsymbol{a}_{j,\ell} + \boldsymbol{c}\,, \tag{2.22}$$

with $M_j \geq 1$ for any $1 \leq j \leq N$, time-dependent amplitude factors $A_{j,\ell} \in C^1(\mathbb{R}_{\geq 0}, \mathbb{R})$, temporal frequencies $\omega_{j,\ell} \in \mathbb{R}$, wave vectors and constant flow directions $\boldsymbol{k}_{j,\ell}, \boldsymbol{a}_{j,\ell} \in S_j$ for any $1 \leq \ell \leq M_j$, $1 \leq j \leq N$, as well as $\boldsymbol{c} \in \mathbb{R}^n$. Furthermore, we presume $|\boldsymbol{a}_{j,\ell}| = 1$ and $|\boldsymbol{k}_{j,\ell}| = \mu_j$ for $\mu_j > 0$, as well as $\boldsymbol{a}_{j,\ell} \cdot \boldsymbol{k}_{j,\ell} = 0$ for any $1 \leq \ell \leq M_j$, $1 \leq j \leq N$. Under these conditions, the nonlinear advection term becomes

$$(\boldsymbol{v} \cdot \nabla)\boldsymbol{v} = (\boldsymbol{c} \cdot \nabla)\boldsymbol{v} + \nabla h\,, \tag{2.23}$$

where $h \in C^1(\mathbb{R}_{\geq 0} \times \mathbb{R}^n, \mathbb{R})$ is defined by

$$\begin{aligned} h(t, \boldsymbol{x}) := \sum_{j=1}^{N} \sum_{\ell=1}^{M_j} \sum_{m=\ell+1}^{M_j} \delta_{j,\ell,m} A_{j,\ell}(t) A_{j,m}(t) \Big(& \cos(\xi_{j,\ell}) \cos(\xi_{j,m}) + \dots \\ & \dots + \frac{\boldsymbol{k}_{j,\ell} \cdot \boldsymbol{k}_{j,m}}{\mu_j^2} \sin(\xi_{j,\ell}) \sin(\xi_{j,m}) \Big)\,, \end{aligned} \tag{2.24}$$

with additionally defined phase variables $\xi_{j,\ell} := \boldsymbol{k}_{j,\ell} \cdot \boldsymbol{x} + \omega_{j,\ell} t$ and amplitude factors $\delta_{j,\ell,m} := -\operatorname{sgn}(\boldsymbol{a}_{j,\ell} \cdot \boldsymbol{k}_{j,m}) \operatorname{sgn}(\boldsymbol{a}_{j,m} \cdot \boldsymbol{k}_{j,\ell})$ for any $1 \leq \ell, m \leq M_j$, $1 \leq j \leq N$.

Proof. Due to the orthogonality $S_j \perp S_\ell$ for all $1 \leq j, \ell \leq N$, $j \neq \ell$, and since $\boldsymbol{k}_{j,\ell}, \boldsymbol{a}_{j,\ell} \in S_j$ for any $1 \leq \ell \leq M_j$, $1 \leq j \leq N$, we can use the splitting of Lemma

2.7 and obtain by inserting (2.22) into $(\boldsymbol{v}\cdot\nabla)\boldsymbol{v}$

$$(\boldsymbol{v}\cdot\nabla)\boldsymbol{v} = \sum_{j=1}^{N}\left(\sum_{\ell=1}^{M_j} A_{j,\ell}(t)\sin(\xi_{j,\ell})\boldsymbol{a}_{j,\ell}\cdot\nabla\right)\left(\sum_{m=1}^{M_j} A_{j,m}(t)\sin(\xi_{j,m})\boldsymbol{a}_{j,m}\right) + (\boldsymbol{c}\cdot\nabla)\boldsymbol{v}\,.$$

It remains to show, that the first sum is ∇h. Let $j\in\{1,\dots,N\}$ be arbitrary and fixed. For the gradient of the j-th sum of h in (2.24) it then follows from Lemma 2.8

$$\begin{aligned}
&\nabla\sum_{\ell=1}^{M_j}\sum_{m=\ell+1}^{M_j}\delta_{j,\ell,m}A_{j,\ell}A_{j,m}\left(\cos(\xi_{j,\ell})\cos(\xi_{j,m}) + \frac{\boldsymbol{k}_{j,\ell}\cdot\boldsymbol{k}_{j,m}}{\mu_j^2}\sin(\xi_{j,\ell})\sin(\xi_{j,m})\right)\\
&\quad= \sum_{\ell=1}^{M_j}\sum_{m=\ell+1}^{M_j}\nabla\delta_{j,\ell,m}A_{j,\ell}A_{j,m}\left(\cos(\xi_{j,\ell})\cos(\xi_{j,m}) + \frac{\boldsymbol{k}_{j,\ell}\cdot\boldsymbol{k}_{j,m}}{\mu_j^2}\sin(\xi_{j,\ell})\sin(\xi_{j,m})\right)\\
&\quad= \sum_{\ell=1}^{M_j}\sum_{m=\ell+1}^{M_j}\Big((A_{j,\ell}\sin(\xi_{j,\ell})\boldsymbol{a}_{j,\ell} + A_{j,m}\sin(\xi_{j,m})\boldsymbol{a}_{j,m})\cdot\nabla\Big)\cdots\\
&\qquad\qquad\cdots(A_{j,\ell}\sin(\xi_{j,\ell})\boldsymbol{a}_{j,\ell} + A_{j,m}\sin(\xi_{j,m})\boldsymbol{a}_{j,m})\\
&\quad\overset{\boldsymbol{a}_{j,\ell}\perp\boldsymbol{k}_{j,\ell}}{=} \sum_{\ell=1}^{M_j}\sum_{m=\ell+1}^{M_j}\Big((A_{j,\ell}\sin(\xi_{j,\ell})\boldsymbol{a}_{j,\ell}\cdot\nabla)A_{j,m}\sin(\xi_{j,m})\boldsymbol{a}_{j,m} + \dots\\
&\qquad\qquad\dots + (A_{j,m}\sin(\xi_{j,m})\boldsymbol{a}_{j,m}\cdot\nabla)A_{j,\ell}\sin(\xi_{j,\ell})\boldsymbol{a}_{j,\ell}\Big)\\
&\quad= \sum_{\ell=1}^{M_j}\sum_{m=\ell+1}^{M_j}(A_{j,\ell}\sin(\xi_{j,\ell})\boldsymbol{a}_{j,\ell}\cdot\nabla)A_{j,m}\sin(\xi_{j,m})\boldsymbol{a}_{j,m} + \dots\\
&\qquad\dots + \sum_{\ell=1}^{M_j}\sum_{m=1}^{\ell-1}(A_{j,\ell}\sin(\xi_{j,\ell})\boldsymbol{a}_{j,\ell}\cdot\nabla)A_{j,m}\sin(\xi_{j,m})\boldsymbol{a}_{j,m}\\
&\quad= \sum_{\ell=1}^{M_j}\sum_{m=1}^{M_j}(A_{j,\ell}\sin(\xi_{j,\ell})\boldsymbol{a}_{j,\ell}\cdot\nabla)A_{j,m}\sin(\xi_{j,m})\boldsymbol{a}_{j,m} - \dots\\
&\qquad\dots - \underbrace{\sum_{\ell=1}^{M_j}(A_{j,\ell}\sin(\xi_{j,\ell})\boldsymbol{a}_{j,\ell}\cdot\nabla)A_{j,\ell}\sin(\xi_{j,\ell})\boldsymbol{a}_{j,\ell}}_{=0,\text{ since }\boldsymbol{a}_{j,\ell}\perp\boldsymbol{k}_{j,\ell}}\\
&\quad= \sum_{\ell=1}^{M_j}(A_{j,\ell}\sin(\xi_{j,\ell})\boldsymbol{a}_{j,\ell}\cdot\nabla)\left(\sum_{m=1}^{M_j}A_{j,m}\sin(\xi_{j,m})\boldsymbol{a}_{j,m}\right)\\
&\quad= \left(\sum_{\ell=1}^{M_j}A_{j,\ell}\sin(\xi_{j,\ell})\boldsymbol{a}_{j,\ell}\cdot\nabla\right)\left(\sum_{m=1}^{M_j}A_{j,m}\sin(\xi_{j,m})\boldsymbol{a}_{j,m}\right).
\end{aligned}$$

Since $j \in \{1, \dots, N\}$ was arbitrary, it follows from the definition (2.24) of h

$$\nabla h = \sum_{j=1}^{N} \left(\sum_{\ell=1}^{M_j} A_{j,\ell} \sin(\xi_{j,\ell}) \boldsymbol{a}_{j,\ell} \cdot \nabla \right) \left(\sum_{m=1}^{M_j} A_{j,m} \sin(\xi_{j,m}) \boldsymbol{a}_{j,m} \right) ,$$

which was left to show (2.23). □

If we compare the two presented flows, under which the nonlinear advection term becomes a gradient, then those from Theorem 2.6 have the advantage of having completely arbitrary wave vectors, but they are not incompressible. In contrast to them, the flows in Theorem 2.9 are incompressible, but their wave vectors and flow directions are restricted to predefined two-dimensional linear subspaces S_j. The form of the nonlinear interaction h in (2.24) shows, that with the approach (2.22) and the conditions in Theorem 2.9 the plane waves within the same two-dimensional linear subspace S_j interact as pairs, while they do not interact with those from other linear subspaces at all, due to the orthogonality $S_j \perp S_\ell$ for $j \neq \ell$ and Lemma 2.7. In each S_j the directions of the wave vectors are completely arbitrary, but the plane waves in the same linear subspace interact at the same scale only, since the wave vectors are restricted to the same length μ_j. However, different subspaces S_j can have different predefined lengths μ_j.

The wave vectors and flow directions of the velocities in Theorem 2.3 can be also seen as being separated by linear subspaces of $\mathbb{R}^n$. In this case there are the linear subspaces $S_{\boldsymbol{k}}$ and $S_{\boldsymbol{a}}$, which are orthogonal to each other, and all wave vectors belong to $S_{\boldsymbol{k}}$ and all flow directions to $S_{\boldsymbol{a}}$. Additionally, the dimensions of these two subspaces are arbitrary, as long as $\dim(S_{\boldsymbol{k}}) + \dim(S_{\boldsymbol{a}}) \leq n$. In contrast to these flows, as already mentioned, the wave vectors and the corresponding flow directions of the velocities in Theorem 2.9 must lie in the same predefined two-dimensional linear subspaces.

Remark 2.9.1. We note that the interacting flows from Theorem 2.9 do not contain the set of flows from Theorem 2.3, even though the nonlinearity in the latter is a gradient as well, albeit zero. However, the sets of both kind of flows intersect since an interacting flow from Theorem 2.9 may produce vanishing nonlinear advection terms and is then a case of a flow as in Theorem 2.3. This can be realized, for example, if there is only one plane wave in each linear subspace S_j.

Remark 2.9.2. We consider the flows in the two-dimensional domain $\mathbb{R}^2$. In this setting, Theorem 2.3 characterizes the possible superposition of waves with arbitrary wave vector lengths, but the same wave vector direction. In contrast, Theorem 2.9 provides the superposition of waves with any wave vector direction, but all must have the same wave vector length. Due to these converse and characteristic kinds of superpositions, we call those as shown in Theorem 2.3 the *radial superposition principle* and those as in Theorem 2.9 the *angular superposition principle* in a two-dimensional setting, as e.g. in shallow water equations, which will be considered in the following chapters. A superposition

with different wave vector lengths and different wave vector directions does not generate a solution in general.

It is also possible to have a superposition of waves by an integral, which produces a gradient nonlinear advection term as well. We will not focus on this kind of flows, but we will still formulate the following theorem about them and refer to them shortly in some places in this work.

Theorem 2.10. *For $n \geq 2$ and $1 \leq N \leq n/2$ let $S_j \subseteq \mathbb{R}^n$ be two-dimensional linear subspaces with $S_j \perp S_\ell$ for all $1 \leq j, \ell \leq N$, $j \neq \ell$. Furthermore, we define within these subspaces the circles $S_j(\mu) := \{\boldsymbol{k} \in S_j \mid |\boldsymbol{k}| = \mu\}$ for $\mu \geq 0$ and any $1 \leq j \leq N$. Consider the velocity field $\boldsymbol{v} : \mathbb{R}_{\geq 0} \times \mathbb{R}^n \to \mathbb{R}^n$ of the traveling wave form*

$$\boldsymbol{v}(t, \boldsymbol{x}) = \sum_{j=1}^{N} \int\limits_{\boldsymbol{k} \in S_j(\mu_j)} A_j(t, \boldsymbol{k}) \sin(\boldsymbol{k} \cdot \boldsymbol{x} + \omega_j(\boldsymbol{k})t) \boldsymbol{a}_j(\boldsymbol{k}) \mathrm{d}\boldsymbol{k} + \boldsymbol{c}\,, \tag{2.25}$$

with constant flow $\boldsymbol{c} \in \mathbb{R}^n$, wave vector lengths $\mu_j > 0$ for any $1 \leq j \leq N$, time-dependent amplitude factors $A_j(\cdot, \boldsymbol{k}) \in C^1(\mathbb{R}_{\geq 0}, \mathbb{R})$, temporal frequencies $\omega_j(\boldsymbol{k}) \in \mathbb{R}$ and constant flow directions $\boldsymbol{a}_j(\boldsymbol{k}) \in S_j(1)$ for any $\boldsymbol{k} \in S_j(\mu_j)$ and $1 \leq j \leq N$. Furthermore, we presume $\boldsymbol{a}_j(\boldsymbol{k}) \cdot \boldsymbol{k} = 0$ for any $\boldsymbol{k} \in S_j(\mu_j)$ and $1 \leq j \leq N$, as well as $||A_j(t, \cdot)||_\infty < \infty$ for any $1 \leq j \leq N$ and $t \geq 0$. Under these conditions, the nonlinear advection term becomes

$$(\boldsymbol{v} \cdot \nabla)\boldsymbol{v} = (\boldsymbol{c} \cdot \nabla)\boldsymbol{v} + \nabla h\,, \tag{2.26}$$

where $h \in C^1(\mathbb{R}_{\geq 0} \times \mathbb{R}^n, \mathbb{R})$ is defined by

$$\begin{aligned} h(t, \boldsymbol{x}) := \sum_{j=1}^{N} \mu_j^2 \int_0^{2\pi} \int_{\varphi_1}^{2\pi} \tilde{A}_j(t, \varphi_1) \tilde{A}_j(t, \varphi_2) \Big(&\cos \xi_j(\varphi_1) \cos \xi_j(\varphi_2) + \ldots \\ &\ldots + \cos(\varphi_1 - \varphi_2) \sin \xi_j(\varphi_1) \sin \xi_j(\varphi_2) \Big) \mathrm{d}\varphi_2 \mathrm{d}\varphi_1\,. \end{aligned} \tag{2.27}$$

For h we use for any two-dimensional subspace S_j an arbitrary orthonormal basis $\boldsymbol{e}_{j,1}, \boldsymbol{e}_{j,2}$ and redefine for all wave vectors $\boldsymbol{k}_j(\varphi) := \mu_j\big(\cos(\varphi)\boldsymbol{e}_{j,1} + \sin(\varphi)\boldsymbol{e}_{j,2}\big) \in S_j(\mu_j)$ the flow directions $\boldsymbol{a}_j(\varphi) := \delta_j(\varphi)\big(-\sin(\varphi)\boldsymbol{e}_{j,1} + \cos(\varphi)\boldsymbol{e}_{j,2}\big) = \boldsymbol{a}_j(\boldsymbol{k}_j(\varphi))$ with $\delta_j(\varphi) \in \{-1, 1\}$, amplitudes $\tilde{A}_j(t, \varphi) := \delta_j(\varphi) A_j(t, \varphi)$ with $A_j(t, \varphi) := A_j(t, \boldsymbol{k}_j(\varphi))$, the temporal frequencies $\omega_j(\varphi) := \omega_j(\boldsymbol{k}_j(\varphi))$ and the phase variables $\xi_j(\varphi) := \boldsymbol{k}_j(\varphi) \cdot \boldsymbol{x} + \omega_j(\varphi)t$ for all $0 \leq \varphi \leq 2\pi$ and any $1 \leq j \leq N$.

Proof. Due to $|\boldsymbol{a}_j(\boldsymbol{k})| = 1$ for any $\boldsymbol{k} \in S_j(\mu_j)$, $1 \leq j \leq N$ and $||A_j(t, \cdot)||_\infty < \infty$ for any $1 \leq j \leq N$, $t \geq 0$ the velocity field (2.25) is well-defined, since for any $t \geq 0$, $\boldsymbol{x} \in \mathbb{R}^n$

and component $1 \leq \ell \leq n$ of $\boldsymbol{v}$ we can estimate

$$|v_\ell(t,\boldsymbol{x})| \leq \sum_{j=1}^{N} \int\limits_{\boldsymbol{k}\in S_j(\mu_j)} |A_j(t,\boldsymbol{k})|\mathrm{d}\boldsymbol{k} + |\boldsymbol{c}| \leq \sum_{j=1}^{N} 2\pi\mu_j ||A_j(t,\cdot)||_\infty + |\boldsymbol{c}| < \infty\,.$$

The function h as in (2.27) is well-defined as well, since we can estimate for any $t \geq 0$ and $\boldsymbol{x} \in \mathbb{R}^n$

$$\begin{aligned}
|h(t,\boldsymbol{x})| &\leq \sum_{j=1}^{N} \mu_j^2 \int_0^{2\pi}\int_{\varphi_1}^{2\pi} 2|A_j(t,\varphi_1)||A_j(t,\varphi_2)|\mathrm{d}\varphi_2\mathrm{d}\varphi_1 \\
&\leq \sum_{j=1}^{N} 2\mu_j^2 \int_0^{2\pi} |A_j(t,\varphi_1)|\mathrm{d}\varphi_1 \int_0^{2\pi} |A_j(t,\varphi_2)|\mathrm{d}\varphi_2 \\
&\leq \sum_{j=1}^{N} 8\pi^2\mu_j^2 ||A_j(t,\cdot)||_\infty^2 < \infty\,.
\end{aligned}$$

Since v in (2.25) is split in parts on different orthogonal linear subspaces S_j, we can use Lemma 2.7 and obtain

$$(\boldsymbol{v}\cdot\nabla)\boldsymbol{v} = (\boldsymbol{c}\cdot\nabla)\boldsymbol{v} + \sum_{j=1}^{N} (\boldsymbol{v}_j\cdot\nabla)\boldsymbol{v}_j\,,$$

with $\boldsymbol{v}_j = \int_{\boldsymbol{k}\in S_j(\mu_j)} A_j(t,\boldsymbol{k})\sin(\xi_j(\boldsymbol{k}))\boldsymbol{a}_j(\boldsymbol{k})\mathrm{d}\boldsymbol{k}$ and $\xi_j(\boldsymbol{k}) := \boldsymbol{k}\cdot\boldsymbol{x} + \omega_j(\boldsymbol{k})t$ for any $j \in \{1,\dots,N\}$. Since the first term is already as in (2.26), it remains to show for any $j \in \{1,\dots,N\}$

$$(\boldsymbol{v}_j\cdot\nabla)\boldsymbol{v}_j = \nabla h_j\,, \tag{2.28a}$$

$$\begin{aligned}
h_j = \mu_j^2 \int_0^{2\pi}\int_{\varphi_1}^{2\pi} \tilde{A}_j(t,\varphi_1)\tilde{A}_j(t,\varphi_2)\Big(&\cos\xi_j(\varphi_1)\cos\xi_j(\varphi_2) + \dots \\
&\dots + \cos(\varphi_1-\varphi_2)\sin\xi_j(\varphi_1)\sin\xi_j(\varphi_2)\Big)\mathrm{d}\varphi_2\mathrm{d}\varphi_1\,.
\end{aligned} \tag{2.28b}$$

Let $j \in \{1,\dots,N\}$ be arbitrary and fixed. First of all we can write

$$\begin{aligned}
\boldsymbol{a}_j(\varphi_2)\cdot\boldsymbol{k}_j(\varphi_1) &= \delta_j(\varphi_2)\big(-\sin(\varphi_2)\boldsymbol{e}_{j,1} + \cos(\varphi_2)\boldsymbol{e}_{j,2}\big)\cdot\mu_j\big(\cos(\varphi_1)\boldsymbol{e}_{j,1} + \sin(\varphi_1)\boldsymbol{e}_{j,2}\big) \\
&= \delta_j(\varphi_2)\mu_j\big(\cos(\varphi_1)\sin(-\varphi_2) + \sin(\varphi_1)\cos(-\varphi_2)\big) \\
&= \delta_j(\varphi_2)\mu_j\sin(\varphi_1-\varphi_2)\,,
\end{aligned}$$

which then leads to

$$\begin{aligned}
\cos(\varphi_1-\varphi_2)\boldsymbol{k}_j(\varphi_1) &= \mu_j\big(\cos(\varphi_2-\varphi_1)\cos(\varphi_1)\boldsymbol{e}_{j,1}+\cos(\varphi_2-\varphi_1)\sin(\varphi_1)\boldsymbol{e}_{j,2}\big)\\
&= \mu_j\Big(\big(\cos(\varphi_2-\varphi_1)\cos(\varphi_1)-\sin(\varphi_2-\varphi_1)\sin(\varphi_1)\big)\boldsymbol{e}_{j,1}\\
&\quad+\big(\cos(\varphi_2-\varphi_1)\sin(\varphi_1)+\sin(\varphi_2-\varphi_1)\cos(\varphi_1)\big)\boldsymbol{e}_{j,2}\\
&\quad+\sin(\varphi_2-\varphi_1)\sin(\varphi_1)\boldsymbol{e}_{j,1}-\sin(\varphi_2-\varphi_1)\cos(\varphi_1)\boldsymbol{e}_{j,2}\Big)\\
&= \mu_j\big(\cos(\varphi_2)\boldsymbol{e}_{j,1}+\sin(\varphi_2)\boldsymbol{e}_{j,2}\big)\\
&\quad+\mu_j\sin(\varphi_2-\varphi_1)\big(\sin(\varphi_1)\boldsymbol{e}_{j,1}-\cos(\varphi_1)\boldsymbol{e}_{j,2}\big)\\
&= \boldsymbol{k}_j(\varphi_2)+\mu_j\sin(\varphi_1-\varphi_2)\big(-\sin(\varphi_1)\boldsymbol{e}_{j,1}+\cos(\varphi_1)\boldsymbol{e}_{j,2}\big)\\
&= \boldsymbol{k}_j(\varphi_2)+\delta_j(\varphi_1)\delta_j(\varphi_2)\big(\boldsymbol{a}_j(\varphi_2)\cdot\boldsymbol{k}_j(\varphi_1)\big)\boldsymbol{a}_j(\varphi_1)\,. \qquad (2.29)
\end{aligned}$$

With this and (2.28b) it then follows

$$\begin{aligned}
\nabla h_j &= \mu_j^2\int_0^{2\pi}\int_{\varphi_1}^{2\pi}\tilde{A}_j(t,\varphi_1)\tilde{A}_j(t,\varphi_2)\Big(\nabla\big(\cos\xi_j(\varphi_1)\cos\xi_j(\varphi_2)\big)\\
&\qquad+\cos(\varphi_1-\varphi_2)\nabla\big(\sin\xi_j(\varphi_1)\sin\xi_j(\varphi_2)\big)\Big)\mathrm{d}\varphi_2\mathrm{d}\varphi_1\\
&= \mu_j^2\int_0^{2\pi}\int_{\varphi_1}^{2\pi}\tilde{A}_j(t,\varphi_1)\tilde{A}_j(t,\varphi_2)\Big(-\sin\xi_j(\varphi_1)\cos\xi_j(\varphi_2)\boldsymbol{k}_j(\varphi_1)\\
&\quad-\cos\xi_j(\varphi_1)\sin\xi_j(\varphi_2)\boldsymbol{k}_j(\varphi_2)+\cos(\varphi_1-\varphi_2)\cos\xi_j(\varphi_1)\sin\xi_j(\varphi_2)\boldsymbol{k}_j(\varphi_1)\\
&\quad+\cos(\varphi_1-\varphi_2)\sin\xi_j(\varphi_1)\cos\xi_j(\varphi_2)\boldsymbol{k}_j(\varphi_2)\Big)\mathrm{d}\varphi_2\mathrm{d}\varphi_1\\
&\overset{(2.29)}{=} \mu_j^2\int_0^{2\pi}\int_{\varphi_1}^{2\pi}\tilde{A}_j(t,\varphi_1)\tilde{A}_j(t,\varphi_2)\Big(-\sin\xi_j(\varphi_1)\cos\xi_j(\varphi_2)\boldsymbol{k}_j(\varphi_1)\\
&\quad-\cos\xi_j(\varphi_1)\sin\xi_j(\varphi_2)\boldsymbol{k}_j(\varphi_2)+\cos\xi_j(\varphi_1)\sin\xi_j(\varphi_2)\boldsymbol{k}_j(\varphi_2)\\
&\quad+\cos\xi_j(\varphi_1)\sin\xi_j(\varphi_2)\delta_j(\varphi_1)\delta_j(\varphi_2)\big(\boldsymbol{a}_j(\varphi_2)\cdot\boldsymbol{k}_j(\varphi_1)\big)\boldsymbol{a}_j(\varphi_1)\\
&\quad+\sin\xi_j(\varphi_1)\cos\xi_j(\varphi_2)\boldsymbol{k}_j(\varphi_1)\\
&\quad+\sin\xi_j(\varphi_1)\cos\xi_j(\varphi_2)\delta_j(\varphi_1)\delta_j(\varphi_2)\big(\boldsymbol{a}_j(\varphi_1)\cdot\boldsymbol{k}_j(\varphi_2)\big)\boldsymbol{a}_j(\varphi_2)\Big)\mathrm{d}\varphi_2\mathrm{d}\varphi_1\\
&= \mu_j^2\int_0^{2\pi}\int_{\varphi_1}^{2\pi}A_j(t,\varphi_1)A_j(t,\varphi_2)\Big(\cos\xi_j(\varphi_1)\sin\xi_j(\varphi_2)\big(\boldsymbol{a}_j(\varphi_2)\cdot\boldsymbol{k}_j(\varphi_1)\big)\boldsymbol{a}_j(\varphi_1)\\
&\quad+\sin\xi_j(\varphi_1)\cos\xi_j(\varphi_2)\big(\boldsymbol{a}_j(\varphi_1)\cdot\boldsymbol{k}_j(\varphi_2)\big)\boldsymbol{a}_j(\varphi_2)\Big)\mathrm{d}\varphi_2\mathrm{d}\varphi_1
\end{aligned}$$

$$
\begin{aligned}
&= \mu_j^2 \int_0^{2\pi} \int_{\varphi_1}^{2\pi} A_j(t,\varphi_1) A_j(t,\varphi_2) \cos\xi_j(\varphi_1) \sin\xi_j(\varphi_2) (\boldsymbol{a}_j(\varphi_2) \cdot \boldsymbol{k}_j(\varphi_1)) \boldsymbol{a}_j(\varphi_1) \mathrm{d}\varphi_2 \mathrm{d}\varphi_1 \\
&\quad + \mu_j^2 \int_0^{2\pi} \int_0^{\varphi_2} A_j(t,\varphi_1) A_j(t,\varphi_2) \cos\xi_j(\varphi_2) \sin\xi_j(\varphi_1) (\boldsymbol{a}_j(\varphi_1) \cdot \boldsymbol{k}_j(\varphi_2)) \boldsymbol{a}_j(\varphi_2) \mathrm{d}\varphi_1 \mathrm{d}\varphi_2 \\
&= \mu_j^2 \int_0^{2\pi} \int_0^{2\pi} A_j(t,\varphi_1) A_j(t,\varphi_2) \cos\xi_j(\varphi_1) \sin\xi_j(\varphi_2) (\boldsymbol{a}_j(\varphi_2) \cdot \boldsymbol{k}_j(\varphi_1)) \boldsymbol{a}_j(\varphi_1) \mathrm{d}\varphi_2 \mathrm{d}\varphi_1 \\
&= \int\limits_{\tilde{\boldsymbol{k}}_1 \in S_j(\mu_j)} \int\limits_{\tilde{\boldsymbol{k}}_2 \in S_j(\mu_j)} A_j(t,\tilde{\boldsymbol{k}}_1) A_j(t,\tilde{\boldsymbol{k}}_2) \cos\xi_j(\tilde{\boldsymbol{k}}_1) \sin\xi_j(\tilde{\boldsymbol{k}}_2) (\boldsymbol{a}_j(\tilde{\boldsymbol{k}}_2) \cdot \tilde{\boldsymbol{k}}_1) \boldsymbol{a}_j(\tilde{\boldsymbol{k}}_1) \mathrm{d}\tilde{\boldsymbol{k}}_2 \mathrm{d}\tilde{\boldsymbol{k}}_1 \\
&= \int\limits_{\tilde{\boldsymbol{k}}_1 \in S_j(\mu_j)} \Bigg(\int\limits_{\tilde{\boldsymbol{k}}_2 \in S_j(\mu_j)} A_j(t,\tilde{\boldsymbol{k}}_2) \sin\xi_j(\tilde{\boldsymbol{k}}_2) \boldsymbol{a}_j(\tilde{\boldsymbol{k}}_2) \mathrm{d}\tilde{\boldsymbol{k}}_2 \cdot \nabla A_j(t,\tilde{\boldsymbol{k}}_1) \sin\xi_j(\tilde{\boldsymbol{k}}_1) \Bigg) \boldsymbol{a}_j(\tilde{\boldsymbol{k}}_1) \mathrm{d}\tilde{\boldsymbol{k}}_1 \\
&= \Bigg(\int\limits_{\tilde{\boldsymbol{k}}_2 \in S_j(\mu_j)} A_j(t,\tilde{\boldsymbol{k}}_2) \sin\xi_j(\tilde{\boldsymbol{k}}_2) \boldsymbol{a}_j(\tilde{\boldsymbol{k}}_2) \mathrm{d}\tilde{\boldsymbol{k}}_2 \cdot \nabla \Bigg) \int\limits_{\tilde{\boldsymbol{k}}_1 \in S_j(\mu_j)} A_j(t,\tilde{\boldsymbol{k}}_1) \sin\xi_j(\tilde{\boldsymbol{k}}_1) \boldsymbol{a}_j(\tilde{\boldsymbol{k}}_1) \mathrm{d}\tilde{\boldsymbol{k}}_1 \\
&= (\boldsymbol{v}_j \cdot \nabla) \boldsymbol{v}_j \,.
\end{aligned}
$$

Since j was arbitrary, (2.28a) holds for any $j \in \{1, \dots, N\}$ and it follows (2.26) with (2.27). □

Remark 2.10.1. For the superposition as in Theorem 2.3 it is also possible to use an integral instead of the inner sum, but due to the arbitrary wave shapes, which make a clear formulation of a corresponding theorem more difficult, we omit further analysis in this direction. Furthermore, in the two-dimensional domain $\mathbb{R}^2$, which we will often consider, the radial superposition by integral is already included in the arbitrary wave shape of the flow in Theorem 2.3.

Theorem 2.11. *The flow* (2.22) *defined in Theorem 2.9, as well as* (2.25) *defined in Theorem 2.10, are divergence-free.*

Proof. It follows directly from the linearity of the divergence operator $\operatorname{div} \boldsymbol{v}$ in $\boldsymbol{v}$ and Lemma 2.4. □

2.2. Explicit solutions in non-rotating fluid models

Now we will see, how the functions described in Section 2.1 can be used in order to solve nonlinear fluid equations explicitly and what set of solutions we obtain. For the set of solutions we will also determine the dimensions, in order to get a better characterization of them and to be able to compare the different sets. In this section we consider simpler

non-rotating fluid models and afterwards in Section 2.3 the rotating Boussinesq equations as a geophysical fluid model.

Here we focus on the incompressible Navier–Stokes equations on an n-dimensional space

$$\frac{\partial \boldsymbol{v}}{\partial t} + (\boldsymbol{v}\cdot\nabla)\boldsymbol{v} = -\frac{1}{\rho_0}\nabla p + \nu\Delta\boldsymbol{v} \tag{2.30a}$$

$$\nabla\cdot\boldsymbol{v} = 0\,, \tag{2.30b}$$

with dimension $n \geq 2$, velocity $\boldsymbol{v} \in C^2(\mathbb{R}_{\geq 0}\times\mathbb{R}^n,\mathbb{R}^n)$ and pressure $p \in C^1(\mathbb{R}_{\geq 0}\times\mathbb{R}^n,\mathbb{R})$ in time $t \geq 0$ and space $\boldsymbol{x} \in \mathbb{R}^n$, as well as constant density $\rho_0 > 0$ and kinematic viscosity $\nu > 0$. We also consider the n-dimensional Euler equations in (2.30) by just setting $\nu = 0$.

2.2.1. Vanishing nonlinear advection term

We start with solutions of the form as in Theorem 2.3. Since the velocity of this form does not produce any gradient linear or nonlinear terms, we can assume the pressure to be space-independent $p(t,\boldsymbol{x}) = \tilde{p}(t)$. Due to the incompressibility of such flows, as shown in Theorem 2.5, the equation (2.30b) is satisfied. Additionally presuming $\psi_{j,\ell} \in C^2(\mathbb{R}_{\geq 0}\times\mathbb{R},\mathbb{R})$ for any wave shape and substituting the velocity field (2.7) with its condition (2.8) into the momentum equation of the Navier–Stokes equations (2.30a) yields, using (2.9), the linear equations in $\psi_{j,\ell}$

$$\sum_{j=1}^{N}\boldsymbol{a}_j\sum_{\ell=1}^{M_j}\Big(\frac{\partial\psi_{j,\ell}}{\partial t} + \omega_{j,\ell}\frac{\partial\psi_{j,\ell}}{\partial\xi} + (\boldsymbol{c}\cdot\boldsymbol{k}_{j,\ell})\frac{\partial\psi_{j,\ell}}{\partial\xi}\Big) = \sum_{j=1}^{N}\boldsymbol{a}_j\sum_{\ell=1}^{M_j}\nu|\boldsymbol{k}_{j,\ell}|^2\frac{\partial^2\psi_{j,\ell}}{\partial\xi^2}\,.$$

We solve this equation for each index separately by solving the following heat equations and choosing the time frequencies:

$$\frac{\partial\psi_{j,\ell}}{\partial t} = \nu|\boldsymbol{k}_{j,\ell}|^2\frac{\partial^2\psi_{j,\ell}}{\partial\xi^2}\,,\quad \omega_{j,\ell} = -\boldsymbol{c}\cdot\boldsymbol{k}_{j,\ell} \qquad \text{for any defined} \quad (j,\ell)\,. \tag{2.31}$$

By the Galilean invariance, which has no effect on the pressure in this case, we may a priori set $\boldsymbol{c} = 0$ when choosing time frequencies $\omega_{j,\ell}$ according to (2.31). We note this may be violated in presence of Coriolis term as in Section 2.3, a forcing as in Section 2.4 or bottom drag as in Chapter 4.

Each set of solutions to the heat equations (2.31) generates an explicit solution to the incompressible Navier–Stokes equations (2.30). In general, these explicit solutions are not constructed by splitting the solutions into lower-dimensional subspaces as described in Lemma 2.7, since these solutions are of the form as in Theorem 2.3 (see discussion after Lemma 2.7).

In a three-dimensional space ($n = 3$) there are two possible cases for the flows from

Theorem 2.3: We can choose $N = 1$, which means that the flow has one direction $\boldsymbol{a}_1$ and arbitrarily many wave vectors $\boldsymbol{k}_{1,\ell}$, lying in the plane orthogonal to the direction $\boldsymbol{a}_1$, e.g. $\boldsymbol{a}_1 = \boldsymbol{e_3}$ and $\boldsymbol{k}_{1,\ell}$ in the horizontal plane. This is related to the so-called *parallel flow* (cf. Wang (1989)), but in plane wave form. Such parallel flows also occur in the Boussinesq equations, see Section 2.3.1.
For the case $N = 2$ we have two flow directions $\boldsymbol{a}_1$ and $\boldsymbol{a}_2$, but only one direction for the wave vectors $\boldsymbol{k}_{1,\ell}$ and $\boldsymbol{k}_{2,\ell}$, which is orthogonal to the plane spanned by $\boldsymbol{a}_1$ and $\boldsymbol{a}_2$. This is similar to a two-dimensional flow with cross flow (cf. Weinbaum and O'Brien (1967)), but again in a plane wave form. For instance, if the wave vector is in the horizontal plane $\boldsymbol{k}_{1,\ell} = \boldsymbol{k}_{2,\ell} = (\boldsymbol{k}, 0)^\intercal \in \mathbb{R}^3$, then with $\boldsymbol{a}_1 = (\boldsymbol{k}^\perp, 0)^\intercal$ we obtain a purely horizontal flow, superposed with a parallel flow for $\boldsymbol{a}_2 = \boldsymbol{e_3}$ as the cross flow component.

In order to make the constraints more clear, we count dimensions of this set of solutions for given M_j, and refer to Remark 2.11.2 below for the infinite dimensional case. The dimension from initial data for (2.31), that are linearly independent, is $m_N := M_1 + \ldots + M_N$. If these are also linearly independent with respect to scaling for each $1 \le j \le N$, which means

$$a_1 \psi_{j,1}(0, b_1 \xi) + \ldots + a_{M_j} \psi_{j,M_j}(0, b_{M_j} \xi) \not\equiv 0\,, \qquad \text{not all} \quad a_\ell,\, b_\ell = 0\,,$$

then this gives linearly independent summands in (2.7). Additionally, we get N dimensions from linearly independent $\boldsymbol{a}_j$, and different wave vectors also generate linear independence. Hence, admissible wave vectors $\boldsymbol{k}_{j,\ell}$ satisfying (2.8) can be independently selected from the orthogonal complement of $\operatorname{span}(\boldsymbol{a}_1, \ldots, \boldsymbol{a}_N)$ in $\mathbb{R}^n$, which has dimension $(n-N)$ and thus contributing $(n-N)m_N$ dimensions to a total of $N+(n-N+1)m_N$ (Galileian invariance and translation in space give another $2n - N$ dimensions).

As mentioned for the three dimensional problem ($n = 3$), we have the two cases $N = 1$ and $N = 2$. For $N = 1$ the dimension is $1 + (3 - 1 + 1)m_1 = 1 + 3m_1$, while for $N = 2$ it is $2 + (3 - 2 + 1)m_2 = 2 + 2m_2$ (and additionally $6 - N$ by Galileian invariance and translation in space). For the two dimensional problem we can only choose one flow direction ($N = 1$), which yields the dimension $1 + (2 - 1 + 1)m_1 = 1 + 2m_1$ (and additional 3 for Galileian invariance and translation in space).

Remark 2.11.1. The representation in the form of (2.7) can be reduced by combining summands of fixed j, for which the wave vectors lie on the same ray, e.g. $\boldsymbol{k}_{j,\ell} = r\boldsymbol{k}_{j,m}$, $r \in \mathbb{R}$. However, the combined function does not necessarily solve a heat equation.

Remark 2.11.2. In fact, the space of solutions is infinite dimensional, since the numbers of summands M_j are arbitrary. As mentioned in Remark 2.10.1, the summation over ℓ can also be replaced by an integral over all admissible wave vectors orthogonal to all flow directions $\boldsymbol{a}_j$.

As a concrete and simple example of solutions to (2.31) and the Navier–Stokes equations (2.30) we can use eigenmode solutions of the heat equations, with arbitrary ampli-

tudes and constant phase shifts $A_{j,\ell}$, $\theta_{j,\ell} \in \mathbb{R}$ for any $1 \leq \ell \leq M_j$ and $1 \leq j \leq N$, and obtain

$$\boldsymbol{v}(t,\boldsymbol{x}) = \sum_{j=1}^{N} \boldsymbol{a}_j \sum_{\ell=1}^{M_j} A_{j,\ell} \mathrm{e}^{-\nu|\boldsymbol{k}_{j,\ell}|^2 t} \sin(\boldsymbol{k}_{j,\ell} \cdot \boldsymbol{x} + \omega_{j,\ell} t + \theta_{j,\ell}) + \boldsymbol{c}\,.$$

For the Euler equations we may proceed in the same way, by just setting $\nu = 0$, so that (2.31) becomes $\frac{\partial \psi_{j,\ell}}{\partial t} = 0$ for any $1 \leq \ell \leq M_j$ and $1 \leq j \leq N$. Hence, the shapes of the travelling wave components of the solutions can be arbitrary functions of ξ and do not explicitly depend on t.

2.2.2. Gradient nonlinear advection term

Another approach to deal with the nonlinear advection term is to consider solutions of the form as in Theorem 2.9. In that way, a nonlinear term remains in the equations, but it is in gradient form, so that it can be compensated by the present pressure gradient. As stated in the theorem, the flow is decomposed into two-dimensional linear subspace of $\mathbb{R}^n$, as in Lemma 2.7, on which the plane wave parts lie in, i.e. the wave vectors and flow directions of the plane waves belong to the same linear subspace. For a two-dimensional space ($n = 2$) this is the whole plane itself, while for a three-dimensional space ($n = 3$) this is a single rotated plane. The following with more than one such plane for $n > 3$ has no direct application, but highlights the underlying structure.

According to Theorem 2.11 the flow defined in Theorem 2.9 satisfies the incompressibility condition (2.30b). Substituting the velocity field $\boldsymbol{v}$ in the form (2.22) with its conditions in Theorem 2.9 and the pressure $p = \tilde{p} - \rho_0 h$, with h as in (2.24), into the momentum equation (2.30a), yields by (2.23) the linear equations in $\boldsymbol{v}$

$$\frac{\partial \boldsymbol{v}}{\partial t} + (\boldsymbol{c} \cdot \nabla)\boldsymbol{v} = -\frac{1}{\rho_0} \nabla \tilde{p} + \nu \Delta \boldsymbol{v}\,.$$

These can be readily solved, so that we obtain solutions of the Navier–Stokes equations (2.30) of the form as in Theorem 2.9, with additional definitions

$$\begin{gathered} p(t,\boldsymbol{x}) = \tilde{p}(t) - \rho_0 h(t,\boldsymbol{x})\,, \quad A_{j,\ell}(t) = B_{j,\ell} \mathrm{e}^{-\nu \mu_j^2 t}\,, \\ B_{j,\ell} \in \mathbb{R}\,, \quad \omega_{j,\ell} = -\boldsymbol{c} \cdot \boldsymbol{k}_{j,\ell}\,, \end{gathered} \tag{2.32}$$

for any $1 \leq \ell \leq M_j$, $1 \leq j \leq N$, with arbitrary $\tilde{p} \in C(\mathbb{R}_{\geq 0}, \mathbb{R})$ and with h as in (2.24). We thus obtain a set of solutions of the incompressible Navier–Stokes equations, where the wave shapes are sinusoidal with arbitrary amplitudes and decay exponentially in time. Notably, the pressure is decaying as the product of the interacting plane waves, faster than each of these. With suitable forcing the decay of such solutions can be compensated, cf. Section 2.4.

For this set of solutions a dimension count is as follows: With the maximum number of linear subspaces $N = \lfloor n/2 \rfloor$ we have the dimension $m_N := M_1 + \cdots + M_N$ for the amplitudes $B_{j,\ell}$, as well as for additional constant phase shifts $\theta_{j,\ell}$ (including translation in space). The wave vectors $\boldsymbol{k}_{j,\ell}$ are in a plane S_j and of the same length μ_j, which gives one dimension for each sinusoidal wave shape. Together, we thus count the dimension $3m_N$ (Galileian invariance with constant vector $\boldsymbol{c}$ adds n). For the two- and three-dimensional space ($n = 2$ and $n = 3$) it makes $3m_1$.

Remark 2.11.3. As before, we actually have an infinitely dimensional solution space. The inner sum of (2.22) over ℓ can be replaced by a general integral. This means, if one proceeds in the same way as above, the Navier–Stokes equations (2.30) have solutions of the form as in Theorem 2.10, with additional definitions

$$p(t,\boldsymbol{x}) = \tilde{p}(t) - \rho_0 h(t,\boldsymbol{x})\,, \quad A_j(t,\boldsymbol{k}) = B_j(\boldsymbol{k})\mathrm{e}^{-\nu\mu_j^2 t}\,,$$
$$B_j(\boldsymbol{k}) \in \mathbb{R}\,, \quad \omega_j(\boldsymbol{k}) = -\boldsymbol{c}\cdot\boldsymbol{k}\,,$$

for any $\boldsymbol{k} \in S_j(\mu_j)$, $1 \le j \le N$, with arbitrary $\tilde{p} \in C(\mathbb{R}_{\ge 0}, \mathbb{R})$ and with h as in (2.27).

For the Euler equations we simply set $\nu = 0$ in (2.30), which yields the same form of solutions, but with constant amplitudes $A_{j,\ell}(t) \equiv B_{j,\ell}$ in the conditions (2.32), i.e. time independent solutions.

2.3. Explicit solutions in rotating Boussinesq equations

After studying explicit solutions in simpler nonlinear fluid models, we now turn to a rotating geophysical fluid model. In this case, the problem is more complex than those studied in Section 2.2, so that more restrictions on the solution sets are expected. Nevertheless, we will still find large and diverse subspaces of explicit solutions. We start with solutions of the form as in Theorem 2.3 in Section 2.3.1 and afterwards we study the occurrence of explicit solutions of the form as in Theorem 2.9 and Theorem 2.10 in Section 2.3.2.

We consider here the viscous rotating Boussinesq equations in the f-plane approximation in $\mathbb{R}^3$

$$\frac{\partial \boldsymbol{v}}{\partial t} + (\boldsymbol{v}\cdot\nabla)\boldsymbol{v} + f\boldsymbol{e_3}\times\boldsymbol{v} + \nabla p - \boldsymbol{e_3}b = \nu\Delta\boldsymbol{v} \tag{2.33a}$$
$$\nabla\cdot\boldsymbol{v} = 0 \tag{2.33b}$$
$$\frac{\partial b}{\partial t} + (\boldsymbol{v}\cdot\nabla)b - \frac{\mathrm{d}\bar{\rho}}{\mathrm{d}z}v_3 = \tilde{\nu}\Delta b\,, \tag{2.33c}$$

with velocity field $\boldsymbol{v}(t,\boldsymbol{x}) \in \mathbb{R}^3$ in space $\boldsymbol{x} \in \mathbb{R}^3$ and time $t \ge 0$, pressure and buoyancy $p(t,\boldsymbol{x})$, $b(t,\boldsymbol{x}) \in \mathbb{R}$, the Coriolis parameter $f \in \mathbb{R}$ with $f \neq 0$, the vertical unit vector $\boldsymbol{e_3}$,

viscosity parameter $\nu \geq 0$, thermal diffusivity $\tilde{\nu} \geq 0$, and reference density field $\bar{\rho}(z)$, where as usual we assume linear dependence on vertical space direction z for linear stratification. More specifically, the buoyancy satisfies $b(t, \boldsymbol{x}) = -g(\rho(t, \boldsymbol{x}) - \bar{\rho}(z))/\rho_0 \in \mathbb{R}$, with fluid density $\rho(t, \boldsymbol{x}) \in \mathbb{R}$, characteristic density ρ_0 and gravitational acceleration g, see e.g. Achatz (2006); Goh and Wayne (2019). We will focus on the viscous case $\nu, \tilde{\nu} > 0$, but briefly remark on the inviscid case $\nu = \tilde{\nu} = 0$.

If we allow the pressure p to grow unboundedly in space, then we note the Galileian invariance upon adding an arbitrary drift $\boldsymbol{c} \in \mathbb{R}^3$ and frequency ω. These terms we also have in the solutions of the form as in Theorem 2.3, Theorem 2.9 and Theorem 2.10, which we will study in the following sections. For these type of solutions this means

$$\boldsymbol{v}(t, \boldsymbol{x}) = \psi(t, \boldsymbol{k} \cdot \boldsymbol{x} - \omega t)\boldsymbol{a} + \boldsymbol{c}\,,$$

where the nonlinear term in the momentum equation (2.33a) becomes $(\boldsymbol{c} \cdot \boldsymbol{k}\frac{\partial \psi}{\partial \xi})\boldsymbol{a}$, with $\xi = \boldsymbol{k}\cdot\boldsymbol{x} - \omega t$ the phase variable of ψ, which is readily compensated by the time derivative term $-\omega \frac{\partial \psi}{\partial \xi}\boldsymbol{a}$ for $\omega = \boldsymbol{c} \cdot \boldsymbol{k}$. The remaining constant Coriolis term $f\boldsymbol{e_3} \times \boldsymbol{c}$ in (2.33a) creates the pressure $p = p_{\boldsymbol{c}}(x, y) := f(c_2 x - c_1 y)$, with $\boldsymbol{c} = (c_1, c_2, c_3)^\intercal$, which we will use in the following as well. If one wants to avoid the pressure to grow unboundedly in space, then one just has to consider $\boldsymbol{c} = 0$ in the upcoming sections.

2.3.1. Vanishing nonlinear advection term

In this section we consider solutions of the form as in Theorem 2.3 to the Boussinesq equations (2.33). This approach provides various explicit solutions, which can be divided into different classes of flows: the *horizontal plane flows*, *parallel flows*, *Kolmogorov flows* and *monochromatic inertia gravity waves*. In the following we will refer to each of this classes. Due to Theorem 2.5 the incompressibility condition (2.33b) is always satisfied. It remains to investigate the equations (2.33a) and (2.33c).

Horizontal plane flow

We first presume here the buoyancy b to be spatially dependent on z only. Then the buoyancy term in (2.33a) can be absorbed into the pressure gradient via the primitive B of b with $\frac{\mathrm{d}}{\mathrm{d}z}B = b$. Now we consider $\boldsymbol{v}$ of the form as in Theorem 2.3 with $N = 1$ and $M_1 = 1$, so only one wave shape $\psi_{1,1} = \psi$, wave vector $\boldsymbol{k}_{1,1} = \boldsymbol{k}$, flow direction $\boldsymbol{a}_1 = \boldsymbol{a}$ and temporal frequency $\omega_{1,1} = \omega$. Later we will see, that this assumption is covering all possible solutions of this kind here, so superpositions with other wave vectors or flow directions is not possible. In order to dispose of the remaining nonlinear term in (2.33c), we have to choose the velocity $\boldsymbol{v}$ to be barotropic, which means $v_3 \equiv 0$, so $a_3 = 0$. What remains are the decoupled linear equations with phase variable $\xi = \boldsymbol{k} \cdot \boldsymbol{x} - \omega t$ and

pressure $p = \tilde{p} + B + p_{\boldsymbol{c}}$,

$$\left(\frac{\partial\psi}{\partial t} - \nu|\boldsymbol{k}|^2\frac{\partial^2\psi}{\partial\xi^2}\right)\boldsymbol{a} = -f\psi\boldsymbol{e_3}\times\boldsymbol{a} - \nabla\tilde{p}$$

$$\frac{\partial b}{\partial t} - \tilde{\nu}\frac{\partial^2 b}{\partial z^2} = 0\,.$$

With the current assumptions it turns out that the left and right hand sides of the first equation must be in the direction $\boldsymbol{a}$ and constant in $\boldsymbol{x}$: Since the third components of $\boldsymbol{a}$ and $\boldsymbol{e_3}\times\boldsymbol{a}$ are zero, it follows that $\tilde{p}$ is z-independent. Orthogonality of $\boldsymbol{a}$ and $\boldsymbol{e_3}\times\boldsymbol{a}$ implies the form $\nabla\tilde{p}(t,x,y) = \hat{p}_1(t,x,y)\boldsymbol{a}+\hat{p}_2(t,x,y)\boldsymbol{e_3}\times\boldsymbol{a}$ and comparing coefficients yields $\hat{p}_1 = -\frac{\partial\psi}{\partial t} + \nu|\boldsymbol{k}|^2\frac{\partial^2\psi}{\partial\xi^2}$ and $\hat{p}_2 = -f\psi$. The latter implies ψ is independent of z, which means $k_3 = 0$ of $\boldsymbol{k}$ and $\boldsymbol{k}\cdot\boldsymbol{a} = 0$ from Theorem 2.3 gives $\boldsymbol{k} = r(-a_2, a_1, 0)^\intercal = r\boldsymbol{e_3}\times\boldsymbol{a}$, for arbitrary $r\in\mathbb{R}$. In the following, without loss of generality, we consider $r = 1$, since other values of r can be absorbed by the general form of the wave shape ψ. Together with $0 = \operatorname{curl}(\nabla\tilde{p}) = \operatorname{curl}(\hat{p}_1\boldsymbol{a} - f\psi\boldsymbol{e_3}\times\boldsymbol{a})$ it follows that $\hat{p}_1 = \hat{p}(t)$ is constant in $\boldsymbol{x}$. The case $\hat{p}_1\equiv 0$ implies geostrophic balance, since then the pressure $\tilde{p}$ is defined by the Coriolis term only.

Since we have shown that $k_3 = a_3 = 0$, this means the velocity $\boldsymbol{v}$ is purely horizontal. This implies our assumption $N = 1$ and $M_1 = 1$ in the beginning, due to the restriction onto a two-dimensional subspace and the orthogonality of the wave vectors and flow directions in Theorem 2.3. Furthermore, superpositions with different length of wave vectors and flow directions are included in the general form of the wave shape ψ as well.

In summary, any solutions to the one-dimensional heat equations

$$\frac{\partial\psi}{\partial t} - \nu|\boldsymbol{k}|^2\frac{\partial^2\psi}{\partial\xi^2} = -\hat{p}\,, \qquad \frac{\partial\tilde{b}}{\partial t} = \tilde{\nu}\frac{\partial^2\tilde{b}}{\partial z^2}\,, \tag{2.34}$$

with arbitrary spatially constant $\hat{p} = \hat{p}(t)$, give solutions to the Boussinesq equations (2.33), that we refer to as *horizontal plane flows*, via

$$\boldsymbol{v}(t,\boldsymbol{x}) = \psi(t,\boldsymbol{k}\cdot\boldsymbol{x}+\omega t)\boldsymbol{a} + \boldsymbol{c} \quad \text{with} \quad a_3 = 0\,, \quad \boldsymbol{k} = \boldsymbol{e_3}\times\boldsymbol{a}\,, \quad \omega = -\boldsymbol{c}\cdot\boldsymbol{k}\,, \tag{2.35a}$$

$$b(t,\boldsymbol{x}) = \tilde{b}(t,z)\,, \tag{2.35b}$$

$$\begin{aligned} p(t,\boldsymbol{x}) &= -f\Psi(t,\boldsymbol{k}\cdot\boldsymbol{x}+\omega t) + \hat{p}(t)\boldsymbol{a}\cdot\boldsymbol{x} + B(t,z) + p_{\boldsymbol{c}}(x,y) \\ &\text{with} \quad \frac{\partial\Psi}{\partial\xi} = \psi(t,\xi)\,, \quad \frac{\partial B}{\partial z} = b(t,z)\,. \end{aligned} \tag{2.35c}$$

Regarding the dimension of the set of solutions, for each nontrivial solution to (2.34) and due to its linear nature, we have a free choice of independent prefactors for ψ and $\tilde{b}$, that generates a two-dimensional set of solutions to (2.33). It is even three-dimensional when also counting the free direction of $\boldsymbol{a}$ with $a_3 = 0$ (translation and

Galilean invariance give 4 additional dimensions).

We emphasize that these horizontal plane flows arise from embedding solutions to the planar Navier–Stokes equations given by the first two components of $\boldsymbol{v}$ as above. Indeed, the velocity field $\boldsymbol{v}$ and buoyancy b do not interact since the velocity field is purely horizontal (no vertical dependence and component), while the buoyancy is purely vertical (independent of the horizontal directions). In Majda (2003) the same idea of vanishing nonlinearity is used and similar solutions are obtained. However, he considers a model without viscosity and Coriolis term.

In the inviscid case $\nu = \tilde{\nu} = 0$ the heat equations in (2.34) imply that ψ and $\tilde{b}$ can be chosen as arbitrary functions of ξ and z respectively. Furthermore, $\tilde{b}$ is independent of time and $\psi(t, \xi) = \psi_0(\xi) - \hat{P}(t)$ with $\hat{P}$ a primitive of $\hat{p}$. In case of $f = 0$ and $b \equiv 0$, the Boussinesq equations (2.33) become rotationally symmetric, so that the plane, on which the horizontal plane flows exist, can be rotated in any direction.

Parallel flow

Related, but differently oriented solutions of similar type arise from the parallel flow approach $\boldsymbol{v}(t, \boldsymbol{x}) = w(t, x, y)\boldsymbol{e_3}$, as done in Wang (1989) for the Navier–Stokes equations. Such a flow is divergence free and the nonlinear advection term $(\boldsymbol{v} \cdot \nabla)\boldsymbol{v}$ vanishes, as does the rotation term $f\boldsymbol{e_3} \times \boldsymbol{v}$. If b is also independent of z, then $p = p_0 z$ for some $p_0 \in \mathbb{R}$ and (2.33) reduces to the inhomogeneous linear system

$$\frac{\partial w}{\partial t} = \nu \Delta_h w + b - p_0 \,, \qquad \frac{\partial b}{\partial t} = \tilde{\nu} \Delta_h b + \frac{\mathrm{d}\bar{\rho}}{\mathrm{d}z} w \,,$$

with horizontal Laplacian Δ_h. Solutions can be written as the constant steady state $b = p_0, w = 0$ plus superposed Fourier modes that decay, and for large scales additionally oscillate in time for stable stratification ($\mathrm{d}\bar{\rho}/\mathrm{d}z$ constant and negative) according the linear dispersion relation; spatially constant modes oscillate in time with frequency $\sqrt{-\mathrm{d}\bar{\rho}/\mathrm{d}z}$. The difference to the horizontal plane flows (2.35) is not only the vertical velocity direction, but also the coupling of the velocity with the buoyancy. However, a superposition with horizontal plane flows (2.35) is in general not possible, since cross terms like

$$a_1 \psi \frac{\partial b}{\partial x} + a_2 \psi \frac{\partial b}{\partial y} + w \frac{\partial \tilde{b}}{\partial z}$$

remain in (2.33c) from $(\boldsymbol{v} \cdot \nabla)b$. An exception is the single mode parallel flow

$$w(t, x, y) = \hat{w}(t, \boldsymbol{k} \cdot \boldsymbol{x}) \,, \quad b(t, x, y) = \hat{b}(t, \boldsymbol{k} \cdot \boldsymbol{x}) \,,$$

for $\boldsymbol{k} = \boldsymbol{e_3} \times \boldsymbol{a}$, whose superposition with horizontal plane flows (2.35) that have $\tilde{b} \equiv 0$ yields an explicit solution.

The form $\boldsymbol{v}(t, \boldsymbol{x}) = w(t, x, y)\boldsymbol{e_3}$ of the parallel flow is more general as what can be constructed by Theorem 2.3, since it is not in plane wave form. In order to get parallel

flows of the form as in Theorem 2.3, one only has to choose $N = 1$ and $M_1 \geq 1$, as well as $\boldsymbol{a}_1 = \boldsymbol{e_3}$, arbitrary $\boldsymbol{k}_{1,\ell} \in \mathbb{R}^2 \times \{0\}$ and $\psi_{1,\ell} \in C^2(\mathbb{R}_{\geq 0} \times \mathbb{R}, \mathbb{R})$ for $1 \leq \ell \leq M_1$.

Kolmogorov flow

Another class of solutions are the Kolmogorov flows, as for instance presented in Balmforth and Young (2005) for the non-rotating Boussinesq equations. Here a time independent forcing of the single wave mode is implemented in the momentum equation (2.33a), but we disregard this for the moment.

Generally, for steady solutions of the form $\boldsymbol{v} = A\cos(k_1 x + k_3 z)\boldsymbol{a}$, the flow direction has to be $\boldsymbol{a} = (-k_3, 0, k_1)^\intercal$ and the pressure $p = A\nu|\boldsymbol{a}|^2 k_3/k_1 \cdot \sin(k_1 x + k_3 z)$. This yields the buoyancy as $b = A\nu|\boldsymbol{a}|^2(k_1 + k_3^2/k_1)\cos(k_1 x + k_3 z)$ and the amplitude A is either zero or the stratification is constrained to

$$\frac{\mathrm{d}\bar{\rho}}{\mathrm{d}z} = \nu\tilde{\nu}|\boldsymbol{a}|^4(1 + k_3^2/k_1^2)\,.$$

Hence, stable stratification (left-hand side negative) only allows for the trivial solution $A = 0$. Unstable stratification (left-hand side positive) permits nontrivial solutions with arbitrary amplitudes. In contrast to the parallel flows and the horizontal plane flows (2.35) these have vertical dependence and vertical velocity component, so that velocity and buoyancy are coupled. Superposition with the parallel flow or horizontal plane flow (2.35) do not yield explicit solutions, since their wave vectors and flow directions are not mutually orthogonal, so that cross terms remain from the nonlinear advection term. Note that viscosity and diffusion are required ($\nu\tilde{\nu} \neq 0$) for nontrivial Kolmogorov flow with buoyancy in the presence of stratification.

With forcing term $\boldsymbol{F} = AB\cos(k_1 x + k_3 z)\boldsymbol{a}$ of the same form as $\boldsymbol{v}$ and an amplitude factor B in addition to A, the solutions are adjusted slightly by the amplitude of the forcing, and nontrivial such solutions must satisfy

$$\frac{\mathrm{d}\bar{\rho}}{\mathrm{d}z} = \tilde{\nu}|\boldsymbol{a}|^2(\nu|\boldsymbol{a}|^2 - B)(1 + k_3^2/k_1^2)\,,$$

while the amplitude factor A of the solution is still arbitrary. In particular, this also allows for nontrivial solutions in the case of stable stratification and shows how forcing can influence the occurrence of steady solutions. In Section 2.4 we will study a more general form of forcing and the resulting steady solutions, as well as in Chapter 3 and Chapter 4 with simplified energy backscatter as forcing terms. Note that for $B \neq 0$ only $\tilde{\nu} \neq 0$ is required for a nontrivial flow of this type with buoyancy in the presence of stratification.

In order to obtain Kolmogorov flows from Theorem 2.3, one proceeds similar as for the horizontal plane flows, but with different orientation: One chooses $N = 1$ and $M_1 = 1$, as well as only one arbitrary wave vector $\boldsymbol{k}_{1,1} = \boldsymbol{k} \in \mathbb{R} \times \{0\} \times \mathbb{R}$ and flow direction $\boldsymbol{a}_1 = \boldsymbol{a} \in \mathbb{R} \times \{0\} \times \mathbb{R}$ with $\boldsymbol{k} \cdot \boldsymbol{a} = 0$. Due to the restriction onto a two-dimensional

subspace and the orthogonality condition, superposition is only possible in one wave vector direction, which is included in the general wave shape $\psi_{1,1} = \psi$.

Monochromatic intertia gravity waves

Other related single mode solution is the so-called monochromatic intertia gravity wave (MIGW), as described in Mied (1976); Drazin (1977) without rotation and in Yau et al. (2004); Achatz (2006) with Coriolis force $f \neq 0$. Notably, for $f = 0$ these have the same velocity form as the Kolmogorov flow, but with phase shifted buoyancy, and these have nonzero temporal frequency.

MIGWs exist in the inviscid case $\nu, \tilde{\nu} = 0$ and are traveling waves with nonzero velocity, depending on a phase variable $\xi = k_1 x + k_3 z - \omega t$ with nonzero squared frequency $\omega^2 = (-\frac{\mathrm{d}\bar{\rho}}{\mathrm{d}z} k_1^2 + f^2 k_3^2)/(k_1^2 + k_3^2)$. Again, the idea is to dispose of the nonlinear advection terms as in Theorem 2.3, but now the time-derivatives compensate the linear terms together with the pressure in case $f^2 \neq -\frac{\mathrm{d}\bar{\rho}}{\mathrm{d}z}$. Specifically, the velocity is $\boldsymbol{v} = A(\cos(\xi)\boldsymbol{a} - \frac{k_3 f}{\omega}\sin(\xi)\boldsymbol{e_2})$ with $\boldsymbol{a} = (-k_3, 0, k_1)^\intercal$ and $A \in \mathbb{R}$, the pressure $p = -Ak_3\frac{\omega^2 - f^2}{k_1 \omega}\cos(\xi)$ and the buoyancy $b = -A\frac{k_1}{\omega}\frac{\mathrm{d}\bar{\rho}}{\mathrm{d}z}\sin(\xi)$.

In the presence of viscosity with $\tilde{\nu} = \nu \neq 0$ the MIGWs turn from stationary into exponentially decaying solutions with the factor for each component given by $\exp(-\nu(k_1^2 + k_3^2)t)$. Exponentially decaying MIGWs with $\tilde{\nu} \neq \nu$ are not possible due to the coupling of velocity and buoyancy in this case.

Superposition with the parallel flow or horizontal plane flow (2.35) do not give explicit solutions due to the missing orthogonality of wave vectors ans flow directions, so that nonlinear cross terms remain, exactly as in the case with the Kolmogorov flow. However, for $f = 0$ and $\nu = \tilde{\nu} \neq 0$ the superposition of MIGW and Kolmorogov flow with the same flow direction $\boldsymbol{a}$ do not produce nonlinear cross terms, since wave vectors and flow directions are orthogonal. Thus, linear terms remain and the superposition of both flows is an explicit solution. Note that in this case the Kolmogorov flow is a steady flow, while the MIGW is exponentially decaying as mentioned above. We have not found such a constructed explicit solution elsewhere.

In order to obtain MIGWs from Theorem 2.3, we can choose $N = 2$ and $M_1 = M_2 = 1$, so that we have only one wave vector $\boldsymbol{k}_{1,1} = \boldsymbol{k}_{2,1} = \boldsymbol{k} \in \mathbb{R}\times\{0\}\times\mathbb{R}$ and two flow directions $\boldsymbol{a}_1 \in \mathbb{R} \times \{0\} \times \mathbb{R}$ with $\boldsymbol{k} \cdot \boldsymbol{a}_1 = 0$ and $\boldsymbol{a}_2 = \boldsymbol{e_2}$. Due to the three-dimensional space and the orthogonality condition, superposition is only possible in one wave vector direction, which is included in the general wave shapes $\psi_{1,1}$ and $\psi_{2,1}$.

2.3.2. Gradient nonlinear advection term

As already mentioned, another special case occurs, when the waves of the flow are interacting nonlinearly and producing a gradient advection term in the equations, as those from Theorem 2.9 and Theorem 2.10. It seems that Walsh (1992) was one of the first to notice that any divergence free Laplace eigenfunctions $\boldsymbol{u}_1$, $\boldsymbol{u}_2$ with the same

eigenvalue λ, i.e. the same wavelength, generate a solution $\boldsymbol{v}_1 + \boldsymbol{v}_2$ to the planar Navier–Stokes equations with viscosity ν and $\boldsymbol{v}_j = \exp(\nu\lambda t)\boldsymbol{u}_j$ for $j = 1, 2$. Due to this approach, the pressure gradient is given by the negative resulting nonlinear advection term. A simple case of this are the so-called *Taylor flows*. Beloshapkin et al. (1989); Majda and Bertozzi (2001) superpose sinusoidal plane waves with the same wave vector length by summation, while Hui (1987) uses integrals, and all of them are causing a gradient nonlinear advection term. As in the previous section, these immediately yield solutions to the rotating Boussinesq equations, similar to the horizontal plane flows (2.35) with decoupled bouyancy. In contrast to these horizontal plane flows, superposition give explicit solutions when using the same wave vector length, but arbitrary wave vector directions.

We will now reproduce such two-dimensional horizontal solutions from a plane wave viewpoint and additionally provide explicit profile of the pressure. Indeed, the pressure is usually not given explicitly in other works. For this purpose, analogous to the horizontal plane flows (2.35), we consider the barotropic case. This means, that the velocity $\boldsymbol{v}$ exists on the horizontal plane and the buoyancy b spatially depends on z only. Thus, the explicit solutions presented in this sections also fall into the category of horizontal plane flows, which we call the *interacting horizontal plane flows* here, due to the nonlinear interactions between the waves.

For better readability, we define here for any vector $\boldsymbol{k} \in \mathbb{R}^2$ the corresponding three-dimensional vectors $\tilde{\boldsymbol{k}} := (\boldsymbol{k}, 0)^\intercal \in \mathbb{R}^3$ and $\tilde{\boldsymbol{k}}^\perp := (\boldsymbol{k}^\perp, 0)^\intercal \in \mathbb{R}^3$. In order to create a gradient nonlinear advection term, we use the angular superposition principle for the considered plane flows as in Theorem 2.9. Since we consider only one horizontal two-dimensional linear subspace, we choose $N = 1$ and arbitrary $M_1 \geq 2$ in Theorem 2.9. It is similar to Majda and Bertozzi (2001), where superposition of arbitrary many plane waves with the same wave vector length is used to solve the planar Navier–Stokes equations. Inserting the velocity $\boldsymbol{v}$ of the form (2.22) with the assumptions above and the conditions in Theorem 2.9 into the Boussinesq equations (2.33) yields the remaining linear system of equations

$$\frac{\partial \boldsymbol{v}}{\partial t} - \nu\Delta\boldsymbol{v} = -f\boldsymbol{e_3} \times \boldsymbol{v} - \nabla\tilde{p}\,, \qquad \frac{\partial \tilde{b}}{\partial t} - \tilde{\nu}\frac{\partial^2 \tilde{b}}{\partial z^2} = 0\,,$$

$$p(t, \boldsymbol{x}) = \tilde{p}(t, \boldsymbol{x}) - h(t, \boldsymbol{x}) + B(t, z)\,,$$

with h defined as in (2.24) and $\frac{\partial B}{\partial z} = \tilde{b}(t, z)$. Similar as before, the left and right hand side of the first equation each have to be zero. The case $\nabla h \neq 0$ means there is no geostropic balance on the nonlinear level. Solving these linear equations yields the explicit solutions of (2.33) as interacting horizontal plane flows

$$\boldsymbol{v}(t,\boldsymbol{x}) = \mathrm{e}^{-\nu\mu^2 t}\sum_{\ell=1}^{M_1} A_\ell \sin(\xi_\ell)\tilde{\boldsymbol{k}}_\ell^\perp + \boldsymbol{c}\,, \tag{2.36a}$$

$$b(t,\boldsymbol{x}) = \tilde{b}(t,z)\,, \tag{2.36b}$$

$$\begin{aligned} p(t,\boldsymbol{x}) = {}& -\mathrm{e}^{-2\nu\mu^2 t}\sum_{\ell=1}^{M_1}\sum_{m=\ell+1}^{M_1} A_\ell A_m\Big(\cos\xi_\ell\cos\xi_m + \frac{\boldsymbol{k}_\ell\cdot\boldsymbol{k}_m}{\mu^2}\sin\xi_\ell\sin\xi_m\Big) \\ & - f\mathrm{e}^{-\nu\mu^2 t}\sum_{\ell=1}^{M_1} A_\ell\cos\xi_\ell + B(t,z) + f(c_2x - c_1y)\,, \end{aligned} \tag{2.36c}$$

with fixed wave vector length $\mu > 0$, phase variables $\xi_\ell := \tilde{\boldsymbol{k}}_\ell\cdot\boldsymbol{x} + \omega_\ell t$, wave vectors $\tilde{\boldsymbol{k}}_\ell \in \mathbb{R}^2\times\{0\}$ with $|\tilde{\boldsymbol{k}}_\ell| = \mu$, frequencies $\omega_\ell = -\boldsymbol{c}\cdot\tilde{\boldsymbol{k}}_\ell$ and arbitrary amplitudes $A_\ell\in\mathbb{R}$ for $1\le\ell\le M_1$, as well as buoyancy $\tilde{b}$ solving the heat equation $\frac{\partial\tilde{b}}{\partial t} = \tilde{\nu}\frac{\partial^2\tilde{b}}{\partial z^2}$ and spatial primitive B of $\tilde{b}$, i.e. $\frac{\partial B}{\partial z} = \tilde{b}(t,z)$. The signs $\delta_{\ell,m}$ from Theorem 2.9 are always $\delta_{\ell,m} = 1$ due to the choice of wave vectors and flow directions.

Analogous to Hui (1987), we may also superpose through an integral over the wave vectors with the same length. We can produce this kind of solutions by Theorem 2.10. Since the setting remains basically the same, we obtain for the flows of the form as in Theorem 2.10 and the assumptions above the same system of linear equations. Thus, the Boussinesq equations (2.33) have the interacting horizontal plane flow solutions

$$\boldsymbol{v}(t,\boldsymbol{x}) = \mathrm{e}^{-\nu\mu^2 t}\int\limits_{\substack{\boldsymbol{k}\in\mathbb{R}^2\\|\boldsymbol{k}|=\mu}} A(\boldsymbol{k})\sin(\tilde{\boldsymbol{k}}\cdot\boldsymbol{x} + \omega(\boldsymbol{k})t)\tilde{\boldsymbol{k}}^\perp\mathrm{d}\boldsymbol{k} + \boldsymbol{c}\,, \tag{2.37a}$$

$$b(t,\boldsymbol{x}) = \tilde{b}(t,z)\,, \tag{2.37b}$$

$$\begin{aligned} p(t,\boldsymbol{x}) = {}& -\mu^2\mathrm{e}^{-2\nu\mu^2 t}\int_0^{2\pi}\int_{\varphi_1}^{2\pi} A(\varphi_1)A(\varphi_2)\Big(\cos\xi(\varphi_1)\cos\xi(\varphi_2) + \ldots \\ & \qquad \ldots + \cos(\varphi_1-\varphi_2)\sin\xi(\varphi_1)\sin\xi(\varphi_2)\Big)\mathrm{d}\varphi_2\mathrm{d}\varphi_1 \\ & - f\mathrm{e}^{-\nu\mu^2 t}\int\limits_{\substack{\boldsymbol{k}\in\mathbb{R}^2\\|\boldsymbol{k}|=\mu}} A(\boldsymbol{k})\cos(\tilde{\boldsymbol{k}}\cdot\boldsymbol{x} + \omega(\boldsymbol{k})t)\mathrm{d}\boldsymbol{k} + B(t,z) + f(c_2x - c_1y)\,, \end{aligned} \tag{2.37c}$$

with fixed wave vector length $\mu > 0$, time frequencies $\omega(\boldsymbol{k}) = -\boldsymbol{c}\cdot\tilde{\boldsymbol{k}}$ and arbitrary amplitudes $A(\boldsymbol{k})\in\mathbb{R}$ for all $\boldsymbol{k}\in\mathbb{R}^2$ with $|\boldsymbol{k}| = \mu$, as well as buoyancy $\tilde{b}$ solving the heat equation $\frac{\partial\tilde{b}}{\partial t} = \tilde{\nu}\frac{\partial^2\tilde{b}}{\partial z^2}$ and spatial primitive B of $\tilde{b}$, i.e. $\frac{\partial B}{\partial z} = \tilde{b}(t,z)$. Regarding the notations from Theorem 2.10 we choose in the double integral of (2.37c) the orthonormal basis vectors $\boldsymbol{e}_1 = (1,0,0)^\intercal$, $\boldsymbol{e}_2 = (0,1,0)^\intercal$ and define the wave vectors

$$\tilde{\boldsymbol{k}}(\varphi) = (\boldsymbol{k}(\varphi),0)^\intercal := \mu(\cos(\varphi)\boldsymbol{e}_1 + \sin(\varphi)\boldsymbol{e}_2)\,,$$

amplitudes $A(\varphi) := A(\boldsymbol{k}(\varphi))$ and phase variables $\xi(\varphi) := \tilde{\boldsymbol{k}}(\varphi) \cdot \boldsymbol{x} + \omega(\boldsymbol{k}(\varphi))t$ for all $0 \leq \varphi \leq 2\pi$. Due to the choice of wave vectors and flow directions the signs from Theorem 2.10 are again always $\delta(\varphi) = 1$.

As for the horizontal plane flows (2.35), the velocity field $\boldsymbol{v}$ and buoyancy b in the interacting horizontal plane flows (2.36) and (2.37) do not influence each other. Thus, velocity $\boldsymbol{v}$ as above is also a solution to the rotating Navier–Stokes equations and the first two velocity components solve the planar Navier–Stokes equations.

We advert to the difference that radial superposition is possible for horizontal plane flows (2.35), while for interacting horizontal plane flows (2.36) and (2.37) angular superposition is used. As a consequence, the phase velocity $v_p = \omega/|\boldsymbol{k}|$ of the horizontal plane flows (2.35) is the same for all superposed traveling wave components. In contrast to that, the phase velocity of the interacting horizontal plane flows (2.36) and (2.37) is different for each superposed traveling wave component, since the temporal frequencies $\omega(\boldsymbol{k})$ change according the wave vector direction $\boldsymbol{k}$, while the wave numbers $|\boldsymbol{k}|$ remain unchanged.

As a dimension count for interacting horizontal plane flows (2.36) with fixed M_1, for each solution b to the heat equation we note that the free amplitudes A_ℓ and free scaling of b generate an $M_1 + 1$ dimensional set. The wave vectors $\boldsymbol{k}_\ell \in \mathbb{R}^2$ of the same length μ form a one-dimensional set for each plane wave component. Together with the free constant phase shifts for each plane wave we have a $3M_1 + 1$ dimensional set of explicit solutions of the equations (2.33) (this includes translation; Galilean invariance gives additional 3 dimensions). In contrast, the interacting horizontal plane flows (2.37) form an overall infinite dimensional set of solutions, since any wave vector direction is considered.

In the inviscid case $\nu = \tilde{\nu} = 0$ the remaining heat equation for $\tilde{b}$ and the factor $\exp(-\nu\mu^2 t)$ of $\boldsymbol{v}$ imply time-independence for the interacting horizontal plane flows (2.36) and (2.37). Hence, there is no decay and b is an arbitrary function of z. Furthermore, in case $f = 0$ and $b \equiv 0$, one obtains rotation symmetry in the Boussinesq equations (2.33), so that the plane, on which the interacting horizontal plane flows exist, can be rotated in any direction.

2.4. Explicit solutions with adapted forcing

In this section we consider incompressible fluid equations with a certain forcing. With the functions presented in Section 2.1 we can determine explicit solutions of such forced nonlinear fluid equations. Here we consider an n-dimensional incompressible fluid equation of the form

$$\frac{\partial \boldsymbol{v}}{\partial t} + (\boldsymbol{v} \cdot \nabla)\boldsymbol{v} = -\nabla p + \mathcal{L}\boldsymbol{v} + \boldsymbol{F} \tag{2.38a}$$

$$\nabla \cdot \boldsymbol{v} = 0\,, \tag{2.38b}$$

with a linear differential operator in space $\mathcal{L}$ and a forcing $\boldsymbol{F} = \boldsymbol{F}(t, \boldsymbol{x})$. Here we allow $\mathcal{L}$ to be more general than a pure Laplacian, similar to Chae and Dubovskiĭ (1996), in order to highlight the broader application. This can be for instance kinetic energy backscatter as in Jansen and Held (2014) and presented here in Chapter 3 and Chapter 4, or stress tensors as in some non-Newtonian fluids, e.g. Chhabra (2010). Thus, this section gives us a first impression about the influence of forcing and linear differential operators on the explicit solutions, their stability and on the dynamics in backscatter models, which we will study in the following chapters.

Based on vanishing or gradient nonlinear terms, we can generate explicit solutions to (2.38) in the presence of suitable forcing. This means, in the same way as shown in Section 2.2 and Section 2.3, we can use the functions presented in Section 2.1 in order to find solutions of the full nonlinear equations (2.38) by reducing it to the linear inhomogeneous equation

$$\frac{\partial \boldsymbol{v}}{\partial t} = \mathcal{L}\boldsymbol{v} + \boldsymbol{F}\,. \tag{2.39}$$

To be more precise, we consider functions $\boldsymbol{F}$ and $\boldsymbol{v}$ in the form as in Theorem 2.3 or Theorem 2.9 respectively, and choose $\boldsymbol{c} = 0$ for simplicity. We note that simpler solutions and forcing in this context has been considered, e.g. in Meshalkin and Sinai (1961); Beloshapkin et al. (1989); Balmforth and Young (2005). Substitution of velocities in the form as in Theorem 2.3 or Theorem 2.9 into (2.38a) yields the inhomogeneous linear equation (2.39), after the pressure gradient compensates the possibly emerging gradient nonlinear advection terms. Note that (2.38b) is also satisfied due to Theorem 2.5 and Theorem 2.11.

We assume that $\mathcal{L}$ generates a semigroup $\mathrm{e}^{\mathcal{L}t}$ and that this respects the form described in Theorem 2.3 or Theorem 2.9 respectively. For instance, $\mathcal{L}$ may consist of differential operators with constant coefficients, such as the already used viscosity term $\mathcal{L} = \nu\Delta$, which yields the heat-semigroup. The homogeneous solution then reads

$$\boldsymbol{v}_{\mathrm{hom}}(t, \boldsymbol{x}) = \left(\mathrm{e}^{\mathcal{L}t}\boldsymbol{v}_0\right)(\boldsymbol{x})\,, \quad t \geq 0\,,$$

and has the form as in Theorem 2.3 or Theorem 2.9 respectively, if the initial condition $\boldsymbol{v}_0$ also has such form. We then solve the inhomogeneous equation with the particular solution

$$\boldsymbol{v}_{\mathrm{p}}(t, \boldsymbol{x}) = \int_0^t \mathrm{e}^{\mathcal{L}(t-s)}\boldsymbol{F}(s, \boldsymbol{x})\mathrm{d}s\,,$$

assuming that the forcing $\boldsymbol{F}$ is such that this integral exists. Then (2.39) with the initial condition $\boldsymbol{v}_0$ possesses the solution

$$\boldsymbol{v}(t, \boldsymbol{x}) = \boldsymbol{v}_{\mathrm{hom}}(t, \boldsymbol{x}) + \boldsymbol{v}_{\mathrm{p}}(t, \boldsymbol{x}) = \left(\mathrm{e}^{\mathcal{L}t}\boldsymbol{v}_0\right)(\boldsymbol{x}) + \int_0^t \mathrm{e}^{\mathcal{L}(t-s)}\boldsymbol{F}(s, \boldsymbol{x})\mathrm{d}s\,. \tag{2.40}$$

The key observation is, that (2.40) is indeed a solution to the nonlinear equation (2.38a)

as well, whenever $\boldsymbol{F}$ has the form as in Theorem 2.3 or Theorem 2.9 respectively, together with the initial condition $\boldsymbol{v}_0$. Furthermore, this ensures that $\boldsymbol{v}$ is divergence free due to Theorem 2.5 and Theorem 2.11, i.e. (2.38b) is also satisfied. In other words, the dynamics of the forced nonlinear equations (2.38) for initial data and forcing under the above constraints is linear.

As usual for inhomogeneous linear equations, if the forcing $\boldsymbol{F}$ is in addition time independent and lies in the range of $\mathcal{L}$, then any preimage $\boldsymbol{v}_s = -\mathcal{L}^{-1}\boldsymbol{F}$ is a steady state of (2.39). This implies that $\boldsymbol{w} = \boldsymbol{v} - \boldsymbol{v}_s$ solves the homogeneous equation $\boldsymbol{w}_t = \mathcal{L}\boldsymbol{w}$ for any solution $\boldsymbol{v}$ of (2.39). This means we have $\boldsymbol{w} = \mathrm{e}^{\mathcal{L}t}\boldsymbol{w}_0$ with $\boldsymbol{w}_0 = \boldsymbol{v}_0 - \boldsymbol{v}_s$, so that (2.40) can be cast as $\boldsymbol{v} = \mathrm{e}^{\mathcal{L}t}(\boldsymbol{v}_0 - \boldsymbol{v}_s) + \boldsymbol{v}_s$. The stability of any such steady state $\boldsymbol{v}_s$ within the linear subspace created by the functions from Theorem 2.3 or Theorem 2.9, respectively, is thus directly determined by spectral properties of the linear operator $\mathcal{L}$. The simplest case of forcing is an eigenfunction $\boldsymbol{F}$ of $\mathcal{L}$ with nonzero real eigenvalue, $\mathcal{L}\boldsymbol{F} = \lambda^{-1}\boldsymbol{F}$ with $\lambda \in \mathbb{R}$ and $\lambda \neq 0$, for which $\boldsymbol{v}_s = -\lambda\boldsymbol{F}$ gives a stationary solution to (2.39) and to (2.38).

We explain the last results with the simple case $\mathcal{L} = \nu\Delta$ and a time-independent forcing $\boldsymbol{F}(\boldsymbol{x})$. A well known example for explicit solutions in this case is the aforementioned Kolmogorov flow, as for instance studied regarding stability properties in a non-rotating Boussinesq setting in Balmforth and Young (2002, 2005). We consider $\boldsymbol{a}_F$, $\boldsymbol{k}_F \in \mathbb{R}^n$ and

$$\mathcal{L} = \nu\Delta\,, \quad \boldsymbol{F}(\boldsymbol{x}) = \int_0^\infty A_F(\xi)\sin(\xi\boldsymbol{k}_F\cdot\boldsymbol{x})\mathrm{d}\xi\,\boldsymbol{a}_F \qquad \text{with} \quad |\boldsymbol{k}_F| = 1\,, \quad \boldsymbol{a}_F\cdot\boldsymbol{k}_F = 0\,,$$

with integrable amplitude function $A_F : \mathbb{R}_{\geq 0} \to \mathbb{R}$, so that

$$\int_0^1 |A_F(\xi)|\mathrm{d}\xi + \int_1^\infty \xi^2|A_F(\xi)|\mathrm{d}\xi < \infty\,.$$

Let $\boldsymbol{v}_0$ be an initial condition of the analogous form with $\boldsymbol{a}_0$, $\boldsymbol{k}_0 \in \mathbb{R}^n$ and

$$\boldsymbol{v}_0(\boldsymbol{x}) = \int_0^\infty A_0(\xi)\sin(\xi\boldsymbol{k}_0\cdot\boldsymbol{x})\mathrm{d}\xi\,\boldsymbol{a}_0 \quad \text{with} \quad |\boldsymbol{k}_0| = 1\,, \quad \boldsymbol{a}_0\cdot\boldsymbol{k}_0 = \boldsymbol{a}_0\cdot\boldsymbol{k}_F = \boldsymbol{a}_F\cdot\boldsymbol{k}_0 = 0\,,$$

and integrable amplitude function $A_0 : \mathbb{R}_{\geq 0} \to \mathbb{R}$ satisfying the same bound as A_F. Then the corresponding solution of (2.39), given by (2.40), can be written as

$$\boldsymbol{v}(t,\boldsymbol{x}) = \int_0^\infty \mathrm{e}^{-\nu\xi^2 t}A_0(\xi)\sin(\xi\boldsymbol{k}_0\cdot\boldsymbol{x})\mathrm{d}\xi\,\boldsymbol{a}_0 + \int_0^t\int_0^\infty \mathrm{e}^{-\nu\xi^2(t-s)}A_F(\xi)\sin(\xi\boldsymbol{k}_F\cdot\boldsymbol{x})\mathrm{d}\xi\mathrm{d}s\,\boldsymbol{a}_F\,.$$

Alternatively, using the steady particular solution of (2.39) given by

$$\boldsymbol{v}_s(\boldsymbol{x}) = \int_0^\infty \frac{A_F(\xi)}{\nu\xi^2}\sin(\xi\boldsymbol{k}_F\cdot\boldsymbol{x})\mathrm{d}\xi\,\boldsymbol{a}_F\,,$$

and additionally assuming sufficiently quick decay of the amplitudes A_F near $\xi = 0$, the

solution above can be reformulated as

$$\boldsymbol{v}(t,\boldsymbol{x}) = \boldsymbol{v}_s(\boldsymbol{x}) + \int_0^\infty \mathrm{e}^{-\nu\xi^2 t}\left(A_0(\xi)\sin(\xi\boldsymbol{k}_0\cdot\boldsymbol{x})\boldsymbol{a}_0 - \frac{A_F(\xi)}{\nu\xi^2}\sin(\xi\boldsymbol{k}_F\cdot\boldsymbol{x})\boldsymbol{a}_F\right)\mathrm{d}\xi\,.$$

It is an explicit solution of (2.39) and (2.38), since the nonlinear advection term vanishes with this choice of wave vectors, as well as flow and forcing directions. To be more precise, this solution is of the form as in Theorem 2.3. The last equation in particular shows, that for this forcing $\boldsymbol{F}$ the unique (up to a constant) bounded equilibrium state $\boldsymbol{v}_s(\boldsymbol{x})$ of (2.39) is asymptotically stable within the subspace of linear dynamics for (2.38).

The velocity $\boldsymbol{v}$ is constructed here as in Theorem 2.3 with $N = 2$ and $M_1 = M_2 = 1$, so at most two flow directions and two wave vector directions, and one part of it is produced by the forcing $\boldsymbol{F}$ with $N = 1$ and $M_1 = 1$, so one direction each. The superposition over different wavelength, which produces different eigenvalues and rate of decay, is realized by the general form of the wave shapes $\psi_{1,1}$ and $\psi_{2,1}$ in Theorem 2.3. Thus, the solutions here are comparable to the presented solutions of the usual unforced Navier–Stokes equations (2.30) in Section 2.2.1 with arbitrary dimension $n \geq 2$. According to the properties of the solutions in the form as in Theorem 2.3, it is also possible to use several forcing terms with different directions, as long as the orthogonality conditions are satisfied. As mentioned in Remark 2.10.1 and Remark 2.11.2, integration over the different directions instead of summation is possible.

In the similar way as shown above, one can also construct forcing $\boldsymbol{F}$ and velocity $\boldsymbol{v}$ in the form as in Theorem 2.10, which create a gradient nonlinear advection term. Instead of integrating over different wave numbers and the same wave vector direction, one integrates over the same wave number and different wave vector directions on a plane, or several planes in case of $n > 3$. The arising nonlinear term in (2.38) is a gradient and compensated by the pressure gradient, so that the linear inhomogeneous equation (2.39) remains again. Such solutions are comparable with those in the unforced setting in Section 2.2.2, where summation is used for superposition instead of an integral.

Remark 2.11.4. In (2.39) we assumed the pressure gradient precisely cancels the possibly arising nonlinear advection term. However, a gradient term $\nabla\tilde{p}$ can remain, if it has the plane wave form. This gradient term can be combined with the forcing term $\boldsymbol{F}$ and results to the new forcing $\tilde{\boldsymbol{F}} = \boldsymbol{F} - \nabla\tilde{p}$. In the simplest case we require $\tilde{p} := \gamma\Psi(\boldsymbol{k}_F\cdot\boldsymbol{x})$ with $\frac{\partial\Psi}{\partial\xi} = \psi$. We then choose $\boldsymbol{F} := \psi(\boldsymbol{k}_F\cdot\boldsymbol{x})\boldsymbol{a}_\gamma$ with $\boldsymbol{a}_\gamma := \boldsymbol{a}_F + \gamma\boldsymbol{k}_F$. It follows $\tilde{\boldsymbol{F}} = \psi(\boldsymbol{k}_F\cdot\boldsymbol{x})\boldsymbol{a}_F$, so we have the same situation as above and can proceed in the same way.

We remark that Chae and Dubovskiĭ (1996) find travelling wave-like solutions in an n-dimensional space with linear forcing term as well. In contrast to our solutions, the forcing is a time dependent factor of the velocity.

We can also use the results of this section in the Boussinesq equations with similar forcing in the momentum equation (2.33a). As for the horizontal plane flows (2.35),

as well as the interacting horizontal plane flows (2.36) and (2.37), the velocity and the buoyancy are decoupled by a suitable choice of wave vector and flow directions, so that a two-dimensional version of (2.38) with Coriolis term remains. The Coriolis term can also be compensated by the pressure gradient, as for the (interacting) horizontal plane flows. A case of solutions of the forced Boussinesq equations with coupled buoyancy and velocity is the aforementioned Kolmogorov flow.

2.5. Comparison and classification of explicit solutions

After the investigation of explicit solutions in Section 2.2 and Section 2.3 constructed by functions presented in Section 2.1, we now compare them with already known explicit solutions. For the Boussinesq equations we have already shown in Section 2.3.1 that some of the solutions can be identified as parallel flows (Wang, 1989), Kolmogorov flows (Balmforth and Young, 2005) or monochromatic inertia gravity waves (Mied, 1976; Yau et al., 2004). Solutions in Section 2.2.1 of the Navier–Stokes and the Euler equations fall into the class of parallel flow (Wang, 1989) or the two-dimensional flow with cross flow (Weinbaum and O'Brien, 1967) in case of three dimensions $n = 3$. Those in Section 2.2.2 and $n = 3$ are two-dimensional explicit solutions as in Walsh (1992), which can be rotated in space.

Here we will shortly exhibit some more explicit solutions of different fluid models that are known and indicate the similarities and differences regarding our explicit solutions presented in the last sections. We also point out, to the best of our knowledge, what is new about our explicit solutions in this thesis.

Before we start, we present more general classes of solutions of fluid equations, which numerous solutions belong to. In two- and three-dimensional spaces $n \in \{2, 3\}$ the class of *generalized Beltrami flows* (Wang, 1990; Drazin and Riley, 2006) is defined by solutions of fluid equations, which satisfy the condition

$$\operatorname{curl}(\boldsymbol{v} \times \operatorname{curl}(\boldsymbol{v})) = 0\,, \tag{2.41}$$

with $\operatorname{curl}(\boldsymbol{F}) = \nabla \times \boldsymbol{F}$ for a vector valued function $\boldsymbol{F} : \mathbb{R}^3 \to \mathbb{R}^3$. For $n = 2$ the function $\boldsymbol{F}$ is just independent of the vertical variable z and the third component F_3 is zero, resulting in $\operatorname{curl}(\boldsymbol{F})$ having the first two components equal zero and a nonzero third component. The condition (2.41) comes from the often used decomposition of the velocity field into an irrotational (gradient) part and a divergence-free (rotational) part, also known as *Helmholtz decomposition*, see e.g. Gregory (1996). Due to this, one often disregards the irrotational gradient part of the momentum equation of a fluid model by taking the curl of this equation and solving the remaining problem in terms of the rotational part of the velocity field, also called *vorticity* (see e.g. Wang, 1990; Drazin and Riley, 2006). Another class is defined, when the argument of the outer curl in (2.41)

is zero, i.e.

$$\boldsymbol{v} \times \operatorname{curl}(\boldsymbol{v}) = 0\,. \tag{2.42}$$

Velocity fields solving (2.42) are called *Beltrami flows*.

It turns out, that for $n \in \{2, 3\}$ the solutions of the form as in Theorem 2.3 with $N = 1$ and $M_1 \geq 1$ or $N = 2$ and $M_1 = M_2 = 1$, as well as those of the form as in Theorem 2.9 and Theorem 2.10 with $N = 1$ and $M_1 \geq 1$, are all generalized Beltrami flows, but no Beltrami flows. See Appendix A for a proof of this statement. We also note another class, the so-called *extended Beltrami flows*, presented in Dyck and Straatman (2020) for the Navier–Stokes equations, to which our solutions in this thesis do not belong as well.

We now turn to the discussion about the relations between the explicit solutions presented in this chapter and known solutions in the literature in some more detail. We first consider solutions of the Euler and Navier–Stokes equations and in the end those of the Boussinesq equations.

We begin with the 2D Euler equations, for which Majda and Bertozzi (2001) characterize in Prop. 2.2 solutions by a nonlinear Poisson equation for the stream function. Weinbaum and O'Brien (1967); Wang (1989, 1990) analogously consider such solutions of the 2D Navier–Stokes equations. In Hui (1987) even an y-dependent linear term is added, causing the solutions to exist on a special co-moving frame. The solutions presented in Section 2.2.1 intersect these sets, but also arise in higher dimensions. Primarily, they generally do not satisfy the conditions of stream function and vorticity, in particular $\Delta\psi(t, x) = F(\psi(t, x))$ from Majda and Bertozzi (2001). These conditions do not allow the superposition of explicit plane wave solutions with different wave length, which is indeed possible for the solutions we have presented. In particular, we found out that the 'only if' in Prop. 2.2 in Majda and Bertozzi (2001) is too strong.

Regarding superpositions, in Hui (1987); Beloshapkin et al. (1989) as well as Majda and Bertozzi (2001) in Prop. 2.5 nonlinear solutions are also generated by superposition of explicit solutions, namely arbitrary superposition of eigenmodes with the same Laplacian eigenvalue (the same eigenvalue arises when the wave length is the same), see also Walsh (1992). This kind of superposition is similar to the angular superposition as in Theorem 2.9 and Theorem 2.10, used in Section 2.2.2. In comparison, the radial superposition as in Theorem 2.3 is different and much more restricted in the directions. However, the superposed solutions in Section 2.2.1 exist for any space dimension, and more importantly, these may be superposed waves with different wave lengths and (certain) different directions, which even have arbitrary wave shapes in case of the Euler equations.

Another example for explicit solutions obtained by superpositions of several flows is presented in Kambe (1986). These consist of a straining flow superposed with several shear flows. Two shear layers can merge to a single one or cancel each other out over

time, depending on the shear layers to be parallel or antiparallel. These differ from the solutions and superpositions that are presented in this thesis, which on the one hand even do not interact at all in the case of the solutions in Section 2.2.1. On the other hand, the plane waves of the interacting flows in Section 2.2.2 relate to each other by wave length and temporal growth-rate, but without merging or canceling.

The well-known parallel flows (see Wang (1989) for a general form for the Navier–Stokes equations) consist of a horizontally dependent vertical flow, which also yields solutions to the rotating Boussinesq equations as shown in Section 2.3.1. However, the horizontal plane flows (2.35) that we identify are differently oriented in the Boussinesq case and depend on a one-dimensional phase variable.

Weinbaum and O'Brien (1967) present generalized Beltrami flows to the Navier–Stokes equations, which are two-dimensional solutions with cross flow or axially symmetric solutions with swirl. They also allow non-constant coefficients for their solutions. Our solutions in Section 2.2.1 for $n = 3$ and $N = 2$ belong to these two-dimensional solutions with cross flow. Weinbaum and O'Brien (1967) also present a cross flow that solves a heat equation forced by a constant pressure gradient. We investigate more general forcing in Section 2.4, which can also affect the pressure (see Remark 2.11.4).

For the 3D incompressible Navier–Stokes equations Chai et al. (2020) derive explicit generalized Beltrami flow solutions with the helical decomposition, which are explicit steady solutions in the 3D Euler equations. These solutions can be understood as a superposition of interacting solutions as in Section 2.2.2 and adjusted parallel flows.

For the Navier–Stokes equations in $\mathbb{R}^n$, $n \geq 2$, and more general linear operators that may also act as forcing, Chae and Dubovskiĭ (1996) find travelling wave-like solutions with single wave vector. For $n = 3$ and usual viscosity Beloshapkin et al. (1989) use a superposition of wave modes with different wave vectors but same wave length for steady forcing and the solutions. In contrast, the superpositions we allow for can be in integral form and for different wave lengths, but restricted directions. We also allow for different type of forcing as discussed in Section 2.4.

Concerning the inviscid rotating 3D Boussinesq equations, Majda (2003) finds solutions with unbounded and spatially linear velocities and pressure (Theorem 2.4 and Theorem 2.7 therein) and also various plane wave-type solutions in the non-rotating case. With rotation and including viscosity, the horizontal plane flows (2.35) are barotropic and geostrophically balanced Rossby-type waves (for the case $\hat{p} \equiv 0$), while the interacting horizontal plane flows (2.36) are unbalanced and general solutions for the same Laplacian eigenvalue. Similar, but different from these, are the unbalanced MIGW (Yau et al., 2004; Achatz, 2006), as discussed in Section 2.3.1.

Lastly, we note that explicit generalized Beltrami flows need not be of (superposed) plane wave form, in particular the explicit Lamb-Oseen vortices are parabolic self-similar solutions (Gallay and Wayne, 2005; Goh and Wayne, 2019).

To the best of our knowledge, the identification of explicit superposed plane wave-type solutions with arbitrary wave lengths in (certain) different directions and in any dimen-

sion has not been done before. The same holds for the explicit solutions constructed by angular superpositions for any dimension, even though for $n \geq 4$ it is realized by splitting the space into two-dimensional subspaces. We also have not seen the explicit representation of solutions, that produce gradient nonlinear advection terms, with the corresponding explicit pressure elsewhere, as well as the investigation of such explicit solutions with a more general type of adjusted forcing.

Furthermore, our plane wave approach for vanishing or gradient advection terms with possible superpositions can be a useful tool for analyzing and determining explicit solutions in fluid models. Due to this, we have identified an explicit superposition of MIGW and Kolmogorow flow, that we have not found elsewhere (see end of Section 2.3.1).

In this chapter we have already seen, how the functions presented in Section 2.1 can be used in order to find explicit solutions in different fluid equations. In Chapter 3 and Chapter 4 we will additionally see, how these functions can be used for analyzing the stability of solutions as well.

3. Explicit Flows and Growth in Geophysical Fluid Models with simplified Backscatter

After the investigation of explicit solutions in various fluid models in Chapter 2, and the impact of more general linear terms as well as forcing on them in Section 2.4, we now turn to geophysical fluid models with simple energy backscatter. More precisely, we consider here the rotating shallow water equations and the rotating Boussinesq equations. We augment both models by simplified backscatter terms. These terms are motivated by the backscatter subgrid parameterization, which is used to ensure energy consistency in numerical simulations of geophysical flows in the oceans (see e.g. Jansen and Held (2014); Zurita-Gotor et al. (2015); Jansen et al. (2019); Juricke et al. (2020); Perezhogin (2020) as well as the introduction in Section 1.1). Therefore, we choose the hyperviscosity as dissipation in these models, which is realized by a negative bi-Laplace operator, and as linear forcing term we use a negative Laplace operator, which is reinjecting energy back into the system. A linear forcing term in the equations leads to the presumption, that the trivial zero solution may be linearly unstable (see e.g. Prugger (2017)).

In fact, we are even able to show more than that: It turns out, that the models we consider here contain explicit solutions of the kind as described in Section 2.1. The hyperviscosity and the backscatter determine the growth rates of such explicit flows and some of them may even grow unboundedly in time. Furthermore, due to the possible radial or angular superposition of these solutions, we are able to show a kind of *unbounded instability* of the trivial flow, where certain infinitesimal perturbations of this state grow unboundedly in time. This kind of instability is not only restricted to the trivial solution, but also extends to some nontrivial explicit steady solutions, which arise in the presence of hyperviscosity and backscatter, and even to some explicit solutions decaying exponentially in time.

In this chapter we study the occurrence, stabilities and further properties of explicit solutions as presented in Section 2.1 in geophysical fluid models with hyperviscosity and simplified backscatter. We start our investigations with the rotating shallow water equations in Section 3.1 and then move to the rotating Boussinesq equations in Section 3.2. As shown in Section 2.2 and Section 2.3, the considered types of solutions simultaneously solve the nonlinear equations and the linear equations that arise by dropping the nonlinear advection term. As a result, we obtain explicit solutions of the nonlinear problem, which form certain linear solution spaces. These include analogues of (interacting) horizontal plane flows, parallel flows, Kolmogorov flows as well as monochromatic inertia

gravity waves (cf. Yau et al., 2004; Balmforth and Young, 2005; Achatz, 2006; Prugger and Rademacher, 2021), which are also discussed in Section 2.3 for the usual rotating Boussinesq equations. Our approach is essentially based on direct computations, though these are at times somewhat tedious.[1]

3.1. Rotating schallow water equations with backscatter

We consider here the rotating shallow water equations with flat bottom topography in the f-plane approximation, in which the usual viscosity is replaced by hyperviscosity and backscatter

$$\frac{\partial \boldsymbol{v}}{\partial t} + (\boldsymbol{v}\cdot\nabla)\boldsymbol{v} = -f\boldsymbol{v}^{\perp} - g\nabla\eta - \begin{pmatrix} d_1\Delta^2 + b_1\Delta & 0 \\ 0 & d_2\Delta^2 + b_2\Delta \end{pmatrix}\boldsymbol{v}\,, \tag{3.1a}$$

$$\frac{\partial \eta}{\partial t} + (\boldsymbol{v}\cdot\nabla)\eta = -(H_0+\eta)\mathrm{div}(\boldsymbol{v})\,, \tag{3.1b}$$

where $\boldsymbol{v} = \boldsymbol{v}(t,\boldsymbol{x}) \in \mathbb{R}^2$ is the velocity field on the whole space $\boldsymbol{x} \in \mathbb{R}^2$ at time $t \geq 0$ and $\eta = \eta(t,\boldsymbol{x}) \in \mathbb{R}$ is the deviation of the fluid layer from the characteristic fluid depth $H_0 > 0$, giving $H_0 + \eta$ as the fluid layer thickness. In addition, $f \neq 0$ is the constant Coriolis parameter, $g > 0$ the gravity acceleration, d_1, $d_2 > 0$ the hyperviscosity or hyperdiffusion parameters and b_1, $b_2 > 0$ the backscatter parameters.

While the physically natural situation is horizontally isotropic backscatter, $d_1 = d_2$, $b_1 = b_2$, we also allow for (weak) anisotropy here. Our motivation for this is to account for an effective anisotropy from the numerical backscatter scheme due to the combination of an anisotropic grid, spatially anisotropic coefficients and the application of filtering (see e.g. Danilov et al., 2019). It turns out that among the phenomena we find, the only one which requires anisotropic backscatter are explicit growing and certain decaying flows in (3.1). However, here the anisotropy can be arbitrarily weak, i.e. $|d_1 - d_2| + |b_1 - b_2|$ can be arbitrarily small. As expected, the consideration of anisotropic backscatter often provide more flexibility, but in the Boussinesq equations (3.21) later in Section 3.2, all general phenomena that we find and consider occur also in the isotropic case.

Remark 3.0.1. We note that the gradient term $\nabla\eta$ in the momentum equation (3.1a) is restricted by (3.1b) this time, in contrast to the free choice of gradient term ∇p in the Navier–Stokes equations (2.30) and the Boussinesq equations (2.33). This additional constraint on the gradient term prevents the use of the angular superposition principle as in Theorem 2.9 and Theorem 2.10, since they create a gradient nonlinear term, which cannot be compensated by $\nabla\eta$ in this case.

We first identify certain explicit flows. According to Theorem 2.3 without superposition ($N = M_1 = 1$), the inviscid rotating shallow water equations without backscatter,

[1] The main results presented in this chapter have been published in Prugger et al. (2022a)

i.e. $b_1 = b_2 = d_1 = d_2 = 0$, possess the explicit plane wave steady solutions

$$\boldsymbol{v} = \phi'(\boldsymbol{k}\cdot\boldsymbol{x})\boldsymbol{k}^\perp\,, \qquad \eta = \frac{f}{g}\phi(\boldsymbol{k}\cdot\boldsymbol{x})\,,$$

for any wave vector $\boldsymbol{k} \in \mathbb{R}^2$ and sufficiently smooth wave shape ϕ. These are also in geostrophic balance, i.e. pressure gradient and Coriolis term are in balance, corresponding to the so-called Rossby waves.

For the case with hyperviscosity and backscatter in (3.1) we seek solutions of the form

$$\boldsymbol{v} = \psi(t, \boldsymbol{k}\cdot\boldsymbol{x})\boldsymbol{k}^\perp\,, \qquad \eta = \frac{f}{g}\phi(\boldsymbol{k}\cdot\boldsymbol{x})\,, \tag{3.2}$$

for any wave vector $\boldsymbol{k} = (k_x, k_y)^\intercal \in \mathbb{R}^2$ and sufficiently smooth wave shapes ψ and ϕ. The time-independence of η results from (3.1b), since $\boldsymbol{v}$ is divergence free as noted in Theorem 2.5 and the advection term vanishes due to the orthogonality of the wave vector of η and the flow direction. Inserting (3.2) into (3.1a) yields the linear equation

$$\frac{\partial\psi}{\partial t}\boldsymbol{k}^\perp + f\left(\frac{\partial\phi}{\partial\xi} - \psi\right)\boldsymbol{k} = -|\boldsymbol{k}|^2 \begin{pmatrix} d_1|\boldsymbol{k}|^2\dfrac{\partial^4\psi}{\partial\xi^4} + b_1\dfrac{\partial^2\psi}{\partial\xi^2} & 0 \\ 0 & d_2|\boldsymbol{k}|^2\dfrac{\partial^4\psi}{\partial\xi^4} + b_2\dfrac{\partial^2\psi}{\partial\xi^2} \end{pmatrix}\boldsymbol{k}^\perp\,.$$

Every vector value in $\mathbb{R}^2$ on the right hand side has a unique representation by the orthogonal basis vectors $\boldsymbol{k}$ and $\boldsymbol{k}^\perp$ on the left hand side. The scalar product with $\boldsymbol{k}^\perp$ and $\boldsymbol{k}$, respectively, gives

$$\frac{\partial\psi}{\partial t} = -|\boldsymbol{k}|^2\left(d_1k_y^2 + d_2k_x^2\right)\frac{\partial^4\psi}{\partial\xi^4} - \left(b_1k_y^2 + b_2k_x^2\right)\frac{\partial^2\psi}{\partial\xi^2}\,, \tag{3.3a}$$

$$f\left(\frac{\partial\phi}{\partial\xi} - \psi\right) = k_xk_y\left((d_1 - d_2)|\boldsymbol{k}|^2\frac{\partial^4\psi}{\partial\xi^4} + (b_1 - b_2)\frac{\partial^2\psi}{\partial\xi^2}\right)\,. \tag{3.3b}$$

We focus on monochromatic solutions first, i.e. which consists of a single Fourier mode, and later investigate possible superposition.

Theorem 3.1. *The rotating shallow water equations with backscatter (3.1) possess the explicit solutions*

$$\boldsymbol{v} = A_1\mathrm{e}^{\mu t}\cos(\boldsymbol{k}\cdot\boldsymbol{x} + \theta)\boldsymbol{k}^\perp\,, \qquad \eta = A_2\frac{f}{g}\sin(\boldsymbol{k}\cdot\boldsymbol{x} + \theta) + s\,, \tag{3.4}$$

with arbitrary shifts θ, $s \in \mathbb{R}$ and the wave vector $\boldsymbol{k} \in \mathbb{R}^2$, growth rate $\mu \in \mathbb{R}$ and

amplitudes A_1, $A_2 \in \mathbb{R}$ *satisfy*

$$\mu = (b_1 - d_1|\boldsymbol{k}|^2)k_y^2 + (b_2 - d_2|\boldsymbol{k}|^2)k_x^2\,, \tag{3.5a}$$

$$\frac{A_2 - A_1}{A_1} f = k_x k_y((d_1 - d_2)|\boldsymbol{k}|^2 + b_2 - b_1)\,, \tag{3.5b}$$

$$A_2 \cdot \mu = 0\,. \tag{3.5c}$$

Proof. The statement follows directly after solving the derived equations (3.3) with the approach (3.2) above. □

We note that (3.5a) is a dispersion relation of growth/decay and wave vector, while (3.5b) is an amplitude relation of the two amplitudes A_1 and A_2 in terms of the wave vector. The equation (3.5c) is an auxiliary compatibility condition. Specifically, (3.1a) possesses explicit solutions (3.4) if the parameters satisfy (3.5), and the time-independence of η coming from (3.1b) requires condition (3.5c), which means amplitude A_2 of η or growth rate μ of $\boldsymbol{v}$ must be zero. In particular, (3.5c) means that these explicit solutions are steady with non-trivial depth variation η, or time-dependent with trivial $\eta \equiv s$.

Notably, solutions with $\mu > 0$ grow exponentially and unboundedly. As mentioned before, we refer to this as *unbounded instability* of the zero state, and more generally of any other solution which admits superposition with such growing explicit solutions. In Section 3.1.2 we will see, that unbounded instability requires anisotropy $b_1 \neq b_2$, $d_1 \neq d_2$, although the differences can be arbitrarily small. In Figure 3.1 we plot the locations of the solutions from Theorem 3.1 in the wave vector space. The blue and red regions picture the sign of the growth rate μ, which characterizes the exponential decay and growth of such explicit solutions. In fact, we show in Section 3.1.2 that the red region describes a subset of real unstable eigenmodes of the linearisation in the zero state as well.

We now proceed as follows: in Section 3.1.1 we will discuss the sets of solutions in terms of their wave vectors, the organizing parameters and possible superpositions. In Section 3.1.2 we then analyze the unbounded instability and the linear stability of explicit steady solutions from Theorem 3.1.

3.1.1. Solution sets and superpositions

In order to analyze the existence of solutions from Theorem 3.1 of the shallow water equations (3.1) in more detail, it is convenient to write the required dispersion relation (3.5a) and the amplitude relation (3.5b) in the form

$$\mu = -(d_1 k_y^2 + d_2 k_x^2)|\boldsymbol{k}|^2 + b_1 k_y^2 + b_2 k_x^2\,, \tag{3.6a}$$

$$0 = ((d_1 - d_2)|\boldsymbol{k}|^2 + b_2 - b_1)k_x k_y + \sigma\,, \tag{3.6b}$$

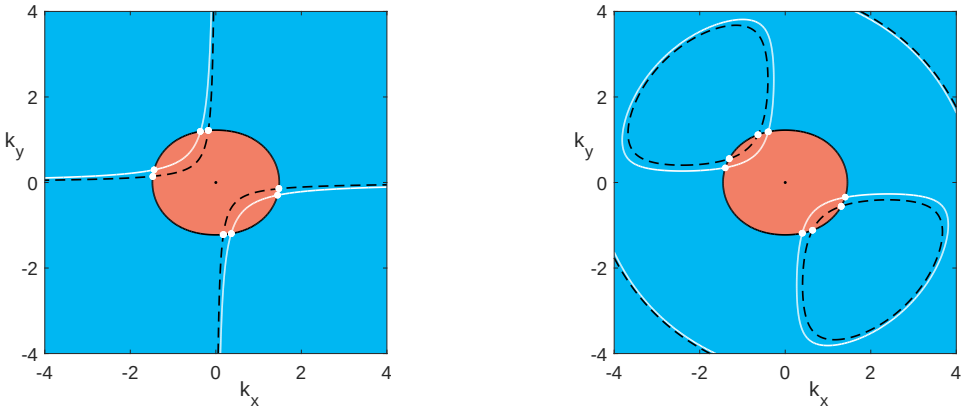

(a) $d_2 = 1.0$ and $A_2 = 0.5$ (b) $d_2 = 1.04$ and $A_2 = -0.5$

Figure 3.1.: The occurrence of explicit solutions from Theorem 3.1 in the wave vector plane with fixed parameters $d_1 = 1.0$, $b_1 = 1.5$, $b_2 = 2.2$, $f = 0.3$, $g = 9.8$, $H_0 = 0.1$, $A_1 = 1.0$ and d_2, A_2 as in the subcaptions. Red regions: $\mu > 0$, i.e. unbounded growth; blue regions: $\mu < 0$; black curves: $\mu = 0$, i.e. steady states. The white curves mark solutions with $A_2 = 0$, the white bullets mark steady solutions with $\mu = 0$. The black dashed curves mark solutions of condition (3.5b) only, for $A_2 \neq 0$ with values as in the subcaptions, which also solve (3.5a) at the white bullets ($\mu = 0$).

with real parameter $\sigma := f(A_1 - A_2)/A_1$ describing the relative difference between the amplitudes of the velocity $\boldsymbol{v}$ and the fluid depth deviation η. Thus, the existence of the considered solutions is completely characterized by (3.6), with $\mu = 0$ or $\sigma = f$ due to (3.5c). Steady solutions must satisfy (3.6a) with $\mu = 0$ and it is then natural to view σ as an adjustment, defined by (3.6b), of the relation between the amplitudes A_1, A_2 depending on the wave vector $\boldsymbol{k}$. For the time-dependent case $\mu \neq 0$ we need $\sigma = f$, so that (3.6b) with this value of σ describes the existence of the solutions, while (3.6a) is considered as a definition for the growth rate μ. The natural free parameter is the wave vector $\boldsymbol{k}$. We will see, that the existence and growth or decay properties of solutions from Theorem 3.1, as well as the locations of unboundedly unstable steady solutions of this kind, are strongly connected with the values of σ, which we therefore consider as an organizing parameter.

We first study the steady solutions of Theorem 3.1 and the structure of their solution set. Afterwards, we analyze the occurrence and shapes of the curves defined by the amplitude relation (3.6b), so that we can use these results in order to determine the time-dependent explicit solutions, i.e. $A_2 = 0$ and $\mu \neq 0$, as well as the steady explicit solutions, for which (3.6a) is satisfied with $\mu = 0$ as well. Then, we study the values of σ, for which steady solutions exist. Clearly any steady solution from Theorem 3.1 has a corresponding value of σ. But not every σ admits such a steady solution and the value of σ for the time-dependent solutions ($\mu \neq 0$) is fixed at $\sigma = f$, since these solutions

require $A_2 = 0$. In the end, we shortly discuss the possible superposition, which extends the set of solutions.

Steady explicit flows

For steady solutions we only need to investigate the wave vectors $\boldsymbol{k}$ satisfying the dispersion relation (3.6a) with $\mu = 0$. These form a simple closed curve around the origin in wave vector space that is symmetric with respect to axis reflection, and whose interior is star shaped, i.e. all points of the set are connected with the origin through a direct line contained in the set, but it need not be convex. We plot an example in Figure 3.1. In order to show this structure, note that for wave vectors $\boldsymbol{k} = r\boldsymbol{k}'$, $\boldsymbol{k}'$ with $|\boldsymbol{k}'| = 1$, the right-hand side of equation (3.6a) is linear in the squared wave vector length $|\boldsymbol{k}|^2 = r^2$ (after using $\boldsymbol{k} = r\boldsymbol{k}'$ with $|\boldsymbol{k}'| = 1$ and division by r^2 in this equation). Furthermore, for any fixed $\boldsymbol{k}'$ there is exactly one $r_0 > 0$, so that $\mu = 0$ for $r = r_0$ and $\mu > 0$ for $0 < r < r_0$, as well as $\mu < 0$ for $r_0 < r$. This means, that μ is positive in the interior of the closed curve of steady solutions (3.4) (red region in Figure 3.1), except for the origin, where $\mu = 0$, and μ is negative outside (blue region in Figure 3.1).

In polar coordinates

$$\boldsymbol{k} = r \begin{pmatrix} \cos\varphi \\ \sin\varphi \end{pmatrix},$$

with angle $\varphi \in [0, 2\pi)$ and wave number $r \geq 0$, the curve for explicit non-trivial steady solutions as in Theorem 3.1, i.e. for their wave vectors $\boldsymbol{k}$ with $\mu = 0$, is parameterized by the angle φ with the wave number given by

$$r = \sqrt{\frac{b_1 \sin^2\varphi + b_2 \cos^2\varphi}{d_1 \sin^2\varphi + d_2 \cos^2\varphi}}\,. \tag{3.7}$$

Generally, these steady solutions have different values of σ defined by (3.6b), i.e. the relative difference of amplitudes A_1 and A_2. In contrast, time-dependent explicit solutions ($\mu \neq 0$) all have the same value $\sigma = f$. In either case, the explicit solutions from Theorem 3.1 form a linear space, since their amplitudes only enter into the ratio $(A_2 - A_1)/A_1$ (so into σ), and are therefore naturally parameterized by an arbitrary amplitude parameter $A \geq 0$, that is a common factor of both A_1 and A_2, which does not change the value of σ.

Set of explicit solutions

In order to investigate the set of explicit solutions of Theorem 3.1, primarily of the time-dependent ones with $A_2 = 0$ and $\mu \neq 0$, we analyze the shapes of the curves defined by the amplitude relation (3.6b). We start with two special cases:

(i) In the isotropic case $b_1 = b_2$ and $d_1 = d_2$, equation (3.6b) requires $\sigma = 0$, i.e. $A_1 = A_2$, so that in this case all non-trivial solutions are steady, i.e. $\mu = 0$, and have $\boldsymbol{k} = 0$ or $\boldsymbol{k}$ on the circle with radius $\sqrt{b_1/d_1}$ defined by dispersion relation (3.6a) (with $\mu = 0$), see Figure 3.2(a). Thus, non-steady solutions ($\mu \neq 0$) of the form (3.4) arise from anisotropy in the hyperdiffusion or backscatter.

(ii) There is also a special anisotropic case. If $d_1 \neq d_2$, then the amplitude relation (3.6b) is satisfied in the origin and on the circle $|\boldsymbol{k}|^2 = (b_1 - b_2)/(d_1 - d_2)$ with $\sigma = 0$, and μ defined by the dispersion relation (3.6a) is always constant on that circle. If additionally $b_1/d_1 = b_2/d_2$, then all solutions of (3.6b) on the circle $|\boldsymbol{k}|^2 = (b_1 - b_2)/(d_1 - d_2)$ also solve (3.6a) with $\mu = 0$, so all of these give steady solutions, which have $\sigma = 0$. In case $b_1/d_1 \neq b_2/d_2$ the value of σ for the steady states is not constant.

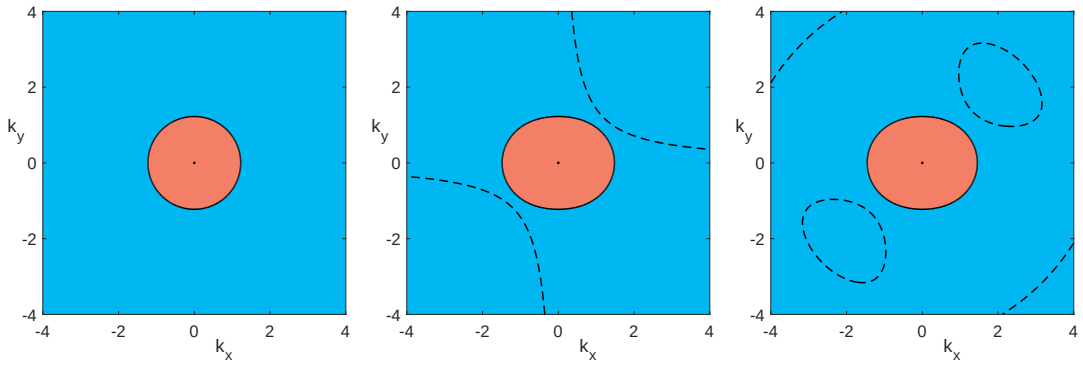

(a) $d_2 = 1.0$, $b_2 = 1.5$, $A_2 = 1.0$ (b) $d_2 = 1.0$, $b_2 = 2.2$, $A_2 = 3.0$ (c) $d_2 = 1.04$, $b_2 = 2.2$, $A_2 = 3.0$

Figure 3.2.: Possible structures of solution curves of the amplitude relation (3.6b) analogous to Figure 3.1. Fixed parameters: $d_1 = 1.0$, $b_1 = 1.5$, $f = 0.5$, $g = 9.8$, $H_0 = 0.1$, $A_1 = 1.0$; It is $\sigma = 0$ in (a) and $\sigma = -1$ in (b) and (c).

It remains to discuss the general anisotropic case, for which we consider the wave vectors in polar coordinates $\boldsymbol{k} = r(\cos\varphi, \sin\varphi)^\intercal$ as above. By symmetry of the amplitude relation (3.6b) it suffices to take $\varphi \in [0, \pi]$. The special cases $\varphi \in \{0, \pi/2, \pi\}$ requires $\sigma = 0$, i.e. steady solutions, and the corresponding wave vectors are

$$\boldsymbol{k} \in \left\{ \begin{pmatrix} 0 \\ 0 \end{pmatrix}, \pm\sqrt{\frac{b_1}{d_1}} \begin{pmatrix} 0 \\ 1 \end{pmatrix}, \pm\sqrt{\frac{b_2}{d_2}} \begin{pmatrix} 1 \\ 0 \end{pmatrix} \right\}.$$

We now consider $\varphi \in (0, \pi) \setminus \{\pi/2\}$. In the case $d_1 = d_2$ solutions of (3.6b) are

$$r = \pm\sqrt{\frac{2\sigma}{(b_1 - b_2)\sin(2\varphi)}}, \qquad \text{for} \quad \operatorname{sgn}(\sigma) = \operatorname{sgn}\big((b_1 - b_2)\sin(2\varphi)\big), \tag{3.8}$$

with $\operatorname{sgn}(\cdot)$ being the sign function (see e.g. Figure 3.2(b)). For $d_1 \neq d_2$ we get

$$r = \sqrt{\frac{b_1 - b_2}{2(d_1 - d_2)} \pm \sqrt{\frac{(b_1 - b_2)^2}{4(d_1 - d_2)^2} - \frac{2\sigma}{(d_1 - d_2)\sin(2\varphi)}}}\,, \tag{3.9}$$

which gives real solutions to (3.6b), if and only if the expressions in the square roots of (3.9) are non-negative. This means, that for fixed angle φ we have two cases:

(i) $b_1 = b_2$ or $\operatorname{sgn}(b_1 - b_2) = -\operatorname{sgn}(d_1 - d_2)$ requires for at least one solution

$$\operatorname{sgn}(\sigma) = -\operatorname{sgn}\big((d_1 - d_2)\sin(2\varphi)\big)\,. \tag{3.10}$$

(ii) $b_1 \neq b_2$ and $\operatorname{sgn}(b_1 - b_2) = \operatorname{sgn}(d_1 - d_2)$ requires for at least one solution

$$\frac{(b_1 - b_2)^2}{8(d_1 - d_2)}\sin(2\varphi) \geq \sigma \qquad \text{for } \varphi \in (0, \tfrac{\pi}{2}) \ \ \big(\text{if } d_1 > d_2, \text{ otherwise } \varphi \in (\tfrac{\pi}{2}, \pi)\big)\,, \tag{3.11a}$$

$$\frac{(b_1 - b_2)^2}{8(d_1 - d_2)}\sin(2\varphi) \leq \sigma \qquad \text{for } \varphi \in (\tfrac{\pi}{2}, \pi) \ \ \big(\text{if } d_1 > d_2, \text{ otherwise } \varphi \in (0, \tfrac{\pi}{2})\big)\,. \tag{3.11b}$$

Two solutions for a fixed angle φ occur if and only if the following three conditions are satisfied:

$$\operatorname{sgn}(b_1 - b_2) = \operatorname{sgn}(d_1 - d_2)\,, \qquad \text{so also } b_1 \neq b_2\,, \tag{3.12a}$$

$$\operatorname{sgn}(\sigma) = \operatorname{sgn}\big((d_1 - d_2)\sin(2\varphi)\big)\,, \tag{3.12b}$$

$$\frac{(b_1 - b_2)^2}{8|d_1 - d_2|}|\sin(2\varphi)| \geq |\sigma|\,. \tag{3.12c}$$

In Figure 3.2 we plot examples, where up to one (Figure 3.2(a) and Figure 3.2(b)) or up to two (Figure 3.2(c)) solutions of (3.6b) for certain angles φ arise for fixed σ. The conditions (3.8)-(3.12) thus determine the occurrence and structures of the solution curves of the amplitude relation (3.6b) depending on the parameter settings. For instance, changing the sign of certain expressions, but not their absolute values, merely rotates the structures by $\pi/2$.

Structure and values of σ

We next discuss the occurrence of explicit steady solutions from Theorem 3.1 in the anisotropic case in more detail, in particular the values of σ, for which explicit steady solutions exist. Strictly speaking, these are the values of σ, for which the corresponding curve defined by the amplitude relation (3.6b) and the one defined by the dispersion relation (3.6a) with $\mu = 0$ intersect, see Figure 3.3. Recall that time-dependent explicit solutions from Theorem 3.1 always have $\sigma = f$.

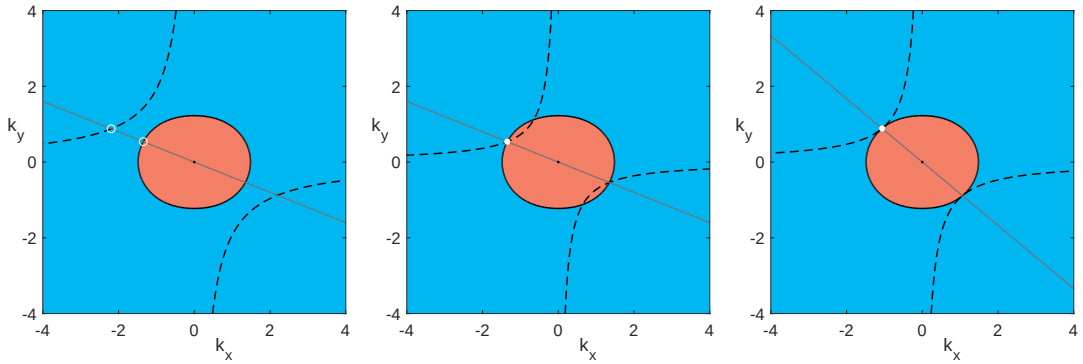

(a) $A_2 = -3.5$, $m = -0.4$ ($\sigma = 1.35$)

(b) $A_2 \approx -0.69$, $m = -0.4$ ($\sigma \approx 0.51$)

(c) $A_2 \approx -1.20$, $m \approx -0.84$ ($\sigma = \sigma(m_\pm) \approx 0.66$)

Figure 3.3.: Solution curves (dashed lines) of the amplitude relation (3.6b) in terms of σ, as well as their intersections with solution curves of the dispersion relation (3.6a) with $\mu = 0$; the gray lines mark $k_y = mk_x$. Denotations as in Figure 3.1 with focus on upper left quadrant. In (a) there are no explicit solutions. In (b) and (c) steady solution occur at intersection point (white dot). Fixed parameters: $d_1 = 1.0$, $d_2 = 1.0$, $b_1 = 1.5$, $b_2 = 2.2$, $f = 0.3$, $g = 9.8$, $H_0 = 0.1$, $A_1 = 1.0$.

To ease the computations, we consider a line $k_y = mk_x$ with the slope $m \in \mathbb{R}$, i.e. $m = \tan\varphi$ in the polar coordinates for wave vectors used before. Inserting this into (3.6) gives the values of k_x, for which the line and the solution curves of (3.6) intersect

$$k_x^2 = \frac{b_1 m^2 + b_2}{(d_1 m^2 + d_2)(1 + m^2)} \qquad \text{and} \tag{3.13a}$$

$$k_x^2 = \frac{\sigma}{m(b_1 - b_2)} \qquad \text{for} \quad d_1 = d_2\,, \tag{3.13b}$$

$$k_x^2 = \frac{b_1 - b_2}{2(d_1 - d_2)(1 + m^2)} \pm \sqrt{\frac{m(b_1 - b_2)^2 - \sigma(d_1 - d_2)(1 + m^2)}{4m(d_1 - d_2)^2(1 + m^2)^2}} \quad \text{for} \quad d_1 \neq d_2\,. \tag{3.13c}$$

The equation (3.13a) is the intersection of the line $k_y = mk_x$ with the curve defined by (3.6a) with $\mu = 0$, while (3.13b) and (3.13c) provides the intersection of the line with the curve defined by (3.6b) in the two corresponding cases (see Figure 3.3(a)).

We next choose σ such that both intersection points are at the same position on the ray (see Figure 3.3(b)). This occurs when the right hand side of (3.13a) equals the right hand side of (3.13b) or (3.13c). In both cases we find $\sigma = \sigma(m)$ is

$$\sigma(m) = \frac{(b_1 d_2 - b_2 d_1)(b_1 m^2 + b_2)m}{(d_1 m^2 + d_2)^2}\,, \tag{3.14}$$

which is an odd function $\sigma(-m) = -\sigma(m)$ and zero for $b_1 d_2 - b_2 d_1 = 0$, the aforementioned special anisotropic case $b_1/d_1 = b_2/d_2$. In the remaining case $b_1 d_2 \neq b_2 d_1$, we note

that $\sigma(m)$ is differentiable and $\sigma(m) \to 0$ for $m \to \pm\infty$, so that it suffices to determine the extrema. The derivative of $\sigma(m)$ is given by

$$\sigma'(m) = \frac{b_1 d_2 - b_2 d_1}{(d_1 m^2 + d_2)^3} \left(-b_1 d_1 m^4 + 3(b_1 d_2 - b_2 d_1) m^2 + b_2 d_2 \right) , \tag{3.15}$$

whose roots, and therefore the location of the extrema, are

$$m_\pm = \pm \sqrt{ \frac{3(b_1 d_2 - b_2 d_1)}{2 b_1 d_1} + \sqrt{ \frac{9(b_1 d_2 - b_2 d_1)^2}{4 b_1^2 d_1^2} + \frac{b_2 d_2}{b_1 d_1} } } . \tag{3.16}$$

Thus, steady explicit solutions from Theorem 3.1 exist for $\sigma \in [\sigma(m_-), \sigma(m_+)]$, for the case $b_1 d_2 - b_2 d_1 > 0$, and $\sigma \in [\sigma(m_+), \sigma(m_-)]$ if $b_1 d_2 - b_2 d_1 < 0$. We may interpret the endpoints $\sigma(m_-)$ and $\sigma(m_+)$, where the solution curves of (3.6) with $\mu = 0$ touch each other (see Figure 3.3(c)), as bifurcation points of explicit steady solutions of the form (3.4). Using the redefinition of the slope $m = \tan\varphi$ we equivalently obtain σ as a function of the wave vector angle φ that was used above. We plot an example of the resulting function $\sigma(\varphi)$ later in Figure 3.6(b).

Remark 3.1.1. As shown above, steady explicit solutions of Theorem 3.1 only exist for $\sigma \in [\sigma(m_-), \sigma(m_+)]$ if $b_1 d_2 - b_2 d_1 > 0$, or $\sigma \in [\sigma(m_+), \sigma(m_-)]$ if $b_1 d_2 - b_2 d_1 < 0$. This in particular means, that even though the amplitudes A_1, A_2 of such explicit solutions can be multiplied with any common factor, they only exist for certain relative difference of A_1 and A_2.

Superpositions of explicit flows

Superpositions of solutions from Theorem 3.1 are also solutions to (3.1), if their wave vectors $\boldsymbol{k}$ all lie on the same line through the origin in the wave vector plane. We plot an example in Figure 3.4. As also shown in Section 2.2.1 and Section 2.3.1, it follows from the radial superposition principle of Theorem 2.3. In contrast to these sections, we are not able to superpose functions with arbitrary wave vector length in the same direction for the problem (3.1), since the occurrence of the considered explicit solutions is restricted here in any direction, as one can see in Figure 3.4.

The superposition provides non-trivial subspaces of initial data to (3.1), in which the dynamics are linear. In the example of Figure 3.4 this space is three-dimensional, since the negated wave vectors give linearly dependent solutions, and this is the maximum possible as shown below. Furthermore, we will show in the following, that we can also use the superposition in order to determine instabilities in certain cases.

3.1.2. Stability analysis of steady solutions

We study the stability of a steady state $(\boldsymbol{v}_s, \eta_s)^\intercal$ of the shallow water equations (3.1) via the linear operator $\mathcal{L} = \mathcal{L}(\boldsymbol{v}_s, \eta_s)$, which results from linearizing (3.1) in $(\boldsymbol{v}_s, \eta_s)^\intercal$. A

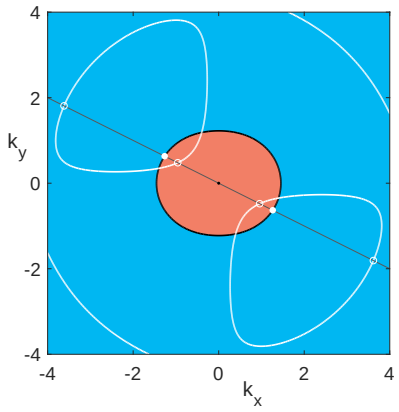

Figure 3.4.: Possible superpositions of explicit solutions from Theorem 3.1 in wave vector space, where the meaning of colors and the parameters are as in Figure 3.1, with $d_2 = 1.04$ and $A_2 = 0$. We mark a line of wave vectors in a fixed direction (gray) and the growing or decaying solutions (white circles) on it, whose superpositions with or without the steady state on the gray line again yield explicit solutions of (3.1).

spectrum of $\mathcal{L}$ with positive real part then implies that the steady solution $(\boldsymbol{v}_s, \eta_s)^\intercal$ is linearly unstable. In the following we will show that the trivial steady state $(\boldsymbol{v}_s, \eta_s)^\intercal \equiv (0,0,0)^\intercal$ is linearly unstable, and in certain cases even unboundedly unstable. The latter means, that unstable perturbations of the steady solution grow unboundedly in time, while in contrast the linear instability is a local property, so that in general the growths of unstable perturbations are bounded in that case. Afterwards, we focus on the stability of non-trivial steady solutions of Theorem 3.1. We first analyze the unbounded instability of these in the full nonlinear equations (3.1) with respect to solutions of Theorem 3.1. Moreover, we study a certain long-wavelength instability in this case and briefly consider the energy of the explicit solutions. Finally, we investigate the linear stability of all steady solutions from Theorem 3.1 with small and large amplitudes.

Linear stability of the trivial steady solution

The linearization of the shallow water equations (3.1) in the trivial homogeneous steady solution $(\boldsymbol{v}_s, \eta_s)^\intercal \equiv (0,0,0)^\intercal$ is exactly (3.1) itself, but without the nonlinear advection terms. The corresponding linear operator $\mathcal{L}$ is then the remaining right-hand side of (3.1). The spectrum of $\mathcal{L}$ in this case can be determined by the dispersion relation

$$d(\lambda, \boldsymbol{k}) := \det(\lambda \mathrm{Id} - \widehat{\mathcal{L}}) = 0\,,$$

with wave vectors $\boldsymbol{k} = (k_x, k_y)^\intercal \in \mathbb{R}^2$, temporal rates of the Fourier modes $\lambda = \lambda(\boldsymbol{k}) \in \mathbb{C}$, which are the eigenvalues when solving the dispersion relation, and $\widehat{\mathcal{L}} = \widehat{\mathcal{L}}(\boldsymbol{k})$ the Fourier

transform of $\mathcal{L}$ given by

$$\widehat{\mathcal{L}}(\boldsymbol{k}) = \begin{pmatrix} -d_1|\boldsymbol{k}|^4 + b_1|\boldsymbol{k}|^2 & f & -\mathrm{i}gk_x \\ -f & -d_2|\boldsymbol{k}|^4 + b_2|\boldsymbol{k}|^2 & -\mathrm{i}gk_y \\ -\mathrm{i}H_0k_x & -\mathrm{i}H_0k_y & 0 \end{pmatrix}.$$

The dispersion relation is thus explicitly

$$d(\lambda, \boldsymbol{k}) = \lambda^3 + c_2\lambda^2 + c_1\lambda + c_0 = 0\,, \tag{3.17}$$

with the coefficients

$$\begin{aligned} c_2 &:= (d_1 + d_2)|\boldsymbol{k}|^4 - (b_1 + b_2)|\boldsymbol{k}|^2\,, \\ c_1 &:= (d_1|\boldsymbol{k}|^4 - b_1|\boldsymbol{k}|^2)(d_2|\boldsymbol{k}|^4 - b_2|\boldsymbol{k}|^2) + gH_0|\boldsymbol{k}|^2 + f^2\,, \\ c_0 &:= -gH_0|\boldsymbol{k}|^2\left((b_1 - d_1|\boldsymbol{k}|^2)k_y^2 + (b_2 - d_2|\boldsymbol{k}|^2)k_x^2\right). \end{aligned}$$

Recall that the explicit solutions of Theorem 3.1 solve the shallow water equations (3.1) with and without the nonlinear terms, since these terms vanish by construction of these solutions. Therefore, the wave vectors $\boldsymbol{k}$ and growth rates μ of these explicit solutions are in fact real solutions of the dispersion relation (3.17) for $\lambda = \mu$. In other words, all the explicit solutions of Theorem 3.1 are real eigenmodes of $\mathcal{L}$ and the values μ defined by the dispersion relation (3.5a) are the corresponding real elements in the spectrum of $\mathcal{L}$. Thus, the possible values for the growth rate μ of the explicit solutions from Theorem 3.1 directly provide part of the spectrum of $\mathcal{L}$, for instance all values of μ on the white and black curves in Figure 3.4. In particular, the occurrence of positive growth rates μ in (3.5a) implies, that the trivial steady solution $(\boldsymbol{v}_s, \eta_s)^\intercal \equiv (0,0,0)^\intercal$ is linearly unstable with respect to the corresponding exponentially growing explicit solutions. For instance, in Figure 3.4 this happens for the wave vectors on the part of the white curves within the red region. More generally, even if the white curves do not intersect the red region, we next show that the whole red region consists of unstable real modes of $\mathcal{L}$. This means, that the trivial solution is always linearly unstable with respect to certain real modes.

We first note that in $\boldsymbol{k} = (0,0)^\intercal$ the dispersion relation (3.17) reduces to

$$d(\lambda, (0,0)^\intercal) = \lambda^3 + f^2\lambda = 0\,,$$

which gives the eigenvalues $\lambda = 0$ and $\lambda = \pm\mathrm{i}f$, all having zero real part. A subset of the unstable spectrum can be determined by the sign of the coefficient $c_0 = -gH_0|\boldsymbol{k}|^2\beta(\boldsymbol{k})$ of the dispersion relation (3.17), where $\beta(\boldsymbol{k})$ is the expression in brackets in the definition of c_0 above. The coefficient c_0 is zero if and only if $\boldsymbol{k} \in \mathbb{R}^2$ satisfies $\beta(\boldsymbol{k}) = 0$, which means that $\lambda = 0$ is in the spectrum of $\mathcal{L}$ with corresponding eigenmodes having such

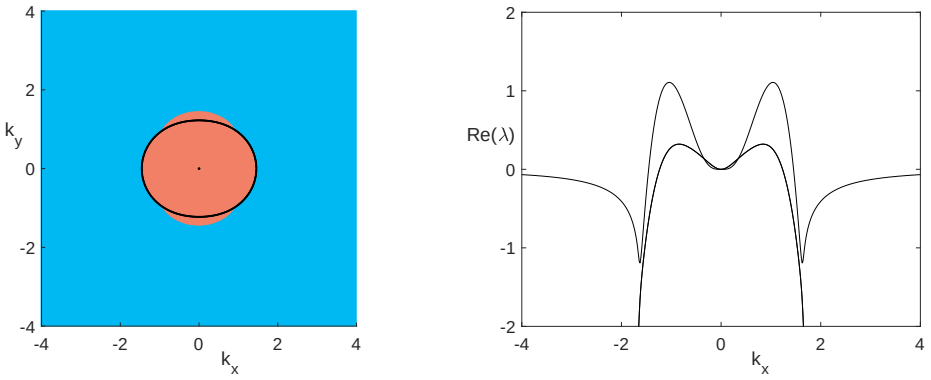

(a) (b)

Figure 3.5.: Information on the spectrum of the linearization of (3.1) in the trivial steady solution $(\boldsymbol{v}_s, \eta_s)^\intercal \equiv (0,0,0)^\intercal$ for parameters $d_1 = 1.0$, $d_2 = 1.04$, $b_1 = 1.5$, $b_2 = 2.2$, $f = -0.3$, $g = 9.8$, $H_0 = 0.1$. (a): Signs of the most unstable real part of elements in the spectrum in terms of the wave vector $\boldsymbol{k}$ of the associated eigenmodes. Real part positive (red region), negative (blue region), black dot and curve correspond to steady solutions of Theorem 3.1. Note the unstable non-real spectrum in addition to, e.g. Figure 3.1. (b): The real part of the spectrum for $k_y = 0$, showing unstable spectrum in the vicinity of the origin.

wave vectors $\boldsymbol{k}$. Furthermore, c_0 is negative if and only if $\beta(\boldsymbol{k}) > 0$, so according to the dispersion relation (3.17) there is at least one positive real value $\lambda > 0$ for each of these wave vectors $\boldsymbol{k}$. We notice, that $\beta(\boldsymbol{k})$ is also exactly the same expression as on the right-hand side of the dispersion relation (3.5a) or (3.6a), which means we obtain the direct relation $\beta(\boldsymbol{k}) = \mu(\boldsymbol{k})$, with $\mu = \mu(\boldsymbol{k})$ from (3.5a) or (3.6a). We have already analyzed the sign of μ in Section 3.1.1. This implies, that the red regions plotted, e.g. in Figure 3.4, correspond to a part of the unstable spectrum of $\mathcal{L}$ which are real and positive. In particular, we conclude that $(\boldsymbol{v}_s, \eta_s)^\intercal \equiv (0,0,0)^\intercal$ is linearly unstable for any choice of parameters with hyperdiffusion and backscatter. However, the spectrum of $\mathcal{L}$ may also contain non-real unstable parts. We plot an example in Figure 3.5(a), where the unstable region extends into the blue region of Figure 3.4. This can be further studied based on the dispersion relation (3.17), but we will not do this here.

The previous investigation regarding the linear instability of the trivial flow in fact shows, that the explicit solutions of the nonlinear equations (3.1) from Theorem 3.1 with $\mu > 0$ are also real unstable eigenmodes. More than that, such perturbations of the trivial flow do not only lead to infinitesimal or local growth, but as explicit solutions of (3.1) they even grow globally and unboundedly in time, implying the unbounded instability of the trivial zero state in such a case.

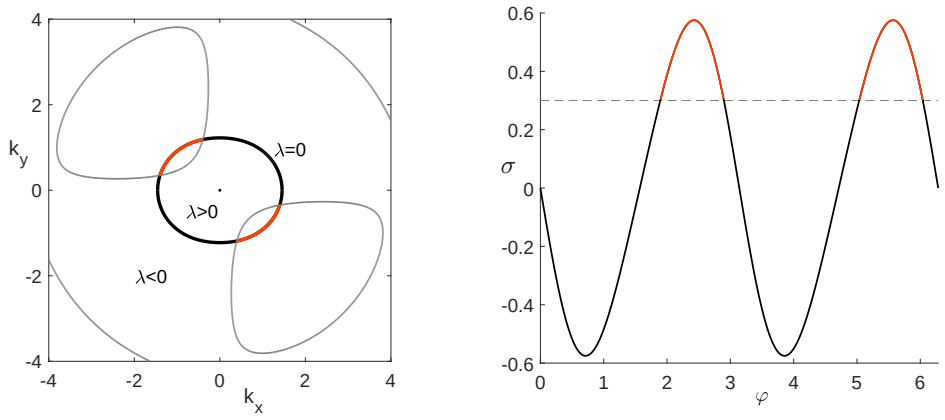

(a) (b)

Figure 3.6.: Examples for unboundedly unstable steady solutions of Theorem 3.1 for the same parameter values as in Figure 3.4. (a) Red arcs mark unboundedly unstable steady solutions. Gray curves mark explicit time-dependent solutions of Theorem 3.1 with $A_2 = 0$. (b) Graph of $\sigma(\varphi)$ defined by (3.6b) with angular direction φ of wave vector $\boldsymbol{k}$. Red parts mark unboundedly unstable cases. Dashed gray line marks the value of the Coriolis parameter f.

Unbounded and long-wavelength instability of nontrivial steady solutions

In the following we show that some of the steady solutions of Theorem 3.1 can be unboundedly unstable as well. We consider parameter values such that some time-dependent explicit solutions from Theorem 3.1 have positive growth rate μ, as in the example of Figure 3.1. Recall that this requires at least weak anisotropy of the hyperdiffusion and backscatter in (3.1). As already shown, steady solutions of Theorem 3.1 exist on the whole curve defined by the dispersion relation (3.5a) with $\mu = 0$ (see Figure 3.6(a) as well as the black curve in Figure 3.4). Now superpositions of explicit solutions from Theorem 3.1, which have the same wave vector direction (e.g. the intersections of white or black curves with the gray line in Figure 3.4), are also explicit solutions of (3.1). In the case of Figure 3.4 these are in particular a non-trivial steady solution $(\boldsymbol{v}_s, \eta_s)^\intercal$ (white dot) and an exponentially growing solution $(\boldsymbol{v}_g, 0)^\intercal$ (white circle in red area). Any superposition $A(\boldsymbol{v}_s, \eta_s)^\intercal + \varepsilon(\boldsymbol{v}_g, 0)^\intercal$, with arbitrary $A, \varepsilon \in \mathbb{R}$, is also an explicit solution of (3.1). In particular, ε can be arbitrarily close to zero. For any $\varepsilon \neq 0$, the resulting solution is exponentially and unboundedly growing in time. Thus, $(\boldsymbol{v}_s, \eta_s)^\intercal$ is an unboundedly unstable steady solution.

This implies the unbounded instability of the explicit steady solutions of Theorem 3.1 corresponding to wave vectors on the red arcs in Figure 3.6(a) (in Figure 3.4 these are between the intersections of black and white curves). These arcs connect the intersection points of the curve defined by the dispersion relation (3.5a) for $\mu = 0$, with that for time-dependent explicit solutions defined by the amplitude relation (3.5b) with $A_2 = 0$.

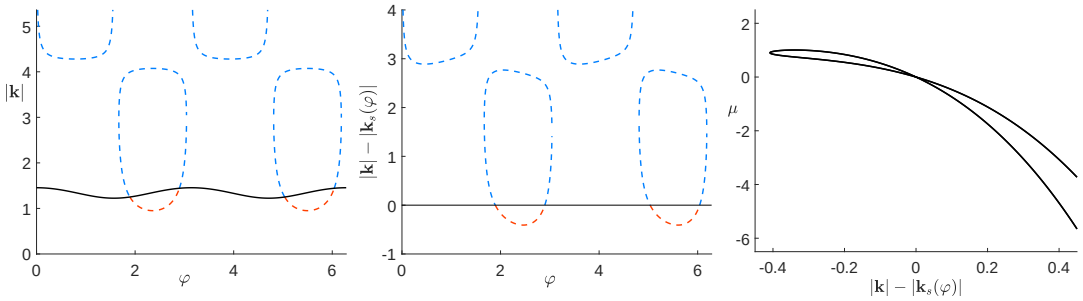

(a) (b) (c)

Figure 3.7.: Illustration of long-wavelength instabilities of explicit flows. (a)-(b): Wave vectors $\boldsymbol{k} = |\boldsymbol{k}|(\cos\varphi, \sin\varphi)^\mathsf{T}$ of explicit solutions from Theorem 3.1 as functions of φ. Black: steady solutions $\boldsymbol{k}_s(\varphi)$; blue: exponentially decaying; red: exponentially growing. (c): Growth rate μ as a function of the difference of wave vector lengths from steady solution. Parameters for all three cases as in Figure 3.4.

Such instability of the other explicit steady solutions (black arcs in Figure 3.6(a)) is not determined in this way, but we will discuss some cases later. However, the transition from the black to the red arcs can be associated with a long-wavelength instability (also called sideband or modulational instability).

We will now show the direct connection of unboundedly unstable steady solutions of Theorem 3.1 with the corresponding values of σ. This is not only useful for checking, if a steady solution of Theorem 3.1 is unboundedly unstable, but also for the investigation of long-wavelength instability. We consider the angle φ of the wave vector $\boldsymbol{k} = \boldsymbol{k}(\varphi)$ and the corresponding value of $\sigma(\varphi) := \sigma(\boldsymbol{k}(\varphi))$ defined by (3.6b). Recall that time-dependent explicit solutions from Theorem 3.1 require $A_2 = 0$, according to (3.5c), which then have $\sigma = f$. Thus, steady solutions with $\sigma(\varphi) = f$ lie at the intersections of the curve for time-dependent solutions (defined by (3.6b) with $\sigma = f$) with the curve for the steady solutions (defined by (3.6a) with $\mu = 0$). Steady solutions "between" those with $\sigma(\varphi) = f$ are unboundedly unstable, since those can be superposed with growing explicit solutions as shown above (cf. red arcs in Figure 3.6(a)), giving explicit solutions of (3.1) again. More precisely, there are at most four angles $\varphi_j \in [0, 2\pi)$, ordered by size, so that $\sigma(\varphi_j) = f$ (cf. Figure 3.6(b)), and steady solutions of Theorem 3.1, whose wave vectors have angles between φ_1 and φ_2, or φ_3 and φ_4, are unboundedly unstable. Hence, a steady solution of Theorem 3.1 is unboundedly unstable if and only if $\operatorname{sgn}(f)\sigma(\varphi) > |f|$, with its corresponding value $\sigma(\varphi)$ (see Figure 3.6(b)).

Towards the long-wavelength instability, we parameterize the set of steady solutions by the angle φ of their wave vectors. In Figure 3.7(a) we plot for each φ the wave vector lengths for which an explicit solution of Theorem 3.1 exists and whether it is steady, exponentially decaying or growing. This also readily shows admissible superpositions

of explicit solutions, since these must have the same angle φ. With respect to these exponentially growing explicit solutions, we thus have stable and unstable steady solutions. The stability change occurs at the intersections of the curves for the steady and the time-dependent solutions, thus providing a long-wavelength instability character at these points, since the difference of wavelength between the steady solution and the unstable mode (the Floquet-Bloch parameter) crosses zero here (see Figure 3.7(b)). Conversely, given any small Floquet-Bloch parameter, one can find a value φ, so that the corresponding steady solution is unstable with respect to the exponentially growing one. See Figure 3.7(c), where the self-intersection point at the origin shows two such points along φ.

Linear stability of non-trivial steady solutions with small and large amplitudes

We now study the linear stability of nontrivial steady solutions from Theorem 3.1. Due to the special property of such solutions to have arbitrary amplitude parameters, we are here interested of their stability for (asymptotically) small and large amplitudes, the natural asymptotic regimes for families of solutions with a free parameter. Since such linear spaces of solutions arise more broadly in fluid equations with nonlinear advection terms, as shown in Section 2.2 and Section 2.3, and for later use in Section 3.2, we set up the notation for the more general setting of an evolution equation with linear term $\mathcal{L}$ and bilinear nonlinearity $\mathcal{B}$ given by

$$\frac{\partial}{\partial t}\boldsymbol{u} = \mathcal{L}\boldsymbol{u} + \mathcal{B}(\boldsymbol{u},\boldsymbol{u}) + \nabla p\,, \tag{3.18}$$

with a pressure p, that is trivial for the rotating shallow water equations (3.1) with $\boldsymbol{u} = (\boldsymbol{v},\eta)^\intercal$, and otherwise will derive from the incompressibility constraint $\nabla\cdot\boldsymbol{v} = 0$.

We assume (3.18) has a family of steady state solutions $\boldsymbol{u} = a\boldsymbol{u}_0$ with amplitude parameter $a \in \mathbb{R}$ and associated (possibly trivial) pressure $p = ap_0$. The spectral stability of the steady state $a\boldsymbol{u}_0$ is determined by the linearized right-hand side of (3.18) in $a\boldsymbol{u}_0$, and thus by the solutions to the generalized eigenvalue problem

$$\lambda\boldsymbol{U} = \mathcal{L}_a\boldsymbol{U} + \nabla P\,, \qquad \mathcal{L}_a := \mathcal{L} + a\mathcal{L}_0\,, \qquad \mathcal{L}_0 := \mathcal{B}(\cdot,\boldsymbol{u}_0) + \mathcal{B}(\boldsymbol{u}_0,\cdot)\,, \tag{3.19}$$

with eigenvalue parameter $\lambda \in \mathbb{C}$, eigenmode $\boldsymbol{U} = (\boldsymbol{v},\eta)^\intercal$ and P either trivial or determined by the linearized constraint $\nabla\cdot\boldsymbol{v} = 0$.

Since the resulting spectrum is locally uniformly continuous with respect to the parameter a, we immediately note that for $|a| \ll 1$ it is close to that for $a = 0$, which is associated to $\mathcal{L}$. Since its spectrum is unstable for the backscatter setting, as shown in the linear stability analysis of the trivial steady solution above, it follows that all the discussed explicit flows with small amplitudes inherit unstable modes of the trivial state, more so for smaller amplitudes. Thus, in the backscatter case (3.1) here, the non-trivial steady solution $a\boldsymbol{u}_0$ is linearly unstable for $|a| \ll 1$.

Regarding large amplitudes, $|a| \gg 1$, we consider eigenvalue parameters that scale with the amplitude, i.e. $\lambda = a\widetilde{\lambda}$, and set $P = a\widetilde{P}$. This gives the (generalized) eigenvalue problem

$$\widetilde{\lambda}\boldsymbol{U} = (a^{-1}\mathcal{L} + \mathcal{L}_0)\boldsymbol{U} + \nabla\widetilde{P}\,. \tag{3.20}$$

The operator of the limiting problem, as $|a| \to \infty$, is $\mathcal{L}_0$. Again by continuity of the spectrum, its stability properties partially predict those of $\mathcal{L}_a$ for $|a| \gg 1$. In particular, an unstable eigenmode of $\mathcal{L}_0$ implies strongly unstable eigenmodes of $\mathcal{L}_a$ for $|a| \gg 1$, since the growth rate $\mathrm{Re}(\lambda) = a\mathrm{Re}(\widetilde{\lambda})$ is proportional to the amplitude a of the steady solution. However, eigenmodes of $\mathcal{L}_a$ for which λ is not proportional to a correspond to growth rates $\widetilde{\lambda} = \lambda/a$, which are going to zero as $|a| \to \infty$, and thus contribute to the kernel of $\mathcal{L}_0$. In particular, $a\boldsymbol{u}_0$ may be linearly unstable for all a even though $\mathcal{L}_0$ does not possess unstable spectrum. Indeed, this turns out to be the case in the present setting. One can see this for the unstable rates $\lambda > 0$ of the explicit flows of Theorem 3.1 from the analysis of unbounded instability above. They are associated with unbounded growth and are constant with respect to the amplitude a of the steady solution, so that in the scaling of $\mathcal{L}_a$ it satisfies $\widetilde{\lambda} = \lambda/a \to 0$ as $a \to \infty$.

Hence, we consider the limiting problem of (3.20) for $|a| \to \infty$

$$\widetilde{\lambda}\boldsymbol{U} = \mathcal{L}_0\boldsymbol{U} + \nabla\widetilde{P}\,,$$

whose spectral properties do not seem to be known analytically for the explicit flows we are concerned with. Specifically, for steady solutions of Theorem 3.1 we have $\boldsymbol{u} = (\boldsymbol{v}, \eta)^\intercal$, the bilinear form of (3.1) is

$$\mathcal{B}\Big((\boldsymbol{v}_1, \eta_1)^\intercal, (\boldsymbol{v}_2, \eta_2)^\intercal\Big) = \begin{pmatrix} -(\boldsymbol{v}_1 \cdot \nabla)\boldsymbol{v}_2 \\ -(\boldsymbol{v}_1 \cdot \nabla)\eta_2 - \eta_1 \nabla \cdot \boldsymbol{v}_2 \end{pmatrix},$$

and the steady state family is generated by $\boldsymbol{u}_0 = (\boldsymbol{v}_0, \eta_0)^\intercal$ from (3.4), i.e. with $\xi = \boldsymbol{k} \cdot \boldsymbol{x}$,

$$\boldsymbol{v}_0 = \cos(\xi)\boldsymbol{k}^\perp\,, \qquad \eta_0 = A_2 \sin\xi + s\,,$$

where $\boldsymbol{k} \in \mathbb{R}^2$ satisfies (3.5a) with $\mu = 0$ and A_2 is chosen so that (3.5b) holds as well. We are then interested in the spectrum of the operator $\mathcal{L}_0$ defined by

$$\begin{aligned}\mathcal{L}_0 \begin{pmatrix} \boldsymbol{v} \\ \eta \end{pmatrix} &= - \begin{pmatrix} (\boldsymbol{v}_0 \cdot \nabla)\boldsymbol{v} + (\boldsymbol{v} \cdot \nabla)\boldsymbol{v}_0 \\ (\boldsymbol{v}_0 \cdot \nabla)\eta + (\boldsymbol{v} \cdot \nabla)\eta_0 + \eta_0 \nabla \cdot \boldsymbol{v} + \eta \nabla \cdot \boldsymbol{v}_0 \end{pmatrix} \\ &= - \begin{pmatrix} \cos(\xi)(\boldsymbol{k}^\perp \cdot \nabla)\boldsymbol{v} - (\boldsymbol{v} \cdot \boldsymbol{k})\sin(\xi)\boldsymbol{k}^\perp \\ \cos(\xi)(\boldsymbol{k}^\perp \cdot \nabla)\eta + A_2(\boldsymbol{v} \cdot \boldsymbol{k})\cos\xi + (A_2 \sin\xi + s)(\nabla \cdot \boldsymbol{v}) \end{pmatrix}.\end{aligned}$$

We immediately note that the kernel of $\mathcal{L}_0$ is infinite dimensional: Any perturbation $\boldsymbol{v}$, η of the same form as the steady flow $\boldsymbol{u}_0$, i.e. $\boldsymbol{v}(\boldsymbol{x}) = \phi_1(\xi)\boldsymbol{k}^\perp$, $\eta(\boldsymbol{x}) = \phi_2(\xi)$ with

arbitrary ϕ_1 and ϕ_2, lies in the kernel of $\mathcal{L}_0$, since $(\boldsymbol{k}^\perp \cdot \nabla)(\boldsymbol{v}, \eta)^\intercal = 0$ as well as $\boldsymbol{v} \cdot \boldsymbol{k} = 0$ and $\nabla \cdot \boldsymbol{v} = 0$.

Next, we show that the spectrum of $\mathcal{L}_0$ is purely imaginary. For this purpose, we consider $\mathcal{L}_0$ on $(L_2(\mathbb{R}^2))^3$ with suitable domain in order to admit Fourier transform with respect to $\zeta = -k_y x + k_x y$. We set $A_2 = s = 0$, i.e. the steady state $\boldsymbol{u}_0$ is in the intersection of the sets of steady and time-dependent solutions as in Figure 3.1, so that

$$\mathcal{L}_0 \begin{pmatrix} \boldsymbol{v} \\ \eta \end{pmatrix} = - \begin{pmatrix} \cos(\xi)(\boldsymbol{k}^\perp \cdot \nabla)\boldsymbol{v} - (\boldsymbol{v} \cdot \boldsymbol{k}) \sin(\xi) \boldsymbol{k}^\perp \\ \cos(\xi)(\boldsymbol{k}^\perp \cdot \nabla)\eta \end{pmatrix}.$$

It is a diagonal operator where $\boldsymbol{v}$ and η are decoupled. Let us change coordinates to $\xi = k_x x + k_y y$, $\zeta = -k_y x + k_x y$. Then ∇ becomes $(k_x \partial_\xi - k_y \partial_\zeta, k_y \partial_\xi + k_x \partial_\zeta)$, so that $\boldsymbol{k}^\perp \cdot \nabla$ turns into $K \partial_\zeta$, where $K := k_x^2 + k_y^2$. We thus obtain

$$\mathcal{L}_0 \begin{pmatrix} \boldsymbol{v} \\ \eta \end{pmatrix} = - \begin{pmatrix} \cos(\xi) K \partial_\zeta \boldsymbol{v} - (\boldsymbol{v} \cdot \boldsymbol{k}) \sin(\xi) \boldsymbol{k}^\perp \\ \cos(\xi) K \partial_\zeta \eta \end{pmatrix},$$

whose Fourier transform with respect to ζ with wave number parameter ϑ read

$$\begin{aligned} \widehat{\mathcal{L}}_0 \begin{pmatrix} \hat{\boldsymbol{v}} \\ \hat{\eta} \end{pmatrix} &= - \begin{pmatrix} \mathrm{i} \cos(\xi) K \vartheta \hat{\boldsymbol{v}} - (\hat{\boldsymbol{v}} \cdot \boldsymbol{k}) \sin(\xi) \boldsymbol{k}^\perp \\ \mathrm{i} \cos(\xi) K \vartheta \hat{\eta} \end{pmatrix} \\ &= - \begin{pmatrix} \mathrm{i} \cos(\xi) K \vartheta \mathrm{Id} - \sin(\xi) \mathrm{A}(\boldsymbol{k}) & 0 \\ 0 & \mathrm{i} \cos(\xi) K \vartheta \end{pmatrix} \begin{pmatrix} \hat{\boldsymbol{v}} \\ \hat{\eta} \end{pmatrix}, \end{aligned}$$

where $\mathrm{A}(\boldsymbol{k}) = \begin{pmatrix} -k_x k_y & -k_y^2 \\ k_x^2 & k_x k_y \end{pmatrix}$.

The lower right entry, which corresponds to η, is a multiplication operator by $\mathrm{i} \cos(\xi) K \vartheta$ and so its spectrum is the range of this function, which is $\mathrm{i} K \vartheta [-1, 1] \subset \mathrm{i}\mathbb{R}$. Since this multiplication operator appears in the upper left entry as a factor of the identity, which commutes with any matrix, $\mathrm{A}(\boldsymbol{k})$ can be brought to normal form. This features a double zero eigenvalue so that the operator on the upper left block possesses purely imaginary spectrum. In particular, the spectrum is neutrally stable.

For A_2, $s \neq 0$ and writing $\boldsymbol{v} = (u, v)^\intercal$ we analogously obtain the transformed operator

$$\widehat{\mathcal{L}}_0 \begin{pmatrix} \hat{\boldsymbol{v}} \\ \hat{\eta} \end{pmatrix} = - \begin{pmatrix} \mathrm{i} \cos(\xi) K \vartheta \hat{\boldsymbol{v}} - (\hat{\boldsymbol{v}} \cdot \boldsymbol{k}) \sin(\xi) \boldsymbol{k}^\perp \\ \mathrm{i} \cos(\xi) K \vartheta \hat{\eta} + \mathbf{B} \hat{\boldsymbol{v}} \end{pmatrix} = \begin{pmatrix} \mathbf{A}_1 & 0 \\ \mathbf{B} & \mathbf{A}_2 \end{pmatrix} \begin{pmatrix} \hat{\boldsymbol{v}} \\ \hat{\eta} \end{pmatrix},$$

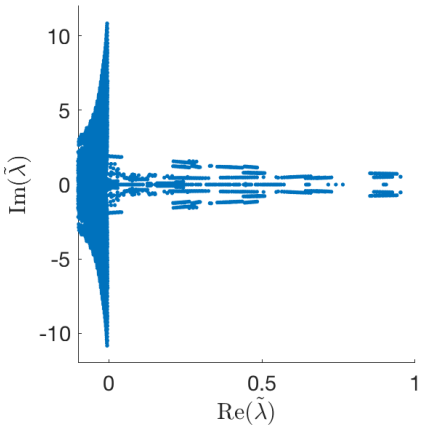

Figure 3.8.: Shown are the eigenvalues with real part larger than -0.1 of an approximation of $\mathcal{L}_1$ with $N = 10$ wave modes, i.e. $3(2N+1)^2$ Fourier modes on the periodic domain $[0, 2\pi/k_x] \times [0, 2\pi/k_y]$, and Bloch modes from the grid with distance $\pi/4$. Parameters are as in Figure 3.4 and $s = 0$. Amplitudes are $A_1 = 1$ and $A_2 = 0$, so $\sigma = f = 0.3$ and the selected steady solution corresponds to the point between the red and black arcs in Figure 3.6(a) with $\boldsymbol{k} \approx (-1.4, 0.35)$.

with

$$\mathbf{A}_1 := -\mathrm{i}\cos(\xi) K\vartheta \mathrm{Id} + \sin(\xi)\mathrm{A}(\boldsymbol{k})\,,$$

$$\mathbf{A}_2 := -\mathrm{i}\cos(\xi) K\vartheta\,,$$

$$\mathbf{B}\hat{\boldsymbol{v}} := -A_2(\hat{\boldsymbol{v}}\cdot\boldsymbol{k})\cos\xi + (A_2\sin\xi + s)\big(k_x\partial_\xi\hat{u} + k_y\partial_\xi\hat{v} + \mathrm{i}\vartheta(k_x\hat{v} - k_y\hat{u})\big)\,.$$

If λ lies in the resolvent set of both operators on the diagonal $\mathbf{A}_1$ and $\mathbf{A}_2$ (by the above result for $A_2 = s = 0$ this includes any non-purely imaginary value), then λ is also in the resolvent set of the present $\widehat{\mathcal{L}}_0$, since

$$(\widehat{\mathcal{L}}_0 - \lambda)^{-1}\begin{pmatrix}\hat{\boldsymbol{v}}\\ \hat{\eta}\end{pmatrix} = \begin{pmatrix}(\mathbf{A}_1 - \lambda\mathrm{Id})^{-1} & 0\\ -(\mathbf{A}_2-\lambda)^{-1}\mathbf{B}(\mathbf{A}_1-\lambda\mathrm{Id})^{-1} & (\mathbf{A}_2-\lambda)^{-1}\end{pmatrix}\begin{pmatrix}\hat{\boldsymbol{v}}\\ \hat{\eta}\end{pmatrix}\,.$$

Hence, as claimed, the asymptotic operator $\mathcal{L}_0$ possesses marginally stable spectrum and we cannot immediately infer linear stability information about the nontrivial steady solution of Theorem 3.1 for large amplitudes. However, numerical computations based on truncated Fourier series suggest, that the spectrum is in fact rather strongly unstable, cf. Figure 3.8.

Energy of explicit solutions

In closing, we briefly consider some energetic aspects of the explicit solutions from Theorem 3.1. The kinetic energy density of solutions to (3.1) is given by $\mathrm{KE}(\boldsymbol{v},\eta) = (H_0+\eta)|\boldsymbol{v}|^2/2$ and the potential energy density by $\mathrm{PE}(\boldsymbol{v},\eta) = g(H_0+\eta)^2/2$. The superposed explicit solutions are generally of the form

$$\begin{aligned}\boldsymbol{v} &= A_s\cos(\xi_s)\boldsymbol{k}^\perp + A_n\mathrm{e}^{\mu_n t}\cos(\xi_n)\boldsymbol{k}^\perp + A_p\mathrm{e}^{\mu_p t}\cos(\xi_p)\boldsymbol{k}^\perp\,,\\ \eta &= \gamma\frac{f}{g}\sin\xi_s + c\,,\end{aligned}$$

with $|\boldsymbol{k}|=1$, phase variables $\xi_a = \kappa_a\boldsymbol{k}\cdot\boldsymbol{x}+\theta_a$ for $a\in\{s,n,p\}$, growth rates $\mu_n<0$ and $\mu_p>0$, wave numbers $\kappa_s,\kappa_n,\kappa_p\in\mathbb{R}$ as well as arbitrary amplitudes $A_a\in\mathbb{R}$ and shifts $\theta_a, c\in\mathbb{R}$ for any $a\in\{s,n,p\}$. The corresponding terms are steady, decaying and growing explicit solutions, determined by (3.4) and (3.5) (compare with steady solutions in red region in Figure 3.6(a) and the possible superpositions with solutions which are decaying or growing in time). The energy densities of these explicit solutions explicitly read

$$\begin{aligned}\mathrm{KE}(\boldsymbol{v},\eta) &= \frac{1}{2}\left(\gamma\frac{f}{g}\sin\xi_s + H_0 + c\right)\left(A_s\cos\xi_s + A_n\mathrm{e}^{\mu_n t}\cos\xi_n + A_p\mathrm{e}^{\mu_p t}\cos\xi_p\right)^2\\ \mathrm{PE}(\boldsymbol{v},\eta) &= \frac{\gamma^2 f^2}{2g}\sin^2\xi_s + \gamma f(H_0+c)\sin\xi_s + \frac{g(H_0+c)^2}{2}\,.\end{aligned}$$

Notably, being cubic in the sine/cosine terms, the kinetic energy in Fourier space features various diadic and triadic combinations of the different wave components of the explicit solution. On the temporal side, the squared linear combination of time-independent, decaying and growing parts yields doubling and adding of the individual rates. The potential energy has no dynamic terms, but we note the constant and $2\kappa_s\boldsymbol{k}$ Fourier modes from the quadratic term.

3.2. Rotating Boussinesq equations with backscatter

We now turn to the investigations of various explicit solutions of the form as provided in Section 2.1 in the rotating Boussinesq equations augmented with hyperdiffusion and backscatter

$$\frac{\partial\boldsymbol{v}}{\partial t} + (\boldsymbol{v}\cdot\nabla)\boldsymbol{v} + f\boldsymbol{e_3}\times\boldsymbol{v} + \nabla p - \boldsymbol{e_3}b = -\begin{pmatrix}d_1&0&0\\0&d_2&0\\0&0&d_3\end{pmatrix}\Delta^2\boldsymbol{v} - \begin{pmatrix}b_1&0&0\\0&b_2&0\\0&0&b_3\end{pmatrix}\Delta\boldsymbol{v}\,, \tag{3.21a}$$

$$\nabla\cdot\boldsymbol{v} = 0\,, \tag{3.21b}$$

$$\frac{\partial b}{\partial t} + (\boldsymbol{v}\cdot\nabla)b + N^2 v_3 = \tilde{\nu}\Delta b\,, \tag{3.21c}$$

with the horizontal hyperviscosity or hyperdiffusion parameters d_1, $d_2 > 0$, horizontal backscatter parameters b_1, $b_2 > 0$ and usual viscosity $d_3 = 0$, $b_3 = -\nu \leq 0$ vertically. For the same reasons as discussed in Section 3.1, we focus on isotropic horizontal hyperviscosity $d_1 = d_2$ and backscatter $b_1 = b_2$, but also consider (weak) anisotropy here as well. Other quantities in (3.21) are the velocity field $\boldsymbol{v}(t, \boldsymbol{x}) \in \mathbb{R}^3$ for $\boldsymbol{x} \in \mathbb{R}^3$, $t \geq 0$, pressure and buoyancy $p(t, \boldsymbol{x})$, $b(t, \boldsymbol{x}) \in \mathbb{R}$, vertical unit vector $\boldsymbol{e_3}$ and thermal diffusivity $\tilde{\nu} \geq 0$. As usual, the buoyancy considered here is of the form $b(t, \boldsymbol{x}) = -g(\rho(t, \boldsymbol{x}) - \overline{\rho}(z))/\rho_0 \in \mathbb{R}$ with fluid density $\rho(t, \boldsymbol{x}) \in \mathbb{R}$ and reference density field $\overline{\rho}(z)$ depending on the vertical space direction z only, and the characteristic density ρ_0. Then $N^2 = -(g/\rho_0)\mathrm{d}\overline{\rho}/\mathrm{d}z$ is the Brunt-Väisälä frequency and we consider the stable stratification $\mathrm{d}\overline{\rho}/\mathrm{d}z < 0$, so $N^2 > 0$.

We emphasize that in the Boussinesq equations (3.21) the pressure gradient ∇p can be chosen completely free (as in (2.30) and (2.33)), in contrast to the gradient term $\nabla\eta$ in the shallow water equations (3.1), which is restricted due to (3.1b). As a result, we are able to use not only the radial superposition principle of Theorem 2.3 for explicit solutions of (3.21), but also the angular superposition principle of Theorem 2.9 and Theorem 2.10 (cf. Remark 3.0.1 for the restriction in the rotating shallow water equations). Furthermore, we will see that even for horizontally isotropic hyperdiffusion and backscatter we can obtain phenomena in the problem (3.21), which are only occurring in the anisotropic case in the shallow water equations (3.1), in particular the unbounded instability in the classes of flows we consider. Not surprisingly, the additional parameters of anistropy often give more freedom of choice. A subtlety is that for one type of monochromatic intertia gravity waves discussed in Section 3.2.2 unbounded growth occurs under stable stratification only in presence of at least some anisotropy.

For comparison and illustration we also discuss briefly the usual horizontal viscous or inviscid cases $d_1 = d_2 = 0$, b_1, $b_2 \leq 0$, unstable stratification $N^2 < 0$, and vertical hyperdiffusion as well as artificial backscatter d_3, $b_3 > 0$. As in Section 3.1, we are especially interested in the parameter relations and stability properties of steady solutions, in particular unbounded instability, as well as in unboundedly growing explicit solutions.

We first investigate the (interacting) horizontal plane flows in Section 3.2.1, which are also studied in Section 2.3.1 and Section 2.3.2, where the velocity is decoupled from the buoyancy. Afterwards, we analyze explicit solutions with vertical structure and coupled buoyancy in Section 3.2.2, which belong to the classes of parallel flows, Kolmogorov flows and monochromatic inertia gravity waves, as also studied in Section 2.3.1.

3.2.1. Horizontal flow and decoupled system

As for the (interacting) horizontal plane flows in Section 2.3.1 and Section 2.3.2, we consider here the barotropic case with horizontal velocity field. Hence, we choose a velocity field $\boldsymbol{v}$ that is independent of the vertical coordinate z and has $v_3 \equiv 0$, as well

as a horizontally independent buoyancy $b = \tilde{b}(t, z)$. This reduces (3.21) to

$$\frac{\partial \boldsymbol{v}}{\partial t} + (\boldsymbol{v} \cdot \nabla)\boldsymbol{v} + f\boldsymbol{v}^\perp + \nabla\tilde{p} = -\begin{pmatrix} d_1\Delta^2 + b_1\Delta & 0 \\ 0 & d_2\Delta^2 + b_2\Delta \end{pmatrix} \boldsymbol{v}\,, \tag{3.22a}$$

$$\nabla \cdot \boldsymbol{v} = 0\,, \tag{3.22b}$$

$$\frac{\partial \tilde{b}}{\partial t} = \tilde{\nu}\frac{\partial^2 \tilde{b}}{\partial z^2}\,, \tag{3.22c}$$

with gradient ∇ and Laplacian operatos Δ, Δ^2 for the horizontal directions $\boldsymbol{x} = (x, y)^\intercal$, velocity $\boldsymbol{v} = \boldsymbol{v}(t, \boldsymbol{x}) \in \mathbb{R}^2$, buoyancy $b = \tilde{b}(t, z)$ and pressure $p = \tilde{p} + B(t, z)$, with $\frac{\partial}{\partial z}B(t, z) = \tilde{b}(t, z)$. Here the buoyancy is decoupled from the velocity field and determined by the linear heat equation (3.22c). On the idealized whole space this can be readily solved by Fourier transform. In the following we will only determine the velocity $\boldsymbol{v}$.

Due to the horizontal structure of the velocity and the decoupling from the buoyancy, such flows are similar to those of the rotating shallow water equations (3.1). In fact, the momentum equations (3.1a) and (3.22a), which determine the velocity $\boldsymbol{v}$, only differ by the gradient terms, which is free in (3.22a) and restricted in (3.1a) by (3.1b). Indeed, the equation (3.1b) is here replaced by the incompressibility condition (3.22b), but it does not restrict the considered explicit solutions as in Section 2.1 in any way (see Theorem 2.5 and Theorem 2.11). Hence, the (interacting) horizontal plane flows of (3.22) are a good comparison for the explicit solutions of the rotating shallow water equations (3.1) in Section 3.1, providing a good picture of the impact of the restriction on the gradient term $\nabla\eta$.

We consider explicit solutions according to Theorem 2.3 with $N = M_1 = 1$. Due to the considered two-dimensional space, the orthogonality of wave vector and flow direction and the general form of wave shapes, we can omit further superpositions as in Theorem 2.3 without loss. With wave shape ψ and pressure profile ϕ we thus have

$$\boldsymbol{v} = \psi(t, \boldsymbol{k} \cdot \boldsymbol{x})\boldsymbol{k}^\perp\,, \qquad \tilde{p} = f\phi(t, \boldsymbol{k} \cdot \boldsymbol{x})\,, \tag{3.23}$$

where $\boldsymbol{k} \in \mathbb{R}^2$ and without loss of generality $|\boldsymbol{k}| = 1$, due to the free choice of ψ and ϕ. Substitution into (3.22a) gives the linear equations for ψ and ϕ,

$$\frac{\partial \psi}{\partial t} = -(d_1 k_y^2 + d_2 k_x^2)\frac{\partial^4 \psi}{\partial \xi^4} - (b_1 k_y^2 + b_2 k_x^2)\frac{\partial^2 \psi}{\partial \xi^2}\,, \tag{3.24a}$$

$$\frac{\partial \phi}{\partial \xi} = \frac{k_x k_y}{f}\left((d_1 - d_2)\frac{\partial^4 \psi}{\partial \xi^4} + (b_1 - b_2)\frac{\partial^2 \psi}{\partial \xi^2}\right) + \psi\,. \tag{3.24b}$$

For the Boussinesq equations with usual viscosity in Section 2.3.1 similar equations arise for horizontal plane flows. However, in that case the pressure gradient fully compensates the buoyancy and the Coriolis term in the equations, which makes the velocity

field geostrophically balanced. In contrast, in the present case, equation (3.24b) for the pressure shape ϕ allows the pressure gradient to not only compensate the full Coriolis term, but also part of the hyperdiffusion and backscatter terms. In particular, the velocity field (3.23) with (3.24) is in general not geostrophically balanced in the anisotropic case. For isotropic hyperdiffusion and backscatter only the Coriolis term remains on the right-hand side of (3.24b), which yields a geostrophic flow $\boldsymbol{v}$.

Superposition principles

The general wave shape ψ in (3.23) also contains the superpositions of arbitrary many sinusoidal waves in the same wave vector direction $\boldsymbol{k}$ and any wave number $|\boldsymbol{k}|$. The arbitrary choice of wave vector length is possible in the Boussinesq equations, since ∇p in the momentum equation (3.21a) is not further constrained, unlike (3.1b) for $\nabla\eta$. It is also possible to superpose by integrating over the wave numbers in the same wave vector direction.

As for the interacting horizontal plane flows in the Boussinesq equations (2.33) in Section 2.3.2, we can use angular superposition of explicit solutions (3.23) here as well. According to Theorem 2.9, we choose finite superposition of waves on a plane $N = 1$ with arbitary $M_1 \in \mathbb{N}$, which results in superposed sinusoidal explicit solutions of the decoupled momentum equation (3.22a)

$$\boldsymbol{v}(t,\boldsymbol{x}) = \sum_{j=1}^{M_1} \mathrm{e}^{\mu_j t} A_j \sin(\boldsymbol{k}_j \cdot \boldsymbol{x} + \theta_j)\boldsymbol{k}_j^{\perp}\,, \tag{3.25a}$$

$$\begin{aligned}\tilde{p}(t,\boldsymbol{x}) = &-\sum_{j=1}^{M_1}\sum_{\ell=j+1}^{M_1} A_j A_\ell \mathrm{e}^{(\mu_j+\mu_\ell)t}\Big(\cos(\xi_j)\cos(\xi_\ell) + \frac{\boldsymbol{k}_j\cdot\boldsymbol{k}_\ell}{s^2}\sin(\xi_j)\sin(\xi_\ell)\Big)\\ &- f\sum_{j=1}^{M_1}\gamma_j \mathrm{e}^{\mu_j t}\cos(\xi_j)\,,\end{aligned} \tag{3.25b}$$

for any fixed wave number $s > 0$, wave vectors $\boldsymbol{k}_j = (k_{j,x}, k_{j,y})^\intercal \in \mathbb{R}^2$ with $|\boldsymbol{k}_j| = s$, arbitrary amplitudes $A_j \in \mathbb{R}\setminus\{0\}$, phase shifts $\theta_j \in \mathbb{R}$ and phase variables $\xi_j = \boldsymbol{k}_j\cdot\boldsymbol{x}+\theta_j$ for any $1 \le j \le M_1$. Again, due to the choice of wave vector and flow direction for each wave, it is $\delta_{j,\ell} = 1$ for all $1 \le j, \ell \le M_1$ in Theorem 2.9. Here, each growth rate μ_j and amplitude γ_j is defined by the dispersion and amplitude relation

$$\mu_j = (b_1 - d_1 s^2)k_{j,y}^2 + (b_2 - d_2 s^2)k_{j,x}^2\,, \tag{3.26a}$$

$$f\frac{\gamma_j - A_j}{A_j} = ((d_1 - d_2)s^2 + b_2 - b_1)k_{j,x}k_{j,y}\,, \tag{3.26b}$$

in order to solve (3.22a). The velocity $\boldsymbol{v}$ in (3.25a) also solves (3.22b) (see Theorem 2.11), and thereby (3.25) with (3.26) is an explicit solution of (3.22).

It is also possible to use angular superposition of explicit solutions by integrating

over the whole circle $S(s) := \{\boldsymbol{k} \in \mathbb{R}^2 \mid |\boldsymbol{k}| = s\}$ for any fixed $s > 0$, according to Theorem 2.10. Hence, we obtain the explicit solutions of (3.22)

$$\boldsymbol{v}(t,\boldsymbol{x}) = \int\limits_{S(s)} A(\boldsymbol{k}) \mathrm{e}^{\mu(\boldsymbol{k})t} \sin(\boldsymbol{k}\cdot\boldsymbol{x} + \theta(\boldsymbol{k}))\boldsymbol{k}^\perp \mathrm{d}\boldsymbol{k}\,, \tag{3.27a}$$

$$\begin{aligned}\tilde{p}(t,\boldsymbol{x}) = &- s^2 \int_0^{2\pi}\int_{\varphi_1}^{2\pi} A_1 A_2 \mathrm{e}^{(\mu_1+\mu_2)t}(\cos\xi_1\cos\xi_2 + \cos(\varphi_1-\varphi_2)\sin\xi_1\sin\xi_2)\mathrm{d}\varphi_2\mathrm{d}\varphi_1 \\ &- f\int\limits_{S(s)} \gamma(\boldsymbol{k})\mathrm{e}^{\mu(\boldsymbol{k})t}\cos(\boldsymbol{k}\cdot\boldsymbol{x}+\theta(\boldsymbol{k}))\mathrm{d}\boldsymbol{k}\,,\end{aligned} \tag{3.27b}$$

with arbitrary amplitudes $A, \gamma \in L^\infty(S(s))$, growth rate $\mu(\boldsymbol{k}) \in \mathbb{R}$ and arbitrary phase shifts $\theta(\boldsymbol{k}) \in \mathbb{R}$ for all $\boldsymbol{k} \in S(s)$. For $j = 1, 2$ and wave vectors $\boldsymbol{k}_j := s(\cos\varphi_j, \sin\varphi_j)^\mathsf{T}$ we define the amplitudes $A_j := A(\boldsymbol{k}_j)$, growth rates $\mu_j := \mu(\boldsymbol{k}_j)$ and phase variables $\xi_j := \boldsymbol{k}_j\cdot\boldsymbol{x} + \theta(\boldsymbol{k}_j)$, for all $0 \le \varphi_j < 2\pi$. Furthermore, growth rate μ and amplitude γ are defined for almost all $\boldsymbol{k} \in S(s)$ by

$$A(\boldsymbol{k})\mu(\boldsymbol{k}) = A(\boldsymbol{k})((b_1 - d_1 s^2)k_y^2 + (b_2 - d_2 s^2)k_x^2)\,, \tag{3.28a}$$

$$f(\gamma(\boldsymbol{k}) - A(\boldsymbol{k})) = A(\boldsymbol{k})k_x k_y((d_1 - d_2)s^2 + b_2 - b_1)\,, \tag{3.28b}$$

corresponding to (3.26) if $A(\boldsymbol{k}) \neq 0$. The velocity $\boldsymbol{v}$ in (3.27a) also solves (3.22b) (see Theorem 2.11), and thereby (3.27) with (3.28) is an explicit solution of (3.22).

Comparing the explicit solutions (3.25) with (3.26), as well as (3.27) with (3.28), with the corresponding explicit solutions (2.36) and (2.37) of the Boussinesq equations without backscatter (2.33), we notice two major differences:
First, in the present case the amplitudes γ_j and $\gamma(\boldsymbol{k})$ of the pressure can be different from those of the velocity. The conditions, or definitions, on the amplitudes are given in (3.26b) and (3.28b) respectively. The reason is that the pressure gradient in the momentum equation (3.22a) can additionally compensate a part of the hyperdiffusion and backscatter terms as well.
Second, the growth rates μ_j and $\mu(\boldsymbol{k})$ can be different, so that each wave is decaying or growing differently from each other.
Both differences require anisotropy in hyperdiffusion or backscatter of the momentum equation, i.e. $d_1 \neq d_2$ or $b_1 \neq b_2$. Indeed, the usual viscosity is isotropic in this sense.

Unbounded instability of steady solutions

Analogous to Section 3.1.2, the possible superpositions of explicit solutions, as discussed above, imply linear subspaces with linear dynamics, in particular unbounded exponential growth of perturbations. Compared with the rotating shallow water equations (3.1), restrictions on wave vectors are absent for the (interacting) horizontal plane flows here. In this section we discuss implications for (in)stability of steady solutions, which are

decribed by (3.25a) with $\mu_j = 0$ in the dispersion relation (3.26a). They also cover steady solutions of the form (3.23) as single wave without superposition. Due to the integration, steady solutions of (3.27) with (3.28) is possible in the isotropic case, providing $\mu(\boldsymbol{k}) = 0$ on a certain whole circle $S(s)$ by (3.28a), but then there is no further superposition of exponentially growing explicit solution possible, in order to show unbounded instability.

Since b_1, b_2, d_1, $d_2 > 0$ in (3.26a) we have $\mu_j > 0$ for any sufficiently small wave numbers s and $\mu_j < 0$ for any sufficiently large ones. In particular, the trivial flow with $\boldsymbol{v} \equiv 0$ is unstable with exponential unbounded growth with respect to any small wave number s. More importantly, the above radial superposition principle immediately implies that the same holds for every single-wave steady solution (3.23). Such steady explicit solutions also arise from (3.25) with $M_1 = 1$ and $\mu_1 = 0$ in (3.26a). Since the definition of μ_j in (3.26a) is exactly the same as in the dispersion relation (3.6a) for the explicit solution from Theorem 3.1 of the shallow water equations (3.1), we can use here the results from Section 3.1.1 about the growth rate μ as well. Hence, for any b_1, b_2, d_1, $d_2 > 0$ the set of solutions with $\mu_j = 0$ forms a simple closed curve around the origin in the wave vector space that is symmetric with respect to axis reflections and whose interior is star shaped. Furthermore, μ_j is positive in the interior of this closed curve, except $\mu_j = 0$ at the origin $\boldsymbol{k} = (0,0)^\intercal$, and μ_j is negative outside the closed curve. Thus, single-wave steady solutions (3.23) exist in any direction and can be radially superposed with explicit solutions with any smaller wave numbers s, which makes them always unboundedly unstable.

However, in the case $b_1/d_1 \neq b_2/d_2$, for fixed s there are up to four wave vectors for which $\mu_j = 0$. In order to see this, note that for $\mu_j = 0$ the dispersion relation (3.26a) is linear in $\cos^2\varphi$ for $\boldsymbol{k}_j = s(\cos\varphi, \sqrt{1-\cos^2\varphi})^\intercal$ in the first quadrant. This provides at most one solution of (3.26a) with $\mu_j = 0$ in this quadrant. Thus, due to the reflection symmetry, there is at most one solution in each quadrant of the wave vector plane, so in total four. Because of the symmetry, the steady states of the form (3.25) can consist of (at most) two different wave vector directions and for those we cannot infer instability by the radial superposition principle as before.

We now show unbounded instability of steady solutions (3.25), which consists of two waves with different wave vector directions, by the angular superposition principle. First, we note that for $b_1/d_1 \neq b_2/d_2$ there is a unique (up to reversing orientation) longest wave vector $\boldsymbol{k}_{\max}$ with length $s_{\max}$, so that (3.26a) is satisfied with $\mu_j = 0$. See Figure 3.9(a) for a typical example. Indeed, due to the aformentioned structures, $\boldsymbol{k}_{\max}$ is along an axis, though the set of $\boldsymbol{k}$ with $\mu_j = 0$ need not be convex. Hence, any steady superposed solution (3.25) with $s = s_{\max}$ is built from $\pm\boldsymbol{k}_{\max}$, which lie on the same line in wave vector space. Thus, we can use the radial superposition principle with the exponentially growing explicit solutions of smaller wave numbers, which leads to unbounded growth with respect to modes on any larger scale. The same applies for steady solutions with minimal wave vector length $s_{\min}$.

Second, we consider steady superposed solutions (3.25) with $s_{\min} < s < s_{\max}$ that can be built from two different directions, cf. the white dots in Figure 3.9(b). Here, we apply the angular superposition principle and superpose with any explicit solution (3.25) on the same scale, i.e. whose wave vector has the same length s, cf. the white circle in Figure 3.9(b). Since for some wave vectors the corresponding μ_j defined by the dispersion relation (3.26a) is positive for the length $s < s_{\max}$, at least for the wave vector $s/s_{\max}\boldsymbol{k}_{\max}$, we again have unbounded instability with respect to a range of modes, here on the same scale.

In case $b_1/d_1 = b_2/d_2$, and thus for the isotropic case as well, we cannot infer the instability of steady superposed solutions (3.25), i.e. steady solutions not of single-wave type, using the above superposition principles, since the wave vectors of nontrivial steady solutions $\{\boldsymbol{k} \in \mathbb{R}^2 \mid \mu(\boldsymbol{k}) = 0\}$, with $\mu(\boldsymbol{k})$ from (3.26a), form a circle with radius $\sqrt{b_1/d_1}$, which means they all have the same length. Thus, explicit solutions (3.25) with $s = \sqrt{b_1/d_1}$ consist only of steady solutions. There are also no steady solutions of the form (3.23) for other wave numbers. However, in some cases unbounded instability still follows from angular superposition with unboundedly growing parallel flows, cf. Section 3.2.2.

Remark 3.1.2. Since the parameter b_1, b_2, d_1, $d_2 > 0$ can be chosen arbitrarily in (3.22), it is natural to consider (3.22a) and (3.22b) as a regularization of the two-dimensional (rotating) Euler equations, when the hyperdiffusion and backscatter parameter are small, as noted in the introduction. The explicit solutions shown here can be important to understand the dynamics of this backscatter regularization, which might provide a better understanding of the dynamics of the two-dimensional (rotating) Euler equations.

In Section 2.2.1 we have shown, that the Euler equations have steady traveling wave solutions of the form as in Theorem 2.3 for any wave vector and any wave shape. The regularization of the Euler equations (3.22a) and (3.22b), with $f = 0$ and isotropic backscatter and hyperdiffusion $b_1 = b_2$ and $d_1 = d_2$, has solutions (3.23) with sinusoidal wave shapes, which we obtain for any wave vector if considering single wave solutions. These explicit solutions decay exponentially to the zero state (for $|\boldsymbol{k}| > \sqrt{b_1/d_1}$) or grow exponentially and unboundedly (for $0 < |\boldsymbol{k}| < \sqrt{b_1/d_1}$). For the same initial conditions similar traveling wave solutions exist for the Euler equations, but they are always time-independent. However, if the backscatter and hyperdiffusion parameter tend to zero, then the growth rates of the explicit solutions in the backscatter model (3.22a) and (3.22b) tend to zero as well (see (3.24a) or (3.26a)), which then correspond to the steady solutions of the Euler equations. Thus, there seems to be a correlation between these explicit solutions and they could provide first hints for the understanding of the relations between the backscatter regularization and the Euler equations.

Although, one needs to be careful with the convergences of the explicit backscatter solutions. If the parameter $b_1 = b_2 = \varepsilon b$ and $d_1 = d_2 = \varepsilon d$ tend to zero for $\varepsilon \to 0$, then the radius of the area for growing solutions $\sqrt{b_1/d_1}$ remain the same for any ε. This means, that most explicit solutions will decay to the trivial state or grow unboundedly for any

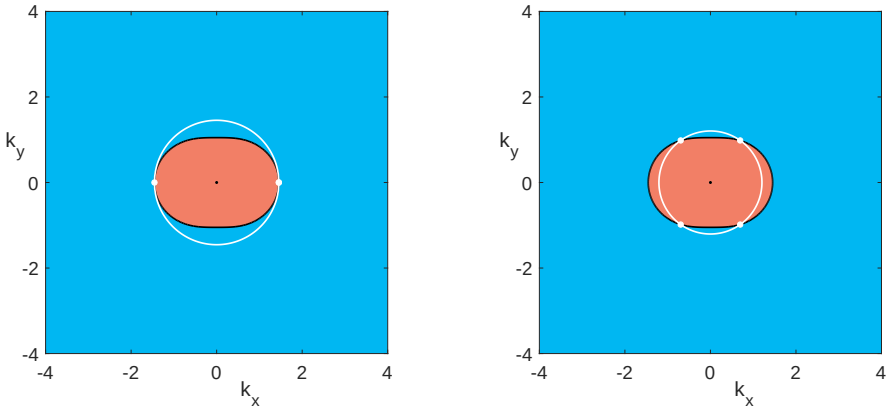

(a) Case $s = s_{\max} = \sqrt{b_2/d_2}$ for steady solutions with largest possible wave number.

(b) Case $s \approx 1.20 < s_{\max}$ for steady solutions with different wave vector directions.

Figure 3.9.: Signs of μ_j as defined in the dispersion relation (3.26a) (red: $\mu_j > 0$, blue: $\mu_j < 0$, black: $\mu_j = 0$) and possible wave vectors for (3.25) for a fixed wave number $s > 0$ (white circles). White dots mark wave vectors of corresponding steady solutions. Fixed parameters are $d_1 = 1.0$, $d_2 = 1.04$, $b_1 = 1.1$, $b_2 = 2.2$, i.e. $b_1/d_1 \neq b_2/d_2$.

$\varepsilon > 0$ and only the magnitudes of their growth rates are varying. For $b_1 = b_2 = \varepsilon^2 b$ and $d_1 = d_2 = \varepsilon d$ the area of wave vectors corresponding to exponentially growing explicit solutions tends to the origin for $\varepsilon \to 0$, while for $b_1 = b_2 = \varepsilon b$ and $d_1 = d_2 = \varepsilon^2 d$ this area grows unboundedly and even more explicit solutions start to grow exponentially. Consequently, most of the explicit solutions in the regularization behave different from the corresponding steady solutions in the Euler equations, even though they depend more and more slowly on time, when backscatter and hyperdiffusion tend to zero.

Linear stability of steady solutions with small and large amplitudes

After the investigation of unbounded instability of steady solutions, we now turn to the linear stability of steady solutions with small and large amplitudes, analogous to Section 3.1.2 for the rotating shallow water equations (3.1). Concerning small amplitudes, we are naturally led to linear and spectral stability of the trivial zero solution again. Instead of analyzing the full spectrum of the linearization of (3.22) in the trivial steady flow $\boldsymbol{v} \equiv 0$, here we restrict attention to instability with respect to eigenmodes of the form of the horizontal plane flows (3.23), which means solutions to (3.24a). The Fourier transform of (3.24a) yields the dispersion relation for perturbation wave vector $\boldsymbol{k} \in \mathbb{R}^2$ and temporal rate $\lambda \in \mathbb{C}$

$$d_\psi(\lambda, \boldsymbol{k}) = -(d_1 k_y^2 + d_2 k_x^2)|\boldsymbol{k}|^2 + b_1 k_y^2 + b_2 k_x^2 - \lambda = 0\,,$$

which is of course equivalent to (3.26a) with $\lambda = \mu_j$ and $\boldsymbol{k} = \boldsymbol{k}_j$. The above discussion about unbounded instability for steady solutions built from single direction wave vectors $\pm\boldsymbol{k}$ implies that the spectrum of the linearization in such steady horizontal plane flows is at least as unstable as that of the zero solution in this wave vector direction. This follows from the fact, that the spectra contain the growth rates of the corresponding explicit solutions in the same direction as well, since as an arbitrary perturbation of the steady solution they also solve the nonlinear equation, which means the linearization in this steady state as well. Of course the result is much stronger in that these modes actually grow unboundedly in the nonlinear Boussinesq equations. In contrast, for the linearization of (3.22) in steady multi-mode horizontal plane flow, similar comparison of its spectrum with that of the zero state holds, but with different wave vector directions and the same wave number $|\boldsymbol{k}| = s$.

However, analogous to Section 3.1.2, any (superposed) steady horizontal plane flow inherits the instability of any unstable mode in the dispersion relation $d_\psi(\lambda, \boldsymbol{k}) = 0$ of the trivial zero solution for sufficiently small amplitudes $0 < |A_j| \ll 1$, $1 \leq j \leq M_1$, though the growth induced by such modes may be bounded. Recall that the explicit solutions of (3.22) also satisfy the full rotating Boussinesq equations (3.21), which admit modes that have vertical structures and are coupled with buoyancy. In Section 3.2.2 we will discuss such explicit solutions of (3.21), which also satisfy these equations without the nonlinear terms. In particular, unboundedly growing flows of this type provide additional explicit unstable modes of the zero solution $\boldsymbol{v} \equiv 0$, which – in contrast to the (interacting) horizontal plane flows – are also influenced by the Brunt-Väisälä frequency N^2, thermal diffusivity $\tilde{\nu}$ and the vertical viscosity. In addition, these imply linear unstable modes for (interacting) horizontal plane flows with sufficiently small amplitudes $0 < |A_j| \ll 1$, $1 \leq j \leq M_1$.

Regarding large amplitudes, where $1 \ll |A_j|$ for at least one j, we first note that, in the notation of Section 3.1.2 and with $\boldsymbol{u} = (\boldsymbol{v}, b)^\intercal$, the bilinear form for the present case reads

$$\mathcal{B}\Big((\boldsymbol{v}_1, b_1)^\intercal, (\boldsymbol{v}_2, b_2)^\intercal\Big) = -\begin{pmatrix} (\boldsymbol{v}_1 \cdot \nabla)\boldsymbol{v}_2 \\ (\boldsymbol{v}_1 \cdot \nabla) b_2 \end{pmatrix}.$$

The steady state family $\boldsymbol{u} = a\boldsymbol{u}_0$ in this case has $\boldsymbol{u}_0 = (\boldsymbol{v}_0, b_0)^\intercal$ with

$$\boldsymbol{v}_0 = \sum_{j=1}^{M_1} A_j \sin(\boldsymbol{k}_j \cdot \boldsymbol{x} + \theta_j)\boldsymbol{k}_j^\perp,$$

where we consider here in this section only horizontal (wave) vectors $\boldsymbol{k} := (\hat{\boldsymbol{k}}, 0)^\intercal$, $\boldsymbol{k}^\perp := (\hat{\boldsymbol{k}}^\perp, 0)^\intercal$ for any $\hat{\boldsymbol{k}} \in \mathbb{R}^2$. Here the third component of $\boldsymbol{v}_0$ vanishes, and b_0 is an arbitrary constant solving (3.22c). In order to find strongly unstable modes, whose growth rates $\lambda = a\tilde{\lambda}$ are proportional to the amplitude parameter a, we study the

generalized eigenvalue problem (3.20) as $|a| \to \infty$, which here reads

$$\widetilde{\lambda} \begin{pmatrix} \boldsymbol{v} \\ b \end{pmatrix} = \mathcal{L}_0 \begin{pmatrix} \boldsymbol{v} \\ b \end{pmatrix} + \begin{pmatrix} \nabla \bar{p} \\ 0 \end{pmatrix}, \qquad \nabla \cdot \boldsymbol{v} = 0, \tag{3.29}$$

with $p = a\bar{p}$ and the operator $\mathcal{L}_0$ defined by

$$\mathcal{L}_0 \begin{pmatrix} \boldsymbol{v} \\ b \end{pmatrix} = - \begin{pmatrix} (\boldsymbol{v}_0 \cdot \nabla)\boldsymbol{v} + (\boldsymbol{v} \cdot \nabla)\boldsymbol{v}_0 \\ (\boldsymbol{v}_0 \cdot \nabla) b \end{pmatrix}.$$

In order to simplify and illustrate the main finding, we investigate the stability of a certain superposed steady solution. We reduce to only two modes, i.e. $A_j = 0$ for $j > 2$, translate so that $\theta_1 = \theta_2 = 0$, and set phase variables $\xi = \boldsymbol{k} \cdot \boldsymbol{x}$, $\zeta = \boldsymbol{k}^\perp \cdot \boldsymbol{x}$ so that we consider an explicit solution (3.25) and (3.26) with a certain wave vector $\boldsymbol{k}$

$$\boldsymbol{v}_0 = A_1 \sin(\xi)\boldsymbol{k}^\perp + A_2 \sin(\zeta)\boldsymbol{k}.$$

We note, that even in the anisotropic case there is at least one wave vector $\boldsymbol{k}$, such that both $\boldsymbol{k}$ and $\boldsymbol{k}^\perp$ correspond to such a steady solution. We omit the full proof, and instead explain the existence of such $\boldsymbol{k}$ based on Figure 3.9. We start with superposed steady solutions with wave number $s = s_{\max}$ as in Figure 3.9(a). Reducing s towards the wave number $s_{\min}$ as in Figure 3.9(b), there is an intermediate value of s such that a wave vector $\boldsymbol{k}$ with $|\boldsymbol{k}| = s$ exists, for which $\boldsymbol{k}$ and $\boldsymbol{k}^\perp$ each correspond to a single mode steady solution. This is ensured by the symmetry of the curve defined by (3.26a) with $\mu_j = 0$. We then obtain

$$\begin{aligned} \mathcal{L}_0 \begin{pmatrix} \boldsymbol{v} \\ b \end{pmatrix} &= - \begin{pmatrix} A_1 \sin(\xi)(\boldsymbol{k}^\perp \cdot \nabla)\boldsymbol{v} + A_2 \sin(\zeta)(\boldsymbol{k} \cdot \nabla)\boldsymbol{v} + \dots \\ \qquad \dots + A_1 \cos(\xi)(\boldsymbol{v} \cdot \boldsymbol{k})\boldsymbol{k}^\perp + A_2 \cos(\zeta)(\boldsymbol{v} \cdot \boldsymbol{k}^\perp)\boldsymbol{k} \\ A_1 \sin(\xi)(\boldsymbol{k}^\perp \cdot \nabla) b + A_2 \sin(\zeta)(\boldsymbol{k} \cdot \nabla) b \end{pmatrix} \\ &= - \begin{pmatrix} \mathcal{L}_1 & 0 \\ 0 & \mathcal{L}_2 \end{pmatrix} \begin{pmatrix} \boldsymbol{v} \\ b \end{pmatrix}, \end{aligned}$$

with a 4-by-4 block diagonal matrix operator in which $\mathcal{L}_1 := \left(\begin{smallmatrix} \mathcal{L}_3 & 0 \\ 0 & \mathcal{L}_2 \end{smallmatrix}\right)$ is a 3-by-3 block matrix operator build from the 2-by-2 matrix operator

$$\mathcal{L}_3 = \mathcal{L}_2 \mathrm{Id} + A_1 \cos(\xi) \mathrm{A}(\boldsymbol{k}) - A_2 \cos(\zeta) \mathrm{A}^\intercal(\boldsymbol{k}),$$

with $\mathrm{A}(\boldsymbol{k})$ as in Section 3.1.2 (for which $\mathrm{A}^\intercal(\boldsymbol{k}) = -\mathrm{A}(\boldsymbol{k}^\perp)$ holds) and the linear operator

$$\mathcal{L}_2 = A_1 \sin(\xi)(\boldsymbol{k}^\perp \cdot \nabla) + A_2 \sin(\zeta)(\boldsymbol{k} \cdot \nabla).$$

Taking the divergence of (3.29) gives, using $\nabla \cdot \boldsymbol{v} = 0$, the linear pressure Poisson equation $\Delta \bar{p} = \nabla \cdot (\mathcal{L}_1 \boldsymbol{v})$. We denote the solution as $\bar{p} = \Delta^{-1} \nabla \cdot (\mathcal{L}_1 \boldsymbol{v})$ and substitution into (3.29)

yields the eigenvalue problem

$$\widetilde{\lambda}\begin{pmatrix}\boldsymbol{v}\\ b\end{pmatrix} = \left(\mathcal{L}_0 + \begin{pmatrix}\nabla\Delta^{-1}\nabla\cdot(\mathcal{L}_1\circ) & 0\\ 0 & 0\end{pmatrix}\right)\begin{pmatrix}\boldsymbol{v}\\ b\end{pmatrix}, \tag{3.30}$$

in which $\circ$ denotes the slot for $\boldsymbol{v}$. The resulting operator on the right-hand side has a diagonal block structure such that the spectrum is the union of the spectra of $-\mathcal{L}_2$ and $-\widetilde{\mathcal{L}}_1$ defined by

$$\widetilde{\mathcal{L}}_1 := \mathcal{L}_1 - \nabla\Delta^{-1}\nabla\cdot(\mathcal{L}_1\circ)\,.$$

We consider the spatial domain $\Omega := \widetilde{\Omega}\times I$, with interval $I\subset\mathbb{R}$ and horizontal rectangular domain $\widetilde{\Omega}\subset\mathbb{R}^2$, so that $\boldsymbol{v}_0$ satisfies periodic boundary conditions on $\widetilde{\Omega}$ for all fixed $z\in I$. The operator $\mathcal{L}_2$ is then skew-adjoint on the space $H^1(\Omega)$ with the same periodic boundary properties. One can directly show this by taking ϕ, ψ from this function space and

$$\begin{aligned}
\langle \mathrm{i}\mathcal{L}_2\phi,\psi\rangle_{L^2(\Omega)} &= \int_\Omega \mathrm{i}\mathcal{L}_2\phi\cdot\overline{\psi}\,\mathrm{d}\boldsymbol{x} = \mathrm{i}\int_\Omega \Big(A_1\sin(\xi)\,\overline{\psi}\,\boldsymbol{k}^\perp + A_2\sin(\zeta)\,\overline{\psi}\,\boldsymbol{k}\Big)\cdot\nabla\phi\,\mathrm{d}\boldsymbol{x}\\
&= -\mathrm{i}\int_\Omega \operatorname{div}\Big(A_1\sin(\xi)\,\overline{\psi}\,\boldsymbol{k}^\perp + A_2\sin(\zeta)\,\overline{\psi}\,\boldsymbol{k}\Big)\cdot\phi\,\mathrm{d}\boldsymbol{x}\\
&= -\mathrm{i}\int_\Omega \Big(A_1\sin(\xi)\boldsymbol{k}^\perp\cdot\nabla\overline{\psi} + A_2\sin(\zeta)\boldsymbol{k}\cdot\nabla\overline{\psi}\Big)\cdot\phi\,\mathrm{d}\boldsymbol{x}\\
&= \int_\Omega \phi\cdot\overline{\mathrm{i}\mathcal{L}_2\psi}\,\mathrm{d}\boldsymbol{x} = \langle\phi,\mathrm{i}\mathcal{L}_2\psi\rangle_{L^2(\Omega)}\,,
\end{aligned}$$

where the periodic boundary properties of ϕ, ψ and $\boldsymbol{v}_0$, as well as the orthogonality of $\boldsymbol{k},\boldsymbol{k}^\perp\in\mathbb{R}^2\times\{0\}$, have been used. Since $\mathcal{L}_2$ is skew-adjoint, it follows for any eigenmode ϕ of $\mathcal{L}_2$ with eigenvalue λ

$$\mathrm{i}\lambda\|\phi\|_2^2 = \langle\mathrm{i}\lambda\phi,\phi\rangle_{L^2(\Omega)} = \langle\mathrm{i}\mathcal{L}_2\phi,\phi\rangle_{L^2(\Omega)} = \langle\phi,\mathrm{i}\mathcal{L}_2\phi\rangle_{L^2(\Omega)} = \langle\phi,\mathrm{i}\lambda\phi\rangle_{L^2(\Omega)} = -\mathrm{i}\overline{\lambda}\|\phi\|_2^2\,,$$

which yields $\mathrm{Re}(\lambda)=0$. Thus, the spectrum of $\mathcal{L}_2$ is purely imaginary. In case the steady solution is a single mode flow, i.e. $A_j=0$ for $j>1$, we readily determine as in Section 3.1.2 that the spectrum of $-\widetilde{\mathcal{L}}_1$ is also purely imaginary, so that the spectrum of $\mathcal{L}_0$ is purely imaginary.

In case of two-wave steady solution, i.e. $A_1A_2\neq 0$, it appears difficult to determine the spectrum of $\widetilde{\mathcal{L}}_1$ analytically and we resort to numerical computations. For this let $(\cdot)_m$ denote the projection onto the mode $\exp(\mathrm{i}\boldsymbol{k}_m\cdot\boldsymbol{x})$. Then

$$(\widetilde{\mathcal{L}}_1\boldsymbol{v})_m = (\mathcal{L}_1\boldsymbol{v})_m - \frac{\boldsymbol{k}_m\cdot(\mathcal{L}_1\boldsymbol{v})_m}{|\boldsymbol{k}_m|^2}\boldsymbol{k}_m = (\mathrm{Id}-\mathrm{B}(\boldsymbol{k}_m))(\mathcal{L}_1\boldsymbol{v})_m\,, \tag{3.31}$$

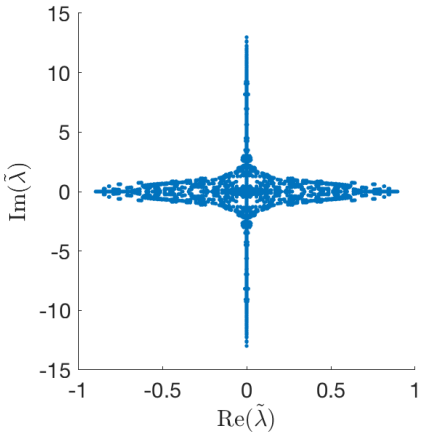

Figure 3.10.: Shown is an approximation of a part of the spectrum of $\widetilde{\mathcal{L}}_1$. Using (3.31) we reduced to two-dimensional wave vectors by fixing the third component of $\boldsymbol{k}_m$ at zero. Here $\boldsymbol{k} = (1,1)^\intercal$, $A_1 = 0.1$, $A_2 = 1$. As in Figure 3.8 we use $N = 10$ wave modes, i.e. $3(2N+1)^2$ Fourier modes on the periodic domain $[0, 2\pi/k_x] \times [0, 2\pi/k_y]$, and Bloch modes in the first component from the grid with distance $\pi/8$. In particular, the spectrum is unstable, so that large amplitude solutions are linear unstable with growth rates proportional to the amplitude.

with suitable matrix $\mathrm{B}(\boldsymbol{k}_m)$. This allows straightforward numerical computation of spectra on truncated Fourier series. We plot results for an example in Figure 3.10, which gives unstable spectrum and thus strong evidence for unstable spectrum of $\mathcal{L}_0$. Notably, this means that for steady solutions (3.25) with two waves $M_1 = 2$ it is possible that linear growth rates are proportional to the amplitude parameter a. In contrast, such modes do not exist for steady single wave flows, since in this case the spectrum of $\mathcal{L}_0$ is purely imaginary, as in Section 3.1.2. Again we remark that we expect the growth induced by these modes is bounded in the nonlinear system.

3.2.2. Flows with vertical structure and coupled buoyancy

The rotating Boussinesq equations with hyperdiffusion and backscatter (3.21) also have explicit solutions of different form, in which the velocity and the buoyancy are coupled, and in which the vertical dependence as well as velocity component are nontrivial. We investigate here the parallel flows, Kolmogorov flows and monochromatic inertia gravity waves, which were also studied for the usual Boussinesq equations (2.33) in Section 2.3. As before, we are in particular interested in the occurrence of unboundedly growing explicit solutions as well as the existence of such steady solutions and their stability properties.

Parallel flow

This class of explicit solutions is well-known in the inviscid and viscous case (e.g. Wang, 1990). It possesses only a vertical velocity component and is therefore different from the (interacting) horizontal plane flows, and has more general dependence on the horizontal space variables. Specifically, parallel flows in (3.21) are of the form

$$\boldsymbol{v}(t,\boldsymbol{x}) = w(t,x,y)\boldsymbol{e_3}\,, \qquad b(t,\boldsymbol{x}) = \tilde{b}(t,x,y)\,, \qquad p(t,\boldsymbol{x}) = \tilde{p}(t)z\,, \tag{3.32}$$

where w and $\tilde{b}$ satisfy, with horizontal Laplace and bi-Laplace operators,

$$\frac{\partial w}{\partial t} + \left(d_3\Delta_h^2 + b_3\Delta_h\right) w + \tilde{p} = \tilde{b}\,, \tag{3.33a}$$

$$\frac{\partial \tilde{b}}{\partial t} - \tilde{\nu}\Delta_h\tilde{b} = -N^2 w\,. \tag{3.33b}$$

Recall that common kinetic energy backscatter, which has $d_3 = 0$ and $b_3 \leq 0$, has no vertical impact so that parallel flows are in fact independent of backscatter. Parallel flows in plane wave form can be superposed with the horizontal plane flows (3.23) that have zero buoyancy, if their wave vector directions $\boldsymbol{k}$ are the same. In this case namely, both solutions satisfy the function form and orthogonality conditions for wave vectors and flow directions of Theorem 2.3, so that radial superposition is possible and gives explicit solutions of (3.21). Thus, a priori, any parallel flow of this form is unboundedly unstable concerning perturbations (3.23) with the same wave vector $\boldsymbol{k}$ and small enough wave number $|\boldsymbol{k}|$ (see analysis of unbounded instability in Section 3.2.1).

Existence and dynamics of parallel flows can be inferred from the dispersion relation of the remaining linear equations (3.33), if we consider the homogeneous case $\tilde{p} \equiv 0$. By Fourier transformation with wave vector $\boldsymbol{k}$ and growth rate μ this is given by

$$\det(\mu\mathrm{Id} - \widehat{\mathcal{L}}) = 0\,, \qquad \widehat{\mathcal{L}} := \begin{pmatrix} -d_3|\boldsymbol{k}|^4 + b_3|\boldsymbol{k}|^2 & 1 \\ -N^2 & -\tilde{\nu}|\boldsymbol{k}|^2 \end{pmatrix},$$

or equivalently as the characteristic polynomial

$$\mu^2 + c_1\mu + c_0 = 0\,, \tag{3.34}$$

where $c_1 := d_3K^2 + (\tilde{\nu} - b_3)K$ and $c_0 := \tilde{\nu}(d_3K - b_3)K^2 + N^2$ with $K := |\boldsymbol{k}|^2 \geq 0$. Steady solutions to (3.33) with $\tilde{p} \equiv 0$ consist of Fourier modes with $\boldsymbol{k} \neq 0$ that solve (3.34) with $\mu = 0$, i.e. $c_0 = 0$. Spatially non-constant solutions to (3.33) with $\tilde{p} \equiv 0$, which grow in time, exist if and only if (3.34) possesses a root with positive real part and $\boldsymbol{k} \neq 0$, and then do so exponentially and unboundedly. Note that both roots have negative real parts only for c_1, $c_0 > 0$ and complex conjugate solutions can be superposed to form a real parallel flow solution.

With vertical viscosity, $d_3 = 0$ and $b_3 < 0$, and focusing on non-constant solutions $\boldsymbol{k} \neq 0$, we have $c_1 > 0$ and $c_0 = -\tilde{\nu}b_3K^2 + N^2$. So steady solutions require unstable

stratification $N^2 < 0$ and quartic wave number $K^2 = N^2/(\tilde{\nu} b_3)$, or $\tilde{\nu} = N^2 = 0$ with any $K > 0$. For $\tilde{\nu} > 0$ also the unstable case $c_0 < 0$ requires unstable stratification $N^2 < 0$, and then $c_0 < 0$ occurs on a disc of wave vectors, for which the corresponding explicit solutions grow exponentially and unboundedly in time.

Regarding small amplitudes, analogous to Section 3.2.1, any steady (or decaying) parallel flow with small amplitude is linearly unstable, though typically not unboundedly, with respect to unstable modes of the trivial steady solution that are inherited for decreasing amplitude. In the large amplitude scaling, the resulting operator $\mathcal{L}_0$ (arising from the nonlinear advection term) for steady parallel flow w_0 is a lower triangular matrix operator with diagonal entries $\mathcal{L}_1 := w_0(x, y)\partial_z$, since steady parallel flows $\boldsymbol{v}_0$ have a vertical component only. Hence, as for the spectrum of $\mathcal{L}_0$ in Section 3.2.1, the spectrum is given by the diagonal entries. For any (smooth) w_0 the operator $\mathcal{L}_1$ is skew self-adjoint, similar to $\mathcal{L}_2$ in Section 3.2.1, and thus the spectrum of $\mathcal{L}_0$ is purely imaginary. Hence, no real parts of the spectrum of the steady parallel flow are proportional to its amplitude parameter a.

Finally, in order to illustrate the abstract structure and in preparation for the flows discussed below, we now briefly consider the artificial case of vertical hyperdiffusion and backscatter d_3, $b_3 > 0$.
Without thermal diffusion ($\tilde{\nu} = 0$), we have $c_0 = N^2$ and $c_1 = \delta_3(K) := (d_3 K - b_3)K$. For stable stratification, $N^2 > 0$, growing Fourier modes occur if and only if $c_1 < 0$ and $c_1^2 \geq 4c_0$, which is equivalent to $K < b_3/d_3$ and $N^2 \leq \delta_3^2(K)/4$, respectively. For $K \in (0, b_3/d_3)$ the global maximum of $\delta_3^2(K)/4$ is $b_3^4/(64d_3^2)$ at $K = K_1 := b_3/(2d_3)$. Its global minimum is zero at $K = 0$ and $K = b_3/d_3$. Specifically, if $N^2 \leq b_3^4/(64d_3^2)$, i.e. the stability of the stratification is sufficiently weak compared with the destabilization by vertical hyperdiffusion and backscatter, then $c_1^2 \geq 4c_0$ for K in a positive interval $I_1 \subset (0, b_3/d_3)$. In particular, $I_1 = \{K_1\}$ if $N^2 = b_3^4/(64d_3^2)$. Hence, a parallel flow (3.32) grows exponentially and unboundedly if it contains a Fourier mode with wave vector $\boldsymbol{k}$ in the annulus $\{\boldsymbol{k} \in \mathbb{R}^2 \,|\, |\boldsymbol{k}|^2 \in I_1\}$.

In the presence of thermal diffusion ($\tilde{\nu} > 0$), we first note that c_0 is a cubic polynomial in K, so c_0 has a local maximum at $K = 0$ and there is a global minimum at some $K > 0$. Specifically, if $0 < N^2 < 4\tilde{\nu} b_3^3/(27d_3^2)$, then $c_0 < 0$ in a positive interval $I_2 \subset (0, b_3/d_3)$. If $N^2 < 0$, then $c_0 < 0$ in an interval $I_3 := [0, K_2)$ for some $K_2 > b_3/d_3$. Hence, in this case, a parallel flow (3.32) grows exponentially and unboundedly if it contains a Fourier mode with wave vector $\boldsymbol{k}$ in the annulus $\{\boldsymbol{k} \in \mathbb{R}^2 \,|\, |\boldsymbol{k}|^2 \in I_2\}$ for not too strongly stable stratification $0 < N^2 < 4\tilde{\nu} b_3^3/(27d_3^2)$, or in the disc $\{\boldsymbol{k} \in \mathbb{R}^2 \,|\, |\boldsymbol{k}|^2 \in I_3\}$ for unstable stratification $N^2 < 0$.

Other modes for $\tilde{\nu} > 0$, that have $c_0 \geq 0$, also yield such growth if $c_1 < 0$ and $c_1^2 \geq 4c_0$. We omit details about this case, but note that $c_1 < 0$ occurs for $K < (b_3 - \tilde{\nu})/d_3$, possibly containing the interval I_2.

Kolmogorov flow

Another well-known class of explicit solutions for the Boussinesq equations in absence of backscatter are the so-called Kolmogorov flows (see, e.g. Balmforth and Young, 2005) with wave vectors of the form $\boldsymbol{k} = (k_x, 0, k_z)^\intercal$, where k_x, $k_z \in \mathbb{R}$. Here we study their occurrence in the presence of horizontal hyperdiffusion and backscatter and start with the plane wave approach

$$\boldsymbol{v}(t,\boldsymbol{x}) = \mathrm{e}^{\mu t}\cos(\boldsymbol{k}\cdot\boldsymbol{x})\boldsymbol{a}\,, \quad b(t,\boldsymbol{x}) = B\mathrm{e}^{\mu t}\cos(\boldsymbol{k}\cdot\boldsymbol{x})\,, \quad p(t,\boldsymbol{x}) = \gamma\mathrm{e}^{\mu t}\sin(\boldsymbol{k}\cdot\boldsymbol{x})\,, \tag{3.35}$$

and the flow direction $\boldsymbol{a} = A_1(0,1,0)^\intercal + A_2(-k_z,0,k_x)^\intercal$. Compared with the Kolmogorov flows in the Boussinesq equations without backscatter and Coriolis force in Section 2.3.1, here we have rotation ($f \neq 0$), time dependence ($\mu \neq 0$) and a nonzero second component of the velocity direction ($A_1 \neq 0$).

A superposition of these Kolmogorov flows with the horizontal plane flow solutions (3.23) is not possible, since the orthogonality conditions for wave vectors and flow directions are not satisfied, neither for the radial superposition in Theorem 2.3 nor for the angular superposition in Theorem 2.9 and Theorem 2.10. It is possible to choose the wave vector $\boldsymbol{k}$ of the Kolmogorov flow so that the orthogonality conditions in Theorem 2.3 are satisfied with a certain horizontal plane flow (3.23), but in this case the Kolmogorov flow constructional becomes a superposition of a horizontal plane flow ($A_1 \neq 0$) and a parallel flow ($A_2 \neq 0$). The same holds for the superposition of the Kolmogorov flow with a parallel flow. However, radial superposition of different Kolmogorov flows is possible, as long as all wave vectors $\boldsymbol{k}$ have the same direction. The same holds for the superposition with such monochromatic inertia gravity waves as discussed later.

We next determine the required relations for the coefficients of (3.35) in order to solve the Boussinesq equations (3.21). For better readability we define the following terms resulting from the hyperdiffusion, backscatter and thermal diffusion:

$$\delta_{\tilde{\nu}}(k_x,k_z) = \tilde{\nu}|\boldsymbol{k}|^2\,, \qquad \delta_j(k_x,k_z) = d_j|\boldsymbol{k}|^4 - b_j|\boldsymbol{k}|^2 \qquad \text{for any } 1 \le j \le 3\,,$$

where $|\boldsymbol{k}|^2 = k_x^2 + k_z^2$. Due to the structure of (3.35), the nonlinear advection operator $(\boldsymbol{v}\cdot\nabla)\boldsymbol{v}$ becomes zero by Theorem 2.3, as well as $(\boldsymbol{v}\cdot\nabla)b = 0$ due to the orthogonality of wave vector and flow direction. Additionally, (3.21b) is satisfied by Theorem 2.5. Hence, inserting (3.35) into (3.21) we find that the coefficients have to satisfy

$$\begin{pmatrix} -f & -k_z(\mu+\delta_1) & 0 & k_x \\ \mu+\delta_2 & -fk_z & 0 & 0 \\ 0 & k_x(\mu+\delta_3) & -1 & k_z \\ 0 & N^2k_x & \mu+\delta_{\tilde{\nu}} & 0 \end{pmatrix} \begin{pmatrix} A_1 \\ A_2 \\ B \\ \gamma \end{pmatrix} = 0\,. \tag{3.36}$$

For $k_x = k_z = 0$ we require $A_1 = 0$ and $B = 0$, which is the trivial zero solution. From

the second row of the 4-by-4 matrix in (3.36) and $f \neq 0$ we immediately find that $A_1 = 0$ implies $A_2 k_z = 0$. In case $A_2 = 0$, the Kolmogorov flow (3.35) is the trivial zero solution, and in case $k_z = 0$, (3.35) is a parallel flow. Hence, we may assume $A_1 \neq 0$. Since (3.36) is a homogeneous linear system in $(A_1, A_2, B, \gamma)^\intercal$, non-trivial solutions require a kernel of the associated matrix. Hence, either there is no nontrivial Kolmogorov flow or a linear space of these, which requires vanishing determinant of this matrix. Assuming $(k_x, k_z)^\intercal \neq (0,0)^\intercal$ and dividing by $-|\boldsymbol{k}|^2$, the determinant of the matrix in (3.36) gives the dispersion relation

$$\mu^3 + c_2\mu^2 + c_1\mu + c_0 = 0\,, \tag{3.37}$$

with coefficients

$$\begin{aligned} c_2 &:= \delta_2 + \delta_{\tilde{\nu}} + |\boldsymbol{k}|^{-2}(\delta_3 k_x^2 + \delta_1 k_z^2)\,,\\ c_1 &:= \delta_2\delta_{\tilde{\nu}} + |\boldsymbol{k}|^{-2}[(\delta_2 + \delta_{\tilde{\nu}})(\delta_3 k_x^2 + \delta_1 k_z^2) + N^2 k_x^2 + f^2 k_z^2]\,,\\ c_0 &:= |\boldsymbol{k}|^{-2}[\delta_2\delta_{\tilde{\nu}}(\delta_3 k_x^2 + \delta_1 k_z^2) + \delta_2 N^2 k_x^2 + \delta_{\tilde{\nu}} f^2 k_z^2]\,. \end{aligned}$$

Steady Kolmogorov flows and linear stability

The condition $\mu = 0$ for steady Kolmogorov flow reduces (3.37) to

$$\delta_2\delta_{\tilde{\nu}}(\delta_3 k_x^2 + \delta_1 k_z^2) + \delta_2 N^2 k_x^2 + \delta_{\tilde{\nu}} f^2 k_z^2 = 0\,. \tag{3.38}$$

For comparison, note that the left-hand side identically equals to zero in the absence of backscatter and hyperviscosity (d_j, $b_j = 0$ for $j = 1, 2, 3$) as well as thermal diffusion ($\tilde{\nu} = 0$), so that in this case steady and nontrivial Kolmogorov flows exist for all $(k_x, k_z)^\intercal \in \mathbb{R}^2 \setminus \{(0,0)^\intercal\}$. In contrast, in the presence of hyperdiffusion and backscatter d_2, $b_2 > 0$, but still without thermal diffusion ($\tilde{\nu} = 0$), only $\delta_2 N^2 k_x^2 = 0$ remains, so that either $k_x = 0$ or $\delta_2 = 0$. The latter means $|\boldsymbol{k}|^2 = b_2/d_2$, so that nontrivial and steady Kolmogorov flows occur on the k_z-axis and the circle in the (k_x, k_z)-plane with radius $\sqrt{b_2/d_2}$, cf. Figure 3.11(b) and Figure 3.11(d). Conversely, we can create steady Kolmogorov flows for any wave vector $(k_x, k_z)^\intercal \neq (0,0)^\intercal$ by suitable choice of d_2, b_2, such that $\delta_2 = 0$.

Concerning stability, analogous to Section 3.2.1, small amplitude steady Kolmogorov flows are unstable, though typically not unboundedly, due to the instability of the zero state under backscatter. In the large amplitude scaling, the resulting operator $\mathcal{L}_0$ is a triangular block matrix operator, similar to the parallel flows in this section, with skew-adjoint parts that imply purely imaginary spectrum. Hence, there are again no growth rates that are proportional to the amplitude of the steady Kolmogorov flow.

A source of unbounded instability of steady Kolmogorov flows are possible superpositions with monochromatic inertia gravity waves discussed below. In the following we

will examine the existence of exponentially and unboundedly growing Kolmogorov flows, which then also proves unbounded instability of steady Kolmogorov flows due to possible superpositions.

Unboundedly growing Kolmogorov flows

For Kolmogorov flows that grow unboundedly in time we need A_2, $k_x \neq 0$, since then the horizontal hyperdiffusion and backscatter are transferred to growing vertical velocity component. They correspond to positive roots of (3.37), which occur as follows in terms of the sign of c_0:

(i) If $c_0 < 0$, then (3.37) has a positive root.

(ii) For $c_0 = 0$, (3.37) has a positive root if and only if $-c_2 + \sqrt{c_2^2 - 4c_1} > 0$.

(iii) For $c_0 > 0$, (3.37) has a positive root if and only if $-c_2 + \sqrt{c_2^2 - 3c_1} > 0$ and $2c_2^3 - 9c_1c_2 + 27c_0 + (6c_1 - 2c_2^2)\sqrt{c_2^2 - 3c_1} \leq 0$.

The conditions in (iii) are derived from the necessity of the cubic polynomial (3.37) having its local minimum at a positive value $\mu > 0$ and its value at the local minimum being non-positive.

For comparison we start with the common situation without backscatter, hyperviscosity and thermal diffusion ($\tilde{\nu}$, b_j, $d_j = 0$ for $j = 1, 2, 3$), where a growing Kolmogorov flow (3.35) requires unstable stratification $N^2 < 0$. Indeed, in this case (3.37) has $c_0 = c_2 = 0$ and $c_1 = |\boldsymbol{k}|^{-2}(N^2k_x^2 + f^2k_z^2)$, so that a positive root occurs if and only if $c_1 < 0$, which requires $N^2 < 0$, and thus growing solutions occur for $k_z^2/k_x^2 < -N^2/f^2$, cf. Figure 3.11(a). More precisely, for such wave vectors a steady flow co-exists with a growing and a decaying flow (on the red regions in Figure 3.11(a)), which turn into a triple steady flow on the boundary, where $c_0 = c_1 = c_2 = 0$ (black curves).

In the presence of horizontal hyperdiffusion and backscatter (b_j, $d_j > 0$ for $j = 1, 2$) growth of Kolmogorov flows (3.35) is possible even for stable stratification $N^2 > 0$. We next focus on case (i) with negative c_0 and omit details of cases (ii) and (iii) with non-negative c_0. However, some examples are plotted in Figure 3.11.

First, we note that for $N^2 > 0$ the coefficient c_0 is negative for sufficiently small k_x and k_z. Its sign is that of the left-hand side of (3.38), whose leading order term as $(k_x, k_z)^\intercal \to (0, 0)^\intercal$ is $|\boldsymbol{k}|^2(-b_2N^2k_x^2 + \tilde{\nu}f^2k_z^2)$ and can be negative only if $N^2 > 0$ and $k_x \neq 0$. Then, to leading order, growing Kolmogorov flows occur for $k_z^2/k_x^2 < b_2N^2/(\tilde{\nu}f^2)$ with $\tilde{\nu} > 0$ (cf. Figure 3.11(e)) and an increase of N^2 or b_2 enlarges this region in the $(k_x, k_z)^\intercal$-plane near the origin, while an increase of $\tilde{\nu}$ or f shrinks it. Rewriting the condition as $N^2 > \tilde{\nu}f^2k_z^2/(b_2k_x^2)$ for a given wave vector, then on the one hand an increase of $\tilde{\nu}$ or f requires sufficiently stable stratification, and on the other hand an increase of b_2 allows for less stable stratification. The leading order term of the left-hand side of (3.38) is always positive in case of unstable stratification $N^2 < 0$, so $c_0 > 0$ near

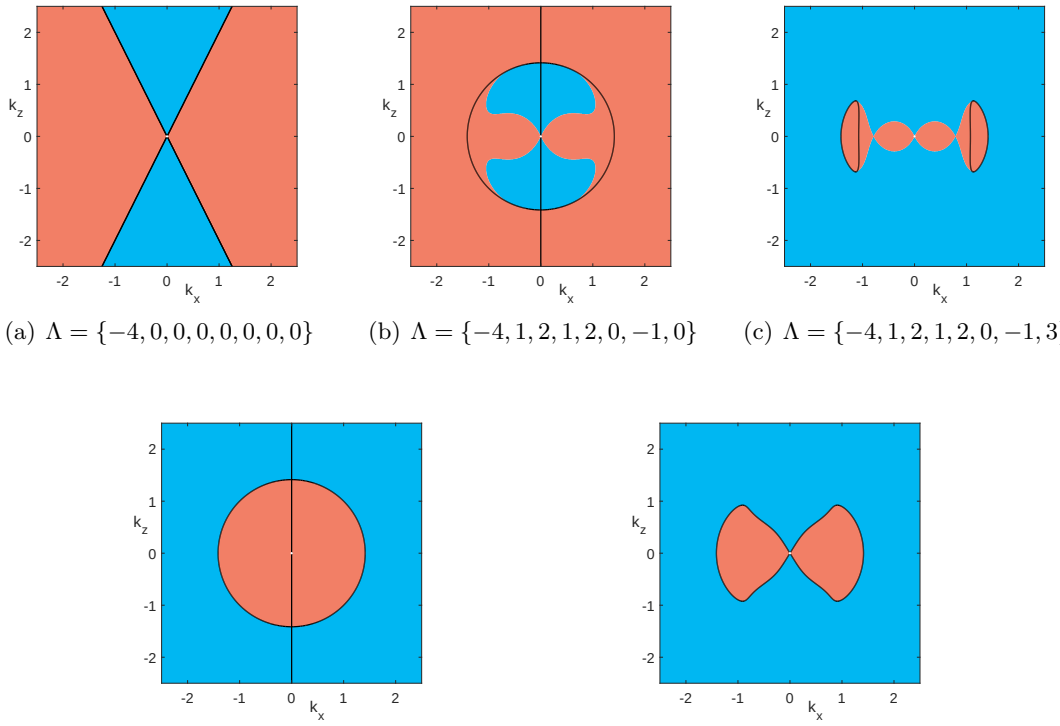

(a) $\Lambda = \{-4, 0, 0, 0, 0, 0, 0, 0\}$ (b) $\Lambda = \{-4, 1, 2, 1, 2, 0, -1, 0\}$ (c) $\Lambda = \{-4, 1, 2, 1, 2, 0, -1, 3\}$

(d) $\Lambda = \{4, 1, 2, 1, 2, 0, -1, 0\}$ (e) $\Lambda = \{4, 1, 2, 1, 2, 0, -1, 3\}$

Figure 3.11.: Unboundedly growing Kolmogorov flows occur for wave vectors $(k_x, k_z)^\intercal$ in the red regions for parameters sets $\Lambda := \{N^2, d_1, b_1, d_2, b_2, d_3, b_3, \tilde{\nu}\}$ (with isotropic backscatter), where the Coriolis parameter is fixed at $f = 1$. Red regions: one of conditions (i), (ii) and (iii) is satisfied; blue regions: none of conditions (i), (ii) and (iii) is satisfied; black curves in (a): locations of $c_0 = c_1 = c_2 = 0$; black curves in (b-e): locations of $c_0 = 0$; white dots: the zero state at $(k_x, k_z)^\intercal = (0, 0)^\intercal$, which is excluded here.

the origin, which refers to the case (iii) above. We omit details on this and provide an example in Figure 3.11(c).

Second, for general $(k_x, k_y)^\intercal$ and vanishing thermal diffusion ($\tilde{\nu} = 0$), only the term $\delta_2 N^2 k_x^2$ remains in c_0. Hence, $c_0 < 0$ for $|\boldsymbol{k}|^2 < b_2/d_2$ with $k_x \neq 0$ and stable stratification $N^2 > 0$ (cf. Figure 3.11(d)), and $c_0 < 0$ for $|\boldsymbol{k}|^2 > b_2/d_2$ with $k_x \neq 0$ and unstable stratification $N^2 < 0$ (cf. Figure 3.11(b)). For $k_x = 0$ we obtain $c_0 = 0$, so we refer to the case (ii) above for the growing Kolmogorov flows. The numerical computations show, that in the examples of Figure 3.11(b) and Figure 3.11(d) the condition in case (ii) is not satisfied for $k_x = 0$, so that here a Kolmogorov flow (3.35) is not growing. Near $\boldsymbol{k} = 0$, the examples of Figure 3.11(b) and Figure 3.11(c) can be considered as perturbations of the example of Figure 3.11(a). We note that decaying or oscillating Kolmogorov flows may co-exist. Notably, in Figure 3.11(b) and Figure 3.11(c) the part of the red region's boundary without black marking stems from a bifurcation of saddle-node-type in terms

of the wave vector, where (3.37) possesses a positive double root. In contrast, the black curves mark locations of steady flows, where $c_0 = 0$.

As also done for the parallel flow, we briefly consider artificial vertical hyperdiffusion and backscatter. Here we focus on the isotropic case $d_j = d > 0$, $b_j = b > 0$, $j = 1, 2, 3$. In this case $\delta := d|\boldsymbol{k}|^4 - b|\boldsymbol{k}|^2 = \delta_j$ for $j = 1, 2, 3$. With thermal diffusion ($\tilde{\nu} > 0$) we then have $c_0 < 0$ for small wave number $|\boldsymbol{k}|^2 < b/d$ (i.e. $\delta < 0$) if stratification is sufficiently stable $N^2 > -\tilde{\nu}|\boldsymbol{k}|^2(f^2k_z^2 + \delta^2|\boldsymbol{k}|^2)/(k_x^2\delta) > 0$, and for large wave number $|\boldsymbol{k}|^2 > b/d$ (i.e. $\delta > 0$) only for sufficiently unstable stratification $N^2 < -\tilde{\nu}|\boldsymbol{k}|^2(f^2k_z^2 + \delta^2|\boldsymbol{k}|^2)/(k_x^2\delta) < 0$. Unlike the growing parallel flows, which require sufficiently weak stable stratification, here the increase of positive N^2 increases the set of wave vectors (within the small wave number region) for growing Kolmogorov flows. Another observation is that for the fixed stratification, stable or unstable, larger thermal diffusion $\tilde{\nu}$ leads to smaller region in wave vector space of growing solutions.

The latter can also be observed numerically without vertical hyperviscosity and backscatter, but vertical usual viscosity $d_3 = 0$, $b_3 < 0$ as shown in Figure 3.11(d) and Figure 3.11(e) for $N^2 > 0$, as well as Figure 3.11(b) and Figure 3.11(c) for $N^2 < 0$.

Monochromatic inertia gravity waves

The last kind of explicit plane wave-type solutions we discuss here are the so-called monochromatic inertia gravity waves (MIGWs), which are for example discussed in Achatz (2006) for the inviscid Boussinesq equations. Here we study their occurrence as well as stability and growing properties in the rotating Boussinesq equations (3.21) with horizontal hyperdiffusion and backscatter. These solutions again form an invariant subspace of linear dynamics, due to the vanishing nonlinear advection terms in the equations and the possible superpositions, but structurally differ from the aforementioned flows. In particular, the wave profile of a MIGW is a time-dependent traveling wave with phase variable $\xi = k_x x + k_z z - \omega t$ and takes the form

$$\boldsymbol{v}(t, \boldsymbol{x}) = A_1 \mathrm{e}^{\mu t} \sin(\xi)(0, 1, 0)^\intercal + A_2 \omega \mathrm{e}^{\mu t} \cos(\xi)(-k_z, 0, k_x)^\intercal \,, \tag{3.39a}$$

$$b(t, \boldsymbol{x}) = B_1 \mathrm{e}^{\mu t} \sin \xi + B_2 \omega \mathrm{e}^{\mu t} \cos \xi \,, \tag{3.39b}$$

$$p(t, \boldsymbol{x}) = \gamma_1 \mathrm{e}^{\mu t} \cos \xi + \gamma_2 \omega \mathrm{e}^{\mu t} \sin \xi \,. \tag{3.39c}$$

The conditions for these flows to be nontrivial explicit solutions of (3.21), with two-dimensional wave vectors $\boldsymbol{k} = (k_x, k_z)^\intercal \in \mathbb{R}^2 \setminus \{(0, 0)^\intercal\}$, in particular depend on the frequency ω. In fact, for $\omega = 0$ these are Kolmogorov flows as above with $A_2 = 0$, and the existence conditions read, after inserting (3.39) into (3.21),

$$\begin{pmatrix} \mu + \delta_2 & 0 & 0 \\ k_z f & -k_x & 0 \\ k_x f & k_z & |\boldsymbol{k}|^2 \\ 0 & \mu + \delta_{\tilde{\nu}} & 0 \end{pmatrix} \begin{pmatrix} A_1 \\ B_1 \\ \gamma_1 \end{pmatrix} = 0 \,, \tag{3.40}$$

with $\delta_j = \delta_j(\boldsymbol{k}) := d_j|\boldsymbol{k}|^4 - b_j|\boldsymbol{k}|^2$ for any $1 \le j \le 3$ and $\delta_{\tilde\nu} = \delta_{\tilde\nu}(\boldsymbol{k}) := \tilde\nu|\boldsymbol{k}|^2$ as before.

For $\omega \neq 0$ the conditions for the existence of MIGWs (3.39) in (3.21) are at first the following eight:

$$\begin{pmatrix} \mu+\delta_2 & 0 & 0 & 0 & 0 & 0 \\ k_z f & -k_x & 0 & \omega^2|\boldsymbol{k}|^2 & 0 & 0 \\ k_x f & k_z & |\boldsymbol{k}|^2 & 0 & 0 & 0 \\ 0 & \mu+\delta_{\tilde\nu} & 0 & 0 & \omega^2 & 0 \\ 1 & 0 & 0 & k_z f & 0 & 0 \\ 0 & -1 & 0 & k_x N^2 & \mu+\delta_{\tilde\nu} & 0 \\ 0 & 0 & 0 & \delta_3 k_x^2 + \delta_1 k_z^2 + \mu|\boldsymbol{k}|^2 & -k_x & 0 \\ 0 & 0 & 0 & (\delta_3-\delta_1)k_x k_z & -k_z & |\boldsymbol{k}|^2 \end{pmatrix} \begin{pmatrix} A_1 \\ B_1 \\ \gamma_1 \\ A_2 \\ B_2 \\ \gamma_2 \end{pmatrix} = 0\,. \tag{3.41}$$

However, most of these can be readily solved directly in terms of the coefficients. In the following we explicitly determine nontrivial solutions (3.39) of (3.21) by the use of (3.40) and (3.41). Afterwards, we shortly discuss the stability of MIGWs and the possible superpositions with other types of explicit flows.

MIGWs with steady phase ($\omega = 0$)

We start with the frequency $\omega = 0$, which gives a certain type of Kolmogorov flows. There is no propagation of the traveling wave profile and the second terms of $\boldsymbol{v}$, b and p in (3.39) vanish. Solutions with

$$k_x = 0\,, \qquad A_1 = 0\,, \qquad B_1 = -\gamma_1 k_z\,, \qquad \mu = -\delta_{\tilde\nu}\,,$$

have $\boldsymbol{v} \equiv 0$, the pressure depends on the buoyancy only, and there are no further conditions on the wave vector $\boldsymbol{k} = (0, k_z)^\intercal$.

Other solutions with $\omega = 0$ satisfy

$$k_x \neq 0\,, \qquad B_1 = A_1 \frac{k_z}{k_x} f\,, \qquad \gamma_1 = -A_1 \frac{f}{k_x}\,, \qquad \mu = -\delta_{\tilde\nu}\,, \qquad \delta_2 = \delta_{\tilde\nu}\,,$$

so $\boldsymbol{v} \neq 0$ for $A_1 \neq 0$. The last of these equations gives a condition on the wave vector $\boldsymbol{k}$, which is equivalent to $d_2|\boldsymbol{k}|^2 - b_2 - \tilde\nu = 0$ and fixes the wave number to $|\boldsymbol{k}|^2 = (b_2+\tilde\nu)/d_2$.

In both cases the growth rate is defined by the thermal diffusion as $\mu = -\tilde\nu|\boldsymbol{k}|^2$, so that all these MIGWs are exponentially decaying for $\tilde\nu > 0$ and steady for $\tilde\nu = 0$. Furthermore, both solutions only depend on parameters of the second momentum equation or the buoyancy equation of (3.21), but are independent of the Brunt-Väisälä frequency N^2.

MIGWs with oscillating phase ($\omega \neq 0$)

We now turn to nontrivial MIGW solutions (3.39) with $\omega \neq 0$. The simplest class are 'vertically varying' MIGWs with

$$k_x = 0\,, \qquad A_1 = -A_2 k_z f\,, \qquad B_1 = B_2 = \gamma_1 = \gamma_2 = 0\,,$$
$$\mu = -\delta_2\,, \qquad \omega = \pm f\,, \qquad \delta_1 = \delta_2\,,$$

so that $b \equiv p \equiv 0$, while $\boldsymbol{v} \neq 0$, in contrast to the case $k_x = \omega = 0$ above. Notably, these solutions depend on the parameters of the horizontal momentum equations of (3.21) only, while the solutions with $k_x = \omega = 0$ only depend on those from the buoyancy equation (3.21c). The last of the above equations is a condition on the wave vector $\boldsymbol{k} = (0, k_z)^\intercal$, which is equivalent to $(d_1 - d_2)k_z^2 + b_2 - b_1 = 0$. Thus, these solutions exist for all $k_z \neq 0$ in the isotropic case, while for $d_1 \neq d_2$ they are restricted to $k_z^2 = (b_1 - b_2)/(d_1 - d_2) > 0$.

Since $\mu = -\delta_2$, these MIGWs are exponentially and unboundedly growing for wave numbers $k_z^2 < b_2/d_2$, and steady for $k_z^2 = b_2/d_2$, thus transferring the horizontal hyperdiffusion and backscatter to growing vertical dependence. In particular, the thermal diffusion $\tilde{\nu}$ and Brunt-Väisälä frequency N^2 have no impact, since these solutions trivially satisfy the buoyancy equation (3.21c) by $v_3 \equiv b \equiv 0$.

Another type are 'zonally varying' MIGWs with the coefficients satisfying

$$A_1 = k_z = 0\,, \qquad B_1 = A_2\Big(N^2 - \frac{(\delta_3 - \delta_{\tilde{\nu}})^2}{4}\Big)k_x\,, \qquad B_2 = A_2\frac{\delta_3 - \delta_{\tilde{\nu}}}{2}k_x\,,$$
$$\gamma_1 = \gamma_2 = 0\,, \qquad \mu = -\frac{\delta_3 + \delta_{\tilde{\nu}}}{2}\,, \qquad \omega^2 = N^2 - \frac{(\delta_3 - \delta_{\tilde{\nu}})^2}{4}\,.$$

These have vanishing pressure and depend only on the parameters of the buoyancy equation and vertical momentum equation of (3.21). In contrast to the MIGW solutions before, these here also depend on the Brunt-Väisälä frequency N^2. Furthermore, different from the solutions before, the growth rate μ and phase frequency ω depend on both, the vertical term δ_3 and the thermal diffusion. Since $\omega^2 > 0$, the last equation is a condition on the wave vector $\boldsymbol{k} = (k_x, 0)^\intercal$, which requires stable stratification $N^2 > 0$ satisfying $(\delta_3 - \delta_{\tilde{\nu}})^2 < 4N^2$. In case $N^2 > 0$ these MIGW solutions exist at least for sufficiently small k_x^2, since δ_3, $\delta_{\tilde{\nu}} \to 0$ as $|\boldsymbol{k}| \to 0$. Due to the equation for the growth rate μ, these MIGWs are exponentially decaying for kinetic energy backscatter, which concerns only the horizontal directions, so $\delta_3 = -b_3|\boldsymbol{k}|^2 > 0$. Hence, this kind of MIGWs are steady or exhibit growth only in the artificial case d_3, $b_3 > 0$ for wave numbers $k_x^2 \leq (b_3 - \tilde{\nu})/d_3$, i.e. only in the case $b_3 > \tilde{\nu}$.

The existence analysis for the remaining MIGW solutions (3.39) with ω, k_x, $A_1 \neq 0$ is more involved. These solutions have the coefficients

$$A_1 = -A_2 k_z f\,, \qquad B_1 = A_1 \frac{k_z}{k_x} f + A_2 \frac{\omega^2}{k_x} |\boldsymbol{k}|^2\,, \qquad B_2 = \frac{A_2}{k_x}(\delta_3 k_x^2 + \delta_1 k_z^2 - \delta_2 |\boldsymbol{k}|^2)\,,$$

$$\gamma_2 = A_2(\delta_1 - \delta_3)\frac{k_x k_z}{|\boldsymbol{k}|^2} + B_2 \frac{k_z}{|\boldsymbol{k}|^2}\,, \qquad \gamma_1 = -A_1 \frac{k_x f}{|\boldsymbol{k}|^2} - B_1 \frac{k_z}{|\boldsymbol{k}|^2}\,, \qquad \mu = -\delta_2\,,$$

with additional conditions, that also define the phase frequency ω, given by

$$\omega^2 = \Big((\delta_3 - \delta_2)(\delta_{\tilde{\nu}} - \delta_2) + N^2\Big)\frac{k_x^2}{|\boldsymbol{k}|^2} + \Big((\delta_1 - \delta_2)(\delta_{\tilde{\nu}} - \delta_2) + f^2\Big)\frac{k_z^2}{|\boldsymbol{k}|^2} > 0\,, \tag{3.42a}$$

$$\begin{aligned}\Big((\delta_{\tilde{\nu}} - \delta_2)N^2 + (\delta_3 - \delta_2)\big((\delta_{\tilde{\nu}} - \delta_2)^2 + \omega^2\big)\Big)k_x^2 + \dots \\ \dots + (\delta_1 - \delta_2)\big((\delta_{\tilde{\nu}} - \delta_2)^2 + \omega^2\big)k_z^2 = 0\,.\end{aligned} \tag{3.42b}$$

The first condition (3.42a) has solutions $(k_x, k_z)^\intercal$ for any parameter: For stable stratification $N^2 > 0$ the factors of k_x^2 and k_z^2 are both positive for $|\boldsymbol{k}|$ sufficiently small, since δ_j, $\delta_{\tilde{\nu}} \to 0$ for $|\boldsymbol{k}| \to 0$ for all $1 \leq j \leq 3$. For unstable stratification $N^2 < 0$ one can first choose $|\boldsymbol{k}|$ sufficiently small, so that the factor of k_z^2 is positive. Then, for a fixed $|\boldsymbol{k}|^2 = s^2$ so that δ_j and $\delta_{\tilde{\nu}}$ are constant for these wave vectors, one can choose $k_x^2 = s^2 - k_z^2$ small enough, so that the term with k_x^2 does not make the whole expression negative.

We omit a complete analysis of the more complicated conditions (3.42) here, but note that the horizontally isotropic case (causing $\delta_1 = \delta_2$) requires unstable stratification $N^2 < 0$ for the existence of unboundedly growing MIGWs of this kind. Both conditions together generate a set of solutions with rather complex structure, as plotted in Figure 3.12 for the cases with stable stratification and (weakly) anisotropic backscatter, as well as unstable stratification with isotropic backscatter, which generate unboundedly growing explicit MIGW solutions.

Due to the equation for the growth rate $\mu = -\delta_2$, these MIGWs are exponentially and unboundedly growing for wave numbers $|\boldsymbol{k}|^2 < b_2/d_2$ and steady solutions for $|\boldsymbol{k}|^2 = b_2/d_2$ (see Figure 3.12). Notably, since $k_x \neq 0$, these flows can transfer the horizontal hyperdiffusion and backscatter (in fact only the meridional component) to growing vertical velocity.

Superpositions and stability

It is possible to superpose MIGWs and Kolmogorov flows to an explicit solution of (3.21), if these have the same direction of wave vectors $\boldsymbol{k}$, so radial superposition according to Theorem 2.3. The superposition can also be in the form of an integral. Note that Kolmogorov flows exist on the whole wave vector space $(k_x, k_z)^\intercal \in \mathbb{R}^2$, while MIGWs in general not. This means, that superposition in one wave vector direction is possible for

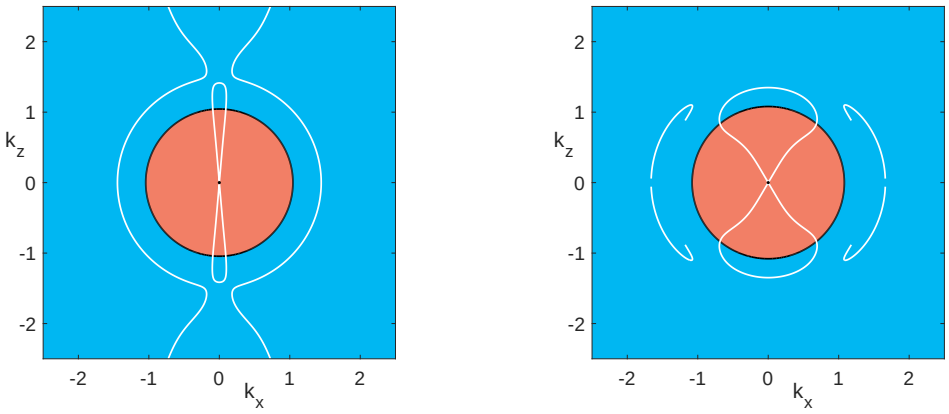

(a) Stable stratification $N^2 = 1$ with anisotropic backscatter $d_2 = 0.11$, $b_2 = 0.12$.

(b) Unstable stratification $N^2 = -0.05$ with isotropic backscatter $d_2 = 0.12$, $b_2 = 0.14$.

Figure 3.12.: Existence of MIGW solutions (3.39) of (3.21) on the wave vector plane $(k_x, k_z)^\intercal$ in the case ω, $A_1 \neq 0$ (white curves) with growth rate μ positive (red), zero (black) or negative (blue). Fixed parameters: $d_1 = 0.12$, $d_3 = 0.0$, $b_1 = 0.14$, $b_3 = -0.1$, $\tilde{\nu} = 0.12$, $f = 0.3$.

arbitrary wave numbers of the Kolmogorov flows, but the wave numbers of the MIGWs is in general restricted, as studied above. Depending on the wave vectors, the Kolmogorov flows and MIGWs in such a superposition can be steady, exponentially growing or decaying.

With this superposition we can prove in certain cases the unbounded instability of steady MIGW solutions due to perturbations with exponentially growing Kolmogorov flows, and vice versa. In previous investigations we found that growing Kolmogorov flows in case $\tilde{\nu} > 0$ may occur only in certain directions. In this case, steady MIGW solutions are unboundedly unstable a priori only in these certain wave vector directions (see investigation of c_0 for Kolmogorov flows for more details). Without thermal diffusion ($\tilde{\nu} = 0$) there are always growing Kolmogorov flows in any direction with $k_x \neq 0$, for stable stratification $N^2 > 0$ at least for all $|\boldsymbol{k}|^2 < b_2/d_2$, and for unstable stratification $N^2 < 0$ for $|\boldsymbol{k}|^2 > b_2/d_2$. Thus, in these cases, the steady MIGWs with $k_x \neq 0$ are always unboundedly unstable with respect to certain Kolmogorov flows. However, steady MIGWs with $k_x = 0$, as well as Kolmogorov flows, are also unboundedly unstable, since there are exponentially and unboundedly growing MIGWs with $k_x = 0$ and $k_z^2 < b_2/d_2$, which they can be superposed with (see the case of 'vertically varying' MIGWs with $\omega \neq 0$ and $k_x = 0$).

As in Section 3.2.1, steady small amplitude MIGWs are unstable due to the unstable trivial zero solution under backscatter. In the large amplitude scaling, the resulting operator $\mathcal{L}_0$ is a triangular block matrix operator with skew-adjoint parts, that imply purely imaginary spectrum as for the Kolmogorov flows. Hence, there are again no unstable eigenvalues that scale with the amplitude parameter of the steady MIGW.

4. Stability and Bifurcations in Shallow Water Equations with simplified Backscatter and Bottom Drag

In the last chapter we have seen, how simplified backscatter in geophysical fluid models affects the occurrence of explicit solutions as well as their growth and stability, in particular unbounded growth and unbounded instability. Such forcing terms also generate sets of steady solutions, that do not occur in the original viscous fluid models, which can even form linear subspaces due to the arbitrary choice of amplitudes and certain superpositions. This is mainly enabled by the specific structure of the solutions, that create vanishing or gradient nonlinear advection terms, as presented in Section 2.1, so that a linear problem remains to be solved. It is expected that adding further terms in the equations would change the occurrence and behavior of solutions again, probably even reducing the set of solutions, in particular with additional nonlinear terms.

In this chapter we include, on top of hyperdiffusion and backscatter, bottom drag terms as an additional physical effect into the models, which has an dissipating character. Since these friction terms need a clearly defined bottom in the models, which is not the case for the Boussinesq equations, we consider here the rotating shallow water equations with hyperdiffusion, backscatter and bottom drag.

It is expected that bottom drag has an stabilizing effect on the dynamics, in particular on the (trivial) steady solutions. Indeed, in Chapter 3 we have seen, that simplified backscatter in the models has an destabilizing character. More than that, varying the parameters without changing the general setting does not change the stability of steady solutions in these models. However, in presence of additional bottom drag we will see, that it is not only possible to make the trivial steady solution stable, but also to change its stability by varying bottom drag parameters. This results in bifurcations of steady solutions at the threshold of instability, similar to Prugger (2017) for the rotating shallow water equations with usual (anisotropic) viscosity and different linear forcing. Such bifurcations do not occur in the models of Chapter 3. Nevertheless, we will also see, that additional bottom drag not necessarily prevents the occurrence of explicit solutions with arbitrary amplitudes completely, even some unboundedly growing ones remain. This indicates some robustness of undesired concentration of energy due to backscatter, which is in contrast to the targeted energy redistribution.

Here we extend (3.1) by linear and nonlinear bottom drag terms in the momentum equations. We refer to, e.g. Kowalik and Whitmore (1991); Grubišić et al. (1995); Satake

(1995); Grianik et al. (2004); Taylor and Sarkar (2008); Zhang et al. (2011); Danilov et al. (2019) for these forms of bottom drag in various contexts. Balmforth and Mandre (2004) uses $C(H_0+\eta)^{-2}$, which does not change the leading order impact. Linear and quadratic bottom drag are often used separately, but here we follow Arbic and Scott (2008), which includes a combination of both. The trivial steady flow is $(\boldsymbol{v}, \eta)^\intercal = (0,0)^\intercal$ and a major goal in this chapter is to understand bifurcations in terms of the linear bottom drag parameter C. It turns out, that the bifurcating nonlinear flows can be associated with Rossby and inertia-gravity waves. Nevertheless, the bifurcation analysis here is a non-standard problem, since the spectrum approaches the origin in the complex plane as the wave number tends to infinity. This lack of spectral gap means that center manifold reduction cannot be used and care has to be taken in the Lyapunov–Schmidt reduction.

This chapter is built up as follows: In Section 4.1 we present the setting, that we will consider in this chapter, followed by spectrum and stability analysis of the model in Section 4.2. Using these results, we continue with the investigation of bifurcating Rossby waves in Section 4.3 and of bifurcating inertia-gravity waves in Section 4.4. Afterwards, we show in Section 4.5 that explicit solutions as in Chapter 3 can occur in the considered model as well. In the end, in Section 4.6, we show some numerical results concerning the studied bifurcating solutions.[1]

4.1. Setting and plane wave reduction

The rotating shallow water equations in an f-plane approximation and augmented with hyperdiffusion, simplified backscatter as well as bottom drag $\boldsymbol{F}$ take the form

$$\frac{\partial \boldsymbol{v}}{\partial t} + (\boldsymbol{v}\cdot\nabla)\boldsymbol{v} = -f\boldsymbol{v}^\perp - g\nabla\eta - \begin{pmatrix} d_1\Delta^2 + b_1\Delta & 0 \\ 0 & d_2\Delta^2 + b_2\Delta \end{pmatrix}\boldsymbol{v} - \boldsymbol{F}(\boldsymbol{v},\eta)\,, \tag{4.1a}$$

$$\frac{\partial \eta}{\partial t} + (\boldsymbol{v}\cdot\nabla)\eta = -(H_0+\eta)\nabla\cdot\boldsymbol{v}\,, \tag{4.1b}$$

with velocity field $\boldsymbol{v} = (v_1, v_2)^\intercal = \boldsymbol{v}(t,\boldsymbol{x}) \in \mathbb{R}^2$ on the space $\boldsymbol{x} = (x,y)^\intercal \in \mathbb{R}^2$ at time $t \geq 0$, deviation $\eta = \eta(t,\boldsymbol{x}) \in \mathbb{R}$ of the fluid layer from the characteristic fluid depth $H_0 > 0$, so η is considered to have zero mean and the thickness of the fluid is $H = H_0+\eta$ (with flat bottom topography), Coriolis parameter $f \in \mathbb{R}$, with $f = 0$ the non-rotational case, and gravity acceleration $g > 0$. The parameters d_1, $d_2 > 0$ provide hyperviscosity and b_1, $b_2 > 0$ the simplified kinetic energy backscatter. The isotropic case $d = d_1 = d_2$ and $b = b_1 = b_2$ appears physically natural and will be in the center of attention here, but for the same reasons as discussed in Section 3.1, the coefficients may differ as well, in particular b_1 and b_2. We refer to the latter as semi-isotropic, but consider also the full anisotropic case $d_1 \neq d_2$ and $b_1 \neq b_2$, since this causes no additional phenomena for

[1] The main results presented in this chapter have been submitted for publication (Prugger et al., 2022b).

the aspects we study. As to the bottom drag, we take the combined form

$$\boldsymbol{F}(\boldsymbol{v},\eta) = \frac{C + Q|\boldsymbol{v}|}{H_0+\eta}\boldsymbol{v}\,, \quad |\boldsymbol{v}| = \sqrt{u^2+v^2}\,, \tag{4.2}$$

where C, $Q \geq 0$ are bottom drag coefficients through which the dissipation enters linearly or quadratically with respect to the velocity $\boldsymbol{v}$, respectively. An important feature for $Q \neq 0$ is the quadratic nature of the velocity drag term, which is common in hydrodynamic drag forces (Steinherr Zazo, 2021), that is once continuously differentiable, but not twice (in $\boldsymbol{v} = 0$).

In addition, we can assume zero mean of η. It follows from (4.1b), which is derived from the mass conservation, see e.g. Vallis (2017). This equation can be written as

$$\frac{\partial \eta}{\partial t} + \nabla \cdot ((H_0+\eta)\boldsymbol{v}) = 0\,,$$

which, e.g. in L^2-spaces on rectangles Ω with periodic boundary conditions, gives again the mass conservation law

$$\frac{\mathrm{d}}{\mathrm{d}t}\int_\Omega \eta \,\mathrm{d}\boldsymbol{x} = 0\,.$$

In fact, an additional constant term in η is the same as changing the characteristic fluid depth H_0 by this constant term in (4.1).

Motivated by the results in Section 3.1, we consider a plane wave approach in (4.1) with wave vector $\boldsymbol{k} = (k_x, k_y)^\intercal \in \mathbb{R}^2$ of the form

$$\boldsymbol{v}(t,\boldsymbol{x}) = \psi(t,\boldsymbol{k}\cdot\boldsymbol{x})\boldsymbol{k}^\perp, \qquad \eta(t,\boldsymbol{x}) = \tilde{\phi}(t,\boldsymbol{k}\cdot\boldsymbol{x})\,, \tag{4.3}$$

for wave shapes ψ, $\tilde{\phi}$ and define the phase variable $\xi := \boldsymbol{k}\cdot\boldsymbol{x}$. In case of isotropic hyperdiffusion and backscatter $d = d_1 = d_2$, $b = b_1 = b_2$, we then obtain by inserting (4.3) into (4.1)

$$\partial_t\psi\,\boldsymbol{k}^\perp = (f\psi - g\partial_\xi\tilde{\phi})\boldsymbol{k} - \left(dk^4\partial_\xi^4\psi + bk^2\partial_\xi^2\psi + \frac{C+Qk|\psi|}{H_0+\tilde{\phi}}\psi\right)\boldsymbol{k}^\perp\,, \tag{4.4a}$$

$$\tilde{\phi}_t = 0\,, \tag{4.4b}$$

where $k := |\boldsymbol{k}| = |\boldsymbol{k}^\perp|$ is the wave number for the plane wave solutions (4.3). Here, the only remaining nonlinearity (with respect to ψ) stems from the bottom drag for $Q \neq 0$, while the advection nonlinearities of the fluid equations are vanished for these plane waves due to Theorem 2.2, Theorem 2.3 and Theorem 2.5. From (4.4b) we see that the wave shape $\tilde{\phi}$ needs to be independent of time t, and for nontrivial wave vector

$\boldsymbol{k}$ equation (4.4a) gives, by comparing the factors of the orthogonal vectors,

$$f\psi = g\partial_\xi \tilde{\phi}\,, \tag{4.5a}$$

$$\partial_t \psi = -dk^4 \partial_\xi^4 \psi - bk^2 \partial_\xi^2 \psi - \frac{C + Qk|\psi|}{H_0 + \tilde{\phi}} \psi\,. \tag{4.5b}$$

From equation (4.5a) it follows that also ψ is independent of t, unless $f = 0$. In case $f = 0$, $\tilde{\phi} \equiv \tilde{\phi}_0 \in \mathbb{R}$ is constant and (4.5b) has the form of a non-smooth quadratic Swift-Hohenberg-type equation with parameter $\tilde{\phi}_0$.

Here the trivial steady solutions appear as $\psi = 0$. If in addition $Q = f = 0$, the remaining linear equation can be solved explicitly. In particular, this forms a linear subset of plane wave-type solutions (4.3) that solve the original nonlinear system (4.1), i.e. these explicit solutions have a free amplitude parameter and can be superposed with each other. Such solutions can also be found in the case $Q = 0$, $f \neq 0$ for anisotropic hyperdiffusion and backscatter, as discussed in Section 4.5.

Remark 4.0.1. In the anisotropic case, $b_1 \neq b_2$ or $d_1 \neq d_2$, we can still reduce to (4.4), by considering only one direction and replacing b, d by b_2, d_2 (or b_1, d_1) as well as choosing the wave vector $\boldsymbol{k} = (1, 0)^\intercal$ (or $\boldsymbol{k} = (0, 1)^\intercal$) in (4.3).

In order to study the bifurcations for both cases $f \neq 0$ and the limit $f = 0$, we rescale the wave shape as $\tilde{\phi} = \tilde{f}\phi$, where $\tilde{f} = f/g$. As for η, here $\tilde{\phi}$ and thus ϕ are assumed to have zero mean. In case $f \neq 0$, substitution into (4.5), and accounting for time-independence of $\tilde{\phi}$ due to (4.4b) as noted above, gives

$$\psi = \partial_\xi \phi, \tag{4.6a}$$

$$0 = -dk^4 \partial_\xi^5 \phi - bk^2 \partial_\xi^3 \phi - \frac{C + Qk|\partial_\xi \phi|}{H_0 + \tilde{f}\phi} \partial_\xi \phi\,. \tag{4.6b}$$

In case $f = 0$, i.e. $\tilde{f} = 0$, zero mean of $\tilde{\phi}$ and (4.5) directly gives

$$\partial_t \psi = -dk^4 \partial_\xi^4 \psi - bk^2 \partial_\xi^2 \psi - \frac{C + Qk|\psi|}{H_0} \psi\,. \tag{4.7}$$

The nonlinear equation (4.7) admits temporal dynamics and thus also contains information on stability with respect to plane wave perturbations of the form (4.3).

Remark 4.0.2. Physically, (4.5a) means that the Coriolis and gradient term are in geostrophic balance. This implies, that bifurcating solutions of this form, as studied in Section 4.3, can be viewed as nonlinear Rossby waves, cf. Pedlosky (1987).

Remark 4.0.3. We briefly consider the limit of fast rotation, so $|f| \to \infty$. With the scaling $\tilde{\phi} = \tilde{f}\phi$ equation (4.6) formally limits to the linear equation with $C = Q = 0$. More generally, let us scale $\psi = \tilde{f}^{-\gamma}\hat{\psi}$, $\tilde{\phi} = \tilde{f}^{1-\gamma}\hat{\phi}$ with $\gamma \in [0, 1]$ in (4.5). Dropping

hats, for $\gamma \in (0,1)$ the limiting equations are the same as for $\gamma = 0$. However, for $\gamma = 1$ we obtain (4.6) with $\tilde{f} = 1$ and $Q = 0$, so that a nonlinear term remains, which results in nontrivial bifurcations.

4.2. Spectrum and spectral stability

We now study in detail the spectrum in the trivial steady flow $(\boldsymbol{v}, \eta)^\intercal = (0,0)^\intercal$ of (4.1). Since (4.1) is a coupled parabolic-hyperbolic system, it is not clear at this point, that standard center manifold reduction can be employed, even on bounded domains. Linearizing (4.1) in the trivial steady flow $(\boldsymbol{v}, \eta)^\intercal = (0,0)^\intercal$ gives the linear operator

$$\mathcal{L} = \begin{pmatrix} -d_1\Delta^2 - b_1\Delta - C/H_0 & f & -g\partial_x \\ -f & -d_2\Delta^2 - b_2\Delta - C/H_0 & -g\partial_y \\ -H_0\partial_x & -H_0\partial_y & 0 \end{pmatrix}. \tag{4.8}$$

The spectrum of $\mathcal{L}$ (e.g. on the space $(L^2(\mathbb{R}^2))^3$) consists of the roots λ of the dispersion relation

$$d(\lambda, k_x, k_y) := \det(\lambda \mathrm{Id} - \widehat{\mathcal{L}}) = 0\,, \tag{4.9}$$

for wave vectors $\boldsymbol{k} = (k_x, k_y)^\intercal \in \mathbb{R}^2$ and with the Fourier transform $\widehat{\mathcal{L}}$ of $\mathcal{L}$

$$\widehat{\mathcal{L}} = \begin{pmatrix} -d_1|\boldsymbol{k}|^4 + b_1|\boldsymbol{k}|^2 - C/H_0 & f & -\mathrm{i}gk_x \\ -f & -d_2|\boldsymbol{k}|^4 + b_2|\boldsymbol{k}|^2 - C/H_0 & -\mathrm{i}gk_y \\ -\mathrm{i}H_0k_x & -\mathrm{i}H_0k_y & 0 \end{pmatrix}.$$

The signs of the real parts $\mathrm{Re}(\lambda)$ of the solutions λ to (4.9) determine the spectral stability of $(\boldsymbol{v}, \eta)^\intercal = (0,0)^\intercal$ with respect to perturbations with wave vectors $\boldsymbol{k}$. Due to the direct relation, we write continuous selections of such solutions in the functional form $\lambda = \lambda(\boldsymbol{k})$. The dispersion relation (4.9) can be written as

$$d(\lambda, k_x, k_y) = \lambda^3 + a_2\lambda^2 + a_1\lambda + a_0 = 0\,, \tag{4.10}$$

with wave vector dependent coefficients

$$\begin{aligned} a_2 &:= (d_1 + d_2)|\boldsymbol{k}|^4 - (b_1 + b_2)|\boldsymbol{k}|^2 + 2C/H_0\,, \\ a_1 &:= (d_1|\boldsymbol{k}|^4 - b_1|\boldsymbol{k}|^2 + C/H_0)(d_2|\boldsymbol{k}|^4 - b_2|\boldsymbol{k}|^2 + C/H_0) + gH_0|\boldsymbol{k}|^2 + f^2\,, \\ a_0 &:= gH_0|\boldsymbol{k}|^2 \left((d_1|\boldsymbol{k}|^2 - b_1)k_y^2 + (d_2|\boldsymbol{k}|^2 - b_2)k_x^2 + C/H_0\right). \end{aligned}$$

We emphasize two aspects concerning the structure of the spectrum:

On the one hand, $\lambda = 0$ is a solution at $\boldsymbol{k} = 0$ for any choice of parameters, whose formal eigenfunction is $(\boldsymbol{v}, \eta)^\intercal = (0, 1)^\intercal$. This perturbs the total fluid mass, so the characteristic fluid depth H_0, and relates to the mass conservation law, as well as the family of trivial steady flows $(\boldsymbol{v}, \eta)^\intercal \equiv (0, h)^\intercal$ of (4.1), for arbitrary $h \in \mathbb{R}$. Hence, these eigenmodes are suppressed when imposing that H_0 is the fixed mean fluid depth, which means η has zero mean. However, it is sometimes convenient to drop this constraint, even though we then need to account for the additional mode.

On the other hand, the presence of hyperdiffusion terms for $d_1 d_2 \neq 0$ implies that there is a continuous solution $\lambda_\infty(\boldsymbol{k})$ with $\mathrm{Re}(\lambda_\infty(\boldsymbol{k})) \to 0$ as $|\boldsymbol{k}| \to \infty$, see blue graph in Figure 4.1(a). Indeed, for $\boldsymbol{k} = r^{-1}\bar{\boldsymbol{k}}$ with $|\bar{\boldsymbol{k}}| = 1$ we obtain

$$\lim_{r \to 0} r^8 d(\lambda, r^{-1}k_x, r^{-1}k_y) = d_1 d_2 \lambda \,, \tag{4.11}$$

which gives the solution $\lambda = 0$ at $r = 0$, i.e. $|\boldsymbol{k}| = \infty$. Hence, there is no spectral gap for the linearization of (4.1) in the trivial solution posed on, e.g. rectangles with periodic boundary conditions. As a consequence, the standard approach of center manifolds cannot be applied in order to reduce the bifurcation from a trivial flow to a finite dimensional ODE. However, in this chapter we will handle this problem by restricting our attention to the existence of certain bifurcating solutions. In the application, the backscatter parameterization is applied to a numerically discretized setting, which effectively cuts the available wave vectors at some large $|\boldsymbol{k}|$. Thus, a spectral gap is retained, but the properties of the present continuum equations are nevertheless relevant, in particular for large-scale settings.

4.2.1. Onset of instabilities

For $\boldsymbol{k} = (k_x, k_y)^\intercal \in \mathbb{R}^2$ and by the Routh-Hurwitz criterion, a solution λ of the dispersion relation (4.10) has $\mathrm{Re}(\lambda) < 0$ if and only if

$$a_2 > 0 \,, \quad a_0 > 0 \,, \quad a_1 a_2 - a_0 > 0 \,. \tag{4.12}$$

More precisely, (4.10) has a zero root $\lambda = 0$ if and only if $a_0 = 0$, and has purely imaginary roots $\lambda = \pm \mathrm{i}\omega \in \mathrm{i}\mathbb{R} \setminus \{0\}$ if and only if $a_1 a_2 - a_0 = 0$ and $a_1 > 0$. For instance, without hyperdiffusion and backscatter $b_j = d_j = 0$ for $j = 1, 2$, the conditions in (4.12) are satisfied for all wave vectors $\boldsymbol{k} \neq 0$ and any bottom drag coefficient $C > 0$, which implies that $(\boldsymbol{v}, \eta)^\intercal = (0, 0)^\intercal$ is spectrally stable in this case (with neutral mode at $\boldsymbol{k} = 0$).

Isotropic case

In case of isotropic hyperdiffusion and backscatter $d_j = d$, $b_j = b$ for $j = 1, 2$, the dispersion relation (4.10) depends on $\boldsymbol{k}$ only through $K := |\boldsymbol{k}|^2$. The spectrum is therefore rotationally symmetric with respect to $\boldsymbol{k} \in \mathbb{R}^2$ in the wave vector plane. Moreover, the coefficients a_2 and a_0 possess the common factor $F(K; C) := dK^2 - bK + C/H_0$, and so

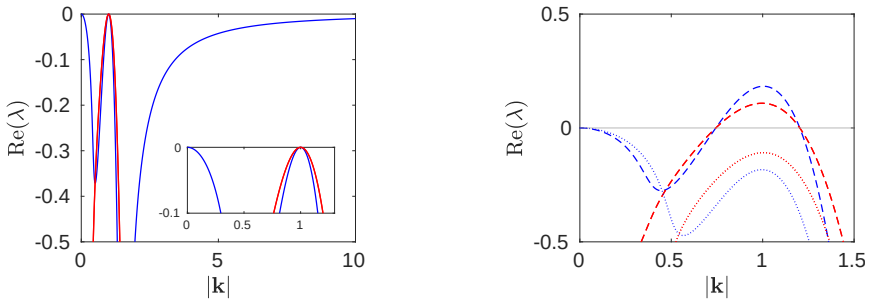

(a) (b)

Figure 4.1.: Samples of spectrum in the isotropic case $d_1 = d_2 = 1$, $b_1 = b_2 = 2$. Other fixed parameters: $f = 0.3$, $g = 9.8$, $H_0 = 0.1$ so that $C_c = 0.1$ and $k_c = 1$. (a) The real spectrum (blue) and the complex spectrum (red) of $\mathcal{L}$ (enlargement in the inset) are simultaneously critical for $C = C_c$ at $\{\boldsymbol{k} \in \mathbb{R}^2 \mid |\boldsymbol{k}| = k_c = 1\}$. (b) Plotted are a stable case at $C = 0.12$ (dotted) and an unstable case at $C = 0.08$ (dashed). In the latter case real and complex spectra have zero real parts for the same wave numbers.

does $a_1 a_2 - a_0$ as well. In addition, a_2 and $a_1 a_2 - a_0$ have the same sign as F, while a_0 the same as KF, so it is additionally zero at $K = 0$. Let $\lambda_j(K; C)$ denote the roots of the dispersion relation (4.10) in some ordering for $j = 1, 2, 3$. It follows that $\lambda_j(K; C) = 0$ occurs at $K = 0$ and at roots of F. The latter emerges when decreasing C below the threshold

$$C_c := \frac{b^2 H_0}{4d}, \tag{4.13}$$

for which $F(K; C_c)$ is non-negative and has a global minimum at the double root in K, that lies at wave vectors with

$$|\boldsymbol{k}| = k_c := \sqrt{\frac{b}{2d}}. \tag{4.14}$$

For $C = C_c$ we choose indices so that $\lambda_1(k_c; C_c) = 0$, $\lambda_2(k_c; C_c) = -\lambda_3(k_c; C_c) = -\mathrm{i}\omega_c$, with

$$\omega_c^2 := a_1|_{C=C_c, |\boldsymbol{k}|=k_c} = g H_0 k_c^2 + f^2, \tag{4.15}$$

and $\mathrm{Re}(\lambda_j(K; C_c)) < 0$ for all $|\boldsymbol{k}| \in \mathbb{R} \setminus \{0, k_c\}$ and $j = 1, 2, 3$. Hence, in the wave vector plane, the critical spectrum away from the origin forms a circle centered at the origin with radius k_c, cf. Figure 4.1(a). And, as C decreases below C_c, the trivial zero solution becomes unstable *simultaneously* via a stationary (similar to a Turing) and an oscillatory (similar to a Turing-Hopf) instability with finite wave number, both in presence of an additional neutrally stable mode with zero wave number, cf. Figure 4.1(b). More precisely, for $0 < C < C_c$ there is a positive interval I_C with $a_0 < 0$ for $K \in I_C$. Hence, in this case the dispersion relation (4.10) has a positive root in the annulus

$|\boldsymbol{k}|^2 \in I_C$ in the wave vector plane.

Regarding the limit of small hyperdiffusion and backscatter parameter $d, b \to 0$, we note that the scalings of C_c and k_c differ, so that fixed k_c requires $C_\mathrm{c} \to 0$, while fixed C_c requires $k_\mathrm{c} \to \infty$.

Any neutral mode corresponds to a class of flows or waves with the usual geophysical terminology, cf. e.g. Pedlosky (1987): Due to the frequency relation (4.15) we refer to waves with $\lambda = \pm \mathrm{i}\omega_\mathrm{c}$ as inertia-gravity waves (IGWs) rather than Poincaré waves. The steady modes with $\lambda = 0$ correspond to Rossby waves in the present f-plane approximation of the Coriolis force. We therefore interpret the instability in the present isotropic case as a backscatter and bottom drag induced simultaneous instability of selected Rossby and inertia-gravity waves.

Anisotropic case

In case of anisotropic hyperdiffusion and/or backscatter ($b_1 \neq b_2$ and/or $d_1 \neq d_2$) with $b_j, d_j > 0$ for $j = 1, 2$, the structure of the spectrum is more complicated. However, in the following we are able to show the property, that the real spectrum is always more unstable than any non-real spectrum. This in particular implies, that the primary instability with respect to C is purely stationary (Rossby waves).

Since the dispersion relation (4.10) explicitly depends on k_x and k_y, the spectrum is anisotropic in the wave vector plane. But, analogous to the isotropic case, a_0 has a factor

$$F(k_x, k_y; C) := d_1|\boldsymbol{k}|^2 k_y^2 + d_2|\boldsymbol{k}|^2 k_x^2 - b_1 k_y^2 - b_2 k_x^2 + C/H_0\,,$$

and a_0 has the same sign as KF. We next show that $F(\boldsymbol{k}; C) = 0$ is the minimal value of $F(\cdot; C)$ at $C = C_\mathrm{c}$ and wave vectors $\boldsymbol{k} = \pm\boldsymbol{k}_\mathrm{c}$ given by

$$C_\mathrm{c} = \frac{b_2^2 H_0}{4d_2}\,, \quad \boldsymbol{k}_\mathrm{c} = (k_\mathrm{c}, 0)^\mathsf{T}\,, \quad k_\mathrm{c} = \sqrt{\frac{b_2}{2d_2}}\,, \quad \text{for } \frac{b_1^2}{d_1} \leq \frac{b_2^2}{d_2}\,, \tag{4.16a}$$

$$C_\mathrm{c} = \frac{b_1^2 H_0}{4d_1}\,, \quad \boldsymbol{k}_\mathrm{c} = (0, k_\mathrm{c})^\mathsf{T}\,, \quad k_\mathrm{c} = \sqrt{\frac{b_1}{2d_1}}\,, \quad \text{for } \frac{b_1^2}{d_1} \geq \frac{b_2^2}{d_2}\,. \tag{4.16b}$$

The critical points of $F(\cdot; C)$ lie at $\boldsymbol{k} = 0$, $\boldsymbol{k} = \pm\boldsymbol{k}_\mathrm{c}$ and (if real)

$$\boldsymbol{k} = \boldsymbol{k}_{m,n} := \left(m\sqrt{\frac{b_1(d_1+d_2) - 2b_2 d_1}{(d_1-d_2)^2}}, n\sqrt{\frac{b_2(d_1+d_2) - 2b_1 d_2}{(d_1-d_2)^2}} \right)\,,$$

for $m, n = \pm 1$. Note that $\boldsymbol{k}_{m,n}$ for $m, n = \pm 1$ are not critical points in the case $d_1 = d_2$. The real critical points $\boldsymbol{k}_{m,n}$ are not minima, since the Hessian matrices of F evaluated at $\boldsymbol{k}_{m,n}$ are indefinite. Indeed, the determinant of the Hessian matrices is always $-16\frac{(b_1(d_1+d_2)-2b_2d_1)(b_2(d_1+d_2)-2b_1d_2)}{(d_1-d_2)^2}$, which is negative for real $\boldsymbol{k}_{m,n}$. Since $F(\cdot; C)$ is coercive and sign symmetric, the global minima are as claimed.

In particular, it is straightforward to switch between the two cases in (4.16) upon varying parameters through the isotropic case. The corresponding scaling of C_c and k_c in (4.16) regarding the limit d_j, $b_j \to 0$ for $j = 1, 2$ is the same as for (4.13) and (4.14) noted above.

Due to the same sign of a_0 and KF, the above analysis of F implies, that the dispersion relation (4.10) has zero roots $\lambda(\boldsymbol{k}, C) = 0$ for $C = C_c$ at $\boldsymbol{k} = 0$ and $\boldsymbol{k} = \boldsymbol{k}_c$ as in (4.16). Since $\partial_\lambda d(0, \boldsymbol{k}_c) = \omega_c^2 = gH_0k_c^2 + f^2 \neq 0$ at $C = C_c$, then by the implicit function theorem there is a unique continuations $\lambda_1 = \lambda_1(\boldsymbol{k}; C)$ as roots of the dispersion relation (4.10) for $\boldsymbol{k}$ near $\pm\boldsymbol{k}_c$. Moreover, $\lambda_1 < 0$ for $\boldsymbol{k}$ near (but not at) $\pm\boldsymbol{k}_c$. The critical wave vectors $\boldsymbol{k}_c$ determined in (4.16a) and (4.16b) differ if $b_1^2/d_1 \neq b_2^2/d_2$, so that $\boldsymbol{k}_c$ lies either on the k_x- or the k_y-axis in the wave vector plane. This is similar to reaction diffusion systems with uni-directional advection (see e.g. Yang, 2019). In case $b_1^2/d_1 = b_2^2/d_2$ the critical wave vectors lie on both axes so there are four critical wave vectors. By continuity, for $C < C_c$ but close to C_c, we have $\lambda_1 > 0$ for wave vectors $\boldsymbol{k}$ in a disc shaped set near any of the two or four critical $\boldsymbol{k}_c$. Specifically, for $b_1^2/d_1 \neq b_2^2/d_2$, this corresponds to the red regions in Figure 4.5 of Section 4.5, and for $b_1^2/d_1 = b_2^2/d_2$ there are four such sets in the wave vector plane.

Remark 4.0.4. In any anisotropic case, the onset of instability upon decreasing C occurs first through steady modes (Rossby waves) with wave vectors on the k_x- and/or k_y-axis, as given in (4.16). This is analogous to a Squire theorem, in the sense that the onset of instability in 2D coincides with the onset in 1D, which trivially holds in the isotropic case. For the anisotropic case, in Appendix B we show that $a_2 > 0$ as well as $a_1a_2 - a_0 > 0$ for $C \geq C_c$ and $\boldsymbol{k} \in \mathbb{R}^2$. Together with $a_0 > 0$ for $C > C_c$ and $\boldsymbol{k} \in \mathbb{R}^2 \setminus \{(0, 0)^\intercal\}$, as well as $a_0 > 0$ for $C = C_c$ and $\boldsymbol{k} \in \mathbb{R}^2 \setminus \{(0, 0)^\intercal, \pm\boldsymbol{k}_c\}$ with $a_0 = 0$ for $\boldsymbol{k} = 0, \pm\boldsymbol{k}_c$ as shown above by the analysis of F, the claim follows by the Routh-Hurwitz criterion (4.12).

4.2.2. Description of the kernels

We summarize here the results on the critical spectrum. In terms of decreasing the bottom drag parameter C, the spectrum of the linear operator $\mathcal{L}$ from (4.8) changes stability at $C = C_c$. The resulting operator $\mathcal{L}_c := \mathcal{L}|_{C=C_c}$ can have the following types of marginally stable spectral structure:

3D A three-dimensional kernel for anisotropic backscatter, satisfying $b_1^2/d_1 \neq b_2^2/d_2$. A sample is shown in Figure 4.2.

5D A five-dimensional kernel for anisotropic backscatter, satisfying $b_1^2/d_1 = b_2^2/d_2$. A sample is shown in Figure 4.3.

∞D For isotropic backscatter, an infinite-dimensional kernel and simultaneously an infinite-dimensional center space, both parameterized by a circle of wave vectors. Samples are shown in Figure 4.1.

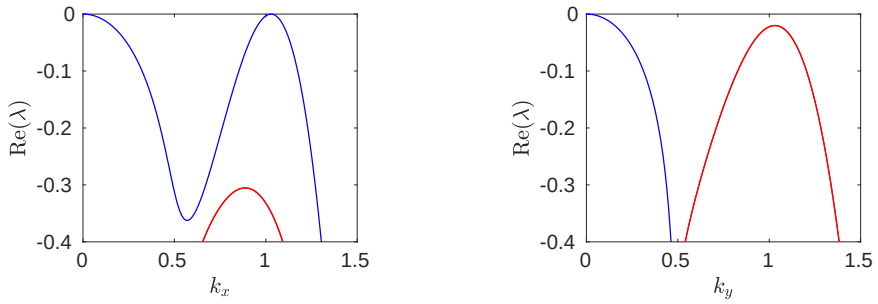

(a) (b)

Figure 4.2.: Sample of critical spectrum in the anisotropic case with $b_1^2/d_1 \neq b_2^2/d_2$. The real spectrum (blue) of $\mathcal{L}$ from (4.8) is critical for $C = C_c$ at $\boldsymbol{k} = (\pm k_c, 0)^\intercal$ as defined in (4.16), with neutral mode at $\boldsymbol{k} = 0$ for any choice of parameters, while the complex spectrum (red) is strictly stable. The parameters are $d_1 = 1$, $d_2 = 1.04$, $b_1 = 1.5$, $b_2 = 2.2$, $f = 0.3$, $g = 9.8$, $H_0 = 0.1$, so that $C_c \approx 0.116$ and $k_c \approx 1.03$.

3D kernel

As shown above, in this case the zero eigenmode of $\mathcal{L}_c$ has its wave vector either on the k_x-axis or on the k_y-axis, and without loss of generality we only discuss the former. Hence, in order to identify the primary bifurcation, it suffices to consider (4.1) in 1D, i.e. $\boldsymbol{x} = (x, 0)^\intercal$ and $x \in [0, 2\pi/k]$ with periodic boundary conditions, where k is the wavenumber for the expected bifurcating nonlinear wave trains. As noted in Remark 4.0.1, the bifurcation problem can be reduced a priori to a scalar equation, and we will proceed with this later based on the isotropic case. As to the linear structure of the full three-component system, we rescale the domain to $[0, 2\pi]$ and restrict $\mathcal{L}$ from (4.8) to 1D. The kernel eigenvectors of $\mathcal{L}$ at $(C, k) = (C_c, k_c)$ as defined in (4.16) are $\widetilde{\boldsymbol{e}}_j := \widetilde{\boldsymbol{E}}_j \mathrm{e}^{\mathrm{i}jx}$ with $\widetilde{\boldsymbol{E}}_j \in \mathbb{C}^3$ and $\widetilde{\boldsymbol{E}}_{-j} = \overline{\widetilde{\boldsymbol{E}}_j}$ for $j = 0, \pm 1$, and

$$\widetilde{\boldsymbol{E}}_j = \begin{pmatrix} 0 \\ 1 \\ -\mathrm{i}jf/(gk_c) \end{pmatrix}, \quad \text{for } j = \pm 1, \quad \widetilde{\boldsymbol{E}}_0 = \begin{pmatrix} 0 \\ 0 \\ 1 \end{pmatrix}. \tag{4.17}$$

Since we have a zero eigenvalue at $\boldsymbol{k} = (0, 0)^\intercal$ for all parameters, it implies $\widetilde{\boldsymbol{e}}_0$ is in the kernel of $\mathcal{L}$ for all C. The first two components of $\widetilde{\boldsymbol{E}}_{\pm 1}$ are orthogonal to $\boldsymbol{k} = (k_x, 0)^\intercal$, which is in accordance with the possibility to reduce to the scalar equation in the form of (4.3), cf. Remark 4.0.1. We note that the eigenvectors depend on the bottom drag parameters only through k_c from (4.16), i.e. $C_c = d_2 H_0 k_c^4$. Consistent with Remark 4.0.2, the kernel eigenvectors $\widetilde{\boldsymbol{e}}_{\pm 1}$ correspond to so-called Rossby waves, e.g. Pedlosky (1987).

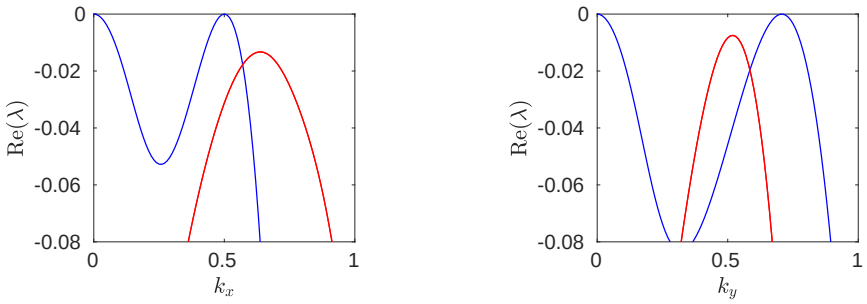

(a) (b)

Figure 4.3.: Sample of critical spectrum in the anisotropic case for $b_1^2/d_1 = b_2^2/d_2$. The real spectrum (blue) of $\mathcal{L}$ from (4.8) is critical for $C = C_c$ at $\boldsymbol{k} = \boldsymbol{k}_c$ with $\boldsymbol{k} = (\pm k_x', 0)^\mathsf{T}$ and $\boldsymbol{k} = (0, \pm k_y')^\mathsf{T}$ as defined in (4.16), with neutral mode at $\boldsymbol{k} = 0$ for any choice of parameters, while the complex spectrum (red) is strictly stable. The parameters are $d_1 = 1$, $d_2 = 4$, $b_1 = 1$, $b_2 = 2$, $f = 0.3$, $g = 9.8$, $H_0 = 0.1$, so that $C_c = 0.025$, $k_x' = 0.5$ and $k_y' \approx 0.71$.

5D kernel

In this case the critical modes in k_x- and k_y-direction of the 3D cases occur simultaneously. Hence, the eigenvectors identified in the 3D case combined represent the kernel of $\mathcal{L}$ from (4.8). The reduction to the respective scalar equations admits a partial unfolding of the bifurcation. In a more complete unfolding one would expect square-type patterns of Rossby waves in orthogonal directions based on the expected bifurcation equations (see e.g. Yang, 2019). However, it is not clear that this can be realized in the present context due to the lack of a spectral gap following from (4.11). In particular, the required Fredholm properties are not immediately clear.

Infinite-dimensional kernel

Here the hyperdiffusion and backscatter are isotropic and the critical eigenmodes of $\mathcal{L}_c$ lie at the origin and on a circle with radius k_c in the wave vector plane. This circle is doubly covered by steady and oscillatory modes. For the steady modes, in contrast to the 3D and 5D cases, any wave vector direction can be selected in order to reduce to a 1D plane wave problem. This is always (4.6b) and allows the analysis of the stationary bifurcation problem independent of the problem with the spectral gap.

Towards bifurcations of oscillatory solutions, we consider a comoving frame $\boldsymbol{x} - \boldsymbol{c}t$ with suitable $\boldsymbol{c} \in \mathbb{R}^2$. This change of variables creates the additional term $-\boldsymbol{c} \cdot \nabla(\boldsymbol{v}, \eta)^\mathsf{T}$ on the left-hand side of (4.1), so that the dispersion relation (4.10) turns into

$$d_{\boldsymbol{c}}(\lambda, \boldsymbol{k}) = d(\lambda - \mathrm{i}\boldsymbol{c} \cdot \boldsymbol{k}, \boldsymbol{k})\,. \tag{4.18}$$

Hence, exactly the purely imaginary spectrum at $C = C_c$ from (4.13) is shifted to the origin. Indeed, if $d(\mathrm{i}\omega, \boldsymbol{k}_\omega) = 0$ for $\omega \in \mathbb{R}$ and some $\boldsymbol{k}_\omega \neq 0$, then $d_{\boldsymbol{c}}(0, \boldsymbol{k}_\omega) = 0$ for

$\boldsymbol{c} = -\omega/|\boldsymbol{k}_\omega|^2\, \boldsymbol{k}_\omega$. This applies for $\omega = \pm\omega_\mathrm{c}$ from (4.15) with any $\boldsymbol{k}_\omega = \boldsymbol{k}_\mathrm{c} = (k_x', k_y')^\mathsf{T}$ satisfying (4.14). Concerning bifurcations, we again consider the simplest case of wave trains, which are 2π-periodic solutions that depend only on the phase variable

$$\zeta = (\boldsymbol{x} - \boldsymbol{c}t) \cdot \boldsymbol{k}_\mathrm{c} = k_x' x + k_y' y + \omega t\,, \tag{4.19}$$

so that $\partial_x = k_x'\partial_\zeta$, $\partial_y = k_y'\partial_\zeta$ and ∂_t becomes $\partial_t + \omega\partial_\zeta$. Hence, in terms of the phase variable ζ, and using $k_\mathrm{c}^4 d\partial_\zeta^4 + k_\mathrm{c}^2 b\partial_\zeta^2 + C_\mathrm{c}/H_0 = dk_\mathrm{c}^4(\partial_\zeta^2+1)^2$ due to (4.13) and (4.14), we obtain for $\omega = -\omega_\mathrm{c}$ the linear operator

$$\mathcal{L}_\mathrm{c} := \begin{pmatrix} \omega_\mathrm{c}\partial_\zeta - dk_\mathrm{c}^4(\partial_\zeta^2+1)^2 & f & -k_x' g\partial_\zeta \\ -f & \omega_\mathrm{c}\partial_\zeta - dk_\mathrm{c}^4(\partial_\zeta^2+1)^2 & -k_y' g\partial_\zeta \\ -k_x' H_0\partial_\zeta & -k_y' H_0\partial_\zeta & \omega_\mathrm{c}\partial_\zeta \end{pmatrix}. \tag{4.20}$$

Its kernel is three-dimensional, spanned by $\boldsymbol{e}_0 = \widetilde{\boldsymbol{e}}_0$ from (4.17) and $\boldsymbol{e}_1$, $\boldsymbol{e}_{-1}$ that have the form $\boldsymbol{e}_j := \boldsymbol{E}_j \mathrm{e}^{\mathrm{i}j\zeta}$ with $\boldsymbol{E}_j \in \mathbb{C}^3$ and $\boldsymbol{E}_{-j} = \overline{\boldsymbol{E}_j}$ for $j = \pm 1$. We choose

$$\boldsymbol{E}_j = \begin{pmatrix} \omega_\mathrm{c} k_x' + j\mathrm{i} f k_y' \\ \omega_\mathrm{c} k_y' - j\mathrm{i} f k_x' \\ k_\mathrm{c}^2 H_0 \end{pmatrix}.$$

The case $\omega = \omega_\mathrm{c}$ is analogous. As in the 3D and 5D cases, the eigenvectors $\boldsymbol{e}_{\pm 1}$ depend on the bottom drag parameters through k_c.

The structure of $\boldsymbol{E}_j$ for $j = \pm 1$ shows, that bifurcating solutions in terms of these modes cannot be of the plane wave form (4.3), which is required for the reduction to the scalar equation (4.6b). Hence, an analysis of the corresponding bifurcations requires to consider the full system. These kernel eigenvectors correspond to the so-called inertia-gravity waves (see e.g. Pedlosky, 1987), so that the bifurcation from these modes can be viewed as inertia-gravity waves and will be studied in Section 4.4. The isotropic case thus simultaneously generates Rossby and inertia-gravity waves, and we expect also mixed waves. Their wave vectors must have length near the critical wave number k_c, but have arbitrary directions.

4.3. Bifurcation of nonlinear Rossby waves

We combine the results of Section 4.2 with the reduction (4.6) presented in Section 4.1 for steady plane wave-type solutions (4.3). Hence, we look in (4.1) for bifurcating solutions of the form

$$\boldsymbol{v} = \partial_\xi \phi(\boldsymbol{k}\cdot\boldsymbol{x})\boldsymbol{k}^\perp\,, \qquad \eta = \tilde{f}\phi(\boldsymbol{k}\cdot\boldsymbol{x})\,, \qquad |\boldsymbol{k}| = |\boldsymbol{k}^\perp| \approx k_\mathrm{c}\,, \tag{4.21}$$

for wave shape ϕ and phase variable $\xi = \boldsymbol{k} \cdot \boldsymbol{x}$, which leads to the reduced steady state equation according to (4.6b)

$$0 = dk^4 \partial_\xi^5 \phi + bk^2 \partial_\xi^3 \phi + \frac{C + Qk|\partial_\xi \phi|}{H_0 + \tilde{f}\phi} \partial_\xi \phi \,.$$

We recall that $k = |\boldsymbol{k}| = |\boldsymbol{k}^\perp|$ is the wave number for the nonlinear plane wave-type solutions (4.3). We remark as before that the nonlinear terms stems from the bottom drag only, the nonlinear advection terms of (4.1) do not enter for this form of plane waves due to Theorem 2.2, Theorem 2.3 and Theorem 2.5. We also recall from (4.0.2) that the bifurcating solutions we investigate here can be viewed as (nonlinear) Rossby waves.

Linear analysis

We augment the stability analysis of the trivial state $(\boldsymbol{v}, \eta)^\intercal = (0,0)^\intercal$ in Section 4.2.1 by including changes in wave number by κ such that $|\boldsymbol{k}| = k_c + \kappa$. We also restrict to the isotropic case and introduce the bifurcation parameter α such that $C = C_c - \alpha H_0$. For $\tau = (\alpha, \kappa) \approx (0,0)$ we expand $\lambda = m\lambda(\tau)$ solving (4.10) with $\lambda(0) = 0$ as

$$\lambda(\tau) = \alpha - 2b\kappa^2 + \mathcal{O}(|\kappa|^3) \,, \tag{4.22}$$

where $m := gk_c^2 H_0/\omega_c^2 > 0$. Hence, the trivial state $(\boldsymbol{v}, \eta)^\intercal = (0,0)^\intercal$ (i.e. $\phi(\xi) \equiv 0$) is unstable for $\alpha > 2b\kappa^2$, and to leading order the stability boundary is given by $\alpha = 2b\kappa^2$.

Steady state equation

We consider the steady state equation in the domain $\xi \in [0, 2\pi]$ under periodic boundary conditions. Analogous to the above linear analysis, we use the parameter κ in the wave number $k = k_c + \kappa$, that allows to detect plane wave-type solutions with wave numbers close to the critical one k_c. With parameters $\tau = (\alpha, \kappa) \approx (0,0)$, we thus obtain

$$G(\phi, \tau) := dk^4 \partial_\xi^5 \phi + bk^2 \partial_\xi^3 \phi + \frac{C_c - \alpha H_0 + Qk|\partial_\xi \phi|}{H_0 + \tilde{f}\phi} \partial_\xi \phi = 0 \,, \tag{4.23}$$

where $G : H^5_{per} \times \mathbb{R}^2 \to L^2$ is Fréchet differentiable. In lack of a reference we provide the following lemma with a short proof, which in particular shows the differentiability of the non-smooth term.

Lemma 4.1. *Let $f : I \to \mathbb{R}$ be a function on the interval $I \subset \mathbb{R}$. For the Nemitsky operator $f_N : \mathcal{U} \subset H^1_{per} \to L^2$ defined by $f_N(\varphi)(x) = f(\varphi(x))$, with $\mathcal{U}$ such that f_N is well-defined, the following holds:*
(a) If f is Lipschitz continuous, then so is f_N.
(b) If f is C^k smooth for $k \in \mathbb{N}$, then so is f_N.

Proof. The Nemitsky operator is well-defined since $\varphi \in H^1_{per}$ is continuous and thus has a bounded range, so that $\|f_N(\varphi)\|_2 \leq 2\pi\|f_N(\varphi)\|_\infty < \infty$ in all cases.

(a) For $\varphi, \psi \in L^2$ and L as the Lipschitz-constant of f, it follows directly the inequality $\|f_N(\varphi) - f_N(\psi)\|_2 \leq L\|\varphi - \psi\|_2$ from the definition of f_N.

(b) We consider $k = 1$ in detail. For $y \in I$ and due to the smoothness of f we have $R(z; y) := f(y + z) - f(y) - f'(y)z = o(|z|)$, i.e. for any $\varepsilon > 0$ there is $\delta > 0$ such that $|z| \leq \delta$ implies $|R(z; y)| \leq \varepsilon|z|$, locally and uniformly in y. For the Nemitsky operator we get $(f_N(\varphi + h) - f_N(\varphi))(x) - f'(\varphi(x))h(x) = R(h(x); \varphi(x))$. With the Sobolev embedding $\|\cdot\|_\infty \leq C\|\cdot\|_{H^1}$, for $\varphi, h \in H^1_{per}$ with $\|h\|_{H^1} \leq \delta/C$ we thus have $|R(h(x); \varphi(x))| \leq \varepsilon|h(x)|$ for all $x \in [0, 2\pi]$, which implies $\|R(h(\cdot); \varphi(\cdot))\|_2 \leq \varepsilon\|h\|_2$. From $\|\cdot\|_2 \leq \|\cdot\|_{H^1}$ we obtain $\|R(h(\cdot); \varphi(\cdot))\|_2/\|h\|_{H^1} \leq \varepsilon$, which implies the Fréchet derivative of f_N is $f'(\varphi(\cdot))$. For general k the proof is the same upon replacing R by the appropriate remainder term of the Taylor expansion of f. □

This lemma provides differentiability of the full operator G from (4.23) due to the additional smoothness in the domain of G and the differentiability of products of differentiable functions.

Any constant ϕ solves (4.23) and without loss we consider the bifurcation from the zero state, since any nonzero trivial solution ϕ corresponds to changing H_0 as noted before. The derivative of G with respect to ϕ in $(\phi, \tau) = (0, 0)$ is given by

$$\mathcal{L}_0 := \partial_\phi G(0, 0) = dk_c^4\partial_\xi^5 + bk_c^2\partial_\xi^3 + \frac{C_c}{H_0}\partial_\xi : H^5_{per} \to L^2\,,$$

which is a Fredholm operator with index zero and with the kernel

$$\ker(\mathcal{L}_0) = \operatorname{span}\{e_j \mid j = 0, \pm 1\}\,, \quad e_j := \mathrm{e}^{\mathrm{i}j\xi}\,.$$

By Fredholm properties the domain and range of $\mathcal{L}_0$ can be split as $H^5_{per} = \ker(\mathcal{L}_0) \oplus \mathcal{M}$ and $L^2 = \ker(\mathcal{L}_0^*) \oplus \operatorname{range}(\mathcal{L}_0)$, where we have $\operatorname{range}(\mathcal{L}_0)^\perp = \ker(\mathcal{L}_0^*)$ with respect to the L^2-inner product $\langle u, v\rangle_{L^2} = \frac{1}{2\pi}\int_0^{2\pi} u\bar{v}\mathrm{d}\xi$. The kernel of the adjoint operator is $\ker(\mathcal{L}_0^*) = \operatorname{span}\{e_j^* \mid j = 0, \pm 1\}$ with $e_j^* = e_j$, analogous to $\ker(\mathcal{L}_0)$. When there is no ambiguity, we denote the inner product $\langle\cdot,\cdot\rangle_{L^2}$ as $\langle\cdot,\cdot\rangle$ in the remainder of Section 4.3.

Lyapunov–Schmidt reduction

The above decompositions define the projections $\tilde{P} : H^5_{per} \to \ker(\mathcal{L}_0)$ along $\mathcal{M}$ and $P : L^2 \to \operatorname{range}(\mathcal{L}_0)$ along $\ker(\mathcal{L}_0^*)$. The projection $\tilde{P}$ with the splitting $\phi = u + w$ for $u \in \ker(\mathcal{L}_0)$ and $w \in \mathcal{M}$ can be written as

$$u = \tilde{P}\phi := \sum_{j=-1}^{1} \langle\phi, e_j\rangle_{H^5} e_j\,, \qquad \langle\phi, e_j\rangle_{H^5} = \sum_{n=0}^{5} \langle\partial_\xi^n\phi, e_j\rangle_{L^2}\,.$$

Since integration by parts under periodic boundary conditions gives

$$\langle \partial_\xi^{n+1}\phi, e_j\rangle_{L^2} = \mathrm{i}j\langle \partial_\xi^n \phi, e_j\rangle_{L^2}\,,$$

it follows for $j = 0, \pm 1$ that $\langle \phi, e_j\rangle_{H^5} = (1+\mathrm{i}j)\langle \phi, e_j\rangle_{L^2}$. Thus, the inner products $\langle\cdot,\cdot\rangle_{H^5}$ and $\langle\cdot,\cdot\rangle_{L^2}$ are equivalent concerning the orthogonality between $\ker(\mathcal{L}_0)$ and $\mathcal{M}$, i.e. $\langle u, w\rangle_{H^5} = 0 \Leftrightarrow \langle u, w\rangle_{L^2} = 0$ for all $u \in \ker(\mathcal{L}_0)$ and $w \in \mathcal{M}$. The projection P in the decomposition of L^2 can be written as

$$P := \mathrm{Id} - \sum_{j=-1}^{1} \langle\cdot, e_j\rangle_{L^2} e_j\,. \tag{4.24}$$

We now consider $u \in \ker(\mathcal{L}_0)$, $w \in \mathcal{M}$ and the projected problem of (4.23)

$$PG(u+w,\tau) = 0\,. \tag{4.25}$$

Differentiating (4.25) with respect to w at zero gives

$$P\partial_\phi G(0,0) = P\mathcal{L}_0 = \mathcal{L}_0 : \mathcal{M} \to \mathrm{range}(\mathcal{L}_0)\,.$$

Thus, by the implicit function theorem, there is an open neighbourhood of $(0,0,0)$ in $\ker(\mathcal{L}_0)\times\mathcal{M}\times\mathbb{R}^2$ of the form $N_0 \times M_0 \times (-\varepsilon,\varepsilon)^2$ and a unique function

$$W : N_0 \times (-\varepsilon,\varepsilon)^2 \to M_0\,,$$

such that $W(0,0) = 0$ and $w = W(u,\tau)$ solves (4.25) for all $(u,\tau) \in N_0 \times (-\varepsilon,\varepsilon)^2$. In order to solve (4.23) it thus remains to determine $(u,\tau) \in N_0 \times (-\varepsilon,\varepsilon)^2$, such that

$$(\mathrm{Id} - P)G(u + W(u,\tau),\tau) = 0\,,$$

which is equivalent to the bifurcation equations

$$\langle G(u+W(u,\tau),\tau), e_j\rangle = 0\,, \qquad j = 0, \pm 1\,. \tag{4.26}$$

For further analysis we write G as

$$G(\phi,\tau) = \mathcal{L}_0\phi + L_\tau\phi + N_C(\phi,\tau) + N_Q(\phi,\tau)\,,$$

with L_τ the linear perturbation by parameters τ, N_C the smooth nonlinear part and N_Q the non-smooth nonlinear part. If we denote $\phi_\xi = \partial_\xi\phi$, then the operators are given by

$$L_\tau := d(k^4 - k_c^4)\partial_\xi^5 + b(k^2 - k_c^2)\partial_\xi^3 - \alpha\partial_\xi\,, \tag{4.27a}$$

$$\begin{aligned} N_C(\phi,\tau) :=& (C_c - \alpha H_0)\left(\frac{1}{H_0 + \tilde{f}\phi} - \frac{1}{H_0}\right)\phi_\xi \\ =& -\frac{C_c - \alpha H_0}{H_0^2}\left(\tilde{f}\phi - \frac{\tilde{f}^2\phi^2}{H_0} + \tilde{f}^3\mathcal{O}(|\phi|^3)\right)\phi_\xi\,, \end{aligned} \tag{4.27b}$$

$$N_Q(\phi,\tau) := \frac{Qk|\phi_\xi|\phi_\xi}{H_0 + \tilde{f}\phi} = \frac{Qk}{H_0}|\phi_\xi|\phi_\xi - \frac{Qk}{H_0^2}|\phi_\xi|\phi_\xi\left(\tilde{f}\phi - \frac{\tilde{f}^2\phi^2}{H_0} + \tilde{f}^3\mathcal{O}(|\phi|^3)\right). \tag{4.27c}$$

Using $\mathcal{L}_0 u = 0$ and $\langle \mathcal{L}_0 w, e_j\rangle = 0$, equations (4.26) become with $\phi = u + W(u,\tau)$

$$\langle G(\phi,\tau), e_j\rangle = \langle L_\tau\phi, e_j\rangle + \langle N_C(\phi,\tau), e_j\rangle + \langle N_Q(\phi,\tau), e_j\rangle = 0\,, \quad j = 0, \pm 1\,. \tag{4.28}$$

There are parameters $A_j \in \mathbb{C}$ for $j = 0, \pm 1$ in a neighbourhood of zero, such that $u = A_0 e_0 + A_1 e_1 + A_{-1} e_{-1} \in N_0 \subset \ker(\mathcal{L}_0)$. For the real bifurcating solutions we have $A_0 \in \mathbb{R}$ and $A_{-1} = \overline{A_1}$. Moreover, we can assume $A_1 = A_{-1} \in \mathbb{R}$ due to the translation symmetry. Denoting $u_\xi = \partial_\xi u$ we obtain

$$u = A_0 + 2A_1\cos(\xi)\,, \qquad u_\xi = \mathrm{i}(A_1 e_1 - A_{-1}e_{-1}) = -2A_1\sin(\xi)\,, \tag{4.29}$$

as well as $\langle u_\xi, e_0\rangle = 0$, $\langle u_\xi, e_1\rangle = \mathrm{i}A_1$ and $\langle u_\xi, e_{-1}\rangle = -\mathrm{i}A_{-1}$.

Due to the equivalence of the inner products $\langle\cdot,\cdot\rangle_{H^5}$ and $\langle\cdot,\cdot\rangle_{L^2}$ concerning the orthogonality between $\ker(\mathcal{L}_0)$ and $\mathcal{M}$ as shown above, and since $e_0 \in \ker(\mathcal{L}_0)$ and $W \in \mathcal{M}$, it follows $\langle W, e_0\rangle_{L^2} = \langle W, e_0\rangle_{H^5} = 0$, so W has always zero mean. Thus, nonzero mean comes from the constant contribution $A_0 \neq 0$ only. Since we focus here on zero mean for η due to mass conservation, we just have to set $A_0 = 0$. However, just for our choice of function spaces and for the completeness of the results, we keep $A_0 \neq 0$.

Now, after the preparation here, we turn to the bifurcation results. Due to the different settings in presence of non-smooth bottom drag or not, which is connected via the different differentiability properties of G from (4.23), we analyze both cases separately in the following subsections. We start with the smooth bottom drag ($Q = 0$) and continue with the non-smooth case ($Q > 0$) afterwards.

4.3.1. Smooth bottom drag

We directly begin with the theorem, that gives the bifurcation and expansion of the small amplitude plane wave-type solutions near $\tau = (\alpha, \kappa) = 0$ and with smooth bottom drag ($Q = 0$). We recall the choice of parameters $C = C_c - \alpha H_0$ with critical bottom drag C_c as in (4.13) and the critical wave number k_c as in (4.14).

Theorem 4.2 (Bifurcation of Rossby waves for $Q = 0$)**.** *Let $Q = 0$ and $\alpha, \kappa \in \mathbb{R}$ sufficiently close to zero, as well as $\boldsymbol{k} \in \mathbb{R}^2$ with $|\boldsymbol{k}| = k_\mathrm{c} + \kappa$. Consider steady plane wave-type solutions to (4.1) of the form (4.21) with 2π-periodic wave shape ϕ and phase variable $\xi = \boldsymbol{k} \cdot \boldsymbol{x}$. These waves are (up to spatial translations) in one-to-one correspondence with solutions A_0, $A_1 \in \mathbb{R}$ near zero of*

$$0 = A_1 \left(\frac{b^2 \tilde{f}}{4dH_0} A_0 + \alpha - 2b\kappa^2 - \frac{17b^2 \tilde{f}^2}{72dH_0^2} A_1^2 + \mathcal{R}_\mathrm{s} \right), \tag{4.30}$$

with remainder term $\mathcal{R}_\mathrm{s} = \tilde{f}\mathcal{O}\left(|A_1|^2(|A_1|^2 + |A_0| + |\alpha| + |\kappa|) + |A_0|(|A_0| + |\alpha|)\right) + \mathcal{O}(|\kappa|^3)$. In addition, the wave shapes are of the form

$$\phi(\xi) = \phi_\mathrm{s}(\xi; \tau) = A_0 + 2A_1 \cos(\xi) + \frac{\tilde{f}}{9H_0} A_1^2 \cos(2\xi) + \mathcal{R}_{\mathrm{s}W}, \tag{4.31}$$

with $\mathcal{R}_{\mathrm{s}W} = \tilde{f}\mathcal{O}\left(|A_1|^2(|A_1| + |A_0| + |\alpha| + |\kappa|)\right)$.

For $A_0 = 0$ and $\tilde{f} \neq 0$, since the coefficient of A_1^3 in (4.30) is negative and the zero state is unstable for $\alpha > 2b\kappa^2$, we always obtain a supercritical pitchfork bifurcation, cf. Figure 4.4(a). After bifurcation, the leading order amplitude is given by

$$|A_1| = \frac{1}{|\tilde{f}|} \sqrt{\frac{72dH_0^2}{17b^2}(\alpha - 2b\kappa^2)}\,.$$

For any fixed $\alpha > 0$ the amplitude $A_1 = A_1(\kappa)$ forms a semi-ellipse with the maximum at $\kappa = 0$ and $|A_1| > 0$ for $\kappa \in (-\kappa_0, \kappa_0)$, with $\kappa_0 = \sqrt{\alpha/(2b)}$ independent of $\tilde{f}$.

The amplitude is proportional to $\sqrt{\alpha}$, while it is inversely proportional to $\tilde{f}$. Hence, the existence of such solutions requires a balance between linear bottom drag C and Coriolis force f, and the amplitude diverges pointwise in $\kappa \in (-\kappa_0, \kappa_0)$ for $\tilde{f} \to 0$. We illustrate this situation in Figure 4.4(b). The amplitudes also diverge pointwise for small hyperdiffusion and backscatter parameters $(d, b) = (\varepsilon\hat{d}, \varepsilon\hat{b})$ as $\varepsilon \to 0$, with $|A_1| = \mathcal{O}(\varepsilon^{-1/2})$. The bifurcating branches in this case appear 'vertical', while the wave number is fixed at $k = k_\mathrm{c} = (\hat{b}/(2\hat{d}))^{1/2}$.

For $\tilde{f} = 0$, the leading order bifurcation equation is given by

$$0 = A_1(\alpha - 2b\kappa^2)\,.$$

The leading order part is independent of A_0 and the value of A_1 can be arbitrary as well for the case $\alpha = 2b\kappa^2$ (or at $\kappa = \pm\kappa_0$), forming 'vertical' bifurcating branches, cf. Figure 4.4. In this case, the corresponding solutions have sinusoidal wave shapes

$$\phi_\mathrm{s}(\xi) = A_0 + 2A_1 \cos(\xi) \in N_0\,,$$

with arbitrary A_0, $A_1 \in \mathbb{R}$, as given in (4.31). This in particular means $w = W(u, \tau) \equiv 0$ from the splitting $\phi = u + w$ with (4.29). Indeed, revisiting the wave-type solutions

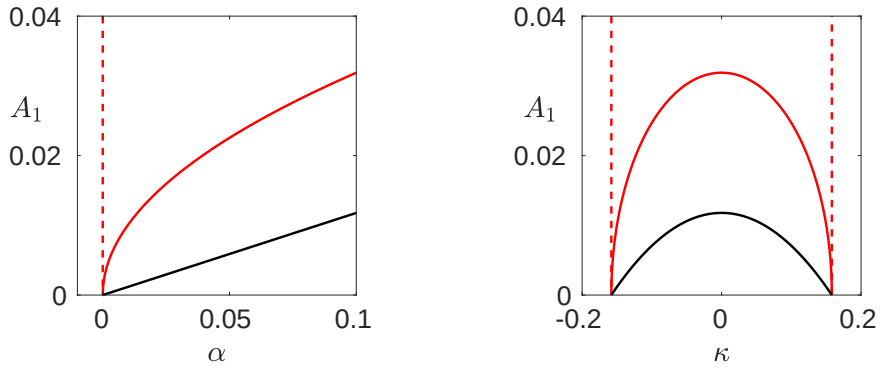

(a) $\kappa = 0$ (b) $\alpha = 0.1$

Figure 4.4.: Leading order amplitudes of bifurcating Rossby waves (Theorem 4.2 and Theorem 4.3) in the isotropic case $d_1 = d_2 = 1$, $b_1 = b_2 = 2$ for smooth ($Q = 0$, red) and non-smooth ($Q = 0.5$, black) cases. Other parameters are $g = 9.8$, $H_0 = 0.1$ so that $C_c = 0.1$. In smooth case, the amplitudes are plotted for $f = 10$ (solid) and $f = 0$ (dashed). In non-smooth case, the amplitude is independent of f.

(4.21) of (4.1), we have here $\eta = \tilde{f}\phi_s = 0$ for $\tilde{f} = 0$ and the amplitude of the velocity $\boldsymbol{v} = \partial_\xi \phi_s(\xi)\boldsymbol{k}^\perp = -2A_1 \sin(\xi)\boldsymbol{k}^\perp$ is free. In Section 4.5 we study related explicit flows, see Remark 4.6.4 and Remark 4.6.6 for details.

Proof of Theorem 4.2. For $Q = 0$, we first solve W from the equation (4.25). We write $PG(\phi, \tau) = P\mathcal{L}_0\phi + PL_\tau\phi + PN_C(\phi, \tau)$. Then we rewrite (4.25) as the fixed point equation for W given by

$$P\mathcal{L}_0 W = -PL_\tau(u + W) - PN_C(u + W, \tau)\,.$$

Using implicit function theorem, and expanding $W = W(u, \tau)$ in $(A_1, A_0, \alpha, \kappa)$ near zero, yields

$$W(u, \tau) = \sum_{j=\pm 1} \frac{C_c \tilde{f}}{2H_0^2 M} e^{2ij\xi} A_j^2 + \widetilde{\mathcal{R}}_W = \frac{\tilde{f}}{9H_0} A_1^2 \cos(2\xi) + \widetilde{\mathcal{R}}_W\,,$$

where $M := 16dk_c^4 - 4bk_c^2 + C_c/H_0 = 9b^2/(4d) > 0$, $\widetilde{\mathcal{R}}_W = \tilde{f}\mathcal{O}\left(|A_1|^2(|A_1| + |A_0| + |\alpha| + |\kappa|)\right)$. Hence, the wave shape has the form

$$\phi(\xi) = \tilde{\phi}_s(\xi; \tau) = A_0 + 2A_1 \cos(\xi) + \frac{\tilde{f}}{9H_0} A_1^2 \cos(2\xi) + \widetilde{\mathcal{R}}_W\,.$$

Now we consider the projections (4.28). For $j = 0$ the projection is trivial, i.e. $\langle G, e_0 \rangle \equiv 0$, since the linear part $\langle \partial_\xi^j \phi, e_0 \rangle = 0$ for $j = 1, 3, 5$, and the integration of the full nonlinear part in (4.23) is given by $\int_0^{2\pi} (H_0 + \tilde{f}\phi)^{-1} \phi_\xi \mathrm{d}\xi = 0$ due to $\log(H_0 + \tilde{f}\phi)$ as the primitive

and the periodic boundary conditions.

Next, we consider the case $j = 1$. We note that the same result applies to the case $j = -1$ due to the assumption $A_1 = A_{-1} \in \mathbb{R}$. For the linear part $\langle L_\tau \phi, e_1 \rangle$ we use the integration by parts and the consideration of periodic boundary conditions in order to show $\langle W_\xi, e_1 \rangle = [W \mathrm{e}^{-\mathrm{i}\xi}]_0^{2\pi}/2\pi + \mathrm{i}\langle W, e_1 \rangle = 0$, since $e_1 \in \ker(\mathcal{L}_0)$ and $W \in \mathcal{M}$. This yields $\langle \phi_\xi, e_1 \rangle = \langle u_\xi, e_1 \rangle = \mathrm{i}A_1$ and in the same way one can show $\langle \partial_\xi^3 \phi, e_1 \rangle = -\mathrm{i}A_1$ as well as $\langle \partial_\xi^5 \phi, e_1 \rangle = \mathrm{i}A_1$. This results in

$$\langle L_\tau \phi, e_1 \rangle = -\mathrm{i}A_1 \left(\alpha - 2b\kappa^2 - 4dk_\mathrm{c}\kappa^3 - d\kappa^4 \right) . \tag{4.32}$$

We consider the nonlinear part that is involving the smooth nonlinear term (4.27b). As to the first and second terms, we respectively compute

$$\begin{aligned} \langle \phi\phi_\xi, e_1 \rangle &= \mathrm{i}A_0A_1 + \frac{\mathrm{i}\tilde{f}}{18H_0} A_1^3 + \mathcal{O}(|A_1|^3(|A_0| + |\alpha| + |\kappa|)) , \\ \langle \phi^2\phi_\xi, e_1 \rangle &= \mathrm{i}A_1^3 + \mathcal{O}(A_0^2|A_1| + |A_0||A_1|^3 + |A_1|^5) . \end{aligned}$$

The remainder terms in $\langle N_C, e_1 \rangle$ are of order $\mathcal{O}(|A_0|^3|A_1| + |A_0||A_1|^3 + |A_1|^5)$. Combining this with the linear and nonlinear terms above, (4.28) becomes

$$\langle G(\phi, \tau), e_1 \rangle = -\mathrm{i}A_1 \left(\alpha - 2b\kappa^2 + \frac{C_\mathrm{c}\tilde{f}}{H_0^2} A_0 - \frac{17C_\mathrm{c}\tilde{f}^2}{18H_0^3} A_1^2 + \widetilde{\mathcal{R}}_\mathrm{s} \right) ,$$

with $\widetilde{\mathcal{R}}_\mathrm{s} = \tilde{f}\mathcal{O}(|A_1|^4 + (|\alpha| + |\kappa|)|A_1|^2 + |A_0||A_1|^2 + |A_0|^2 + |\alpha||A_0|) + \mathcal{O}(|\kappa|^3)$. Substituting the value (4.13) and dividing out the factor $-\mathrm{i}$, implies the bifurcation equation (4.30) with $\mathcal{R}_\mathrm{s} = \widetilde{\mathcal{R}}_\mathrm{s}$ and the wave shape reduces to (4.31). □

4.3.2. Non-smooth bottom drag

For the non-smooth case $Q \neq 0$ we note, that G is not smooth in ϕ anymore, but at least once continuously differentiable in ϕ, so that we can still use the same method to derive the bifurcation equations. We first give the bifurcation in the following theorem. We again recall the choice of parameters $C = C_\mathrm{c} - \alpha H_0$ with critical bottom drag C_c as in (4.13) and the critical wave number k_c as in (4.14).

Theorem 4.3 (Bifurcation of Rossby waves for $Q \neq 0$)**.** *Let $Q \neq 0$ and $\alpha, \kappa \in \mathbb{R}$ sufficiently close to zero, as well as $\boldsymbol{k} \in \mathbb{R}^2$ arbitrary with $|\boldsymbol{k}| = k_\mathrm{c} + \kappa$. Consider steady plane wave-type solutions to (4.1) of the form (4.21) with 2π-periodic wave shape ϕ and phase variable $\xi = \boldsymbol{k} \cdot \boldsymbol{x}$. These waves are (up to spatial translations) in one-to-one correspondence with solutions A_0, $A_1 \in \mathbb{R}$ near zero of*

$$0 = A_1 \left(\frac{b^2\tilde{f}}{4dH_0} A_0 + \alpha - 2b\kappa^2 - \frac{16Q\sqrt{b}}{3\pi H_0\sqrt{2d}} |A_1| + \mathcal{R}_{ns} \right) , \tag{4.33}$$

with remainder term $\mathcal{R}_{\text{ns}} = Q\mathcal{R}_1 + \tilde{f}\mathcal{R}_2 + Q\tilde{f}\mathcal{R}_3 + \mathcal{O}(|\kappa|^3)$ *and*

$$\begin{aligned}
\mathcal{R}_1 &= \mathcal{O}(A_1(|A_1| + |A_0| + |\alpha| + |\kappa|))\,, \\
\mathcal{R}_2 &= \mathcal{O}(A_1(|A_1| + |A_0| + |\alpha| + |\kappa|)) + \mathcal{O}(|A_0||\alpha|) + \tilde{f}\mathcal{O}(|A_0|^2)\,, \\
\mathcal{R}_3 &= \mathcal{O}(|A_0||A_1| + |A_1|^2)\,.
\end{aligned}$$

The wave shape has the form

$$\phi(\xi) = \phi_{\text{ns}}(\xi;\tau) = A_0 + 2A_1\cos(\xi) + \mathcal{O}(|A_1|(|A_1| + |A_0| + |\alpha| + |\kappa|))\,. \tag{4.34}$$

Analogous to the smooth case, the leading order bifurcation occurs at the leading order stability boundary of zero state if and only if $A_0 = 0$. Upon dividing out A_1 in (4.33), the leading order bifurcation equation (4.33) at $A_0 = 0$ reduces to

$$0 = \alpha - 2b\kappa^2 - \frac{16Q\sqrt{b}}{3\pi H_0\sqrt{2d}}|A_1|\,. \tag{4.35}$$

Since the coefficient of the term $A_1|A_1|$ in (4.33) is negative and the zero state is unstable for $\alpha > 2b\kappa^2$, the bifurcation is always a degenerate supercritical pitchfork. The 'degenerate' means the bifurcating branch behaves linearly in α near zero rather than in the usual square root form for the smooth case, cf. Figure 4.4(a).

In contrast to the smooth case in Theorem 4.2, the coefficient of $|A_1|$ in (4.35) is independent of the parameter $\tilde{f}$. This implies that the balance between linear bottom drag C and Coriolis force f is invisible at leading order, and thus the 'vertical branch' does not occur for any $\tilde{f}$.

From the leading order amplitude at $A_0 = 0$, namely

$$|A_1| = \frac{3\pi H_0\sqrt{2d}}{16Q\sqrt{b}}\left(\alpha - 2b\kappa^2\right)\,,$$

derived from (4.33) or (4.35), we readily see that it behaves parabolic in κ, cf. Figure 4.4(b). The parameter Q of the non-smooth bottom drag enters through only a prefactor so that the value of amplitude is monotonically decreasing in Q. In contrast to the smooth case, for small hyperdiffusion and backscatter parameter $(d, b) = (\varepsilon\hat{d}, \varepsilon\hat{b})$ as $\varepsilon \to 0$, the amplitude is always finite, thus the 'vertical branch' does not occur.

Remark 4.3.1. For $Q \to 0$ in (4.33) the quadratic term in $|A_1|$ goes to zero and the remainder term limits to $\mathcal{R}_{\text{ns}} = \tilde{f}\mathcal{R}_2 + \mathcal{O}(|\kappa|^3)$. Compared with the bifurcation equation (4.30) for $Q = 0$ there may be additional terms of order $\tilde{f}\mathcal{O}(|A_1|(|A_0| + |\alpha| + |\kappa|))$. We expect that it can be shown with a refined analysis that such terms do not occur, which would prove that the bifurcation equation (4.33) is continuous with respect to Q at $Q = 0$.

Remark 4.3.2. For $f = 0$ we consider the evolution equation (4.7), which provides temporal dynamics and therefore we are able to determine stability of bifurcating steady solutions. Due to above proof of supercriticality, these are stable under perturbations of the same form (4.21) and with the same wave vector. For $f \neq 0$ one has to transform the system of equations (4.6) into an evolution equation first, which yields an integro-differential equation. However, its stability analysis is beyond the scope of this paper.

In the remainder of the present subsection we give a proof of Theorem 4.3. In contrast to the smooth case in Section 4.3.1, we need to estimate the function W of the decomposition $\phi = u + W(u, \tau)$ instead of expanding it, since G does not have enough smoothness in ϕ. Since W inherits the differentiability of G by the implicit function theorem, we can approximate near the zero state via

$$W(u, \tau) = \partial_u W(0, 0)u + \partial_\alpha W(0, 0)\alpha + \partial_\kappa W(0, 0)\kappa + o(\|u\|_{H^5} + |\tau|)\,.$$

Since W solves (4.25), it follows from differentiation that the first derivatives of W are zero, which means $W = o(\|u\|_{H^5} + |\alpha| + |\kappa|)$. Indeed, we even obtain the approximation

$$W(u, \tau) = \mathcal{O}(\|u\|_{H^5}(\|u\|_{H^5} + |\tau|))\,, \tag{4.36}$$

which is shown in Appendix C. We refine this estimate even further in the following lemma.

Lemma 4.4. *The function W can be written as*

$$W(A_1, A_0, \alpha, \kappa) = h(A_1, A_0, \alpha, \kappa) \cdot A_1\,,$$

with a continuous function $h = \mathcal{O}(|A_1| + |A_0| + |\alpha| + |\kappa|)$.

Proof. We know that (4.23) is satisfied for $\phi \equiv const$ and any parameter α, κ, Q. Due to the implicit function theorem and the uniqueness of $W(A_1, A_0, \alpha, \kappa)$ this means, that $W(0, A_0, \alpha, \kappa) \equiv 0$ for any parameter A_0, α, κ. Since G from (4.23) is continuously differentiable in ϕ, it follows that W is continuously differentiable in A_1 (from implicit function theorem). Due to that it follows from the mean value theorem, that for any A_1, A_0, α, κ there is an $\widetilde{A}_1 = \widetilde{A}_1(A_1, A_0, \alpha, \kappa) \in [0, A_1]$, so that

$$\partial_{A_1} W(\widetilde{A}_1, A_0, \alpha, \kappa) = \frac{W(A_1, A_0, \alpha, \kappa) - W(0, A_0, \alpha, \kappa)}{A_1 - 0} = \frac{W(A_1, A_0, \alpha, \kappa)}{A_1}\,,$$

which means we can express W as

$$W(A_1, A_0, \alpha, \kappa) = \partial_{A_1} W(\widetilde{A}_1, A_0, \alpha, \kappa) \cdot A_1\,.$$

The function $h(A_1, A_0, \alpha, \kappa) := \partial_{A_1} W(\widetilde{A}_1, A_0, \alpha, \kappa)$ is continuous in A_1, A_0, α, κ, since $\partial_{A_1} W$ and $\widetilde{A}_1$ are continuous. Due to $W(u, \tau) = \mathcal{O}((\|u\|_{H^5} + |\tau|)\|u\|_{H^5})$ as in (4.36), we also obtain the estimate of h as in the statement. □

Remark 4.4.1. We can also approximate the values of u and W by the Sobolev embedding theorem. Since we consider $u, W \in H^5(0, 2\pi)$, it follows by the Sobolev embedding theorem that $u, W \in C^{4,1/2}([0, 2\pi], \mathbb{R})$. In addition, there is a constant $a > 0$ so that $\|v\|_{C^{4,1/2}} \leq a\|v\|_{H^5}$ for all $v \in H^5$.

Proof of Theorem 4.3. The wave shape (4.34) follows directly from the decomposition $\phi = u + W$, the estimate of W from Lemma 4.4 and the form of u in (4.29). With the given approximations above we can estimate the smooth and non-smooth nonlinear parts in the projection (4.28).

We first consider $j = 0$. As noted we make the splitting $\phi = u + w$, where $\phi \in H^5_{per}$ and u from (4.29) is even in ξ. As proved in the beginning of Section 4.3, by the implicit function theorem there exists a unique function W with values in M_0 such that $w = W(u, \tau)$ solves the projected problem (4.25) near zero. We prove in Appendix D that in the space of even function in H^5_{per}, i.e. for even $\phi \in H^5_{per}$, such a function W is even in ξ. Combining these we conclude that the solution $\phi = u + W$ to the steady state equation (4.23) is always even. The operators L_τ, N_C, N_Q from (4.27) map even functions to odd functions, thus for any even and 2π-periodic function ϕ the functions $L_\tau\phi$, $N_C(\phi)$, $N_Q(\phi)$ have zero mean on any interval of length 2π. It follows that for such ϕ the right-hand side of (4.28) vanishes for $j = 0$, i.e.

$$\langle G(\phi, \tau), e_0\rangle \equiv 0\,.$$

We now consider $j = 1$. For $j = -1$ we get the same result due to the parameter choice $A_1 = A_{-1} \in \mathbb{R}$. Defining $\mathcal{R}_W := \mathcal{O}(|A_1|(|A_1| + |A_0| + |\alpha| + |\kappa|))$ we approximate the absolute value with Remark 4.4.1 and Lemma 4.4

$$\big||u_\xi + W_\xi| - |u_\xi|\big| \leq |u_\xi + W_\xi - u_\xi| \leq a\|W\|_{H^5} = \mathcal{R}_W\,,$$

which in particular means $|u_\xi + W_\xi| = |u_\xi| + \mathcal{R}_W$. This gives

$$|u_\xi + W_\xi|(u_\xi + W_\xi) = |u_\xi|u_\xi + |u_\xi|W_\xi + (u_\xi + W_\xi)\mathcal{R}_W\,.$$

Thus, the leading order part in $\langle N_Q, e_1\rangle$ can be approximated by

$$\langle|\phi_\xi|\phi_\xi, e_1\rangle = \langle|u_\xi|u_\xi, e_1\rangle + \langle|u_\xi|W_\xi + (u_\xi + W_\xi)\mathcal{R}_W, e_1\rangle = \frac{16\mathrm{i}}{3\pi}|A_1|A_1 + A_1\mathcal{R}_W\,,$$

where we used the form of u_ξ given in (4.29). Note that the coefficient $\frac{16}{3\pi}\mathrm{i}$ results from the nature of the absolute value and reflects the non-smooth nature, similar to Steinherr Zazo and Rademacher (2020). The higher order parts of $\langle N_Q, e_1\rangle$ are

$$\langle|\phi_\xi|\phi_\xi(\tilde{f}\phi - \frac{\tilde{f}^2\phi^2}{H_0} + \tilde{f}^3\mathcal{O}(|\phi|^3)), e_1\rangle = \tilde{f}A_1\mathcal{O}(|A_0||A_1| + |A_1|^2)\,.$$

The smooth nonlinear term $\langle N_C, e_1\rangle$ can be estimated by

$$\langle(\tilde{f}\phi - \frac{\tilde{f}^2\phi^2}{H_0} + \tilde{f}^3\mathcal{O}(|\phi|^3))\phi_\xi, e_1\rangle = \mathrm{i}\tilde{f}A_0A_1 + \tilde{f}A_1\left(\mathcal{R}_W + \tilde{f}\mathcal{O}(|A_0|^2)\right).$$

Analogous to the proof of Theorem 4.2 we have $\langle\phi_\xi, e_1\rangle = \langle\partial_\xi^5\phi, e_1\rangle = \mathrm{i}A_1$ as well as $\langle\partial_\xi^3\phi, e_1\rangle = -\mathrm{i}A_1$, which leads to the linear part as in (4.32). Combining all terms, (4.28) then becomes

$$\langle G(\phi,\tau), e_1\rangle = -\mathrm{i}A_1\left(\frac{C_\mathrm{c}\tilde{f}}{H_0^2}A_0 + \alpha - 2b\kappa^2 - \frac{16Qk_\mathrm{c}}{3\pi H_0}|A_1| + \mathcal{R}_\mathrm{ns}\right),$$

where $\mathcal{R}_\mathrm{ns} = Q\mathcal{R}_W + \tilde{f}\mathcal{R}_2 + Q\tilde{f}\mathcal{R}_3 + \mathcal{O}(|\kappa|^3)$ with $\mathcal{R}_2 = \mathcal{R}_W + \mathcal{O}(|A_0||\alpha|) + \tilde{f}\mathcal{O}(|A_0|^2)$, $\mathcal{R}_3 = \mathcal{O}(|A_0||A_1| + |A_1|^2)$. Substituting the values (4.13) and (4.14) and dividing out the factor $-\mathrm{i}$, it follows the bifurcation equation (4.33). □

4.4. Bifurcation of nonlinear inertia-gravity waves

In this section we consider one-dimensional bifurcations due to the purely imaginary spectrum in the case of marginal stability for isotropic hyperdiffusion and backscatter. We focus entirely on the non-smooth case $Q \neq 0$, which gives non-standard bifurcation equations and is more subtle than that in Section 4.3.2.

We recall from Section 4.2 that in the isotropic case pattern forming stationary and oscillatory modes destabilize simultaneously.

To set up Lyapunov–Schmidt reduction, we consider the preparation (4.20) started with the problem (4.1), but with deviations κ from the critical wave number k_c and s from the critical wave speed $-\omega_\mathrm{c}$. This means, we choose a critical wave vector $\boldsymbol{k}_\mathrm{c} = (k_x', k_y')^\intercal$ satisfying (4.14), consider the phase (4.19) of the traveling wave solutions and change variables to $\chi, \tilde{\chi} \in \mathbb{R}$ via

$$\boldsymbol{x} = \left((1+\kappa)^{-1}\chi + st\right)/|\boldsymbol{k}_\mathrm{c}|^2\,\boldsymbol{k}_\mathrm{c} + \tilde{\chi}\boldsymbol{k}_\mathrm{c}^\perp\,, \tag{4.37}$$

seeking solutions that are independent of $\tilde{\chi}$. Then, with $\boldsymbol{U} = (\boldsymbol{v}, \eta)^\intercal$ and parameters $\tau = (\alpha, s, \kappa)$, the existence of such travelling waves of (4.1) near the critical modes of (4.20) can be cast in the form

$$G(\boldsymbol{U};\tau) = \mathcal{L}_\tau\boldsymbol{U} - \mathcal{B}(\boldsymbol{U};\tau) - B_Q(\boldsymbol{U}) - N(\boldsymbol{U};\tau) = 0\,, \tag{4.38}$$

with suitable linear $\mathcal{L}_\tau$ and nonlinear $\mathcal{B}$, B_Q, N as defined in the following. The term $\mathcal{B}(\boldsymbol{U};\tau)$ will contain all smooth quadratic terms with respect to $\boldsymbol{U}$, $N(\boldsymbol{U};\tau) = \mathcal{O}(|\boldsymbol{U}|^3)$ the higher order terms, and

$$B_Q(\boldsymbol{U}) = \begin{pmatrix} \frac{Q}{H_0}|\boldsymbol{v}|\boldsymbol{v} \\ 0 \end{pmatrix}$$

is the quadratic non-smooth term. The linear part $\mathcal{L}_\tau$ at $\alpha = s = 0$ is given by $\mathcal{L}_\mathrm{c}$ from (4.20) with ∂_ζ replaced by $(1+\kappa)\partial_\chi$, i.e. $\mathcal{L}_\mathrm{c}$ depends on κ. We split $\mathcal{L}_\tau$ into α-, s- and

κ-dependent parts

$$\mathcal{L}_\tau := \mathcal{L}_\mathrm{c}(\kappa) + \alpha \begin{pmatrix} 1 & 0 & 0 \\ 0 & 1 & 0 \\ 0 & 0 & 0 \end{pmatrix} - (1+\kappa)s \begin{pmatrix} 1 & 0 & 0 \\ 0 & 1 & 0 \\ 0 & 0 & 1 \end{pmatrix} \partial_\chi \,. \tag{4.39}$$

The linear operator $\mathcal{L}_\mathrm{c}(\kappa)$ is then given by

$$\mathcal{L}_\mathrm{c}(\kappa) := \mathcal{L}_\mathrm{c} + \kappa\mathcal{K}\,, \tag{4.40}$$

$$\mathcal{K} := \begin{pmatrix} \omega_\mathrm{c}\partial_\chi - dk_\mathrm{c}^4\mathcal{S} & 0 & -k_x' g\partial_\chi \\ 0 & \omega_\mathrm{c}\partial_\chi - dk_\mathrm{c}^4\mathcal{S} & -k_y' g\partial_\chi \\ -k_x' H_0\partial_\chi & -k_y' H_0\partial_\chi & \omega_\mathrm{c}\partial_\chi \end{pmatrix},$$

$$\mathcal{S} := (2+\kappa)\left(\kappa(2+\kappa)\partial_\chi^2 + 2(\partial_\chi^2+1)\right)\partial_\chi^2\,,$$

where $\mathcal{L}_\mathrm{c}$ is the operator (4.20) with ∂_ζ replaced by ∂_χ. Note that $\mathcal{L}_\mathrm{c}(0) = \mathcal{L}_\mathrm{c}$. We consider $G : X \times \mathbb{R}^3 \to Y$ with $X := H^4_{\mathrm{per}}([0,2\pi]) \times H^4_{\mathrm{per}}([0,2\pi]) \times H^1_{\mathrm{per}}([0,2\pi])$ and $Y := (L^2([0,2\pi]))^3$. Due to Lemma 4.1 G from (4.38) is then continuously differentiable. The following lemma admits to apply Lyapunov–Schmidt reduction in order to solve (4.38) near $(\boldsymbol{U},\tau)^\intercal = (0,0)^\intercal$.

Lemma 4.5. *For $\tau = 0$ the linear operator $\mathcal{L}_\tau = \mathcal{L}_\mathrm{c} : X \to Y$, defined in (4.39) and (4.20), is a Fredholm operator with index zero. Its generalized kernel and that of its adjoint are three-dimensional.*

Proof. We will show that for $\tau = 0$ the operator $\mathcal{L}_\tau = \mathcal{L}_\mathrm{c}(0) = \mathcal{L}_\mathrm{c}$ is a compact perturbation of a Fredholm operator. To see this, let us define the following diagonal operator and matrix Nemitsky operators:

$$D : X \to Y\,, \qquad D := \begin{pmatrix} \widetilde{D}(k_x') & 0 & 0 \\ 0 & \widetilde{D}(k_y') & 0 \\ 0 & 0 & \omega_\mathrm{c}\partial_\chi \end{pmatrix},$$

$$\text{with} \quad \widetilde{D}(k) := (\omega_\mathrm{c} - gH_0k^2/\omega_\mathrm{c})\partial_\chi - dk_\mathrm{c}^4(\partial_\chi^2+1)^2\,,$$

$$R : Y \to Y\,, \qquad R := \begin{pmatrix} 1 & 0 & -k_x' g/\omega_\mathrm{c} \\ 0 & 1 & -k_y' g/\omega_\mathrm{c} \\ 0 & 0 & 1 \end{pmatrix},$$

$$S : X \to X\,, \qquad S := \begin{pmatrix} 1 & 0 & 0 \\ 0 & 1 & 0 \\ -k'_x H_0/\omega_\mathrm{c} & -k'_y H_0/\omega_\mathrm{c} & 1 \end{pmatrix}.$$

Each of the diagonal elements in D is a Fredholm operator, which implies D is. The matrix R is invertible and since on Y all components come from the same space, then R is also boundedly invertible. For the operator $S : X \to X$ the same argument applies to the upper left block since the first two components of X are the same. The entire operator S is well defined since the last row maps into $H^1([0, 2\pi])$ due to the inclusion $H^4([0, 2\pi]) \subset H^1([0, 2\pi])$. Using the inverse matrix, which is of the same form, this also implies that S is boundedly invertible.

The product $\check{\mathcal{L}}_\mathrm{c} := RDS$ of boundedly invertible and Fredholm operators is a Fredholm operator and takes the form

$$\check{\mathcal{L}}_\mathrm{c} = \begin{pmatrix} \omega_\mathrm{c}\partial_\chi - dk_\mathrm{c}^4(\partial_\chi^2+1)^2 & \frac{gH_0k'_xk'_y}{\omega_\mathrm{c}}\partial_\chi & -k'_x g\partial_\chi \\ \frac{gH_0k'_xk'_y}{\omega_\mathrm{c}}\partial_\chi & \omega_\mathrm{c}\partial_\chi - dk_\mathrm{c}^4(\partial_\chi^2+1)^2 & -k'_y g\partial_\chi \\ -k'_x H_0\partial_\chi & -k'_y H_0\partial_\chi & \omega_\mathrm{c}\partial_\chi \end{pmatrix}.$$

The difference to $\mathcal{L}_\mathrm{c}$ reads

$$\check{\mathcal{L}}_\mathrm{c} - \mathcal{L}_\mathrm{c} = \begin{pmatrix} 0 & \frac{gH_0k'_xk'_y}{\omega_\mathrm{c}}\partial_\chi - f & 0 \\ f + \frac{gH_0k'_xk'_y}{\omega_\mathrm{c}}\partial_\chi & 0 & 0 \\ 0 & 0 & 0 \end{pmatrix},$$

which is a compact perturbation of $\mathcal{L}_\mathrm{c}$ since the range of $\check{\mathcal{L}}_\mathrm{c} - \mathcal{L}_\mathrm{c}$ lies in the compact subset $H^3([0, 2\pi]) \times H^3([0, 2\pi]) \times \{0\}$ of Y. Hence, the unperturbed operator $\mathcal{L}_\mathrm{c}$ shares the Fredholm property of $\check{\mathcal{L}}_\mathrm{c}$. The index is zero since its kernel and the kernel of its adjoint have the same dimension.

The kernel of the adjoint operator $\mathcal{L}_\mathrm{c}^*$ to (4.20) is spanned by $\boldsymbol{e}_0^* = \boldsymbol{e}_0$ and $\boldsymbol{e}_1^*$, $\boldsymbol{e}_{-1}^*$ of the form $\boldsymbol{e}_j^* := \boldsymbol{E}_j^* \mathrm{e}^{\mathrm{i}j\chi}$ with $\boldsymbol{E}_j^* \in \mathbb{C}^3$. We recall the eigenvectors $\boldsymbol{e}_j = \boldsymbol{E}_j \mathrm{e}^{\mathrm{i}j\chi}$ of $\mathcal{L}_\mathrm{c}$ and choose $\boldsymbol{E}_j^*$ as

$$\boldsymbol{E}_j = \begin{pmatrix} \omega_\mathrm{c}k'_x + j\mathrm{i}fk'_y \\ \omega_\mathrm{c}k'_y - j\mathrm{i}fk'_x \\ k_\mathrm{c}^2 H_0 \end{pmatrix}, \quad \boldsymbol{E}_j^* = \frac{1}{m}\begin{pmatrix} \omega_\mathrm{c}k'_x + j\mathrm{i}fk'_y \\ \omega_\mathrm{c}k'_y - j\mathrm{i}fk'_x \\ k_\mathrm{c}^2 g \end{pmatrix}, \tag{4.41}$$

with $m = 2\omega_\mathrm{c}^2 k_\mathrm{c}^2$, so that $\langle \boldsymbol{E}_j, \boldsymbol{E}_j^* \rangle = 1$ for $j = 0, -1, 1$.

Consider the dispersion relation (4.18) expressed via (4.10). At the critical bottom drag and wave number the constant coefficient a_0 with respect to the eigenvalue parameter λ vanishes, and the linear coefficient a_1 is $-2\omega_\mathrm{c}^2$. This is non-zero so that there is no double root and thus no generalized eigenfunction for $\mathcal{L}_\mathrm{c}$ and its adjoint. □

Remark 4.5.1. The lemma also holds for $\mathcal{L}_\tau$ with perturbations of τ from zero. In order to prove this, one shows that $\mathcal{L}_c(\kappa)$ is a Fredholm operator by replacing $(1+\kappa)\partial_\chi$ by ∂_ζ, so that one obtains again the linear operator $\mathcal{L}_c$ from (4.20) and proceeds exactly in the same way as in the proof of Lemma 4.5. The other terms of $\mathcal{L}_\tau$ in (4.39) give a Fredholm or are a compact operator and form an order τ perturbation, which does not change the index for $|\tau| \ll 1$.

Due to Lemma 4.5 we can split the domain and range analogous to Section 4.3 as $X = \ker(\mathcal{L}_c) \oplus \mathcal{M}$ and $Y = \ker(\mathcal{L}_c^*) \oplus \operatorname{range}(\mathcal{L}_c)$, where $\operatorname{range}(\mathcal{L}_c)^\perp = \ker(\mathcal{L}_c^*)$ with respect to the inner product $\langle \boldsymbol{U}, \boldsymbol{V}\rangle_Y = \frac{1}{2\pi}\int_0^{2\pi}\langle \boldsymbol{U}(\chi), \boldsymbol{V}(\chi)\rangle_{\mathbb{C}^3} \mathrm{d}\chi$ and the kernel of the adjoint operator $\ker(\mathcal{L}_c^*) = \operatorname{span}\{\boldsymbol{e}_j^* \mid j = 0, \pm 1\}$ as in the proof of Lemma 4.5. With the inner product for $\boldsymbol{U}$, $\boldsymbol{V} \in X$ given by $\langle \boldsymbol{U}, \boldsymbol{V}\rangle_X = \langle U_1, V_1\rangle_{H^4} + \langle U_2, V_2\rangle_{H^4} + \langle U_3, V_3\rangle_{H^1}$, we split $\boldsymbol{U} = u + w$ with $u \in \ker(\mathcal{L}_c)$ and $w \in \mathcal{M}$ by the projection $\tilde{P} : X \to \ker(\mathcal{L}_c)$, which can be written as

$$u = \tilde{P}\boldsymbol{U} := \sum_{j=-1}^{1} \langle \boldsymbol{U}, \boldsymbol{e}_j^*\rangle_X \boldsymbol{e}_j \,.$$

The projection $P : Y \to \operatorname{range}(\mathcal{L}_c)$ along $\ker(\mathcal{L}_c^*)$ can be written as

$$P := \mathrm{Id} - \sum_{j=-1}^{1} \langle \cdot, \boldsymbol{e}_j^*\rangle_Y \boldsymbol{e}_j \,,$$

which gives the reduced problem of (4.38)

$$PG(u + w; \tau) = 0 \,. \tag{4.42}$$

As in Section 4.3, by the implicit function theorem there is an open neighbourhood of $(0,0,0)$ in $\ker(\mathcal{L}_c) \times \mathcal{M} \times \mathbb{R}^3$ of the form $N_0 \times M_0 \times (-\varepsilon, \varepsilon)^3$ and a unique function $W : N_0 \times (-\varepsilon, \varepsilon)^3 \to M_0$, such that $W(0,0) = 0$ and $w = W(u;\tau)$ solves (4.42) for all $(u, \tau) \in N_0 \times (-\varepsilon, \varepsilon)^3$. We will make use of the following estimate, which holds for possibly smaller ε and N_0:

$$W(u;\tau) = \mathcal{O}(\|u\|_X(\|u\|_X + |\tau|)) \,. \tag{4.43}$$

While this is in some sense standard, we give the proof in Appendix C.

In order to solve (4.38) it remains to determine $(u, \tau) \in N_0 \times (-\varepsilon, \varepsilon)^3$ such that

$$(\mathrm{Id} - P)G(u + W(u,\tau);\tau) = 0 \,,$$

which is equivalent to the bifurcation equations

$$\langle G(u + W(u;\tau);\tau), \boldsymbol{e}_j^*\rangle_Y = 0 \,, \quad j = 0, \pm 1 \,. \tag{4.44}$$

The next theorem gives the bifurcation near $\tau = (\alpha, s, \kappa) = 0$. We recall the choice of parameters $C = C_c - \alpha H_0$ with critical bottom drag C_c as in (4.13), the critical wave

length k_c as in (4.14) and the critical wave speed ω_c as in (4.15).

Theorem 4.6 (Bifurcation of inertia-gravity waves for $Q \neq 0$)**.** *Let $Q \neq 0$ and $\alpha, \kappa \in \mathbb{R}$ sufficiently close to zero, as well as $\boldsymbol{k}_c = (k_x', k_y')^\intercal$ arbitrary with $|\boldsymbol{k}_c| = k_c$. Consider 2π-periodic steady traveling wave-type solutions $(\boldsymbol{v}, \eta)^\intercal$ of (4.1) with the phase variable $\zeta = (1+\kappa)^{-1}\chi - (\omega_c - s)t$. These waves are (up to spatial translations) in one-to-one correspondence with solutions s, A_0, A_1 near zero of*

$$0 = A_1 \left(-s + \kappa \frac{f^2}{\omega_c} - \frac{g k_c^2}{2\omega_c} A_0 + \mathcal{R}_{gw} \right) , \tag{4.45a}$$

$$0 = A_1 \left(\alpha + \frac{C_c}{H_0^2} A_0 - \frac{2Q k_c}{H_0} \left(I_1 + \frac{k_c^2 g H_0}{2f^2 + k_c^2 g H_0} I_2 \right) |A_1| + \mathcal{R}_{gw} \right) , \tag{4.45b}$$

with remainder term $\mathcal{R}_{gw} = \mathcal{O}(|A_0|^2 + |A_1|^2 + |\tau|^2)$ and positive quantities

$$I_1 = \frac{1}{2\pi} \int_0^{2\pi} \sqrt{f^2 + k_c^2 g H_0 \cos(\chi)^2} \mathrm{d}\chi \, , \tag{4.46a}$$

$$I_2 = \frac{1}{2\pi} \int_0^{2\pi} \sqrt{f^2 + k_c^2 g H_0 \cos(\chi)^2} \cos(2\chi) \mathrm{d}\chi \, . \tag{4.46b}$$

With $\boldsymbol{x}$ as in (4.37) and remainder term $\mathcal{R}_W = \mathcal{O}(|A_1|(|A_0| + |A_1| + |\tau|))$, these waves have the form

$$\begin{pmatrix} \boldsymbol{v} \\ \eta \end{pmatrix} (t, \boldsymbol{x}) = A_0 \begin{pmatrix} 0 \\ 0 \\ 1 \end{pmatrix} + 2A_1 \begin{pmatrix} \omega_c k_x' \cos\zeta - f k_y' \sin\zeta \\ \omega_c k_y' \cos\zeta + f k_x' \sin\zeta \\ k_c^2 H_0 \cos\zeta \end{pmatrix} + \mathcal{R}_W \, . \tag{4.47}$$

Note that (4.45a) specifies the deviation through s from the traveling wave velocity and (4.45b) the amplitude $|A_1|$. Since the coefficient of $A_1|A_1|$ in (4.45b) is negative and the zero state is unstable for $\alpha > 0$ and $A_0 = 0$, the bifurcation is always supercritical in the form of a degenerate pitchfork. The parameter A_0 modifies the mean so that it should be fixed at zero when considering that η has zero mean. In contrast to the bifurcation of Rossby waves, linear term in κ appears and balances the deviation s in (4.45a). The quadratic term in κ enters (4.45b) through the remainder term $\mathcal{R}_{gw}$. Nevertheless, it suffices to get supercritical bifurcation for sufficiently small κ.

Proof of Theorem 4.6. We derive the bifurcation equations (4.45) from (4.44). For $j = 0$ the equation is trivial, since $\boldsymbol{e}_0^* = (0, 0, 1)^\intercal$ and with $\boldsymbol{U} = (\boldsymbol{v}, \eta)^\intercal$ the third component of G can be written as the derivative

$$G_3(\boldsymbol{U}; \tau) = -\partial_\chi (1+\kappa)(\boldsymbol{k}_c \cdot \boldsymbol{v})(H_0 + \eta) - (s - \omega_c)(1+\kappa)\partial_\chi \eta \, ,$$

whose integral vanishes on the space of periodic functions.

Next we consider $j = \pm 1$. Since the range of $\mathcal{L}_c$ is orthogonal to the kernel of $\mathcal{L}_c^*$, the linear part (4.39) of G can be replaced by

$$L_\tau := \mathcal{L}_\tau - \mathcal{L}_c = \mathcal{O}(|\tau|)\,.$$

With (4.38) the non-trivial bifurcation equations (4.44) can be written as

$$\langle L_\tau u, \boldsymbol{e}_j^* \rangle_Y - \langle \mathcal{B}(u;\tau), \boldsymbol{e}_j^* \rangle_Y - \langle B_Q(u), \boldsymbol{e}_j^* \rangle_Y = \mathcal{R}_j\,, \quad j = \pm 1\,, \tag{4.48}$$

where $\mathcal{R}_j$ is a remainder term, which includes $L_\tau W = \mathcal{O}(|\tau|\|W\|_X)$ and

$$\mathcal{B}(u+W;\tau) - \mathcal{B}(u;\tau) = \mathcal{O}(\|W\|_X(\|u\|_X + \|W\|_X))\,,$$

as well as $B_Q(u+W) - B_Q(u) = (\|W\|_X(\|u\|_X + \|W\|_X))$. The latter follows from the reverse triangle inequality for the euclidean norm of $\boldsymbol{v}$ within B_Q, and we then obtain

$$\mathcal{R}_j = \mathcal{O}(\|W\|_X(\|u\|_X + \|W\|_X + |\tau|))\,.$$

Next, we derive the leading order part in (4.48). Analogous to Section 4.3, u in (4.48) can be written in terms of the amplitudes $A_j \in \mathbb{C}$ with $j = -1, 0, 1$ for the kernel modes $\boldsymbol{e}_j$ of $\mathcal{L}_c$ as

$$u = A_0\boldsymbol{e}_0 + A_1\boldsymbol{e}_1 + A_{-1}\boldsymbol{e}_{-1}\,.$$

Here $A_{-1} = \overline{A_1}$, and since $\boldsymbol{e}_0 = (0,0,1)^\intercal$ is real we have $A_0 \in \mathbb{R}$. The modes $\boldsymbol{e}_1$, $\boldsymbol{e}_{-1}$ are given in (4.41). As in Section 4.3, by translation symmetry we can assume that $A_1 = A_{-1} \in \mathbb{R}$. Hence, since (4.48) for $j = 1$ is the complex conjugate of $j = -1$ it suffices to consider $j = 1$. Also, due to (4.43) and exactly as in Lemma 4.4 in Section 4.3.2, the line of equilibria with constant η and $\boldsymbol{v} = 0$ implies that $W = \mathcal{O}(|A_1|(|A_0| + |A_1| + |\tau|))$. Hence,

$$\mathcal{R}_1 = \mathcal{O}(|A_1|(|A_0|^2 + |A_1|^2 + |\tau|^2))\,. \tag{4.49}$$

We also write $u = (\tilde{\boldsymbol{v}}, \tilde{\eta})^\intercal$ in the following so that

$$\tilde{\boldsymbol{v}} = A_1 \begin{pmatrix} \omega_c k_x' + \mathrm{i} f k_y' \\ \omega_c k_y' - \mathrm{i} f k_x' \end{pmatrix} \mathrm{e}^{\mathrm{i}\chi} + A_1 \begin{pmatrix} \omega_c k_x' - \mathrm{i} f k_y' \\ \omega_c k_y' + \mathrm{i} f k_x' \end{pmatrix} \mathrm{e}^{-\mathrm{i}\chi}\,,$$

$$\tilde{\eta} = A_0 + A_1 k_c^2 H_0 (\mathrm{e}^{\mathrm{i}\chi} + \mathrm{e}^{-\mathrm{i}\chi})\,.$$

This corresponds to the solutions (4.47) after the transformation of the phase variable, since $(\boldsymbol{v}, \eta)^\intercal = u + W$.

We first consider the term involving the smooth quadratic terms of (4.1) given by

$$\mathcal{B}(u;\tau) = (1+\kappa)(\tilde{\boldsymbol{v}} \cdot \boldsymbol{k}_c) \begin{pmatrix} \partial_\chi \tilde{\boldsymbol{v}} \\ \partial_\chi \tilde{\eta} \end{pmatrix} + (1+\kappa) \begin{pmatrix} 0 \\ \tilde{\eta}\, \boldsymbol{k}_c \cdot \partial_\chi \tilde{\boldsymbol{v}} \end{pmatrix} - \frac{C_c - \alpha H_0}{H_0^2} \begin{pmatrix} \tilde{\eta}\tilde{\boldsymbol{v}} \\ 0 \end{pmatrix}\,.$$

Here ∇ from (4.1) is replaced by $(1+\kappa)\boldsymbol{k}_{\mathrm{c}}\partial_\chi$ due to the choice of variables. It is straightforward that the first term $(\tilde{\boldsymbol{v}}\cdot\boldsymbol{k}_{\mathrm{c}})(\partial_\chi\tilde{\boldsymbol{v}},\partial_\chi\tilde{\eta})^{\intercal}$ is orthogonal to the kernel of $\mathcal{L}_{\mathrm{c}}^*$ and thus does not enter into (4.48). For the second term we compute and obtain $\boldsymbol{k}_{\mathrm{c}}\cdot\partial_\chi\tilde{\boldsymbol{v}} = \mathrm{i}A_1\omega_{\mathrm{c}}k_{\mathrm{c}}^2(\mathrm{e}^{\mathrm{i}\chi}-\mathrm{e}^{-\mathrm{i}\chi})$, and further

$$\langle\begin{pmatrix}0\\ \tilde{\eta}\,\boldsymbol{k}_{\mathrm{c}}\cdot\partial_\chi\tilde{\boldsymbol{v}}\end{pmatrix},\boldsymbol{e}_1^*\rangle_Y = \mathrm{i}A_0A_1\omega_{\mathrm{c}}k_{\mathrm{c}}^2\overline{\boldsymbol{E}_{1,3}^*} = \mathrm{i}\frac{\omega_{\mathrm{c}}g}{m}k_{\mathrm{c}}^4A_0A_1\,,$$

where $\boldsymbol{E}_{1,3}^*$ is the third component of $\boldsymbol{E}_1^*$. As to the third term, we compute

$$\langle\begin{pmatrix}\tilde{\eta}\tilde{\boldsymbol{v}}\\ 0\end{pmatrix},\boldsymbol{e}_1^*\rangle_Y = A_0\langle\begin{pmatrix}\tilde{\boldsymbol{v}}\\ 0\end{pmatrix},\boldsymbol{e}_1^*\rangle_Y = A_0A_1\frac{\omega_{\mathrm{c}}^2+f^2}{m}k_{\mathrm{c}}^2\,, \tag{4.50}$$

and thus obtain

$$\langle\mathcal{B}(u;\tau),\boldsymbol{e}_1^*\rangle_Y = \mathrm{i}\frac{\omega_{\mathrm{c}}g}{m}k_{\mathrm{c}}^4A_0A_1 - \frac{C_{\mathrm{c}}(\omega_{\mathrm{c}}^2+f^2)}{mH_0^2}k_{\mathrm{c}}^2A_0A_1 + \mathcal{O}(|\tau||A_0||A_1|)\,. \tag{4.51}$$

Next, we consider the term in (4.48), which involves the non-smooth quadratic term

$$\langle B_Q(u),\boldsymbol{e}_1^*\rangle_Y = \langle\begin{pmatrix}\frac{Q}{H_0}|\tilde{\boldsymbol{v}}|\tilde{\boldsymbol{v}}\\ 0\end{pmatrix},\boldsymbol{e}_1^*\rangle_Y\,,$$

where

$$|\tilde{\boldsymbol{v}}| = 2|A_1|k_{\mathrm{c}}\sqrt{\omega_{\mathrm{c}}^2\cos(\chi)^2+f^2\sin(\chi)^2} = 2|A_1|k_{\mathrm{c}}\sqrt{f^2+k_{\mathrm{c}}^2gH_0\cos(\chi)^2}\,.$$

We thus compute and obtain

$$\langle B_Q(u),\boldsymbol{e}_1^*\rangle_Y = \frac{2k_{\mathrm{c}}^3Q}{H_0m}|A_1|A_1((\omega_{\mathrm{c}}^2+f^2)I_1+(\omega_{\mathrm{c}}^2-f^2)I_2)\,, \tag{4.52}$$

where the decisive coefficients I_1, I_2 are characterized by the non-smooth nonlinearity as in (4.46)

$$I_1 := \frac{1}{2\pi}\int_0^{2\pi}\sqrt{f^2+k_{\mathrm{c}}^2gH_0\cos(\chi)^2}\mathrm{d}\chi\,, \tag{4.53}$$

$$I_2 := \frac{1}{2\pi}\int_0^{2\pi}\sqrt{f^2+k_{\mathrm{c}}^2gH_0\cos(\chi)^2}\cos(2\chi)\mathrm{d}\chi\,. \tag{4.54}$$

In contrast to the analogous integrals in Section 4.3.2, here we cannot find explicit expressions. However, for the qualitative result it suffices to determine the signs. Clearly,

$I_1 > 0$ and to show that $I_2 > 0$ we abbreviate $r(\chi) := \sqrt{f^2 + k_c^2 g H_0 \cos(\chi)^2}$ and compute

$$\begin{aligned}
\pi I_2 &= \sum_{j=0}^{3} \int_{j\pi/4}^{(j+1)\pi/4} r(\chi)\cos(2\chi)\mathrm{d}\chi \\
&= \int_0^{\pi/4} r(\chi)\cos(2\chi)\mathrm{d}\chi + \int_{\pi/2}^{3\pi/4} r(\chi)\cos(2\chi)\mathrm{d}\chi \\
&\quad + \int_{\pi/4}^{\pi/2} r(\chi)\cos(2\chi)\mathrm{d}\chi + \int_{3\pi/4}^{\pi} r(\chi)\cos(2\chi)\mathrm{d}\chi \\
&= \int_0^{\pi/4} \underbrace{\big(r(\chi) - r(\chi+\frac{\pi}{2})\big)}_{>0 \ (*)} \underbrace{\cos(2\chi)}_{>0}\,\mathrm{d}\chi + \int_{\pi/4}^{\pi/2} \underbrace{\big(r(\chi) - r(\chi+\frac{\pi}{2})\big)}_{<0 \ (**)} \underbrace{\cos(2\chi)}_{<0}\,\mathrm{d}\chi > 0\,,
\end{aligned}$$

where $(*)$ holds since $\cos(\chi)^2 > 1/2 > \cos(\chi+\pi/2)^2$ for $\chi \in [0, \pi/4)$, and $(**)$ holds since $\cos(\chi)^2 < 1/2 < \cos(\chi+\pi/2)^2$ for $\chi \in (\pi/4, \pi/2]$.

Concerning the linear part of (4.48), we first note that due to $\mathcal{L}_\tau$ in (4.39)

$$L_\tau = \alpha \begin{pmatrix} 1 & 0 & 0 \\ 0 & 1 & 0 \\ 0 & 0 & 0 \end{pmatrix} - (1+\kappa)s \begin{pmatrix} 1 & 0 & 0 \\ 0 & 1 & 0 \\ 0 & 0 & 1 \end{pmatrix} \partial_\chi + \kappa\,\mathcal{K}\,. \tag{4.55}$$

We next compute $\langle L_\tau u, \boldsymbol{e}_1^* \rangle_Y$. As in (4.50) we obtain

$$\langle \begin{pmatrix} 1 & 0 & 0 \\ 0 & 1 & 0 \\ 0 & 0 & 0 \end{pmatrix} u, \boldsymbol{e}_1^* \rangle_Y = \langle \begin{pmatrix} \tilde{\boldsymbol{v}} \\ 0 \end{pmatrix}, \boldsymbol{e}_1^* \rangle_Y = A_1 k_c^2 \frac{\omega_c^2 + f^2}{m}\,.$$

Further, for the comoving frame term with factor s we can use

$$\langle \partial_\chi u, \boldsymbol{e}_1^* \rangle_Y = \mathrm{i} A_1 \frac{2k_c^2 \omega_c^2}{m}\,. \tag{4.56}$$

Regarding $\mathcal{K}$ as in (4.40), we are only interested in the leading order terms and thus consider $\mathcal{K}|_{\kappa=0}$. Here $\mathcal{S}|_{\kappa=0}$ from (4.40) simplifies and for the projection onto $\boldsymbol{e}_1^*$ we note that $(\partial_\chi^2 + 1)\mathrm{e}^{\mathrm{i}j\chi} = 0$, so that the relevant diagonal part of $\mathcal{K}|_{\kappa=0}$ is $\omega_c \left(\begin{smallmatrix} 1 & 0 & 0 \\ 0 & 1 & 0 \\ 0 & 0 & 1 \end{smallmatrix}\right) \partial_\chi$, for which we can use (4.56). The remaining terms of the third column in $\mathcal{K}$ give

$$-g\langle (\boldsymbol{k}_c, 0)^\intercal \partial_\chi \tilde{\eta}, \boldsymbol{e}_1^* \rangle_Y = -\mathrm{i} A_1 g H_0 k_c^2 \langle (\boldsymbol{k}_c, 0)^\intercal, \boldsymbol{E}_1^* \rangle_Y = -\mathrm{i} A_1 g H_0 k_c^4 \frac{\omega_c}{m}\,,$$

which is the same as the term created by the third row, so it is doubled. Gathering terms we have

$$\langle L_\tau u, \boldsymbol{e}_1^* \rangle_Y = \Big(\alpha(\omega_c^2 + f^2) + 2\mathrm{i}(-s\omega_c + \kappa f^2)\omega_c\Big) \frac{k_c^2}{m} A_1 + \mathcal{O}(|\tau|^2 |A_1|)\,, \tag{4.57}$$

where we have used $\omega_c^2 - gH_0k_c^2 = f^2$. Concerning (4.48) we observe that the order of the remainder in (4.49) includes the error term in (4.57) and (4.51). Using the results (4.51), (4.52) and (4.57), then (4.48) becomes

$$\left(\alpha(\omega_c^2+f^2) + 2\mathrm{i}(-s\omega_c+\kappa f^2)\omega_c\right)\frac{k_c^2}{m}A_1 - \mathrm{i}\frac{\omega_c g}{m}k_c^4 A_0A_1 + \frac{C_c(\omega_c^2+f^2)}{mH_0^2}k_c^2A_0A_1$$

$$-\frac{2k_c^3Q}{H_0m}|A_1|A_1((\omega_c^2+f^2)I_1+(\omega_c^2-f^2)I_2) = \mathcal{O}(|A_1|(|A_0|^2+|A_1|^2+|\tau|^2))\,. \quad (4.58)$$

Upon defining the order of the remainder terms $\mathcal{R}_{gw} := \mathcal{O}(|A_0|^2+|A_1|^2+|\tau|^2)$ and dividing by k_c^2/m, (4.58) can be split into real and imaginary parts as

$$0 = A_1\left(2(-s\omega_c+\kappa f^2)\omega_c - \omega_c g k_c^2 A_0 + \mathcal{R}_{gw}\right)$$

$$0 = A_1\left(\alpha(\omega_c^2+f^2) + C_c\frac{\omega_c^2+f^2}{H_0^2}A_0 - \frac{2Qk_c}{H_0}|A_1|((\omega_c^2+f^2)I_1+(\omega_c^2-f^2)I_2) + \mathcal{R}_{gw}\right).$$

Using $\omega_c^2 - f^2 = k_c^2gH_0$ as well as $\omega_c^2+f^2 = 2f^2+k_c^2gH_0$ and rearranging terms, we obtain the bifurcation equations (4.45). □

Remark 4.6.1. The term A_0 in the bifurcation equation (4.33) from Theorem 4.3 has an additional factor $\tilde{f}$ compared with the same term in the bifurcation equation (4.45b). This is a result of the scaling of η by $\eta = \tilde{f}\phi(\boldsymbol{k}\cdot\boldsymbol{x})$ in the form of solutions (4.21) considered in Section 4.3. Since (4.33) is the bifurcation equation for ϕ, the constant perturbation of η in Theorem 4.3 is parameterized by $\tilde{f}A_0$, while in Theorem 4.6 it is A_0. Thus, the constant perturbation of η has the same factor in both bifurcation equations, which means Rossby waves and inertia-gravity waves emerge simultaneously in the isotropic case. This coincides with the simultaneous stationary and oscillatory instability for isotropic backscatter as shown in Section 4.2.1.

4.5. Explicit nonlinear flows with arbitrary amplitudes

Inspired by the results in Chapter 3, we are now interested in explicit flows in the presence of bottom drag. Such solutions can be found in (4.1) for smooth bottom drag, so we restrict to $Q = 0$ in this section. In contrast to the determined bifurcating solutions in Section 4.3.1, these have arbitrary amplitudes and can depend on time, where some of them even grow unboundedly in time. The certain linear behavior of such flows and the unbounded exponential growth are hints of possible issues in the simulations with backscatter and bottom drag, like undesired concentrations of energy in certain scales.

We are in particular looking for such steady flows. We will not only see, that some of the solutions discussed in this section are also some of those determined in Section 4.3.1, showing the consistency of both results. The corresponding solutions also exist for a larger set of parameters here, thus extending some results of our previous bifurcation

analysis. We will also briefly comment on the set of unboundedly growing explicit flows, but we will not discuss them in detail as in Chapter 3.

When restricting to the case $Q = 0$, we can find explicit flows of the plane wave form, which results from vanishing nonlinear advection terms in (4.1) due to Theorem 2.3,

$$\boldsymbol{v} = A\mathrm{e}^{\mu t}\cos(\boldsymbol{k}\cdot\boldsymbol{x}+\theta)\boldsymbol{k}^{\perp}\,, \qquad \eta = 0\,. \tag{4.59}$$

The restriction $\eta = 0$ is required due to the presence of η in the denominator of the bottom drag term (4.2). This is also a special case of the solutions (4.3). Substituting (4.59) into (4.1) gives the conditions for these explicit flows

$$\mu = (b_1 - d_1|\boldsymbol{k}|^2)k_y^2 + (b_2 - d_2|\boldsymbol{k}|^2)k_x^2 - C/H_0\,, \tag{4.60a}$$

$$0 = q(\boldsymbol{k}) := k_x k_y\Big((d_1 - d_2)|\boldsymbol{k}|^2 + b_2 - b_1\Big) + f\,. \tag{4.60b}$$

Since the conditions (4.60) are independent of A, each solution yields a 'vertical branch' of explicit flows (4.59), parameterized by $A \in \mathbb{R}$. In the steady case $\mu = 0$ this can be viewed as bifurcating from the trivial state for fixed parameters, cf. Figure 4.4(a) (dashed). The wave vectors $\boldsymbol{k}$, for which explicit flows of the form (4.59) exist, lie on a union of curves determined by the condition (4.60b). Their growth rates $\mu = \mu(\boldsymbol{k})$ are given by the dispersion relation (4.60a), so that the wave vectors of steady flows lie on the intersections with curves determined by (4.60a) for $\mu = 0$.

For $\delta \in \{0, \pm 1\}$ let us define

$$\Gamma_\delta := \{\boldsymbol{k} \in \mathbb{R}^2 \mid q(\boldsymbol{k}) = 0,\ \mathrm{sgn}(\mu(\boldsymbol{k})) = \delta\}\,.$$

Steady flows of the form (4.59) exist if and only if $\Gamma_0 \neq \emptyset$ (the intersection of black and blue curves in Figure 4.5), exponentially and unboundedly growing such flows if and only if $\Gamma_1 \neq \emptyset$ (the intersection of red regions and blue curves in Figure 4.5), and exponentially decaying ones have wave vectors $\boldsymbol{k} \in \Gamma_{-1}$ (the intersection of white regions and blue curves in Figure 4.5), which is always non-empty, except of the isotropic case with rotation, where solutions (4.59) do not exist.

The explicit flows (4.59) with $\boldsymbol{k} \in \Gamma_1$ grow unboundedly and exponentially in the nonlinear systems, and thus form a linear and unbounded part of the unstable manifold of the trivial state due to the arbitrary choice of the amplitude A. This holds analogously for the stable manifold if $\boldsymbol{k} \in \Gamma_{-1}$. Since explicit flows (4.59) with (4.60) also satisfy (4.1) without the nonlinear terms, they are selected real eigenmodes of the linearization in the trivial state. In particular, the existence of an explicit flow (4.59) requires a solution to the eigenvalue problem of (4.8) studied in Section 4.2 with $\lambda = \mu$. In fact, for μ from (4.60a) the term $-|\boldsymbol{k}|\mu$ has the same sign as a_0 in the dispersion relation (4.10). Thus, for any $\boldsymbol{k} \neq 0$ with $\mu > 0$ it follows $a_0 < 0$ and a positive real eigenvalue exists for these $\boldsymbol{k}$. This means, that regions with positive μ in the wave vector plane (the red regions in Figure 4.5) give subspaces of unstable real eigenmodes of trivial states, see Chapter 3

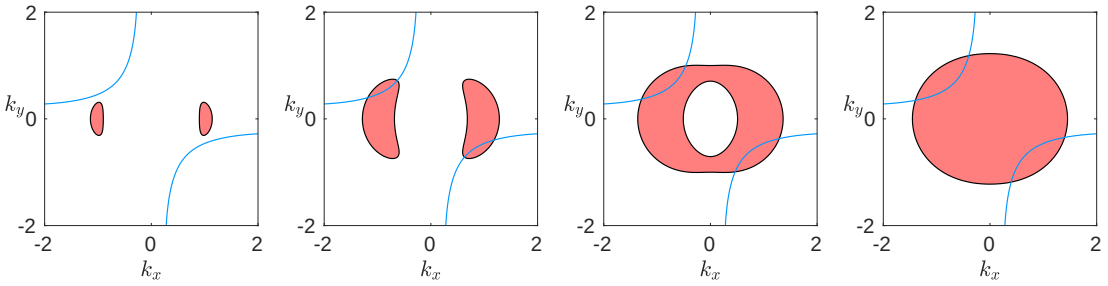

(a) $C = 0.11$ (b) $C = 0.08$ (c) $C = 0.05$ (d) $C = 0$

Figure 4.5.: Sample of the locations of explicit flows (4.59) of (4.1) in the wave vector plane. The parameters are $d_1 = 1$, $d_2 = 1.04$, $b_1 = 1.5$, $b_2 = 2.2$, $f = 0.3$, $g = 9.8$, $H_0 = 0.1$, $Q = 0$, so that $C_c \approx 0.116$. Red: $\mu > 0$; white: $\mu < 0$; black: $\mu = 0$; blue: the wave vectors satisfying (4.60b). The steady explicit flows are indicated by the intersections of black and blue curves. $\mu = 0$ at the origin is excluded in each figure.

for a broader discussion in the case $C = 0$.

The bottom drag parameter C only affects the growth rate μ, which one can directly see in (4.60), and has a monotonically stabilizing effect on the explicit flows. Steady flows (4.59) cannot exist if there are no steady eigenmodes, since these explicit flows also solve the linearization in the trivial flow, cf. Section 4.2. Hence, for $C > C_c$ from (4.13) or (4.16) we have $\Gamma_0 = \Gamma_1 = \emptyset$. At $C = 0$, for sufficiently small k_x and k_y, the leading order term of μ is given by the positive quantity $b_1 k_y^2 + b_2 k_x^2$, which means any explicit flow with $\boldsymbol{k} \approx 0$ is growing. For $C > 0$, the leading order term of μ for small k_x and k_y is given by $-C/H_0$, and for large $(k_x, k_y)^\intercal$ by $-(d_1 k_y^2 + d_2 k_x^2)|\boldsymbol{k}|^2$. Both quantities are negative, thus the explicit flows are decaying for $\boldsymbol{k}$ close to and sufficiently far from the origin in the wave vector plane. We plot examples in Figure 4.5 that illustrate these situations.

Remark 4.6.2. We briefly comment on linear stability properties of the explicit flows (4.59) for small amplitudes $A \approx 0$. As discussed for the explicit solutions in Section 3.2, for $A \approx 0$ a part of the spectrum of the linearization in the explicit flows is close to the spectrum of the underlying trivial flow. Since this is unstable precisely for $C < C_c$, the explicit flows (4.59) with small amplitudes $A \approx 0$ are also unstable. From the results in Section 3.2 we expect, that the explicit flows are unstable for all A, although we do not have a proof. For $|A| \gg 1$ it might be possible to exploit the scaling argument in Section 3.2.

Remark 4.6.3. We briefly consider fast rotation $|f| \gg 1$, which requires large wave numbers $|\boldsymbol{k}| \gg 1$ to solve (4.60b). Since the right-hand side of (4.60a) is negative for $|\boldsymbol{k}| \gg 1$ (and fixed C), there are no steady explicit flows of the form (4.59) in this regime. However, as noted in Remark 4.0.3, $|f| \to \infty$ with $\tilde{\phi} = \tilde{f}\phi$ gives the formal limit $\psi = \partial_\xi \phi$

and $0 = (dk^2\partial_\xi^2 + b)\partial_\xi^2\psi$. These have the steady solutions of the form $\psi(\xi) = A\cos(\xi)$, $\phi(\xi) = A\sin(\xi)$ with $k = \sqrt{b/d}$, which are different of the solutions (4.59).

We are now investigating the number of different steady explicit flows (4.59) occurring for fixed parameters. This is equivalent to the different intersections of the curves defined by (4.60a) and (4.60b) in the wave vector plane with $\mu = 0$. We organize this analysis by the types of isotropy of hyperdiffusion and backscatter terms and consider both, the rotational and non-rotational case.

Steady solutions in isotropic case

For isotropic hyperdiffusion and backscatter, $d_1 = d_2 := d$ and $b_1 = b_2 := b$, explicit flows (4.59) exist if and only if $f = 0$ due to (4.60b). The condition (4.60a) reduces to $\mu = \mu(K) = (b - dK)K - C/H_0$ with $K := |\boldsymbol{k}|^2$, and the solutions correspond to those of (4.7), which is linear in this case ($Q = 0$).

Steady explicit flows (4.59) exist (i.e. $\Gamma_0 \neq \emptyset$) for $0 < C \leq C_c$, but not for $C > C_c$. $\mu(K)$ has for $C = C_c$ a double root at $K = k_c^2$, with k_c from (4.14), and the wave vectors of steady explicit flows form a circle with radius $|\boldsymbol{k}| = k_c$. Hence, in terms of decreasing C, the primary bifurcation of the steady explicit flows from a trivial flow occurs at $C = C_c$, with a vertical branch as in Figure 4.4(a) (dashed), parameterized by the amplitude A.

For $0 < C < C_c$ the negative parabola $\mu(K)$ has two different roots and is monotonically shifted upwards upon decreasing C, so that the wave vectors of the steady explicit flows (4.59) form two concentric circles, whose radii depend monotonically on C, cf. a sample in Figure 4.6(a). The whole area in the annulus define Γ_1, which is not empty. For each $C \in (0, C_c]$ the steady explicit flows form vertical branches and are analogous to (4.31) for $f = 0$, cf. Figure 4.4(a) (dashed). We recall that the case $C = 0$ has been studied in Section 3.2.

Remark 4.6.4. With isotropic hyperdiffusion and backscatter, as well as $f = Q = 0$, the bifurcating Rossby-type waves of Theorem 4.2 coincide with a part of the unbounded branches of explicit steady flows (4.59). Indeed, it is $\eta = 0$ for $f = 0$ since $\eta = \tilde{f}\phi_s$ (cf. Section 4.1) and the wave vectors of the bifurcating wave shapes (4.31) satisfy $0 = \alpha - 2b\kappa^2 - 4dk_c\kappa^3 - d\kappa^4$, which follows from the bifurcation equation (4.30) with resolving the rest terms (cf. (4.32)). This coincides with the wave vectors defined by (4.60a) upon setting $C = C_c - \alpha H_0$, $|\boldsymbol{k}| = k_c + \kappa$ and $\mu = 0$.

Recall that $w = W(u, \tau) \equiv 0$ for $f = Q = 0$ in Theorem 4.2. Note that the bifurcation analysis requires $|\alpha|$ and $|A_1|$ to be sufficiently small in Theorem 4.2 due to the use of the implicit function theorem, whereas (4.59) can have arbitrary $A \in \mathbb{R}$ and $\alpha \in [0, C_c/H_0]$, which are thus an extension of these solutions in the case $f = 0$.

For $f \neq 0$ the steady explicit flows (4.59) do not exist, whereas the bifurcation analysis gives plane wave-type solutions (4.21) with (4.31) for wave vectors in an open neighbourhood of the circle with radius k_c. Recall the bifurcation diagram in Figure 4.4(a) (red solid).

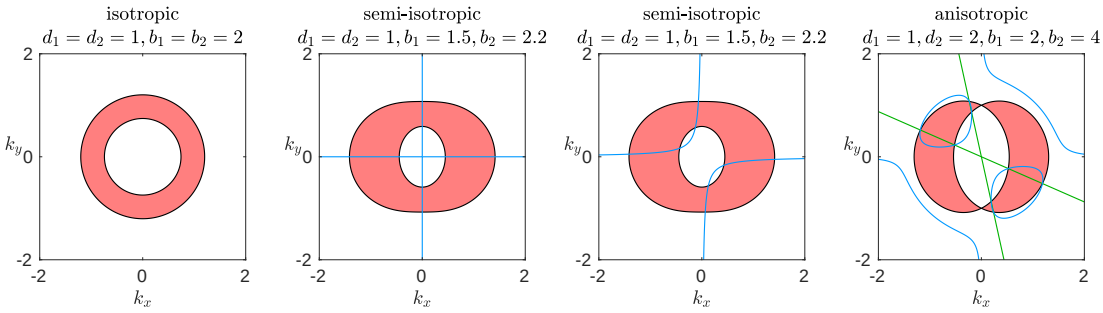

(a) $f = 0$, $C = 0.08$ (b) $f = 0$, $C = 0.04$ (c) $f = 0.05$, $C = 0.04$ (d) $f = 0.2$, $C = 0.1$

Figure 4.6.: Sample of the locations of explicit flows (4.59) of (4.1) in the wave vector plane; (a) existence for any wave vector, (b-d) existence on blue curves only. Red: $\mu > 0$; white: $\mu < 0$; black: $\mu = 0$; blue: wave vectors satisfying (4.60b). Common parameters: $g = 9.8$, $H_0 = 0.1$, $Q = 0$. In (d), there are two intersections of blue and black curves on each ray (green) in the second and fourth quadrant.

Steady solutions in semi-isotropic case

In the semi-isotropic case $b_1 \neq b_2$ and $d_1 = d_2 := d$, as well as without rotation $f = 0$, one needs $k_x = 0$ or $k_y = 0$ due to (4.60b). Hence, in this case steady solutions have wave vector on the axes in the wave vector plane only. Due to the remaining fourth order polynomial (4.60a) with $\mu = 0$ and even exponents, there are up to two different steady solutions at each axis in the wave vector plane, so in total up to four. Moreover, in case of existing two wave vectors of steady solutions on the same axis in the wave vector plane implies, that the interval between them belongs to wave vectors of exponentially growing explicit flows. An example of the occurrence of steady, growing and decaying explicit flows (4.59) for this situation is depicted in Figure 4.6(b).

In the rotational case $f \neq 0$ the equations (4.60) reduce to

$$0 = -d|\boldsymbol{k}|^4 + b_1 k_y^2 + b_2 k_x^2 - C/H_0\,,$$
$$0 = (b_2 - b_1) k_x k_y + f\,,$$

where the second equation implies k_x, $k_y \neq 0$. Thus, we can reformulate to the second component $k_y = f/((b_1 - b_2)k_x)$ and inserting this form of k_y into the first equation and defining $K_x := k_x^2 > 0$ leads to

$$0 = -dK_x^4 + b_2 K_x^3 - \left(\frac{2df^2}{(b_1 - b_2)^2} + \frac{C}{H_0}\right) K_x^2 + \frac{b_1 f^2}{(b_1 - b_2)^2} K_x - \frac{df^4}{(b_1 - b_2)^4}\,. \tag{4.61}$$

This is a fourth order polynomial with always four sign changes of the coefficients, so that due to the Descartes' rule of signs it has up to four different positive roots. So with $k_x = \pm\sqrt{K_x}$ we have up to eight intersections of the curves. Since $\sqrt{K_x}$ and

$-\sqrt{K_x}$ represent the same solution, but with opposite sign of wave vector, there are up to four different steady solutions (4.59) in this case. The wave vectors of these steady solutions can be precisely determined by the roots of the polynomial (4.61). Similarly, the wave vectors on the curve defined by $k_y = f/((b_1 - b_2)k_x)$ with $\mu(\boldsymbol{k}) > 0$ belong to exponentially growing explicit flows. An example of the occurrence of different explicit flows (4.59) for this situation is depicted in Figure 4.6(c).

Steady solutions in anisotropic case

For anisotropic hyperdiffusion and backscatter $b_1 \neq b_2$ and $d_1 \neq d_2$, and without rotation $f = 0$, both $k_x = 0$ and $k_y = 0$ solve (4.60b). This leads to the same situation as for the semi-isotropic case with $f = 0$. Thus, there are up to four different steady solutions in this case, up to two at each axis.

Additionally to these solutions, if $(b_1 - b_2)/(d_1 - d_2) > 0$, wave vectors on the circle with radius $|\boldsymbol{k}| = k_0 := \sqrt{(b_1 - b_2)/(d_1 - d_2)}$ also solve (4.60b). The remaining condition (4.60a) with $\mu = 0$ and $|\boldsymbol{k}| = k_0$ implies

$$C = C_0 := \frac{(b_1 - b_2)(b_2 d_1 - b_1 d_2)H_0}{(d_1 - d_2)^2}\,.$$

The sign of C_0 is indefinite, i.e. $\operatorname{sgn}(C_0) = \operatorname{sgn}((b_1 - b_2)(b_2 d_1 - b_1 d_2))$. The case $C_0 = 0$ for $b_2 d_1 = b_1 d_2$ also occurs in Section 3.1.1 as a special anisotropic case.

We claim that $C_0 < C_\mathrm{c}$. For C_c given by (4.16a) (the case (4.16b) is analogous) we compute

$$C_\mathrm{c} - C_0 = \frac{(b_2(d_1 + d_2) - 2b_1 d_2)^2 H_0}{4d_2(d_1 - d_2)^2}\,,$$

which is strictly positive and never zero since

$$\begin{aligned} b_2(d_1 + d_2) - 2b_1 d_2 &= (b_2^2 d_1 + b_2^2 d_2 - 2b_1 b_2 d_2)/b_2 \\ &\geq (b_1^2 d_2 + b_2^2 d_2 - 2b_1 b_2 d_2)/b_2 = d_2(b_1 - b_2)^2/b_2 > 0\,, \end{aligned}$$

where the first inequality is derived from the condition $b_2^2 d_1 \geq b_1^2 d_2$ in (4.16a). In general, if $(b_1 - b_2)/(d_1 - d_2) > 0$ and $(b_1 - b_2)(b_2 d_1 - b_1 d_2) \geq 0$, then we have $0 \leq C_0 < C_\mathrm{c}$, and there exists a positive k_0 such that for $C = C_0$ the steady explicit flows (4.59) exist on the entire circle with radius k_0 in the wave vector plane. If $(b_1 - b_2)(b_2 d_1 - b_1 d_2) < 0$, then $C_0 < 0$ and thus C does not reach C_0 since $C > 0$, so that the steady explicit flows do not exist on the aforementioned circle for any $C \geq 0$. See examples for these two cases in Figure 4.7.

In addition, this implies that the linear operator $\mathcal{L}$ from (4.8) has an infinite-dimensional kernel at $C = C_0$ in this case. However, the underlying trivial state is not marginally stable since $C_0 < C_\mathrm{c}$ for any choice of parameters, which means it is already unstable. We shortly note that the explicit flows (4.59) with $|\boldsymbol{k}| = k_0$ are all exponentially decaying for $C_0 < C$ and exponentially growing for $0 \leq C < C_0$.

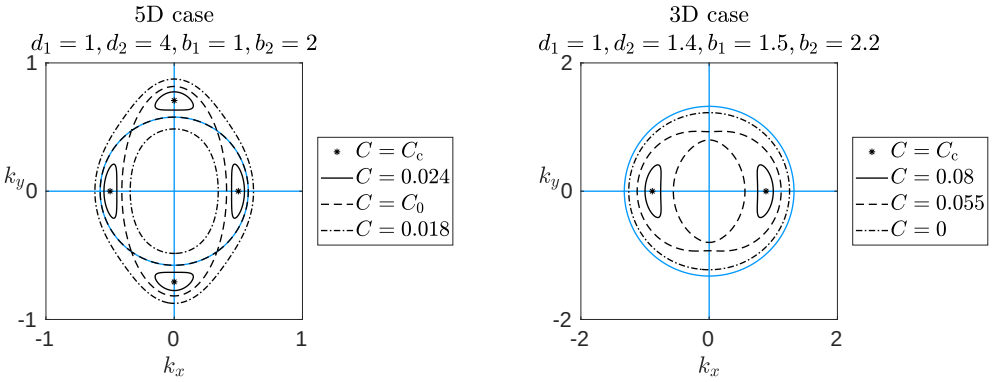

(a) $C_c = 0.025$, $C_0 \approx 0.022$ (b) $C_c \approx 0.086$, $C_0 \approx -0.044$

Figure 4.7.: Sample of locations of the wave vectors for steady explicit flows (4.59) of (4.1) for anisotropic hyperdiffusion and backscatter on the intersections of blue curves and the different types of black curves. Black: $\mu = 0$ with different types for different values of C. Blue: the wave vectors satisfying (4.60b). Common parameters: $f = 0$, $g = 9.8$, $H_0 = 0.1$.

Remark 4.6.5. Since $C_0 < C_c$, the primary bifurcation of the steady explicit flows upon decreasing C does not occur for wave vectors on the circle with radius k_0. Equivalently, the primary instability of the trivial solution (i.e. marginally stable spectrum of $\mathcal{L}$) does not occur at $C = C_0$, so that these solutions do not correspond to a bifurcation analyzed in Section 4.3.

In the rotational case $f \neq 0$ it is more involved to determine the number of steady solutions or intersections of the corresponding curves. If we consider the wave vectors in polar coordinates $\boldsymbol{k} = r(\cos\varphi, \sin\varphi)^\mathsf{T}$, then (4.60) with $\mu = 0$ becomes

$$0 = a_1 r^4 - a_2 r^2 + C/H_0\,, \tag{4.62a}$$

$$0 = a_3 r^4 - a_4 r^2 + f\,, \tag{4.62b}$$

with $a_1(\varphi) := d_1 \sin^2\varphi + d_2 \cos^2\varphi$, $a_2(\varphi) := b_1 \sin^2\varphi + b_2 \cos^2\varphi$, $a_3(\varphi) := \frac{d_1 - d_2}{2} \sin(2\varphi)$ and $a_4(\varphi) := \frac{b_1 - b_2}{2} \sin(2\varphi)$. If we consider (4.62a), then for $r > 0$ and fixed angle $\varphi \in [0, 2\pi)$ this fourth order polynomial has always two sign changes of the coefficients (or one for $C = 0$). Due to the Descartes' rule of signs it thus has up to two different positive roots (or one for $C = 0$). Since both equations (4.62) need to be satisfied, this means there are not more than two different steady solutions for a fixed direction φ of their wave vector $\boldsymbol{k}$ (or one for $C = 0$). In certain cases there are two different steady solutions in one wave vector direction φ, see Remark 4.6.7.

These numbers are upper bounds and determined for a fixed angle φ, so not the total numbers for all angles $\varphi \in [0, 2\pi)$ together, which we are primary interested in. We omit an analytical investigation of the total number of intersections, but analyzing this numerically, we determined up to four different intersections of the corresponding curves,

so up to four different steady solutions (4.59) for fixed parameters. Figure 4.6(d) shows an example of such a possible setting including the non-empty sets Γ_1 and Γ_{-1}.

Remark 4.6.6. For anisotropic hyperdiffusion and backscatters, based on Remark 4.0.1 we can a priori reduce to an analogue of (4.6) and prove bifurcations as in Theorem 4.2. However, such steady solutions have wave vectors constrained to the axes in the wave vector plane and require sufficiently small bifurcation parameters.

For $f = 0$ the steady explicit flows (4.59) not only exist for wave vectors on the axes, but also elsewhere (cf. Figure 4.7(a)), and the parameter $\alpha = (C_c - C)/H_0$ is not necessarily small. Additionally, exponentially growing explicit flows exist for instance between the steady ones on the axes in wave vector plane, which are not described by Theorem 4.2. Hence, for $f = 0$, the explicit flows (4.59) are not contained in the reduction of Remark 4.0.1 and have unconstrained amplitude and growth.

Likewise, for $f \neq 0$, the steady explicit flows (4.59) are not part of this reduction since their wave vectors do not lie on the axes in the wave vector plane. The same applies for the exponentially growing solutions, which do not exist on the axes, cf. Figure 4.5.

Remark 4.6.7. We consider the anisotropic case with a fixed but arbitrary angle φ of the wave vector $\boldsymbol{k}$ in polar coordinates as above. In certain cases both equations (4.62) can be solved at the same time with two different values $r > 0$, so the highest possible number of different positive solutions of (4.62a) in one wave vector direction.

Due to (4.62b) and $f \neq 0$, we need $\sin(2\varphi) \neq 0$. For these angles φ, a necessary condition for both polynomials (4.62) to have two common real roots is to share the same symmetric axis of their graphs, i.e. $\frac{a_2}{2a_1} = \frac{a_4}{2a_3}$, which is equivalent to $b_2 d_1 = b_1 d_2$. Under this condition, so both polynomials in (4.62) have the same symmetric axis, one can vary C, which is only in (4.62a), or f, which is only in (4.62b), in order to get the same real roots as well. An example of this situation is depicted in Figure 4.6(d).

In the semi-isotropic case $b_1 \neq b_2$ and $d_1 = d_2$ we have $a_3 \equiv 0$. Thus, by (4.62b), there are at most one steady explicit solution in a wave vector direction φ, which must have $r = \sqrt{f/a_4} > 0$.

4.6. Numerical results

In order to illustrate and underline our analytical results, we present here some results from numerical computations. In particular, we confirm the analytically determined branches of nonlinear Rossby and inertia-gravity waves by numerical continuation. For this we have implemented (4.1) for y-independent solutions in the MATLAB package *pde2path* (Uecker et al., 2014; Uecker, 2022). We thus consider waves that depend on the x-variable only, which is scaled so that the onset of instability occurs on the normalized domain $[0, 2\pi]$ with periodic boundary conditions. We plot some of the results in Figure 4.8 for an isotropic case, and in Figure 4.9 for an anisotropic case. As determined analytically, they show supercritical bifurcations of Rossby and inertia-gravity waves

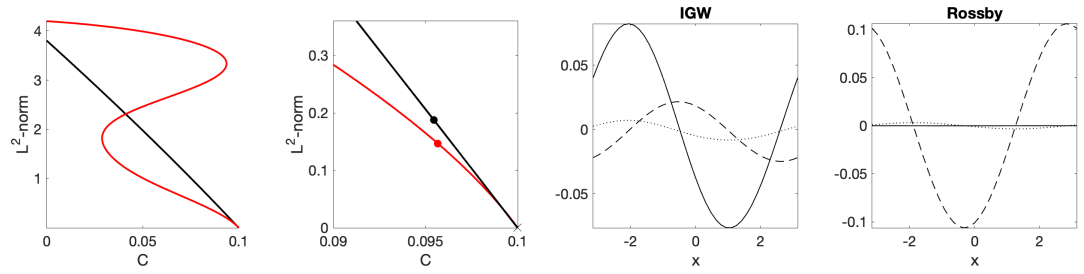

(a) (b) (c) (d)

Figure 4.8.: (a) Numerically computed branches of nonlinear Rossby waves (black) and inertia-gravity waves (red) in the isotropic case $d_1 = d_2 = 1$, $b_1 = b_2 = 2$; (b) Magnification of (a). Marks on the branches are the solutions plotted in panels (c) and (d) with v_1 solid, v_2 dashed and η dotted. Other parameters are $Q = 0.05$, $f = 0.3$, $g = 9.8$ and $H_0 = 0.1$, so that $C_c = 0.1$.

by decreasing the bottom drag parameter C as well. In all cases we found that the branches extend (after two folds in the isotropic case) to $C = 0$, i.e. purely nonlinear bottom drag. We do not show the various bifurcation points along the branches, that are detected numerically.

Due to the numerical discretization there is a spectral gap for large wavenumbers, and we can directly consider stability of the bifurcating waves, i.e. including perturbations that are not of plane wave type as well, what we are not able to do analytically for the more relevant case $f \neq 0$. For this setting and with isotropic backscatter and hyperdiffusion, where steady and oscillatory modes are critical simultaneously, the numerical results show that corresponding bifurcating solutions are all unstable (see Figure 4.8). In fact, the instability occurs already for purely x-dependent perturbations of the same wave number as the solutions. For both, the Rossby and inertia-gravity waves, the unstable eigenvalues near bifurcation are a complex conjugate pair. The unstable eigenfunction for Rossby waves has the shape of an inertia-gravity wave, and vice versa. This indicates that the instability stems from the interaction between Rossby and inertia-gravity waves.

For anisotropic backscatter only steady modes are critical at the primary instability, and Rossby waves bifurcate supercritically as predicted analytically. As expected, we find that inertia-gravity waves bifurcate at some smaller value of C (see Figure 4.9). Interestingly, the bifurcating nonlinear Rossby waves turn out to be spectrally stable against general two-dimensional perturbations. The Rossby waves seem to remain spectrally stable until $C \approx 0.01$ and become spectrally unstable when further deacreasing C towards $C = 0$.

In order to determine stability of the spectrum, we have implemented a Floquet-Bloch transform in the x-direction by replacing ∂_x with $\partial_x - \mathrm{i}\gamma_x$, with Floquet-Bloch wavenumber parameter $\gamma_x \in [-\pi, \pi]$ in the linearization. Since the waves are constant in the y-direction, we use a direct Fourier transform in this direction with wave number

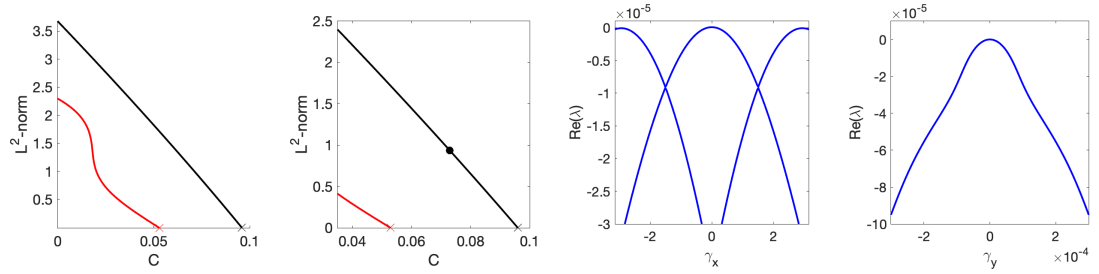

(a) (b) (c) (d)

Figure 4.9.: (a) Numerically computed branches of nonlinear Rossby waves (black) and inertia-gravity waves (red) in the anisotropic case $d_1 = 1$, $d_2 = 1.04$, $b_1 = 1.5$, $b_2 = 2$; (b) Magnification of (a). Other parameters are $Q = 0.05$, $f = 0.3$, $g = 9.8$ and $H_0 = 0.1$, so that $C_c = 0.1$. (c) Floquet-Bloch spectrum near zero for $\gamma_x \in [-\pi, \pi]$ and (d) Fourier spectrum for $\gamma_y \approx 0$ of the marked solution on the branch in (b), suggesting spectral stabilty.

$\gamma_y \in \mathbb{R}$. We found that the most unstable growth rate is zero and stems from the translation eigenmode at $\gamma_x = \gamma_y = 0$. Thus, the sidebands are stable as plotted in Figure 4.9(c) and Figure 4.9(d). This implies that the combined backscatter and bottom drag can stabilize Rossby waves, meaning that backscatter not only induces the bifurcation of waves, but also a selection of waves in the dynamics. This would lead to undesired results in the numerics, as e.g. physically unrealistic solutions.

5. Outlook

5.1. Two-layer shallow water equations with backscatter and bottom drag

Based on the results in Chapter 4, further research can be done in similar, but more complex models. The two-layer shallow water equations is the perfect model for the next step, since it is similar to the single-layer shallow water equations in Chapter 4 and additionally is a model with stratification. It consists of two vertically thin fluid layers compared to their horizontal scale, which lie on top of each other. The upper layer has the constant density $\rho_1 > 0$, velocity $\boldsymbol{v}_1$ and fluid layer thickness h_1, while the bottom layer has the constant density $\rho_2 > \rho_1$ and the velocity and height $\boldsymbol{v}_2$ and h_2. The bottom friction is then only affecting the bottom layer directly, so it appears only there. Together with additional hyperdiffusion and backscatter terms the equations then read

$$\frac{\partial \boldsymbol{v}_1}{\partial t} + (\boldsymbol{v}_1 \cdot \nabla)\boldsymbol{v}_1 = - f\boldsymbol{v}_1^{\perp} - g\nabla(h_1 + h_2) - \begin{pmatrix} d_{1,1}\Delta + b_{1,1} & 0 \\ 0 & d_{1,2}\Delta + b_{1,2} \end{pmatrix} \Delta \boldsymbol{v}_1 \tag{5.1a}$$

$$\frac{\partial h_1}{\partial t} + (\boldsymbol{v}_1 \cdot \nabla)h_1 = - h_1 \nabla \cdot \boldsymbol{v}_1 \tag{5.1b}$$

$$\begin{aligned} \frac{\partial \boldsymbol{v}_2}{\partial t} + (\boldsymbol{v}_2 \cdot \nabla)\boldsymbol{v}_2 = &- f\boldsymbol{v}_2^{\perp} - g\nabla(\tfrac{\rho_1}{\rho_2}h_1 + h_2) - \begin{pmatrix} d_{2,1}\Delta + b_{2,1} & 0 \\ 0 & d_{2,2}\Delta + b_{2,2} \end{pmatrix} \Delta \boldsymbol{v}_2 \\ &- \frac{C + Q|\boldsymbol{v}_2|}{h_2}\boldsymbol{v}_2 \end{aligned} \tag{5.1c}$$

$$\frac{\partial h_2}{\partial t} + (\boldsymbol{v}_2 \cdot \nabla)h_2 = - h_2 \nabla \cdot \boldsymbol{v}_2 \,, \tag{5.1d}$$

where the parameters are as in (4.1) respectively. See Vallis (2017) for more details about the usual multi-layer model without backscatter, hyperdiffusion and bottom drag.

One sees, that (5.1) consists of two almost independent singe-layer shallow water equations with backscatter and bottom drag. They are only coupled by the gradients of the fluid thickness h_1 and h_2. This coupling does not seem to be too restrictive, so we expect that some of the results from Chapter 4 can be used in this two-layer model as well. Furthermore, one can also study different variations of the model, e.g. usual viscosity in the upper layer and backscatter with hyperdiffusion and bottom drag in the bottom layer. It would be particularly interesting to see, how the instability and bifurcation of Rossby and inertia-gravity waves (as shown in Chapter 4) in the bottom layer would affect the dynamics in the upper layer. It is certainly also possible that

the upper layer has an effect on the bottom layer, so that the bifurcation results as in Chapter 4 are different, or in general one could discover dynamics, which we do not have in the single-layer equations.

In the two-layer model (5.1) one can use an aspect, which we have shown in Chapter 4, but we could not use it for the single-layer case due to mass conservation. In the bifurcation of Rossby and inertia-gravity waves in the presence of backscatter and bottom drag we have shown, that they also consist of a constant term A_0 in their deviation η, which is the same as changing the characteristic fluid depth H_0 by this constant term. Due to mass conservation and since we fixed the value of H_0, it was just natural to fix $A_0 = 0$.

However, in the two-layer model we can also vary A_0 of the bifurcating Rossby and inertia-gravity waves, if they exist in the bottom layer, and it is not violating the mass conservation. The thickness of the bottom layer can be described by $h_2 = H_2 + \eta_2$, with characteristic fluid depth of the bottom layer H_2 and its deviation η_2. If η_2 contains constant terms, it just changes H_2, which means the characteristic fluid depth of the bottom layer changes. This can be explained by changing the amount of the fluid, which has either density ρ_1 or ρ_2. If e.g. $A_0 > 0$, then the bottom layer gets thicker, which can be interpreted as a part of the fluid from the upper layer with density ρ_1 gets the density ρ_2, so descending to the bottom layer. This can happen by cooling the upper layer, since the density of fluids is in relation with the temperature. In this case, the upper layer needs to get thinner correspondingly at the same time, in order to keep the total mass conserved, which does not need to happen linearly. For $A_0 < 0$ the situation is the other way round, which can be explained by heating the bottom layer. Thus, in the two-layer model we can use the results from Chapter 4 with $A_0 \neq 0$ and it would be interesting to see, how this affects the dynamics in both layers.

5.2. Equatorial fluid models with β-plane approximation

The rotating geophysical fluid equations, that we have in particular considered in Chapter 3 and Chapter 4, have a constant Coriolis parameter f. Even though the Coriolis force varies with the latitude, it is still appropriate to consider a constant Coriolis parameter when studying flows at the mid-latitudes only, where the Coriolis force changes insignificantly. Such a model is called *f-plane approximation*.

However, for equatorial regions for instance it is not a proper model, since there the Coriolis force varies strongly and even changes its sign, when crossing the equator. In order to correctly model such effects, one uses for the equatorial regions the so-called *β-plane approximation*. In such a model one replaces the constant Coriolis parameter f by a linear and y-dependent parameter βy, with $\beta \in \mathbb{R} \setminus \{0\}$. Even though this is a little change, mathematically this is a completely different problem with different dynamics, so that other analytical methods have to be used.

Interestingly, in order to analyze such a β-plane model one can successfully use the so-called *Hermite polynomials* $H_n(y)$ with degree $n \in \mathbb{N}$. The special features of such

Hermite polynomials are first, that $H_n(y)\mathrm{e}^{-y^2/2}$ form an orthogonal basis of $L^2(\mathbb{R})$, and second, that they solve the linear ODE for degree $n \in \mathbb{N}$

$$v'' - yv' = -nv\,. \tag{5.2}$$

One immediately sees, that the latter property is the key for this specific approach, due to the linear parameter $-y$. The property (5.2) can also be seen as an eigenvalue problem or dispersion relation, so that Hermite polynomials can be used for the analysis of waves. See Matsuno (1966); Chan and Shepherd (2013) for more details, where this approach is used for the equatorial shallow water equations without viscosity.

In the analyses of Matsuno (1966); Chan and Shepherd (2013) the nonlinear advection terms are neglected in order to obtain a linear ODE of the form (5.2). An open question is, if one can combine this approach with ours, since our method provides the reduction to the required linear equation without just neglecting the nonlinear advection terms, so that solutions would also solve the full nonlinear equations. Furthermore, it would be interesting to find out, for what models such an approximation could also be useful, e.g. for those with usual viscosity, with backscatter and hyperdiffusion or even with bottom drag. We believe that in particular fluid models with certain adapted forcing as in Section 2.4 have explicit solutions with shapes build by Hermite polynomials. If steady solutions exist, then determining stability and even unbounded instability (if superposition is possible) as done in Chapter 3 would be the next step, and maybe even bifurcation analysis as in Chapter 4.

5.3. Application of results in numerical backscatter scheme

Since the here considered models with simplified backscatter arise from numerical simulations of subgrid effects, it is not clear to what extent one can compare the presented results with real physical phenomena. Instead, we provide an outlook of how the results here can appear in the numerical computations. The following are just ideas and assumption of the occurrence and effects of our results in the numerical simulations and further investigations need to be made. Just for simplicity, as well as better graphical representation and explanation, we consider a discretization of a domain, where the values of the backscatter and hyperviscosity parameter are given in each grid cell.

If we have a region, where the parameter in each grid cell are the same (cf. Figure 5.1(a)), then numerical solutions on this domain approximate explicit solutions on the same domain in the continuum setting. This also means, that the numerical solutions also behave similar to the explicit ones, so they might grow unboundedly under certain circumstances. However, it might also be that they grow, but not unboundedly, due to the numerical discretization. Nevertheless, both cases are undesired in numerical computations and it is one aspect for further investigation.

When analyzing such (unboundedly) growing solutions with these assumptions, one sees two problems of the occurrence of such a situation in the discrete setting:

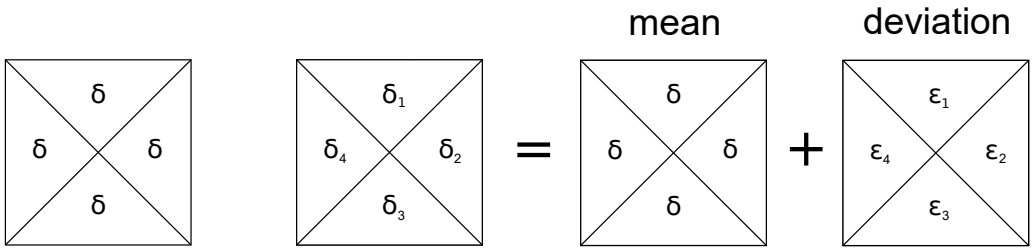

(a) Homogeneous backscatter parameter.

(b) Inhomogeneous backscatter parameter splitted in regional mean value and corresponding deviations.

Figure 5.1.: Simplified examples for situations of backscatter parameter values in the discretized setting. (a) The situation as in the analytical investigations. (b) The values how they more likely could appear in numerical computations. In each grid cell there are backscatter parameter with the same values $\delta := (d_1, d_2, b_1, b_2)$ or different ones in each grid cell $\delta_j := (d_{1,j}, d_{2,j}, b_{1,j}, b_{2,j})$ with corresponding deviations $\varepsilon_j := (\varepsilon_{1,j}, \varepsilon_{2,j}, \varepsilon_{3,j}, \varepsilon_{4,j})$.

First, it is improbable that on a whole region the backscatter parameter are exactly the same. However, it might happen that the backscatter and hyperviscosity parameter differ only slightly on a whole region (cf. Figure 5.1(b)), so they consist of the mean value of these parameters on the whole region plus a corresponding deviation. Considering the mean values, (unboundedly) growing solutions can arise, and the additional deviations are like disturbances, that can cause solutions which still grow, if the disturbance is not too large. So an open question for further investigations is, how large the deviations (ε_j in Figure 5.1(b)) must be, so that the arising solutions do not grow.
The second problem is, that the unboundedly growing solutions are large scale flows, since their wave vectors lie in the unstable region around the origin of the wave vector space (red regions as e.g. in Figure 3.4). This means, that the considered region with at least similar backscatter and hyperviscosity parameter must be large enough in order to contain such unboundedly growing solutions. However, the size of the region of unstable wave vectors is given by the ratio $\sqrt{b_1/d_1}$ and $\sqrt{b_2/d_2}$, which can be very large. This means, that also in smaller domains the flows with smaller scales might be affected and grow, since their wave vectors could lie in the larger unstable region of wave vectors. This situation is even given with very small backscatter parameter, e.g. with $b_1 = 10^{-10}$ and $d_1 = 10^{-20}$ the ratio and size of unstable wave vectors are of order $\mathcal{O}(10^5)$. Hence, even for finer discretization with smaller backscatter and hyperviscosity parameter, which is a better approximation of our continuum setting, such growing solutions might appear.

Hence, our results show, that under certain circumstances (unboundedly) growing solutions may arise in numerical simulations. The remaining open questions for further investigations are, under which circumstances exactly they can occur (size of required domain and deviations ε_j) and how they influence the numerical computations. The

next step would also be to clarify, if and when bifurcating Rossby and inertia-gravity waves from Section 4.3 and Section 4.4 occur in the same discrete settings and how they behave. As already mentioned in Section 1.1, such bifurcating flows might be physically unrealistic flows (see Guan et al. (2022) and the references therein), which also needs to be clarified.

As the last step it would be interesting to understand, if such growing flows occur and how they behave with time-dependent parameter, which are also coupled with additional energy equations in order to control the reinjection of energy by backscatter. It might be that the presented growing waves do not exist in such a non–autonomous and dynamic model. However, it could also lead to certain disturbances in the computations, since growing waves might not disappear completely and reappear, so that the algorithms unnecessarily have to deal with too strong artificial growing.

Appendices

A. Solutions are generalized Beltrami flows

Here we show that our solutions presented in Chapter 2 are all generalized Beltrami flows, but not Beltrami flows. Since the Beltrami condition (2.41) is quadratic in the velocity $\boldsymbol{v}$, it is sufficient to check the condition for angular and radial superposition of two different waves.

For the radially superposed solutions of the form as in Theorem 2.3 we consider the velocity

$$\boldsymbol{v} = \psi_1(\boldsymbol{k}_1 \cdot \boldsymbol{x})\boldsymbol{a}_1 + \psi_2(\boldsymbol{k}_2 \cdot \boldsymbol{x})\boldsymbol{a}_2\,,$$

with $\boldsymbol{k}_1 \perp \boldsymbol{a}_1$, $\boldsymbol{k}_1 \perp \boldsymbol{a}_2$, $\boldsymbol{k}_2 \perp \boldsymbol{a}_1$ and $\boldsymbol{k}_2 \perp \boldsymbol{a}_2$. Due to the arbitrary wave shapes we additionally can assume without loss $|\boldsymbol{k}_1| = |\boldsymbol{k}_2| = |\boldsymbol{a}_1| = |\boldsymbol{a}_2| = 1$. We note that the case $N = 1$ and $M_1 \geq 1$ is equivalent to $\boldsymbol{a}_1 = \boldsymbol{a}_2$ and the case $N = 2$ and $M_1 = M_2 = 1$ is equivalent to $\boldsymbol{k}_1 = \boldsymbol{k}_2$.

Now we compute each term of the condition (2.41) separately. First we obtain

$$\operatorname{curl}(\boldsymbol{v}) = \nabla \times \boldsymbol{v} = \nabla \times \psi_1\boldsymbol{a}_1 + \nabla \times \psi_2\boldsymbol{a}_2 = \psi_1'\boldsymbol{k}_1 \times \boldsymbol{a}_1 + \psi_2'\boldsymbol{k}_2 \times \boldsymbol{a}_2 = \psi_1'\tilde{\boldsymbol{a}}_1 + \psi_2'\tilde{\boldsymbol{a}}_2\,,$$

where $\tilde{\boldsymbol{a}}_j$ are unit vectors orthogonal to $\boldsymbol{k}_j$ and $\boldsymbol{a}_j$ according to the right-hand rule of the cross product for $j \in \{1, 2\}$. With this we then get

$$\boldsymbol{v} \times \tilde{\boldsymbol{a}}_1 = \psi_1\boldsymbol{a}_1 \times \tilde{\boldsymbol{a}}_1 + \psi_2\boldsymbol{a}_2 \times \tilde{\boldsymbol{a}}_1 = \psi_1\boldsymbol{k}_1 + \sin(\varphi_1)\psi_2\boldsymbol{k}_1\,,$$

where φ_1 is the angle between $\boldsymbol{a}_2$ and $\tilde{\boldsymbol{a}}_1$. For the case $\boldsymbol{a}_1 = \boldsymbol{a}_2$ it is $\sin(\varphi_1) = 1$ and for $\boldsymbol{k}_1 = \boldsymbol{k}_2$ we have $\sin(\varphi_1) \in (-1, 1)$. Analogously we obtain $\boldsymbol{v} \times \tilde{\boldsymbol{a}}_2 = \psi_2\boldsymbol{k}_2 + \sin(\varphi_2)\psi_1\boldsymbol{k}_2$ and one can show that $\varphi_2 = \varphi_1 = \varphi$ for both cases by comparing the angles of the corresponding vectors. With the last results it follows then

$$\boldsymbol{v} \times \operatorname{curl}(\boldsymbol{v}) = \psi_1'\boldsymbol{v} \times \tilde{\boldsymbol{a}}_1 + \psi_2'\boldsymbol{v} \times \tilde{\boldsymbol{a}}_2 = \psi_1\psi_1'\boldsymbol{k}_1 + \sin(\varphi)\psi_2\psi_1'\boldsymbol{k}_1 + \sin(\varphi)\psi_1\psi_2'\boldsymbol{k}_2 + \psi_2\psi_2'\boldsymbol{k}_2\,,$$

which is in general not zero. Thus, the corresponding solutions do not satisfy (2.42) and are therefore no Beltrami flows. Now using the last equation and the fact $\boldsymbol{k} \times \boldsymbol{k} = 0$ for any $\boldsymbol{k} \in \mathbb{R}^3$ we finally obtain

$$\operatorname{curl}(\boldsymbol{v} \times \operatorname{curl}(\boldsymbol{v})) = \nabla \times (\psi_1\psi_1'\boldsymbol{k}_1 + \sin(\varphi)\psi_2\psi_1'\boldsymbol{k}_1 + \sin(\varphi)\psi_1\psi_2'\boldsymbol{k}_2 + \psi_2\psi_2'\boldsymbol{k}_2)$$

$$
\begin{aligned}
&= \sin(\varphi)\psi_1'\nabla\psi_2 \times \boldsymbol{k}_1 + \sin(\varphi)\psi_2'\nabla\psi \times \boldsymbol{k}_2 \\
&= \sin(\varphi)\psi_1'\psi_2'(\boldsymbol{k}_2 \times \boldsymbol{k}_1 + \boldsymbol{k}_1 \times \boldsymbol{k}_2) \\
&= \sin(\varphi)\psi_1'\psi_2'(-\boldsymbol{k}_1 \times \boldsymbol{k}_2 + \boldsymbol{k}_1 \times \boldsymbol{k}_2) = 0\,,
\end{aligned}
$$

which proves that the considered solutions of the form as in Theorem 2.3 are all generalized Beltrami flows.

For the angular superposed solutions of the form as in Theorem 2.9 with $N = 1$ and $M_1 \geq 1$ and Theorem 2.10 we consider the velocity

$$
\boldsymbol{v} = A_1 \sin(\boldsymbol{k}_1 \cdot \boldsymbol{x})\boldsymbol{k}_1^\perp + A_2 \sin(\boldsymbol{k}_2 \cdot \boldsymbol{x})\boldsymbol{k}_2^\perp\,,
$$

where without loss we assume only the horizontal plane $\boldsymbol{k}_1$, $\boldsymbol{k}_2$, $\boldsymbol{k}_1^\perp$, $\boldsymbol{k}_2^\perp \in \mathbb{R}^2 \times \{0\}$ and $|\boldsymbol{k}_1| = |\boldsymbol{k}_2| = |\boldsymbol{k}_1^\perp| = |\boldsymbol{k}_2^\perp| = \mu$. For simplicity we denote $\sin_j = \sin(\boldsymbol{k}_j \cdot \boldsymbol{x})$ and $\cos_j = \cos(\boldsymbol{k}_j \cdot \boldsymbol{x})$ for $j \in \{1, 2\}$. We then get

$$
\operatorname{curl}(\boldsymbol{v}) = \nabla \times \boldsymbol{v} = A_1 \cos_1 \boldsymbol{k}_1 \times \boldsymbol{k}_1^\perp + A_2 \cos_2 \boldsymbol{k}_2 \times \boldsymbol{k}_2^\perp = -\mu^2(A_1 \cos_1 + A_2 \cos_2)\boldsymbol{e_3}\,.
$$

With this we then obtain

$$
\begin{aligned}
\boldsymbol{v} \times \operatorname{curl}(\boldsymbol{v}) &= -\mu^2 \boldsymbol{v} \times (A_1 \cos_1 + A_2 \cos_2)\boldsymbol{e_3} \\
&= \mu^2(A_1^2 \cos_1 \sin_1 \boldsymbol{k}_1 + A_1 A_2 \cos_1 \sin_2 \boldsymbol{k}_2 + A_1 A_2 \sin_1 \cos_2 \boldsymbol{k}_1 + A_2^2 \cos_2 \sin_2 \boldsymbol{k}_2)\,,
\end{aligned}
$$

which is in general not zero. Thus, the corresponding solutions do not satisfy (2.42) and are therefore no Beltrami flows. Using the last result we now obtain again with $\boldsymbol{k} \times \boldsymbol{k} = 0$

$$
\begin{aligned}
\operatorname{curl}(\boldsymbol{v} \times \operatorname{curl}(\boldsymbol{v})) &= \mu^2 \nabla \times (A_1^2 \cos_1 \sin_1 \boldsymbol{k}_1 + A_1 A_2 \cos_1 \sin_2 \boldsymbol{k}_2 \\
&\qquad + A_1 A_2 \sin_1 \cos_2 \boldsymbol{k}_1 + A_2^2 \cos_2 \sin_2 \boldsymbol{k}_2) \\
&= -\mu^2 A_1 A_2 \sin_1 \sin_2(\boldsymbol{k}_1 \times \boldsymbol{k}_2 + \boldsymbol{k}_2 \times \boldsymbol{k}_1) \\
&= -\mu^2 A_1 A_2 \sin_1 \sin_2(\boldsymbol{k}_1 \times \boldsymbol{k}_2 - \boldsymbol{k}_1 \times \boldsymbol{k}_2) = 0\,,
\end{aligned}
$$

which proves that the considered solutions of the form as in Theorem 2.9 with $N = 1$ and $M_1 \geq 1$ and Theorem 2.10 are all generalized Beltrami flows.

B. Signs of a_1, a_2 and $a_1 a_2 - a_0$

Since a_2 is a quadratic polynomial in $K := |\boldsymbol{k}|^2$ with a positive quadratic coefficient, it possesses a global minimum which is positive for $C > C_1 := (b_1 + b_2)^2 H_0/(8(d_1 + d_2))$. Since $C_c > C_1$, we have $a_2 > 0$ for $C \geq C_c$ and $\boldsymbol{k} \in \mathbb{R}^2$.

We also find that $a_1 > 0$ for $C \geq C_c$. Without loss of generality, assume $C_c = b_1^2 H_0/(4d_1)$. The global minimum of $d_j K^2 - b_j K + C/H_0$ equals to $4d_j C/H_0 - b_j^2$ which

is non-negative for $C \geq C_c$ and $j = 1, 2$. Hence $a_1 > 0$ for $C \geq C_c$ and $\boldsymbol{k} \in \mathbb{R}^2$.

We next show that $a_1 a_2 - a_0 > 0$ for all $\boldsymbol{k} \in \mathbb{R}^2$ and $C \geq C_c$. The previous implies that a_1, $a_2 > 0$ for all $\boldsymbol{k} \in \mathbb{R}^2$ and $C \geq C_c$. Concerning a_0, we first of all have $a_0 = 0$ for $\boldsymbol{k} = (0,0)^\intercal$. For $C > C_c$ we have $a_0 > 0$ for all $\boldsymbol{k} \in \mathbb{R}^2 \setminus \{(0,0)^\intercal\}$, and for $C = C_c$ it holds that $a_0 > 0$ for all $\boldsymbol{k} \neq (0,0)^\intercal, \pm\boldsymbol{k}_c$ and $a_0 = 0$ for $\boldsymbol{k} = (0,0)^\intercal, \pm\boldsymbol{k}_c$. We make the dependence of $a_0 = a_0(k_x, k_y)$ on $\boldsymbol{k}$ explicit in the following. Since $a_2 > 0$ for all $\boldsymbol{k} \in \mathbb{R}^2$ and $C \geq C_c$ we may compute

$$\begin{aligned}\frac{a_0(k_x,k_y)}{a_2} &= \frac{gH_0|\boldsymbol{k}|^2\left((d_1|\boldsymbol{k}|^2 - b_1)|\boldsymbol{k}|^2 + (d_2|\boldsymbol{k}|^2 - b_2)|\boldsymbol{k}|^2 + 2C/H_0\right)}{(d_1+d_2)|\boldsymbol{k}|^4 - (b_1+b_2)|\boldsymbol{k}|^2 + 2C/H_0} \\ &\quad - \frac{gH_0|\boldsymbol{k}|^2\left((d_1|\boldsymbol{k}|^2 - b_1)k_x^2 + (d_2|\boldsymbol{k}|^2 - b_2)k_y^2 + C/H_0\right)}{(d_1+d_2)|\boldsymbol{k}|^4 - (b_1+b_2)|\boldsymbol{k}|^2 + 2C/H_0} \\ &= gH_0|\boldsymbol{k}|^2 - \frac{a_0(k_y,k_x)}{a_2}\,.\end{aligned}$$

Note that the wave vector components in a_0 on the right-hand side are swapped. It follows for all $\boldsymbol{k} \in \mathbb{R}^2$ and $C \geq C_c$ that

$$\begin{aligned}a_1 - \frac{a_0(k_x,k_y)}{a_2} &= (d_1|\boldsymbol{k}|^4 - b_1|\boldsymbol{k}|^2 + C/H_0)(d_2|\boldsymbol{k}|^4 - b_2|\boldsymbol{k}|^2 + C/H_0) + \frac{a_0(k_y,k_x)}{a_2} + f^2 \\ &\geq f^2 > 0\,,\end{aligned}$$

since the polynomials in $|\boldsymbol{k}|$ in the brackets are non-negative for $C \geq C_c$. In particular, $a_1 a_2 - a_0 > 0$ for all $\boldsymbol{k} \in \mathbb{R}^2$ and $C \geq C_c$, since $a_2 > 0$ for these parameters.

C. Proof of estimate (4.36) and (4.43)

The proof relies on rewriting (4.25) or (4.42) as a fixed point equation for W. We first write $PG(V;\tau) = L_0 V + L_\tau V + \mathcal{N}_\tau(V)$ with nonlinear part $\mathcal{N}_\tau(V) = \mathcal{O}(\|V\|_X^2)$ and corresponding solution space X, as well as linear parts L_0, which is τ-independent, and L_τ as the perturbation by parameters τ, i.e. $\|L_\tau\| = \mathcal{O}(|\tau|)$. More precisely, for Section 4.3 these are $V = \phi$, $L_0 = P\mathcal{L}_0$, $L_\tau = PL_\tau$ and $\mathcal{N}_\tau = P(N_C + N_Q)$, while for Section 4.4 $V = \boldsymbol{U}$, $L_0 = P\mathcal{L}_c$, $L_\tau = P(\mathcal{L}_\tau - \mathcal{L}_c)$ and $\mathcal{N}_\tau = P(-\mathcal{B} - B_Q - N)$ from (4.38). Using $V = u + W$, $L_0 u = 0$ and that L_0 is boundedly invertible from $\mathcal{M}$ to range$(\mathcal{L}_0)$ or range$(\mathcal{L}_c)$, we rewrite $PG = 0$ as the fixed point equation for W given by

$$-(L_0 + L_\tau)W = L_\tau u + \mathcal{N}_\tau(u+W) \Leftrightarrow W = -(L_0 + L_\tau)^{-1}(L_\tau u + \mathcal{N}_\tau(u+W))\,. \quad \text{(C.1)}$$

Since a priori $\|W\| = \mathcal{O}(|\tau| + \|u\|_X)$ and $L_0 + L_\tau$ is boundedly invertible for sufficiently small $|\tau|$ and $\|u\|_X$, we find constants C_1, $C_2 > 0$ such that

$$\|(L_0+L_\tau)^{-1}L_\tau u\|_X \le C_1|\tau|\|u\|_X\,,$$
$$\|(L_0+L_\tau)^{-1}\mathcal{N}_\tau(u+W)\| \le C_2(\|u\|_X^2+\|W\|_X^2)\,.$$

From (C.1) we then obtain

$$\begin{aligned} &\|W\|_X \le C_1|\tau|\|u\|_X + C_2(\|u\|_X^2+\|W\|_X^2) \\ \Rightarrow\quad &\|W\|_X(1-C_2\|W\|_X) \le C_1|\tau|\|u\|_X + C_2\|u\|_X^2\,. \end{aligned} \tag{C.2}$$

Choosing τ and u sufficiently small gives $C_2\|W\|_X \le \frac{1}{2}$ and then (C.2) implies

$$\|W\|_X \le 2C_1|\tau|\|u\|_X + 2C_2\|u\|_X^2\,,$$

which proves (4.36) and (4.43).

D. Proof for even parity of W

Analogous to the proof of Theorem 4.2, we rewrite (4.25) as the fixed point equation for W given by

$$P\mathcal{L}_0 W = -P(L_\tau\phi + N_C(\phi,\tau) + N_Q(\phi,\tau))\,, \tag{D.1}$$

with operators as in (4.27). We consider the even function ϕ. The operators L_τ, N_C, N_Q map even functions to odd functions, and the projection P from (4.24) maps odd functions to odd functions. Thus, the term on the right-hand side of (D.1) is odd. We write the periodic function W as a Fourier series $W = \sum_{\ell\in\mathbb{Z}} w_\ell \mathrm{e}^{\mathrm{i}\ell\xi}$ with $w_\ell \in \mathbb{C}$, and write the odd periodic function on the right-hand side of (D.1) as $\sum_{m=1}^{\infty} R_m \sin(m\xi)$ with $R_m \in \mathbb{R}$. Then, (D.1) becomes

$$\sum_{\ell\in\mathbb{Z}} \widehat{P}\widehat{\mathcal{L}}_0(\ell) w_\ell \mathrm{e}^{\mathrm{i}\ell\xi} = \sum_{m=1}^{\infty} R_m \sin(m\xi)\,,$$

where $\widehat{\mathcal{L}}_0(\ell) = \mathrm{i}\ell(dk_c^4\ell^4 - bk_c^2\ell^2 + C/H_0)$, which is an odd function in ℓ, and $\widehat{P} = \mathrm{Id}$ since $W \in \mathcal{M}$. Hence, $\widehat{P}\widehat{\mathcal{L}}_0(\ell) = \widehat{\mathcal{L}}_0(\ell)$ and its inverse is also odd. We project the both sides of the above equation onto $\mathrm{e}^{\mathrm{i}\ell\xi}$ and $\mathrm{e}^{-\mathrm{i}\ell\xi}$ (with the inner product $\langle\cdot,\cdot\rangle = \langle\cdot,\cdot\rangle_{L^2}$), respectively and obtain

$$\begin{aligned} \widehat{\mathcal{L}}_0(\ell)w_\ell = \langle R_\ell\sin(\ell\xi), \mathrm{e}^{\mathrm{i}\ell\xi}\rangle \quad &\Leftrightarrow \quad w_\ell = (\widehat{\mathcal{L}}_0(\ell))^{-1}\langle R_\ell\sin(\ell\xi), \mathrm{e}^{\mathrm{i}\ell\xi}\rangle\,, \\ \widehat{\mathcal{L}}_0(-\ell)w_{-\ell} = \langle R_\ell\sin(\ell\xi), \mathrm{e}^{-\mathrm{i}\ell\xi}\rangle \quad &\Leftrightarrow \quad w_{-\ell} = (\widehat{\mathcal{L}}_0(-\ell))^{-1}\langle R_\ell\sin(\ell\xi), \mathrm{e}^{-\mathrm{i}\ell\xi}\rangle\,. \end{aligned}$$

Since $\langle R_\ell\sin(\ell\xi), \mathrm{e}^{\mathrm{i}\ell\xi}\rangle = -\langle R_\ell\sin(\ell\xi), \mathrm{e}^{-\mathrm{i}\ell\xi}\rangle \in \mathrm{i}\mathbb{R}$, we have $w_\ell = w_{-\ell} \in \mathbb{R}$. It follows that W is even and real.

References

Achatz, U. (2006). *Gravity-Wave Breakdown in a Rotating Boussinesq Fluid: Linear and Nonlinear Dynamics*. Habilitation, University of Rostock, Germany.

Arbic, B. K. and Scott, R. B. (2008). On quadratic bottom drag, geostrophic turbulence, and oceanic mesoscale eddies. *Journal of Physical Oceanography*, 38(1):84–103.

Balmforth, N. J. and Mandre, S. (2004). Dynamics of roll waves. *Journal of Fluid Mechanics*, 514:1–33.

Balmforth, N. J. and Young, Y.-N. (2002). Stratified Kolmogorov flow. *Journal of Fluid Mechanics*, 450:131–167.

Balmforth, N. J. and Young, Y.-N. (2005). Stratified Kolmogorov flow. II. *Journal of Fluid Mechanics*, 528:23–42.

Bateman, H. (1915). Some recent researches on the motion of fluids. *Monthly Weather Review*, 43(4):163 – 170.

Beloshapkin, V. V., Chernikov, A. A., Natenzon, M. Y., Petrovichev, B. A., Sagdeev, R. Z., and Zaslavsky, G. M. (1989). Chaotic streamlines in pre-turbulent states. *Nature*, 337:133–137.

Burgers, J. M. (1948). A mathematical model illustrating the theory of turbulence. volume 1 of *Advances in Applied Mechanics*, pages 171–199. Elsevier.

Chae, D. and Dubovskiĭ, P. (1996). Travelling wave-like solutions of the Navier-Stokes and the related equations. *Journal of Mathematical Analysis and Applications*, 204(3):930–939.

Chai, J., Wu, T., and Fang, L. (2020). Single-scale two-dimensional-three-component generalized-Beltrami-flow solutions of incompressible Navier–Stokes equations. *Physics Letters A*, 384(34):126857.

Chan, I. H. and Shepherd, T. G. (2013). Balance model for equatorial long waves. *Journal of Fluid Mechanics*, 725:55–90.

Chhabra, R. P. (2010). Non-Newtonian Fluids: An Introduction. In Krishnan, J., Deshpande, A., and Kumar, P., editors, *Rheology of Complex Fluids*, pages 3–34. Springer, New York, NY.

Danilov, S., Juricke, S., Kutsenko, A., and Oliver, M. (2019). Toward consistent subgrid momentum closures in ocean models. In Eden, C. and Iske, A., editors, *Energy Transfers in Atmosphere and Ocean*, pages 145–192. Springer, Cham.

Doering, C. R. and Gibbon, J. D. (1995). *Applied Analysis of the Navier–Stokes Equations*. Cambridge Texts in Applied Mathematics. Cambridge University Press, Cambridge.

Drazin, P. G. (1977). On the instability of an internal gravity wave. *Proceedings of the Royal Society of London. Series A, Mathematical and Physical Sciences*, 356(1686):411–432.

Drazin, P. G. and Riley, N. (2006). *The Navier–Stokes Equations: A Classification of Flows and Exact Solutions*, volume 334 of *London Mathematical Society Lecture Note Series*. Cambridge University Press, Cambridge.

Dyck, N. J. and Straatman, A. G. (2020). Exact solutions to the three-dimensional Navier–Stokes equations using the extended Beltrami method. *Journal of Applied Mechanics*, 87(1). 011004.

Foias, C. and Temam, R. (1989). Gevrey class regularity for the solutions of the Navier–Stokes equations. *Journal of Functional Analysis*, 87(2):359–369.

Gallay, T. and Wayne, C. E. (2005). Global stability of vortex solutions of the two-dimensional Navier–Stokes equation. *Communications in Mathematical Physics*, 255:97–129.

Ghaemsaidi, S. J. and Mathur, M. (2019). Three-dimensional small-scale instabilities of plane internal gravity waves. *Journal of Fluid Mechanics*, 863:702–729.

Goh, R. and Wayne, C. E. (2019). Vortices in stably-startified rapidly rotating Boussinesq convection. *Nonlinearity*, 32(5):R1–R52.

Gregory, R. D. (1996). Helmholtz's theorem when the domain is infinite and when the field has singular points. *The Quarterly Journal of Mechanics and Applied Mathematics*, 49(3):439–450.

Grianik, N., Held, I. M., Smith, K. S., and Vallis, G. K. (2004). The effects of quadratic drag on the inverse cascade of two-dimensional turbulence. *Physics of Fluids*, 16(1):73–78.

Grubišić, V., Smith, R. B., and Schär, C. (1995). The effect of bottom friction on shallow-water flow past an isolated obstacle. *Journal of Atmospheric Sciences*, 52(11):1985–2005.

Guan, Y., Chattopadhyay, A., Subel, A., and Hassanzadeh, P. (2022). Stable a posteriori LES of 2D turbulence using convolutional neural networks: Backscattering analysis and generalization to higher Re via transfer learning. *Journal of Computational Physics*, 458:111090.

Hui, W. H. (1987). Exact solutions of the unsteady two-dimensional Navier–Stokes equations. *Journal of Applied Mathematics and Physics (ZAMP)*, 38(5):689–702.

Jansen, M. F., Adcroft, A., Khani, S., and Kong, H. (2019). Toward an energetically consistent, resolution aware parameterization of ocean mesoscale eddies. *Journal of Advances in Modeling Earth Systems*, 11(8):2844–2860.

Jansen, M. F. and Held, I. M. (2014). Parameterizing subgrid-scale eddy effects using energetically consistent backscatter. *Ocean Modelling*, 80:36–48.

Juricke, S., Danilov, S., Koldunov, N., Oliver, M., Sein, D. V., Sidorenko, D., and Wang, Q. (2020). A kinematic kinetic energy backscatter parametrization: from implementation to global ocean simulations. *Journal of Advances in Modeling Earth Systems*, 12(12):e2020MS002175.

Kambe, T. (1986). A class of exact solutions of the Navier–Stokes equation. *Fluid Dynamics Research*, 1(1):21–31.

Kowalik, Z. and Whitmore, P. M. (1991). An investigation of two tsunamis recorded at Adak, Alaska. *Science of Tsunami Hazards*, 9(2):67–83.

Lelong, M. P. and Dunkerton, T. J. (1998). Inertia–gravity wave breaking in three dimensions. Part I: Convectively stable waves. *Journal of the Atmospheric Sciences*, 55(15):2473 – 2488.

Majda, A. (2003). *Introduction to PDEs and Waves for the Atmosphere and Ocean*, volume 9 of *Courant Lecture Notes in Mathematics*. New York University, Courant Institute of Mathematical Sciences, New York; American Mathematical Society, Providence, RI.

Majda, A. J. and Bertozzi, A. L. (2001). *Vorticity and Incompressible Flow*. Cambridge Texts in Applied Mathematics. Cambridge University Press, Cambridge.

Majda, A. J. and Wang, X. (2006). *Nonlinear Dynamics and Statistical Theories for Basic Geophysical Flows*. Cambridge University Press, Cambridge.

Matsuno, T. (1966). Quasi-geostrophic motions in the equatorial area. *Journal of the Meteorological Society of Japan. Ser. II*, 44(1):25–43.

Meshalkin, L. D. and Sinai, I. G. (1961). Investigation of the stability of a stationary solution of a system of equations for the plane movement of an incompressible viscous liquid. *Journal of Applied Mathematics and Mechanics*, 25(6):1700–1705.

Mied, R. P. (1976). The occurrence of parametric instabilities in finite-amplitude internal gravity waves. *Journal of Fluid Mechanics*, 78(4):763–784.

Olbers, D., Willebrand, J., and Eden, C. (2012). *Ocean Dynamics*. Springer, Berlin, Heidelberg.

Onuki, Y., Joubaud, S., and Dauxois, T. (2021). Simulating turbulent mixing caused by local instability of internal gravity waves. *Journal of Fluid Mechanics*, 915:A77.

Pedlosky, J. (1987). *Geophysical Fluid Dynamics*. Springer, New York, NY, 2nd edition.

Perezhogin, P. A. (2020). Testing of kinetic energy backscatter parameterizations in the nemo ocean model. *Russian Journal of Numerical Analysis and Mathematical Modelling*, 35(2):69–82.

Petcu, M., Temam, R. M., and Ziane, M. (2009). Some mathematical problems in geophysical fluid dynamics. In *Handbook of Numerical Analysis. Volume XIV. Special volume: Computational Methods for the Atmosphere and the Oceans*, volume 14 of *Handook of Numerical Analysis*, pages 577–750. Elsevier/North-Holland, Amsterdam.

Porta Mana, P. and Zanna, L. (2014). Toward a stochastic parameterization of ocean mesoscale eddies. *Ocean Modelling*, 79:1–20.

Prugger, A. (2017). Flachwassergleichung mit Diffusion: Stabilität und Verzweigung von Wellen. Master's thesis, University of Bremen.

Prugger, A. and Rademacher, J. D. M. (2021). Explicit superposed and forced plane wave generalized Beltrami flows. *IMA Journal of Applied Mathematics*, 86(4):761–784.

Prugger, A., Rademacher, J. D. M., and Yang, J. (2022a). Geophysical fluid models with simple energy backscatter: explicit flows and unbounded exponential growth. *Geophysical & Astrophysical Fluid Dynamics*, 116(5-6):374–410.

Prugger, A., Rademacher, J. D. M., and Yang, J. (2022b). Rotating shallow water equations with bottom drag: bifurcations and growth due to kinetic energy backscatter. *arXiv preprint arXiv:2209.06651*.

Rubio, A. M., Julien, K., Knobloch, E., and Weiss, J. B. (2014). Upscale energy transfer in three-dimensional rapidly rotating turbulent convection. *Physical Review Letters*, 112:144501.

Satake, K. (1995). Linear and nonlinear computations of the 1992 Nicaragua earthquake tsunami. *Pure and Applied Geophysics*, 144(3-4):455–470.

Schneider, G. and Uecker, H. (2017). *Nonlinear PDEs: A Dynamical Systems Approach*, volume 182 of *Graduate Studies in Mathematics*. American Mathematical Society, Providence, Rhode Island.

Stakgold, I. (1971). Branching of solutions of nonlinear equations. *SIAM Review*, 13(3):289–332.

Steinherr Zazo, M. (2021). *Bifurcation Analysis for Systems with Piecewise Smooth Nonlinearity and Applications*. PhD thesis, University of Bremen.

Steinherr Zazo, M. and Rademacher, J. D. M. (2020). Lyapunov coefficients for Hopf bifurcations in systems with piecewise smooth nonlinearity. *SIAM Journal on Applied Dynamical Systems*, 19(4):2847–2886.

Taylor, J. R. and Sarkar, S. (2008). Stratification effects in a bottom Ekman layer. *Journal of Physical Oceanography*, 38(11):2535–2555.

Temam, R. (1995). *Navier–Stokes Equations and Nonlinear Functional Analysis*. Society for Industrial and Applied Mathematics, Philadelphia, Pa., 2nd edition.

Temam, R. (2001). *Navier–Stokes equations: Theory and numerical analysis*. AMS Chelsea Publishing, American Mathematical Society, Providence, RI. Reprint of the 1977 edition, Studies in Mathematics and its Applications, North-Holland Publishing Co., Amsterdam.

Uecker, H. (2022). Continuation and bifurcation in nonlinear PDEs –algorithms, applications, and experiments. *Jahresbericht der Deutschen Mathematiker-Vereinigung*, 124(1):43–80.

Uecker, H., Wetzel, D., and Rademacher, J. D. M. (2014). pde2path - a Matlab package for continuation and bifurcation in 2D elliptic systems. *Numerical Mathematics: Theory, Methods and Applications*, 7(1):58–106.

Vallis, G. K. (2017). *Atmospheric and Oceanic Fluid Dynamics: Fundamentals and Large-Scale Circulation*. Cambridge University Press, Cambridge, 2nd edition.

van der Toorn, R. (2019). Elementary properties of non-linear Rossby–Haurwitz planetary waves revisited in terms of the underlying spherical symmetry. *AIMS Mathematics*, 4(2):279–298.

Walsh, O. (1992). Eddy solutions of the Navier–Stokes equations. In Heywood, J. G., Masuda, K., Rautmann, R., and Solonnikov, V. A., editors, *The Navier–Stokes equations II – theory and numerical methods (Oberwolfach, 1991)*, volume 1530 of *Lecture Notes in Mathematics*, pages 306–309. Springer, Berlin, Heidelberg.

Wang, C. Y. (1989). Exact solutions of the unsteady Navier–Stokes equations. *Applied Mechanics Reviews*, 42(11S):S269–S282.

Wang, C. Y. (1990). Exact solutions of the Navier–Stokes equations – the generalized Beltrami flows, review and extension. *Acta Mechanica*, 81:69–74.

Weinbaum, S. and O'Brien, V. (1967). Exact Navier–Stokes solutions including swirl and cross flow. *The Physics of Fluids*, 10(7):1438–1447.

Wiedemann, E. (2011). Existence of weak solutions for the incompressible Euler equations. *Annales de l'institut Henri Poincaré. Analyse non linéaire*, 28(5):727–730.

Yang, J. (2019). *Diffusion, Advection and Pattern Formation*. PhD thesis, University of Bremen.

Yau, K.-H., Klaassen, G. P., and Sonmor, L. J. (2004). Principal instabilities of large amplitude inertio-gravity waves. *Physics of Fluids*, 16(4):936–951.

Zanna, L., Porta Mana, P., Anstey, J., David, T., and Bolton, T. (2017). Scale-aware deterministic and stochastic parametrizations of eddy-mean flow interaction. *Ocean Modelling*, 111:66–80.

Zhang, J., Lu, X., Wang, P., and Wang, Y. P. (2011). Study on linear and nonlinear bottom friction parameterizations for regional tidal models using data assimilation. *Continental Shelf Research*, 31(6):555–573.

Zurita-Gotor, P., Held, I. M., and Jansen, M. F. (2015). Kinetic energy-conserving hyperdiffusion can improve low resolution atmospheric models. *Journal of Advances in Modeling Earth Systems*, 7(3):1117–1135.